Department of Applied Geology

Hydrogeology of the Lake Muir–Unicup Catchment, Western Australia: an ecologically important area experiencing hydrologic change

Margaret G. Smith

This thesis is presented for the Degree of
Doctor of Philosophy
of
Curtin University

August 2010

Declaration

To the best of my knowledge and belief this thesis contains no material previously published by any other person except where due acknowledgement has been made. This thesis contains no material which has been accepted for the award of any other degree or diploma in any university.

Abstract

Identified in the Western Australian Government's 1996 Salinity Action Plan as an important natural diversity area at risk from changing hydrology, the Lake Muir–Unicup Natural Diversity Catchment is in need of urgent management to minimise impacts to lake hydrology and vegetation health. Many of the wetlands in the south of the catchment have been designated under the Ramsar Convention as Wetlands of International Importance. Other wetlands elsewhere in the catchment have been prioritised according to the Convention guidelines and are awaiting to be officially listed.

In the 1980 to 1990s changing hydrology related to land clearing was considered to result in dry-land salinisation. Although low pH groundwater was noted during the groundwater monitoring between 1997 and 2001, the implications of groundwater acidification were not realised. Groundwater acidification cannot be taken in isolation, and it quickly became apparent that a viable management plan could not be formulated until the hydrogeology and geochemistry were better understood.

The aquifers present today are the result of a landscape that evolved during and since Australia and Antarctica rifted apart. The separation of these two land masses has resulted in the formation and preservation of five regolith units that make up the three aquifers: the surficial; the sedimentary; and the fractured and/or weathered basement rock aquifers. The late Eocene topography was modelled using known depth to basement rock and reprocessed airborne magnetic data, enabling the lateral and verticals extent of the aquifers to be determined.

The hydraulic head data within the mapped aquifers led to the identification of a closed groundwater basin in the south of the study area with groundwater TDS values up to three times seawater.

Three distinct hydrochemical facies have been recognised and in keeping with the marine aerosol signature the majority of the groundwater is a Na–Cl type water. The fractured and/or weathered basement rock aquifer in the south of the study area contains a water where the major cations are Ca and Na and is referred to as a Ca–

Na–Cl type water. Anthropogenic process have resulted in the a Na–Mg–SO_4 type water associated with draining a peat swamp with the aim of mining the peat.

All three aquifers contain iron rich water, and pyrite has been identified in the sedimentary aquifer and fractured and/or weathered basement rock aquifer. Of the three aquifers the sedimentary aquifer is the most likely to contain groundwaters with pH up to 6.3 that have minimal buffering capacity.

Acknowledgements

I would like to thank my supervisors Dr. Ron Watkins, Dr. David Gray, Dr. Mehrooz Aspandiar and Dr. Stephen Appleyard. All have given invaluable support.

This project was made possible through the Department of Environment and Conservation, CRC Landscape Environments and Mineral Exploration and CSIRO. The Department of Environment and Conservation provided financial support and access to the study area and bore network. Mr. Roger Hearn, Mr. Ian Wheeler and Mr. Peter Geste all helped in the data collection. Financial support was given by CRC Landscape Environments and Mineral Exploration. CSIRO provided an office, computing facilities and access to Wet Chemical Laboratory and the Electron Beam and XRD Laboratory without which the project would have been harder to complete.

I am very grateful to the people at CSIRO who took time out from their busy schedule, listened to my questions and gave carefully considered answers. This included Dr. R Fitzpatrick, Dr. R. Anand, and Dr. Ian Robertson.

I would like to thank Mr Paul Wilkes from the Department of Exploration Geophysics at Curtin University of Technology for re-processing the airborne magnetic geophysics, Michael Verrall for conducting the XRD work on the samples and Mr. Mike Walsh for helping write computer routines to run PHREEQC.

I would like to thank my Mum for her support.

Table of Contents

Figures

Tables

Appendix Tables

1 Introduction

1.1 BACKGROUND

Acidic groundwater is widespread in southern Western Australia, but was ignored as an environmental issue by land and water salinisation during the 1990s. Concern about land and water salinisation, and current and future loss of agricultural land, led to a review of salinisation in 1996 (Government of Western Australia, 1996a; 1996b). It was estimated that about 1.8 million hectares of farmland were salt affected and that this area would double within 25 years (Government of Western Australia, 1996a). In 1996 about a third of the State's divertible water resources were brackish or saline and salinity was a major threat to natural (biological) diversity.

One method of dealing with land salinisation in southern Western Australia detailed by the Government of Western Australia (Government of Western Australia, 2000) is the excavation of 'deep drains'. Such drains intersect the saline groundwater allowing drainage of the saline water and its discharge to topographic low points such as lakes. The aim of the drain is to lower the watertable to below the root depth of crops. Drainage of this type has been embraced by many land managers to help ameliorate salinisation with more than 10 000 km of drains (Shand and Degens, 2008) constructed to depths up to 3 m.

Review of the water quality within these drains revealed some to be discharging saline water with pH < 2 (Fitzpatrick and Shand, 2008; Shand and Degens, 2008; Shand et al., 2008) and containing elevated levels of Al, Mn, Co, Ni, and Pb (Tapley et al., 2004). Mann (1983) identified groundwater with pH values < 4 underlying extensive areas of the Yilgarn Craton. Mann (1983) favoured a model where weathering of basement rocks was releasing ferrous ion (Fe^{2+}) into solution, which was subsequently oxidised according to the reaction:

$$4Fe^{2+} + 6H_2O + O_2 \rightarrow 4FeOOH + 8H^+ \quad (1.1)$$

The release of H^+ causes the pH the fall.

Further work by McArthur et al. (1989; 1991) considered alternative groundwater processes. These authors agreed with Mann's proposal that the acidity is formed by the oxidation of Fe^{2+} but disagreed as to the source of the Fe^{2+}. They argued that the iron-rich water is formed by the microbial reduction of iron oxyhydroxides (McArthur et al., 1991). The microbial reduction of Fe^{2+} to form pyrite and microbial oxidation of pyrite to form SO_4^{2-} and H^+ has gained recognition over the last 20 to 30 years especially for low temperature environments as such as affecting groundwater.

Since the initial work in the 1980s and early 1990s, inland acidic groundwater in southern Western Australia has received little attention. However, numerous studies have looked at acidic water associated with acid sulfate soils and acid mine drainage. Potential acid sulfate soils are found in coastal mangroves, salt marshes, estuaries and tidal lakes. Pyrite in water-logged soils is chemically stable but once the land is drained, e.g. for development or agriculture, the pyrite oxidises and sulfuric acid forms. Acid mine drainage (AMD) is also due to the oxidation of pyrite and other sulfide minerals. Water permeating mined rock containing pyrite becomes acidic as the pyrite oxidises. Acid water from these two sources have cost governments and private companies billions of dollars to manage or remediate, both in Australia and overseas.

Recognising the potential cost of acid sulfate soils and acid mine drainage, the Western Australian Government realised that the cause and risk of local inland acidic water (and the mobilisation of trace metals) were unknown. Prior to 2004, the risk posed by acidic, metal laden water on Western Australian aquatic ecosystems had not been investigated. Only limited work on inland eastern Australian acidic groundwater existed (Fitzpatrick et al., 2003; Macumber, 1992; Merry et al., 2002; Rosicky et al., 2002) and its relevance to Western Australian conditions was uncertain. Thus, there was a clear need for further study of the acidic groundwater in southern Western Australia.

1.2 LAKE MUIR–UNICUP NATURAL DIVERSITY CATCHMENT

The Western Australian Government's 1996 salinity review identified 'Recovery Catchments' for water and natural diversity that needed remediation (Government of Western Australia, 1996b). The Natural Diversity Recovery Program was charged

> (to) *ensure that critical and regionally significant natural areas, particularly wetlands are protected in perpetuity* (Government of Western Australia, 1996b).

The Lake Muir–Unicup Natural Diversity Catchment (managed by the Western Australian Department of Environment and Conservation (DEC)) was identified as a high priority area, with fresh water wetlands of world significance at risk of water salinisation (Figure 1–1). Within the Lake Muir–Unicup Natural Diversity Catchment, and covering an area of 10 631 ha, is the 'Muir-Byenup System' of wetlands that are listed as 'wetlands of international significance' under the Ramsar Convention (Figure 1–1). Other wetlands in the Lake Muir–Unicup Natural Diversity Catchment have been prioritised according to the Ramsar Convention guidelines and are awaiting official listing. The 'Muir-Byenup' group of wetlands is one of five remaining breeding/feeding habitats for the Australasian Bittern (*Botaurus poiciloptilus*) and in Australia there are about 2500 individuals left, with their numbers in decline (Garnett and Crowley, 2000).

In developing the Lake Muir–Unicup Natural Diversity Catchment Management Plan (Department of Environment and Conservation, *in prep*) it became apparent that little was known about the hydrogeology or groundwater that could threaten vegetation and many of the lakes. From previous regional mapping, the geology and associated aquifers beneath the lakes could not be resolved. A sedimentary aquifer had been recognised (De Silva, 2000; 2004) but the lateral and vertical extent within the Lake Muir–Unicup Natural Diversity Recovery Catchment was not known. Lakes fed by shallow local groundwater were not distinguished from those that were maintained by deeper regional groundwater flows associated with the sedimentary aquifer. Knowledge of groundwater geochemistry was limited, and groundwater salinity was the only water quality parameter addressed in the Management Plan for the catchment.

Figure 1–1 Location of the study area showing the boundaries of the Lake Muir–Unicup Natural Diversity Recovery Catchment and Muir–Byenup System.

A review of bore water data in 2001 revealed that in places the saline groundwater was acidic (Smith et al., 2005). Acidic water may mobilise metals and metalloids which can cause harm to ecosystems and result in a loss of diversity if the water is discharged into watercourses or evaporation basins. In particular, acidic groundwater is known to dissolve Al whence it is highly toxic to plants and fish. Additional bores were constructed in the catchment in 2003 with the aim of increasing our knowledge of the aquifers and groundwater movement and quality. Preliminary groundwater investigations revealed water samples where Total Acidity exceeded Total Alkalinity and elevated levels of Cd, Cr, Cu and Ni were identified (Smith et al., 2004).

The Department of Environment and Conservation realised that to manage the hydrology of the lakes within the Lake Muir–Unicup Natural Diversity Recovery Catchment, a series of research projects were needed. The first project which is the basis of this research thesis was to clarify the catchment geology, hydrogeology and

groundwater geochemistry. This research will be combined with additional research projects on catchment surface hydrology, catchment land use and predicted changes in climate to enable the hydrology of the lakes in the Lake Muir–Unicup Natural Diversity Recovery Catchment to be advanced.

1.3 AIMS AND SCOPE

The groundwater in the Lake Muir–Unicup Natural Diversity Recovery Catchment needs to be managed in order to prevent more vegetation loss and to help the environment make a healthy transition as the groundwater budget and water quality change. Thus the aims of this research are to:

- Establish the lateral and vertical extent of the aquifers within the catchment;
- Elucidate the geochemical processes active within the groundwater of the catchment; and
- Identify groundwater at risk of acidification within the catchment.

A comprehensive groundwater study needs to integrate geology, hydrogeology and geochemistry of the catchment. Saline groundwater has been noted as a risk to the lake systems, but concern over acidification of groundwater has intensified as acid groundwater discharging into lakes can potentially cause deterioration of lake health. Before addressing the groundwater acidification this study needs to refine the geology and hydrogeology for the catchment. Current understanding of the hydrogeology in the Lake Muir–Unicup area (De Silva, 2000; 2004; Smith, 2003) is based on regional geology (Wilde and Walker, 1984).

This research project has collected and analysed rock and groundwater samples, and utilised the extensive geological information collected as part of the 2003 exploration program. In this thesis the geological information will be combined with geophysical data to develop an understanding of the geology, hydrogeology and hydrogeochemistry of the catchment.

1.4 OVERVIEW OF THE STUDY

Pivotal to the discussion of the groundwater geochemistry is the term groundwater acidification which is incompletely defined in many geochemistry texts. Chapter 2 addresses the concept of acidification. Since groundwater interacts with the aquifer media this chapter also summarises groundwater evolution.

The geomorphology, climate, soils, vegetation and salinisation of the study area are documented in Chapter 3 and the methods used in the study are described in Chapter 4.

The local geology, aquifers and groundwater flow are discussed in Chapters 5 and 6. Chapter 5 details the local geology, placing it in the context of the regional geological setting and using it to develop a greater understanding of the aquifers within the catchment. Chapter 6 focuses upon description of the rocks and physical properties of the aquifers before examining groundwater flow and areas of groundwater recharge and discharge.

Groundwater geochemistry is the subject of Chapter 7 and the acidification is discussed in light of the processes described in Chapter 2. Chapter 7 includes discussion of the chemical interaction of the groundwater with the aquifer media.

The finding reported in Chapters 5 to 7 are summarised in Chapter 8 along with recommendations for future research.

1.5 TERMINOLOGY AND NOTATION

1.5.1 Spelling

Names given to lakes and wetlands within the Lake Muir–Unicup Natural Diversity Recovery Catchment are based on aboriginal names. The spelling used in this study is that appearing on the Department of Environment and Conservation maps. Other government agencies have sometimes employed alternative spellings e.g. Bokarup Swamp (DEC) verses the Bokerup climatic station. As Bokerup with an *e* is the official spelling for the Bureau of Meteorology (BOM) site this spelling is used in this study when referring to the climate station BOM 9673.

The spelling of Werillup Formation has been addressed by Clarke et al. (2003) and their preferred spelling has been used in this study.

1.5.2 Definitions

The International Commission of Stratigraphy does not recognise the term Tertiary (Gradstein et al., 2004), but the term Tertiary appears widely in the literature of the study area (De Silva, 2004; Smith, 2003; Wilde and Walker, 1984). If the referenced authors have not refined the time scale into Epoch or Stage then the term Tertiary is retained when referring to their work. The value of the term inset-valley verses terms such as palaeochannel is reviewed in Chapter 5.

2 Alkalinity and acidity

2.1 INTRODUCTION

Geochemical reactions occurring as groundwater flows through the aquifer may directly or indirectly influence groundwater acidity and alkalinity. Reactions that yield or consume H^+ or OH^- have a direct affect on the groundwater acidity and alkalinity. Increased alkalinity can result from weathering of most rocks, and redox reactions such as the chemical reduction of iron and sulfate. Oxidation reactions, notably the oxidation of sulfide and ferrous iron contribute to groundwater acidity.

Other geochemical reactions, such as cation exchange and evaporation, indirectly influence the acidity and alkalinity by changing the concentration of major ions in the groundwater. Should groundwater become saturated with respect to minerals like calcite and sepiolite ($MgSi_3O_6(OH)_2$) the precipitation of these minerals will affect alkalinity.

This chapter summarises the geochemical processes that may affect the geochemical composition of the groundwater in the study area. Prior to this summary, the concept of groundwater acidity and alkalinity is reviewed.

2.2 NATURE OF GROUNDWATER ACIDITY AND ALKALINITY

Alkalinity is a parameter frequently measured as part of routine groundwater analysis and is defined as the capacity of a system to neutralise an acid (Appelo and Postma, 2005; Drever, 1997; Langmuir, 1997; Stumm and Morgan, 1996). While understanding of alkalinity is central to aquatic and groundwater chemistry, it is often less than perfectly understood (Morel and Hering, 1993).

Increasingly, field workers and land managers in Western Australia are having to address groundwater acidity. Like alkalinity, the concept is often poorly understood. Whereas pH is a good indicator of acidic groundwater it is a poor indicator of acidity.

That is, groundwater with a Net Acidity, but with a near neutral pH will not be recognised.

One of the problems is that theoretical definitions and laboratory measurements of alkalinity and acidity are conceptually and practically different (Kirby and Cravotta III, 2005a). This is compounded by a plethora of terms such as alkalinity, caustic alkalinity, p-alkalinity, acidity, mineral acidity and CO_2-acidity. The geochemical and hydrogeology texts vary in the detail when discussing acidity and alkalinity and frequently do not mention the limitation of the calculations or measurements. This led Kirby and Cravotta III (2005a; 2005b) to review the theoretical and practical aspects of alkalinity and acidity. Before the theoretical definitions and laboratory measurements of alkalinity and acidity are summarised the carbonate system is reviewed.

2.3 CARBONATE EQUILIBRIA AND GROUNDWATER

The carbonate system dominates groundwater alkalinity (Drever, 1997; Freeze and Cherry, 1979; Langmuir, 1997; Stumm and Morgan, 1996). Carbon dioxide (CO_2) combines with water to form carbonic acid (H_2CO_3) which dissociates into the bicarbonate ion (HCO_3^-) and carbonate ion (CO_3^{2-}).

The carbonate system and equilibrium constants at 25°C can be expressed as (Appelo and Postma, 2005):

$$CO_{2(g)} + H_2O \leftrightarrow H_2CO_3^* \qquad K_H = 10^{-1.5} \qquad (2.1)$$

$$H_2CO_3^* \leftrightarrow H^+ + HCO_3^- \qquad K_1 = 10^{-6.3} \qquad (2.2)$$

$$HCO_3^- \leftrightarrow H^+ + CO_3^{2-} \qquad K_2 = 10^{-10.3} \qquad (2.3)$$

where $H_2CO_3^*$ is both hydrated CO_2 ($CO_{2(aq)}$) and carbonic acid (H_2CO_3). Mass balance equations and their constants are valid for the activity of ions but not the ion concentrations (Appelo and Postma, 2005; Drever, 1997). The activity of an ion is the measured total concentration corrected for the effects of electrostatic shielding and for the presence of aqueous complexes (Appelo and Postma, 2005). Activity of an ion is represented by square brackets [*i*]. The concentration is generally represented as m_i where *m* is molar concentration and *i* is the ion.

To understand carbonate alkalinity in relation to groundwater, some important soil processes must first be explained. Biological and hydrochemical processes are capable of producing carbon dioxide and carbonic acid. Carbon dioxide is produced by decay of organic matter (oxidation) and respiration from plant roots. Organic matter decays in the soil according to the reaction:

$$O_{2(g)} + CH_2O \rightarrow CO_{2(g)} + H_2O \qquad (2.4)$$

where CH_2O is a simple carbohydrate used to designate organic matter. Respiration from plant roots may be represented by the reaction (Drever, 1997):

$$C_{106}H_{263}O_{110}N_{16}P + 138O_2 \rightarrow 106CO_2 + 16NO_3^- + HPO_4^{2-} + 122H_2O + 18H^+ \quad (2.5)$$

The $CO_{2(g)}$, from organic matter decay and respiration combines with water to form carbonic acid according the reaction (2.1).

The P_{CO_2} (partial pressure of CO_2) in soil is typically between 10^{-3} to 10^{-1} compared to the atmospheric P_{CO_2} $10^{-3.5}$ (Freeze and Cherry, 1979). Water in equilibrium with atmospheric CO_2 (P_{CO_2} $10^{-3.5}$) has a pH of 5.7, but as the P_{CO_2} increases pH falls. Henry's constant for reaction (2.1) is $K_H = 10^{-1.5}$ and can be rewritten as follows:

$$\frac{[H_2CO_3^*]}{[P_{CO_2}]} = 10^{-1.5} \qquad (2.6)$$

In the unsaturated zone, where the soil water is in contact with the gaseous environment, the system is considered an open system with respect to CO_2, with CO_2 replenished by oxidation of organic matter and root respiration (reactions 2.4 and 2.5). Once the CO_2-enriched soil water encounters groundwater, the system can be either closed or open with respect to CO_2. Diffusion of CO_2 through water is slow (Appelo and Postma, 2005) so the system can be considered closed if this is the sole source of CO_2. In an open system CO_2 can be replenished by oxidation of organic matter, or derived from alternative sources by groundwater flow.

Carbonic acid can release two protons. The relative distribution of dissolved carbonate species is dependent on the pH of the solution. Reaction (2.2) can be rewritten as:

$$\frac{[HCO_3^-]}{[H_2CO_3^*]} = \frac{10^{-6.3}}{10^{-pH}} \qquad (2.7)$$

Therefore, at pH 6.3 the activities of HCO_3^- and $H_2CO_3^*$ are equal. At pH < 6.3 the activity of HCO_3^- decreases and the activity of $H_2CO_3^*$ increases (Figure 2–1). Similarly reaction (2.3) can be rewritten as:

$$\frac{[CO_3^{2-}]}{[HCO_3^-]} = \frac{10^{-10.3}}{10^{-pH}} \qquad (2.8)$$

At pH 10.3 the activities of HCO_3^- and CO_3^{2-} are equal and at pH > 10.3 the activity of HCO_3^- decreases and the activity of CO_3^{2-} increases (Figure 2–1). Assuming a constant total inorganic carbon (TIC) or $\sum CO_2$ of 0.01 mol/L where $TIC = m_{H_2CO_3^*} + m_{HCO_3^-} + m_{CO_3^{2-}}$ the activities of CO_2 species in water are evident in Figure 2–1.

2.4 ALKALINITY

2.4.1 Theoretical alkalinity

Drever (1997) has defined alkalinity based on the charge balance equation:

$$m_{H^+} + m_{K^+} + m_{Na^+} + 2m_{Ca^{2+}} + 2m_{Mg^{2+}} + \text{other cationic species} =$$
$$m_{Cl^-} + 2m_{SO_4^{2-}} + m_{NO_3^-} + m_{HCO_3^-} + 2m_{CO_3^{2-}} + m_{OH^-} + \text{other anionic species}$$

(such as borates, phosphates, and silicates) (2.9)

where *m* is the molar concentration.

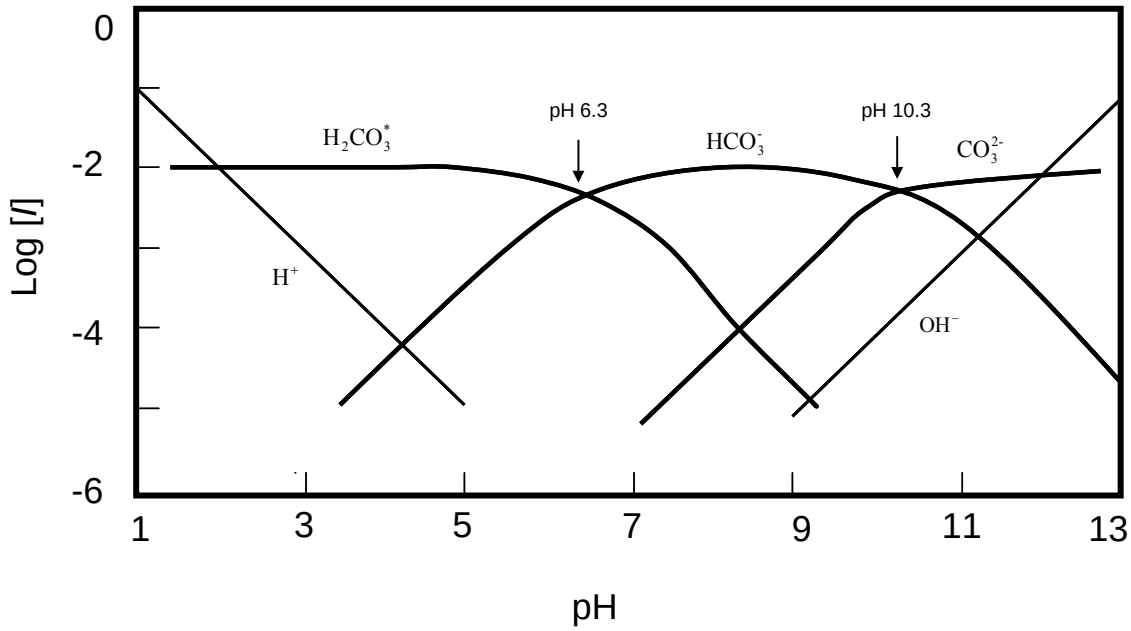

Figure 2–1 Activities of CO_2 species in water as a function of pH assuming constant TIC at 0.01mol/L and T 25°C. At pH 6.3 the activities of $H_2CO_3^*$ and HCO_3^- are equal and at pH 10.3 the activities of CO_3^{2-} and HCO_3^- are equal. Activities of H^+ and OH^- are defined by pH (Drever, 1997).

Conservative species (such as K^+, Na^+, Ca^{2+}, Mg^{2+}, Cl^-, SO_4^{2-} and NO_3^-) are unaffected by changes in pH, pressure or temperature. The borates, phosphates, and silicates are in most instances considered insignificant and excluded (Drever, 1997). Equation (2.9) becomes:

$$\text{Sum (conservative cation species) - sum (conservative anion species)}$$

$$= m_{HCO_3^-} + 2m_{CO_3^{2-}} + m_{OH^-} - m_{H^+}$$

$$= \text{alkalinity} \qquad (2.10)$$

Hydroxide and H^+ are considered negligible and equation (2.10) is reduced to:

$$\text{Carbonate alkalinity} = m_{HCO_3^-} + 2m_{CO_3^{2-}} \approx \text{alkalinity} \qquad (2.11)$$

The P_{CO_2} and $H_2CO_3^*$ are not involved in the charge balance equation (2.10). An increase in P_{CO_2} will cause an increase in $m_{HCO_3^-}$ according to the reactions:

$$CO_2 + H_2O + CO_3^{2-} \rightarrow 2HCO_3^- \quad (2.12)$$

$$CO_2 + H_2O \rightarrow H^+ + HCO_3^- \quad (2.13)$$

In the reaction (2.12) an increase in HCO_3^- is offset by the decrease in CO_3^{2-} and in reaction (2.13) increase in HCO_3^- is balanced by an increase in H^+.

Within the range of most natural waters this definition based on electron neutrality is adequate, but with waters that have an acid component it is necessary to understand the concepts of speciation and the mass balance equations.

Strum and Morgan (1996) and Morel and Hering (1993) expanded the definition based on electron neutrality by: using the relevant mass balance equations; defining a reference point; and introducing the concept of principal components. For a set reference condition (*f*) alkalinity is defined as:

for $f = 0$ alkalinity = $[HCO_3^-] + 2[CO_3^{2-}] + [OH^-] - [H^+]$ (2.14)

for $f = 1$ p-alkalinity = $[OH^-] + [CO_3^{2-}] - [H_2CO_3^*] - [H^+]$ (2.15)

for $f = 2$ Caustic alkalinity = $[OH^-] - 2[H_2CO_3^*] - [HCO_3^-] - [H^+]$ (2.16)

where $f = \frac{C_B}{C}$ and C is moles/L of an acid in the aqueous solution that is titrated with C_B moles/L of strong base (Stumm and Morgan, 1996). Depending on the TIC concentration the reference conditions for $f = 0$ to 2 are pH ≈ 4.5, 8.3 and 11, respectively. Assuming the activity is approximately equal to molar concentration then for $f = 0$ the alkalinity is equivalent to the alkalinity defined by electron neutrality equation (2.10) but for $f = 1$ or $f = 2$ the components that contribute to alkalinity change. The changing carbonate components and contributions to alkalinity relate to the mass balance defined by reactions (2.1) to (2.3).

Table 2-1 Principal component (highlighted in bold) and equivalents per mole positive and negative contribution to alkalinity at pH 4.5, 8.3 and 11 (after Kirby and Cravotta III, 2005a).

Reference condition (f)	Approximate pH	$H_2CO_3^*$	HCO_3^-	CO_3^{2-}	OH^-	H^+
0	4.5	**0**	1	2	1	-1
1	8.3	-1	**0**	1	1	-1
2	11	-2	-1	**0**	1	-1

At pH 4.5 $H_2CO_3^*$ is the principal component and does not contribute to alkalinity or acidity, but at pH 8.3 it contributes -1 equivalent per mole to alkalinity and at pH 11 it contributes -2 equivalent per mole to alkalinity (Table 2-1). The principal component at pH 8.3 is HCO_3^-, but at pH 4.5 the HCO_3^- contributes 1 equivalent per mole to alkalinity and -1 equivalent per mole at pH 11. At pH 11 CO_3^{2-} is the principal component and at pH 8.3 and 4.5 CO_3^{2-} contributes 1 and 2 equivalent per mole to alkalinity.

In groundwater the reference condition for alkalinity is generally $f = 0$ or the alkalinity at pH 4.5. Thus equation (2.14) is the most important when dealing with groundwater.

2.4.2 Measured alkalinity

The alkalinity of a sample of water is its acid-neutralizing capacity. Being the sum of all titratable bases, alkalinity is an aggregate property. The major bases are from the carbonate group but measured values include generally minor contributions from borates, phosphates, and silicates which are ignored when calculating the alkalinity of a sample (Drever, 1997). The aggregate property of alkalinity is generally obtained by adding a strong acid titrant, H_2SO_4 or HCl to a known volume of the sample of known pH until a pH of 4.5 is reached. The alkalinity is reported as 'Alkalinity at pH 4.5 = ___ mg/L $CaCO_3$' (American Public Health Association, 1999). Alkalinity by standard titration reports only positive results. This is in contrast to equation (2.9) where large negative values of alkalinity could be calculated.

Below pH values of 8.3 less than 1% of the carbonic acid is present as CO_3^{2-} (Figure 2–1) thus it is often ignored (Appelo and Postma, 2005) and from equation (2.14) only the first term (HCO_3^-) becomes important. If it is assumed that all the alkalinity is from the carbonate group (there are no other bases) the relevant contribution of HCO_3^- and CO_3^{2-} can be calculated from the mass balance equations (2.17) and (2.18) derived from equations (2.2) and (2.3) (Appelo and Postma, 2005):

$$\text{Log}[CO_3^{2-}] = \log K_2 + pH + \log[HCO_3^-] \quad (2.17)$$

$$\text{Log}[H_2CO_3^*] = \log K_1 - pH + \log[HCO_3^-] \quad (2.18)$$

where the activity is assumed to approximate concentrations (mole/L) and pH is the initial pH. In groundwater, the measured alkalinity is standardised (American Public Health Association, 1999) and reproducible. Unlike the calculated alkalinity, negative alkalinity values are not possible from titrations. The exception to this is the gran titration which enables small negative values (Appelo and Postma, 2005), but these are often not reported by laboratories.

2.5 ACIDITY

2.5.1 Theoretical acidity

Acidity is the opposite of alkalinity, being the capacity of a system to neutralise a base (Appelo and Postma, 2005; Drever, 1997; Stumm and Morgan, 1996). Unlike alkalinity, where the carbonate system tends to dominate, and contributions from other aqueous species are considered minimal, there are many aqueous species capable of donating protons and thus producing acidity. These include strong acids, weak acids and hydrolysable salts. It is important in the determination of acidity to understand the proton approach in mass balance equations and reference points as defined by Stumm and Morgan (1996) and Morel and Hering (1993) and summarised by Kirby and Cravotta III (2005a; 2005b).

Acidity due to the carbonate system is defined by equations (2.19) to (2.21) (Stumm and Morgan, 1996). Comparison of these equations with equations (2.14) to (2.16) shows that acidity is the reverse of alkalinity. Thus at pH 4.5 or for $f = 0$ the principal

component is $H_2CO_3^*$. As pH rises $H_2CO_3^*$ can donate protons (reactions 2.2 and 2.3) and the concentrations of HCO_3^- and CO_3^{2-} increase. At pH 4.5 acidity is defined as:

$$\text{for } f = 0 \qquad \text{mineral acidity} = [H^+] - [HCO_3^-] - 2[CO_3^{2-}] - [OH^-] \qquad (2.19)$$

with H^+ contributing 1 equivalent per mole, HCO_3^- and OH^- contributing -1 equivalent per mole and CO_3^{2-} contributing -2 equivalent per mole to acidity (Table 2-2). At pH 8.3, HCO_3^- becomes the principal component and does not contribute to acidity. From Table 2-2 it can be seen that $H_2CO_3^*$ and H^+ contribute one equivalent per mole to acidity and CO_3^{2-} and OH^- contribute a negative equivalent per mole to acidity at pH 8.3. This is also evident from the acidity definition for $f = 1$ below:

$$\text{for } f = 1 \qquad CO_2\text{-acidity} = [H_2CO_3^*] + [H^+] - [CO_3^{2-}] - [OH] \qquad (2.20)$$

Carbonate ion becomes the principal component at pH 11 and the negative and positive contributions to acidity are evident from Table 2-2 and equation (2.21):

$$\text{for } f = 2 \qquad \text{acidity} = 2[H_2CO_3^*] + [HCO_3^-] + [H^+] - [OH] \qquad (2.21)$$

Table 2-2 Principal component (highlighted in bold) and equivalents per mole positive and negative contribution to acidity 4.5, 8.3 and 11 (after Kirby and Cravotta III, 2005a).

Reference condition (f)	Approximate pH	$H_2CO_3^*$	HCO_3^-	CO_3^{2-}	OH^-	H^+
0	4.5	**0**	-1	-2	-1	1
1	8.3	1	**0**	-1	-1	1
2	11	2	1	**0**	-1	1

2.5.2 Calculated acidity

The concept of principal component becomes important when determining the relative contributions to acidity from the Fe(III), Fe(II), Al and SO_4 species. Kirby and Cravotta III (2005a) illustrated the contribution to acidity for a simple Fe(III)/SO_4 solution (Figure 2–2). The reference condition remains the same as for the carbonate

species, thus for $f = 0$ or pH ≈ 4.5 $Fe(OH)_2^+$ is the principal component for Fe(III). For $f = 1$ or pH ≈ 8.3 $Fe(OH)_3^0$ and SO_4^{2-} are the principal components for the Fe(III) and SO_4 species, respectively. For $f = 1$ the contributions to acidity (equivalents per mole) have been tabulated by Kirby and Cravotta III (2005a) using the PHREEQC database and are given in Figure 2–2.

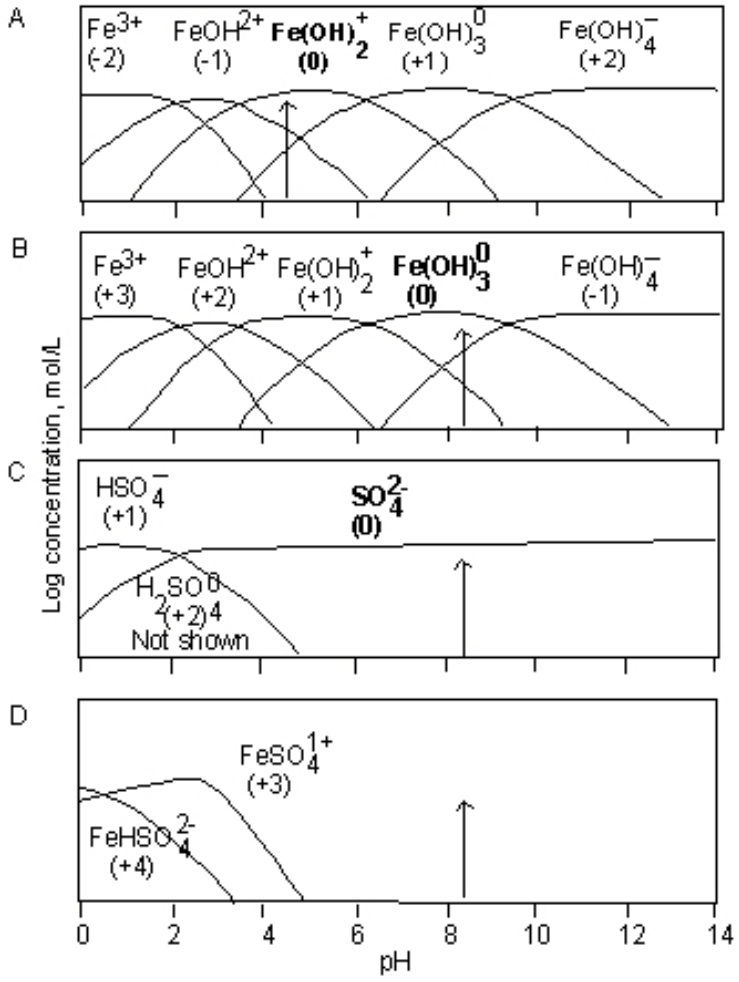

Figure 2–2 Schematic of Fe(III) and SO_4 speciation: A) Alkalinity species at pH 4.5; B) Fe(III) acidity species at pH 8.3; C) SO_4 acidity species at pH 8.3 and D) Fe(III)/SO_4 acidity species (other SO_4 species are off-scale as Fe(III) complexes are low in concentration at pH > 5 (source Kirby and Cravotta III, 2005a).

Table 2-3 Positive and negative contribution to acidity at pH 8.3 (Kirby and Cravotta III, 2005a).

	Acidity due to species, eq/mol (at pH 8.3)						
	+5	+4	+3	+2	+1	0	-1
Fe(II)			$FeHSO_4^+$	Fe^{2+} $FeSO_4^0$ $FeHCO_3^+$	$FeOH^+$ $FeCO_3^0$	$Fe(OH)_2^0$	
Fe(III)	$Fe_3(OH)$	$FeHSO_4^{2+}$ $Fe_2(OH)_2^{4+}$	Fe^{3+} $FeSO_4^+$ $Fe(SO_4)_2^-$	$FeOH^{2+}$	$Fe(OH)_2^+$	$Fe(OH)_3^0$	$Fe(OH)_4^-$
Al		$AlHSO_4^{2+}$	Al^{3+} $AlSO_4^+$ $Al(SO_4)_2^-$	$AlOH^{2+}$	$Al(OH)_2^+$	$Al(OH)_2^0$	$Al(OH)_4^-$
Mn(II)				Mn^{2+} $MnSO_4^0$	$MnOH^+$	$Mn(OH)_2^0$	
H_2S					H_2S H^+	HS^-	S^{2-} OH^-
CO_2					$H_2CO_3^*$	HCO_3^-	CO_3^{2-}
Non metal SO4				$H_2SO_4^0$	HSO_4^-	SO_4^{2-}	

At pH 8.3 the contributions to acidity can be calculated as:

$$\text{Acidity(eq/L)} = 3m_{FeHSO_4^+} + 2m_{Fe^{2+}} + 2m_{FeSO_4^0} + 2m_{FeHCO_3^+} + m_{FeOH^+} + m_{FeCO_3^0} + 5m_{Fe_3(OH)_4^{5+}} + 4m_{FeHSO_4^{2+}} + 4m_{Fe_2(OH)_2^{4+}} + 3m_{Fe^{3+}} + 3m_{FeSO_4^+} + 3m_{Fe(SO_4)_2^-} + 2m_{FeOH^{2+}} + m_{Fe(OH)_2^+} - m_{Fe(OH)_4^-}..$$

± the metals and complexes as listed in Table 2-3 (2.22)

Additional metals and complexes can be added as necessary. This equation can be simplified to (Kirby and Cravotta III, 2005b):

$$\text{acidity}_{\text{calculated}}, \text{eq/L} = \sum_{i}^{\text{all speces}} \varepsilon_i m_i \qquad (2.23)$$

where at pH 8.3 ε_i is the number of equivalents per mole of the i^{th} species that contributes either positive or negative acidity and m_i is the concentration in mol/L of the i^{th} species.

Often, acidity related to CO_2 is not required, or considered negligible. In groundwater, the dissolved CO_2 is not in equilibrium with the atmosphere and on reaching surface the CO_2 will degas until the CO_2 attains equilibrium with the atmosphere (Kirby and Cravotta III, 2005b). In acid mine drainage, CO_2 is considered short lived and therefore its contribution to acidity is negligible (Kirby and Cravotta III, 2005a). Thus, equation (2.23) can be redefined as non-CO_2 acidity (Kirby and Cravotta III, 2005b) or:

$$\text{non-}CO_2 \text{ acidity}_{\text{calculated}}, \text{eq/L} = \sum_{i}^{\substack{\text{all species} \\ \text{less CO2}}} \varepsilon_i m_i \qquad (2.24)$$

where at pH 8.3 ε_i is the number of equivalents per mole of the i^{th} species that contributes either positive or negative acidity and m_i is the concentration in mol/L of the i^{th} species.

Often, this level of information is not available for groundwater when determining the acidity of the water. Hedin et al. (1994) derived a formula for calculating acidity for water with a pH < 4.5 in mg/L $CaCO_3$:

$$50[1000(10^{-\text{pH}}) + \frac{2(\text{Fe (II)})}{56} + \frac{3(\text{Fe (III)})}{56} + \frac{2(\text{Mn})}{55} + \frac{3(\text{Al})}{27}] \qquad (2.25)$$

where Fe(II), Fe(III), Mn and Al are in mg/L. This formula does not differentiate the acidity contribution from individual Fe(II), Fe(III), Mn and Al species as in equation (2.22). From Table 2-3 and equation (2.22) it can be seen that equation (2.25) does not include acidity from SO_4^{2-} complexes. Kirby and Cravotta III (2005a) showed that while equation (2.25) does not include acidity from SO_4^{2-} complexes, the formula over-

estimates the contributions from Fe(III). Because these two effects tend to cancel each other, equation (2.25) gives a reasonable estimate of Acidity. The other concern about equation (2.25) is that pH is the negative $\log_{10}$ of the activity of H^+ and not the negative $\log_{10}$ of the concentration of H^+. All other species in equation (2.25) are in mg/L or concentration rather than activity. At pH > 2 activity corrections to H^+ will be small and the concentration of the other species will dissipate any corrections applied to the pH activity (Kirby and Cravotta III, 2005a).

A further issue with equation (2.25) is that individual species Fe(II) and Fe(III) are not routinely determined. In recognising this, Kirby and Cravotta III (2005b) have refined equation (2.25) as follows:

$$\text{acidity}_{\text{calculated}}\ (\text{mg/L CaCO}_3) = 50[1000(10^{-\text{pH}}) + \frac{2(\text{Fe})}{55.8} + \frac{2(\text{Mn})}{54.9} + \frac{3(\text{Al})}{27.0}] \quad (2.26)$$

where the dissolved metal concentrations are in mg/L and Fe is the total dissolved iron concentration. This calculation has been used for water samples with pH 2.5 to 8.3 (Kirby and Cravotta III, 2005b) while equation (2.25) was initially designed for water with a pH < 4.5 (Hedin et al., 1994). However, equation (2.25) is no longer constrained by pH (Hedin, 2006).

2.5.3 Measured acidity

To obtain the acidity due to dissolved CO_2 of a water sample, a strong base titrant such as NaOH is added till pH 8.3 is obtained. Hydrated $H_2CO_3^*$ is converted to HCO_3^- via equation (2.2). It is reported as 'the acidity at pH 8.3 = ____ mg/L $CaCO_3$' (American Public Health Association, 1999). This method measures acidity as defined by equation (2.20).

Acidity may also be produced through oxidation or hydrolysis of metallic ions such as those of iron, aluminium and manganese. To determine acidity due to metals a 'Hot acid titration' is employed (American Public Health Association, 1999). For this method if the initial pH > 4 then H_2SO_4 is added to lower the pH to 4 or less. Hydrogen peroxide is then added and the sample boiled before titrating to pH 8.3. The reactions occurring at each step are listed in Kirby and Cravotta III (2005b) and are summarised here. The addition of H_2SO_4 converts HCO_3^- according to:

$$0.5H_2SO_4 + HCO_3^- \rightarrow H_2CO_3^* + 0.5SO_4^{2-} \quad (2.27)$$

The addition of H_2O_2 oxidises metals according to:

$$Fe^{2+} + 0.5H_2O_2 + H^+ \rightarrow Fe^{3+} + H_2O \quad (2.28)$$

$$Fe^{3+} + 2H_2O \rightarrow Fe(OH)_2^+ + 2H^+ \quad (2.29)$$

$$Fe(OH)_2^+ + H_2O \rightarrow Fe(OH)_{3(s)} + H^+ \quad (2.30)$$

and the metal acidity is converted to H^+ acidity which can be titrated.

This method of titration does not measure acidity from the $H_2CO_3^*$ as the sample is boiled and CO_2 degasses according to:

$H_2CO_3^*$ (original in sample) + $H_2CO_3^*$ (from equation (2.27)) $\rightarrow$

$CO_{2(g)}$ (from original $H_2CO_3^*$ in sample) + $CO_{2(g)}$ (derived from HCO_3^- and H_2SO_4 in equation (2.27)) + $2H_2O$ (2.31)

The acidity is calculated by the following (American Public Health Association, 1999):

$$\text{Acidity (mg/L}CaCO_3) = \frac{[(A \times B) - (X \times Y)] \times 50000}{\text{mL sample}} \quad (2.32)$$

where A = mL NaOH titrant used to pH 8.3, B = normality of NaOH, X = mL of H_2SO_4 used to pH 4 and Y = normality of H_2SO_4. This method over estimates the addition of H_2SO_4. The addition of H_2SO_4 converts HCO_3^- to $H_2CO_3^*$ (reaction 2.27) which degasses as $CO_{2(g)}$ on boiling (reaction 2.31). It will take fewer equivalents of base to titrate back to the original sample pH than equivalents of acid required to lower the original pH to 4 (Kirby and Cravotta III, 2005b). During addition of H_2O_2, oxidation may cause metal hydroxide precipitation thus, underestimating acidity.

2.6 NET ALKALINITY AND NET ACIDITY

The importance of understanding how the acidity is calculated or measured becomes apparent when determining the Net Acidity or Net Alkalinity. Conceptually Net Acidity is simply expressed as:

$$\text{Net Acidity} = \text{Total Acidity} - \text{Total Alkalinity} \quad (2.33)$$

However, as seen from the previous sections the calculated and measured values incorporate different aspects of acidity. The Net Acidity can be either measured or determined from a combination of measured and calculated values.

The 'Hot Acidity' reports a Net Acidity (as mg/L $CaCO_3$) (Hedin, 2006; Kirby and Cravotta III, 2005a; 2005b). However, the 'Hot Acidity' method is often erroneously used as a Total Acidity (Edwards and Turney, 1997; Koryak et al., 2004). The use of the 'Hot Acidity' as a Total Acidity rather than the Net Acidity explains the findings by Koryak et al. (2004) that the 'Hot Acidity' consistently gave lower acidity values when compared to those obtained by other methods and that this discrepancy increased in water as the pH increased and approached 7. Prior to the 20th edition of the 'Standard methods for the examination of water and wastewater' (American Public Health Association, 1999) negative values for the 'Hot Acidity' were reported as zero. According to Hedin (2006) many laboratories still do not report negative acidity values.

The Net Acidity (as mg/L $CaCO_3$) can also be obtained from the calculated Total Acidity minus Alkalinity $_{\text{(titrated to pH 4.5)}}$ according to (Hedin, 2006; Kirby and Cravotta III, 2005a; 2005b):

$$\text{Total Acidity}_{\text{(calculate, equation (2.24 or 2.25))}} - \text{Alkalinity}_{\text{(Titration to pH 4.5)}} \quad (2.34)$$

Many government agencies rely on laboratory determined alkalinities for groundwater samples. In Western Australia, the long travel distances can prevent the water samples for alkalinity titrations reaching the laboratory within recommended holding time of 24 hours, let alone the 6 hour limit if biological activity is anticipated (American Public Health Association, 1999). Groundwater samples, once extracted, are no longer in equilibrium (Appelo and Postma, 2005) and samples that contain both bicarbonate alkalinity and Fe^{2+} are unstable (Hedin, 2006). While every effort is made to minimise aeration of the sample, some oxidation of the sample will occur and iron oxidation and hydrolysis is possible according the equation (Appelo and Postma, 2005):

$$2Fe^{2+} + 4HCO_3^- + 0.25O_2 + 5H_2O \rightarrow 2Fe(OH)_{3(s)} + 4H_2CO_3 \quad (2.35)$$

Iron hydrolysis will consume bicarbonate alkalinity and in samples with a positive Net Acidity the pH will fall especially once the alkalinity is consumed. In samples with a positive Net Alkalinity the pH will remain relatively stable, but the bicarbonate

alkalinity will be consumed and the Total Alkalinity$_{(\text{Titration to pH 4.5})}$ value will decrease. Problems relating to a delay in titrating the sample for alkalinity are overcome by determining the alkalinity in the field.

Laboratory determined pH values can differ from field pH. This will change the calculated acidity (equations 2.25 or 2.26) (Hedin, 2006). However, at pH 3.5 the water sample will contain ~0.316 mg/L of H^+ which will only contribute ~16 mg/L to the total acidity in equation (2.25) or (2.26). Degassing of CO_2 during storage can raise the pH, again altering the Total Acidity calculation but by less than 1 mg/L if the pH is 7. To overcome this problem the field pH should be used.

In this study the Total Acidity was calculated using equation (2.26) and Net Acidity using equation (2.34)

2.7 GROUNDWATER EVOLUTION PROCESSES

2.7.1 Mineral dissolution

Models for the hydrochemical evolution of groundwater (with a low to moderate TDS) in igneous and high-grade metamorphic crystalline rock terrains was developed by Chebotarev (1955) and Garrels and Mackenzie (1967). Such models were developed for groundwaters within a closed system with respect to CO_2 and had initial P_{CO_2} of around $10^{-1.5}$ atm. It has been further developed by numerous workers e.g. Banks and Frengstad (2006).

In igneous terrains, plagioclase feldspar and mafic minerals react faster than quartz or K-feldspar (Appelo and Postma, 2005). Plagioclase feldspar forms a solid solution with end-members albite ($Na(AlSi_3O_8)$) and anorthite ($Ca(Al_2Si_2O_8)$) (Neuendorf et al., 2005). Incongruent dissolution of the two end-members, albite and anorthite, to kaolinite is according to following reactions (Appelo and Postma, 2005):

$$2NaAlSi_3O_8 + 2H^+ + 9H_2O \rightarrow Al_2Si_5O_5(OH)_2 + 2Na^+ + 4H_4SiO_4 \quad (2.36)$$

$$CaAl_2Si_2O_8 + 2H^+ + H_2O \rightarrow Al_2Si_2O_5(OH_4) + Ca^{2+} \quad (2.37)$$

From these two reactions it can be seen that increased concentrations of Ca^{2+} and Na^+ will occur in groundwater that is reacting with plagioclase feldspar. Chemical weathering of silicates consumes H^+ ions and thus the groundwater pH will tend to rise.

In unpolluted groundwater, carbonic acid is an important source of protons. Dissociation of H_2CO_3 gives H^+ and HCO_3^- (Reaction (2.2)). Thus, groundwater moving through an aquifer dominated by plagioclase feldspar-bearing rocks will evolve towards an alkaline Na–Ca–HCO_3 type water.

However, groundwater from the Norwegian igneous terrain is depleted in aqueous Ca. Banks and Frengstad (2006) argued that Na–Ca–HCO_3 dominated groundwater is hydrochemically 'immature' water and that the chemical evolution of such waters beyond the point of calcite saturation will result in a high pH (8.0 to 8.5), Na-rich, Ca-depleted groundwater. To assess this they looked at two possibilities:

- that Ca depletion is due to calcite saturation and precipitation as suggested by Garrels and Mackenzie (1967); and/or
- cation exchange is effective.

They argued that at pH ~8.2, Na-rich, Ca-depleted groundwater is the result of calcite saturation and precipitation. Cation exchange (summarised below) while possible would not explain the calcite saturation indices that approach zero at pH 8 and exceed zero in the highest pH water.

2.7.2 Calcite process

Calcite precipitation and dissolution is influenced by many factors within the environment. These include changes in P_{CO2}, evaporation, and common ion effect. The concentration of CO_2 (carbon dioxide) tends to increase in groundwater near the watertable. Carbon dioxide is a product of plant decay and plant root respiration in the soil zone. The CO_2 is dissolved in infiltrating water that recharges the groundwater, thus the P_{CO2} increases from an atmospheric P_{CO2} of about $10^{-3.5}$ to a soil P_{CO2} of about 10^{-1} (Appelo and Postma, 2005). As P_{CO2} increases the infiltrating water tends to become less saturated with respect to calcite. Photosynthesis consumes CO_2. In lakes and rivers the process of photosynthesis has been documented as increasing pH from 6 or 7 to about 10 on a diurnal basis and for waters to become saturated with respect to calcite. However, the kinetics of calcite precipitation is generally too slow for the precipitation to occur during diurnal cycles.

Evaporation is known to cause precipitation of calcite in soil. As shallow groundwater or soil water evaporates the concentration of Ca^{2+} in the remaining water increase. If the water becomes saturated with respect of calcite then precipitation may occur.

The addition of Ca, HCO_3 or CO_3 from sources other than the dissolution of calcite may super saturate the water with respect to calcite. An example of this is the dissolution of gypsum. Gypsum is more soluble that calcite and thus calcite can form according to the following reaction (Langmuir, 1997):

$$CaSO_4 \cdot 2H_2O_{(gypsum)} + 2HCO_3^- \rightarrow CaCO_3 + SO_4^{2-} + 2H_2O + CO_2$$

2.7.3 Cation exchange

Cation exchange is a process where cations associated with the aquifer media may exchange with cations in solution in the groundwater (Appelo and Postma, 2005; Drever, 1997; Freeze and Cherry, 1979; Stumm and Morgan, 1996). The aquifer media can act as an adsorbent as demonstrated by cation exchange at the salt/fresh water interface within coastal areas. When seawater (Na–Cl type water) moves into a fresh groundwater aquifer dominated by a Ca–HCO_3 type water, sodium replaces the calcium absorbed onto the aquifer medium according to the formula:

$$Na^+ + 1/2\,Ca - X_2 \rightarrow Na - X + 1/2\,Ca^{2+} \qquad (2.38)$$

were X represents the counter ion on the exchanger. The water at the interface becomes a Ca–Cl type water. The reverse process takes place if fresh water flushes a salt water aquifer and the aquifer media will now adsorbs Ca^{2+} and release Na^+ producing a Na–HCO_3 type water at the interface.

The distribution of species is given by the law of mass action (Appelo and Postma, 2005):

$$K_{Na\backslash Ca} = \frac{[Na - X][Ca^{2+}]^{0.5}}{[Ca - X_2]^{0.5}[Na^+]} = \frac{\beta_{Na}[Ca^{2+}]^{0.5}}{\beta_{Ca}^{0.5}[Na^+]} \qquad (2.39)$$

where β_I is activity of each exchangeable ion expressed as an equivalent fraction:

$$\beta_I = \frac{meqI - X_i \text{ per kg sediment}}{CEC} \qquad (2.40)$$

Typical exchange coefficients for $K_{Na\backslash Ca}$ and $K_{Na\backslash Mg}$ are 0.4 (0.3–0.6) and 0.5 (0.4–0.6), respectively (Appelo and Postma, 2005). Expressed as an equivalent fraction, equation (2.39) conforms to the *Gaines-Thomas* convention (Appelo and Postma, 2005). The *Gapon* convention based on molar fractions and is not given here.

The ability of a material to adsorb cations is dependent on mineral structure and the specific surface of the mineral accessible to water (Appelo and Postma, 2005). Different regolith materials do not have the same proficiency for the exchange of cations. Typical cation exchange capacities (CEC) of regolith materials are listed in Table 2-4. Kaolinite has a typical CEC between 30–150 meq/kg (Appelo and Postma, 2005) that is strongly dependent on pH (Langmuir, 1997). This is low compared to other clays such as montmorillonite or smectite which have a CEC of between 800 and 1500 and independent of pH (Langmuir, 1997). Organic matter has a high CEC of between 1500 and 4000 meq/kg that is pH dependent. According to Scheffer and Schachtschabel (2002), quoted in Appelo and Postma (2005), the pH dependence of CEC per kg organic carbon can be taken into account as follows:

$$\mathrm{CEC} = 510 \times \mathrm{pH} - 590 \qquad (2.41)$$

and at pH 5 the CEC would be about 1960 meg/kg of organic carbon.

Table 2-4 Cation exchange capacities of common regolith material (Appelo and Postma, 2005; Langmuir, 1997).

Regolith material	*Cation exchange capacity (meq/kg)*
Kaolinite	30–150 (pH dependant)
Halloysite	50–100
Smectite-Montmorillonite	800–1500
Vermiculite	1000–2000
Glauconite	50–400
Illite	200–500
Chlorite	100–4000
Allophane	up to 1000
Goethite and hematite	up to 1000 (pH dependant)
Organic matter (at pH 8)	1500–4000 (pH dependant)

2.7.4 Groundwater evolution in closed basins

Building on the work of Garrels and Mackenzie (1967), Hardie, Eugster and Jones (Eugster and Hardie, 1978; Eugster and Jones, 1979; Hardie and Eugster, 1970) investigated the evolution of brines in closed basins and developed the brine evolution model (EJH model). They recognised chemical pathways which evaporating water would follow after precipitation of select minerals; calcite, sepiolite and gypsum (Figure 2–3).

In the initial model, Hardie and Eugster (1970) recognised 3 main end-member brine types Na–Ca–Mg–Cl, Na–Mg–SO_4–Cl and Na–CO_3–SO_4–Cl (Figure 2–3) and showed how the final composition of a brine is determined by the initial composition of the water from which the brine was derived. They showed how relative concentrations of Ca^{2+}, Mg^{2+}, SO_4^{2-} and alkalinity constrain the pathway taken by the evaporating waters.

The model works on the concept of chemical divides. For calcite ($CaCO_3$) to be continuously precipitated as water is progressively evaporated two conditions must be met (Hardie and Eugster, 1970): the molar proportions of Ca^{2+} and CO_3^{2-} lost from solution must be equal; and that the ion activity product (IAP) for $(aCa^{2+} \bullet aCO_3^{2-})$ in solution must remain constant at constant *P* and *T*. Initial molar proportions of Ca^{2+} and CO_3^{2-} in groundwater are unlikely to be equal and thus the concentrations of Ca^{2+} and CO_3^{2-} will change as calcite is precipitated. For the IAP to stay constant any increase in Ca^{2+} must result in a decrease in CO_3^{2-} and *vice versa*. Thus the precipitation of calcite will determine if the evaporating water will become carbonate rich or carbonate poor. The next minerals to precipitate are sepiolite from carbonate rich waters or gypsum from carbonate poor waters (Figure 2–3).

Sepiolite ($MgSi_3O_6(OH)_2$) is a clay mineral that when precipitated removes Mg^{2+}, SiO_2 and alkalinity (either as HCO_3^- or CO_3^{2-}) from the water according to the equation:

$$Mg^{2+} + 3H_4SiO_4 + 2HCO_3^- \rightarrow MgSi_3O_6(OH)_2 + 2CO_2 + 6H_2O \qquad (2.42)$$

As sepiolite precipitates the increase or decrease in alkalinity will depend on the initial molar ratio of Mg^{2+} to the alkalinity. The two brines that result after the precipitation of

sepiolite are the Na–Mg–SO_4–Cl brine from the Mg^{2+} rich water, and the Na–CO_3–SO_4–Cl brine from the alkalinity rich water (Figure 2–3).

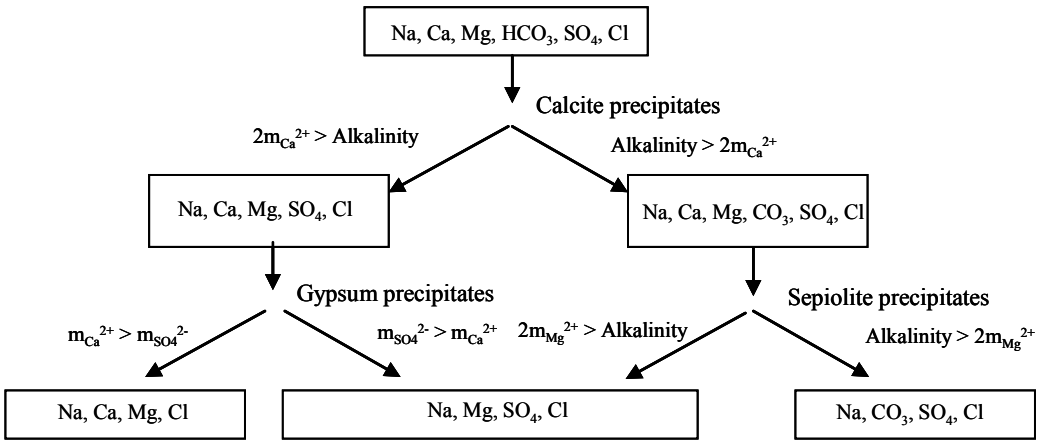

Figure 2–3 Original model for closed-basin brine evolution (Hardie and Eugster, 1970) as modified by Drever (1997) (ratios in equivalents).

Since the original work by Hardie and Eugster (1970) it has been suggested that other minerals can precipitate and include magnesium-rich smectite, dolomite or high-magnesium calcite (Eugster and Hardie, 1978; Eugster and Jones, 1979).

Gypsum precipitates if the Ca^{2+} concentration is greater than the alkalinity concentration. Precipitation removes both Ca^{2+} and SO_4^{2-} in equal molar proportions, but again the IAP for $(aCa^{2+} \bullet aSO_4^{2-})$ must remain constant. Therefore, the concentrations of Ca^{2+} and SO_4^{2-} in the evaporating water will change as gypsum is precipitated (Eugster and Hardie, 1978) leading to the development of either a Na–Ca–Mg–Cl brine or a Na–Mg–SO_4–Cl brine.

The initial work of Hardie and Eugster (1970) was subsequently modified (Eugster and Hardie, 1978; Eugster and Jones, 1979) showing how pathways were decided prior to the precipitation of calcite based on the molar concentrations of Ca^{2+} and Mg^{2+} to alkalinity (Figure 2–4). While maintaining the concept of chemical divides more pathways were added to account for more specific brines.

The EJH model does not take into account how other reactions influence brine evolution such as selective dissolution of crust and sediment coatings, ion exchange processes and redox reactions, although they were noted (Eugster and Jones, 1979). Thus the model does not account for acidic brines as these will include redox reactions.

To account for acidic brines a separate pathway was added to the model (Figure 2–4) (Long et al., 1992a). The pathway was based on the work from Lake Tyrrell, an inland playa lake that contains solutes of a marine chemical signature (Long et al., 1992a).

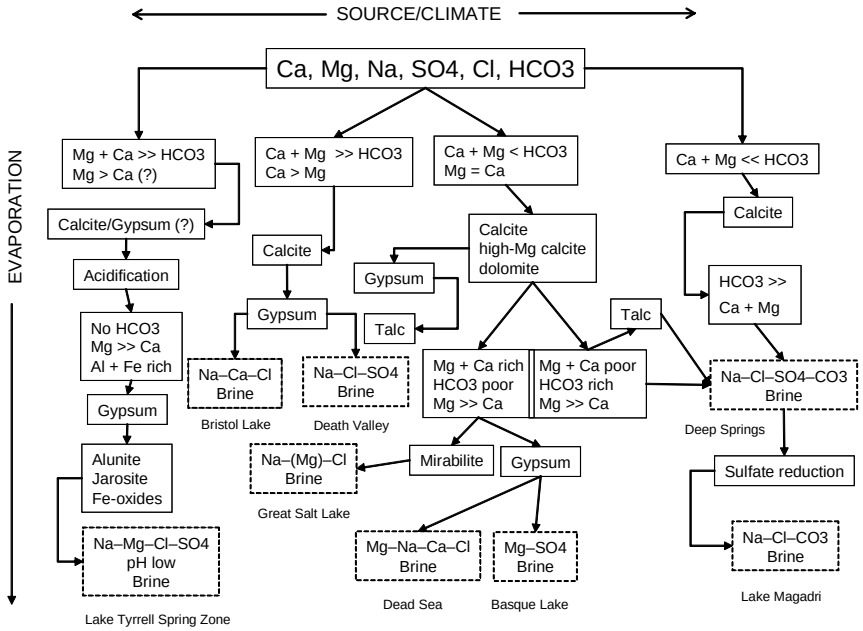

Figure 2–4 Model for the evolution of acid brines in closed basins by Long et al. (1992) based on EJH model (Eugster and Hardie, 1978; Eugster and Jones, 1979; Hardie and Eugster, 1970).

The evaporation pathway for development of the acidic brine requires that calcite and possibly gypsum are precipitated. Precipitation of calcite will remove some of the alkalinity. Acidification then occurs removing any remaining alkalinity allowing the water to become enriched in Mg, Al and Fe. Calcium is further removed as gypsum is precipitated resulting in a Na–Mg–Cl–SO_4 brine with low pH and high amounts of Al and Fe. Under the low pH conditions alunite and jarosite precipitate, thus removing both K^+ and SO_4^{2-} from the waters. Long et al. (1992) proposed this last pathway to

explain the acid-hypersaline lakes and groundwater across the southern half of the Australian continent.

2.8 GROUNDWATER REDOX REACTIONS

The importance of microorganisms has gained recognition over the last 20 to 30 years especially for low temperature anaerobic environments as often found in groundwater. The redox processes that contribute to the groundwater acidity or alkalinity are complex. The general concepts are understood and the stoichiometric equations are found in most geochemical textbooks (Appelo and Postma, 2005; Drever, 1997; Langmuir, 1997), but the exact mechanisms are not well understood (Ehrlich, 2002). Numerous laboratory experiments have been designed to examine the contributing factors, both physical and microbiological. One concept that has been developed is that of sequential redox reactions (Appelo and Postma, 2005; Drever, 1997; Stumm and Morgan, 1996). It relates to the order of electron acceptors that are involved in degradation (oxidation) of organic matter. As redox conditions change the terminal electron acceptors change according to the thermodynamics of the reaction (Appelo and Postma, 2005; Stumm and Morgan, 1996). The sequence of microbial mediated redox reactions have been diagrammatically represented by Stumm and Morgan (1996) and are reproduced in Figure 2–5. The expected redox reactions in groundwater are listed in Table 2-5 and Table 2-6.

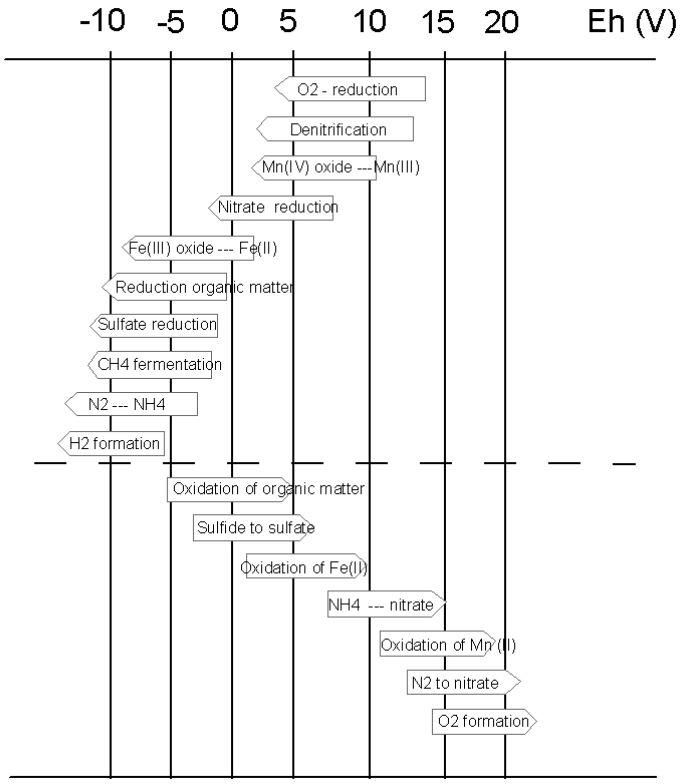

Figure 2–5 Sequence of microbial mediated redox reaction from Stumm and Morgan (1996) showing how the redox process overlap and different reaction can occur under the same conditions.

Organic matter is an important component in redox reactions occurring in groundwater. Organic matter may be aerobically oxidised to CO_2 and H_2O (reaction (2.4)). Initially bacteria uses oxygen to carry out aerobic respiration (Ledin and Pedersen, 1996) and oxygen serves as the terminal electron acceptor. Oxygen is the preferred electron acceptor by most bacteria. However, the solubility of oxygen in water is low and depleted relatively quickly. Once oxygen is depleted in the groundwater, anoxic oxidation of organic matter occurs. The terminal electron acceptors become NO_3^-, Fe(III), Mn(IV), SO_4^{2-} and CO_2. The products of carbon oxidation are CO_2 and H_2O in the presence of suitable microorganisms and sufficient quantities of NO_3^-, Fe(III), Mn(IV), SO_4^{2-}. If there is insufficient oxidant (NO_3^-, Fe(III), Mn(IV), SO_4^{2-}) the organic matter is partly oxidised to acetate, CO_2 and H_2.

2.9 PYRITE

2.9.1 Formation at low temperatures

Iron(II) monosulfide is a precursor to pyrite formation at low temperatures. Rickard (1995) showed experimentally that at 25°C and under reducing conditions (*Eh* < -3 V) precipitation of iron(II) monosulfide proceeds via two competing pathways:

$$Fe^{2+} + H_2S \rightarrow FeS_{(s)} + 2H^+ \qquad (2.43)$$

referred to as the hydrogen sulfide pathway; and

$$Fe^{2+} + 2HS^- \rightarrow Fe(HS)_{2(s)} \qquad (2.44)$$

$$Fe(HS)_{2(s)} \rightarrow FeS_{(s)} + H_2S \qquad (2.45)$$

referred to as the bisulfide pathway.

The relative dominance between the two competing pathways is dependent on pH and total concentration of sulfide. The concentration of Fe(II) has no effect on the predominance of either pathway as an increase in the iron concentration will increase

Table 2-5 Summary of bacterial assisted redox process under oxic conditions.

Electron donor	*Electron acceptor*	*pH*	*Process*	*Representative strains*	*Source*
Fe(II)	O_2	acidic	Fe(II) oxidation	*Thiobacillus ferrooxidans*	Kappler and Straub, 2005
Fe(II)	O_2	neutral	Fe(II) oxidation	*Gallionella ferruginea*	Kappler and Straub, 2005
Sulfide	O_2	acidic	Sulfide oxidation	*Thiobacillus ferrooxidans*	Ehrlich, 2002
Sulfide	O_2	neutral	Sulfide oxidation	*Thiobacillus thioparus* (halophilic)	Ehrlich, 2002
Organic matter	O_2		O_2 reduction by SO_4^{2-} reduction bacteria		Ehrlich, 2002

Table 2-6 Summary of bacterial assisted redox process under anaerobic conditions.

Electron donor	*Electron acceptor*	*pH*	*Process*	*Representative strains*	*Source*
Fe(II)	NO_3^-	neutral	NO_3^- dependent Fe(II) oxidation	*Acidovorax sp.* strain BrG1	Kappler and Straub, 2005
Organic matter	Fe(III)	Acidic	Fe(III) reduction	*Thiobacillus thiooxidans*	Kappler and Straub, 2005
Organic matter	Fe(III)	neutral	Fe(III) reduction	*Shewanella oneidensis*	Kappler and Straub, 2005
H_2S	Fe(III)	Acid to neutral	Fe(III) reduction	Abiotic	Ehrlich, 2002
sulfide	NO_3^-	neutral	NO_3^- dependent sulfide oxidation	*Thiobacillus denitrificans*	Ehrlich, 2002
lactate	O_2		SO_4^{2-} reduction		Ehrlich, 2002 Kjeldsen et al, 2005
Organic matter	SO_4^{2-}		SO_4^{2-} reduction		Ehrlich, 2002
Inorganic H2/CO2	SO_4^{2-}		SO_4^{2-} reduction	*Desulfovibrio desulfuricans*	Ehrlich, 2002

the rates of both processes equally. Rickard (1995) showed that at pH 5 and total dissolved sulfide 10^{-1} M (3200 mg/L) the two pathways have equal dominance precipitating iron(II) monosulfide that is then available to form pyrite.

Pyrite forms from both abiotic and biotic processes. The abiotic process can be divided into the polysulfide pathway and H_2S pathway (Butler et al., 2004). The polysulfide pathway at T 25°C and under reducing conditions (*Eh* -3 V) is described by the net reaction:

$$FeS_{(s)} + S^{2-}_{n\ (aq)} \rightarrow FeS_{2\ (s)} + S^{2-}_{n-1\ (aq)} \qquad (2.46)$$

and the H_2S pathway by the reaction

$$FeS_{(s)} + H_2S_{(aq)} \rightarrow FeS_{2\ (s)} + H_{2(g)} \qquad (2.47)$$

The polysulfide pathway dominates at the oxic/anoxic interface and is important at pH > 7.5 whereas, the H_2S pathway dominates in the reduced environment below the oxic/anoxic interface (Butler et al., 2004). The abiotic rate of 10^{-17} to 10^{-12} mol/L/day (Rickard, 1997) is up to 10^4 to 10^5 times slower than the measured rates from biotic process (Canfield et al., 1998).

2.9.2 Oxidation

Pyrite oxidation is described by the following reactions (Langmuir, 1997):

$$FeS_{2(S)} + 7/2\,O_2 + H_2O \rightarrow Fe^{2+} + 2SO_4^{2-} + 2H^+ \qquad (2.48)$$

$$Fe^{2+} + 1/4\,O_2 + H^+ \rightarrow Fe^{3+} + 1/2\,H_2O \qquad (2.49)$$

$$Fe^{3+} + 3H_2O \rightarrow Fe(OH)_{3(s)} + 3H^+ \qquad (2.50)$$

$$FeS_{2(S)} + 14Fe^{3+} + 8H_2O \rightarrow 15Fe^{2+} + 2SO_4^{2-} + 16H^+ \qquad (2.51)$$

The oxidant (O_2) in reaction (2.48) oxidises the sulfur component to produce SO_4^{2-}. The iron component is not oxidised, but the Fe^{2+} is released into solution. Then Fe^{2+} can be oxidised to Fe(III) oxides and hydroxides via reactions (2.49) and (2.50). Under aerobic conditions at near neutral pH the reaction rate for reaction (2.49) is

fast with a predicted half life for Fe^{2+} ranging between 12 hours, 7 hours and 4.3 minutes for pH 5, 6 and 7, respectively (Appelo and Postma, 2005; Langmuir, 1997; Stumm and Morgan, 1996). Aqueous Fe^{3+} at these pH values is not stable and is precipitated as Fe(III) oxides and hydroxides (reaction (2.50)). At lower pH values aqueous Fe^{3+} is stable and becomes the oxidant in reaction (2.51).

2.10 JAROSITE PRECIPITATION AND DISSOLUTION

Jarosite ($KFe_3(SO_4)_2(OH)_6$) commonly occurs in acid sulfate soils and acid mine drainage water where pyrite has been oxidised (Welch et al., 2008). In Australia, jarosite has been identified in coastal acid sulfate soils (Fitzpatrick and Shand, 2008), hypersaline evaporated basins such as Lake Tyrell (Long et al., 1992b) and in "deep" drains constructed to remediate dryland salinity in Western Australia (Fitzpatrick and Shand, 2008). The need for greater understanding of jarosite and its potential disruption to remediation strategies for acid sulfate soils has lead to many studies looking at its formation and dissolution (Brown, 1971; Liu et al., 2009; Welch et al., 2007; Welch et al., 2008).

Early work on the stability of jarosite found the mineral stable under acidic oxidizing conditions (Brown, 1971). The formation of jarosite was found to be influenced by pH and bacterial oxidation. Bacterial oxidation by *Thiobacillus ferroxidans* is reduced at pH < 1.5 and > 2.3 with the optimal jarosite precipitation being between pH 1.6 to 1.7 (Liu et al., 2009). The concentration of Fe^{2+} also influences the precipitation of jarosite at low pH. Jarosite precipitation increases with increased Fe^{2+} concentration (Liu et al., 2009).

Dissolution of jarosite and production of acid can be produced by the following reaction (Welch et al., 2008):

$$KFe_3(SO_4)_2(OH)_6 + 3H_2O \rightarrow 3Fe(OH)_3 + K^+ + 3H^+ + 2SO_4^{2-} \quad (2.52)$$

The presence of organic material has been found to contribute to the dissolution of jarosite and this could have implication in areas with acidic peat swamps (Chu et al., 2006).

3 Site description

3.1 LOCATION AND SIZE

The Lake Muir–Unicup Natural Diversity Recovery Catchment is located about 65 km east of Manjimup and 100 km west of Mt Barker, near the south coast of Western Australia (Figure 1–1). It has an area of around 700 square kilometres (km^2) between 463 000–490 000 mE and 6 173 000–6 209 000 mN (MGA Zone 50). The Muirs Highway (Hwy.) divides the area roughly in half with unsealed roads providing access to the rest of the catchment (Figure 1–1 and Figure 3–1).

3.2 GEOMORPHOLOGY

In the northeast of the study area ferricrete covered uplands of the Darling Plateau slope southward to poorly drained flats of broad-valley floors, forming part of the Ravensthorpe Ramp (Beard, 1999; Cope, 1975). The Tone River skirts the northwest corner of the study area (Figure 3–1). In the south, the study area is bounded by a plateau which rises 40 to 60 m above the poorly drained flats. The plateau has been cut by modern drainage which flows to the Deep River (Figure 1–1) in the southwest and the Frankland River (Figure 1–1 and Figure 3–1) in the southeast.

The study area consist of low hills or rises, plateaus, broad-valleys floors and valleys with low gradients (Figure 3–1). Bounding the study area are the low hills in the northeast (300 m AHD) and the plateau in the south (235 m AHD). The study area is divided into northern and southern sections by dissected hills that form two westerly sloping ridges, extending from the eastern boundary at 280 m AHD and terminate east of Pindicup Lake (Figure 3–1). The dissected character of these ridges gives rise to the undulating nature of the ground surface.

In the north and south of the study area, poorly drained flats on the broad-valley floors have low gradients. In the north, the flats measure 7 km across at Wingebellup Road but narrow to 2 km near the northern end of Yarnup Road. Elevations range from 210 m in the west to 220 m AHD in the east over a distance of about 18 km. Ferricrete covered hillocks rise from the valley floor giving a gentle undulating form to the landscape north of Unicup Lake. The poorly drained flats in the south of the

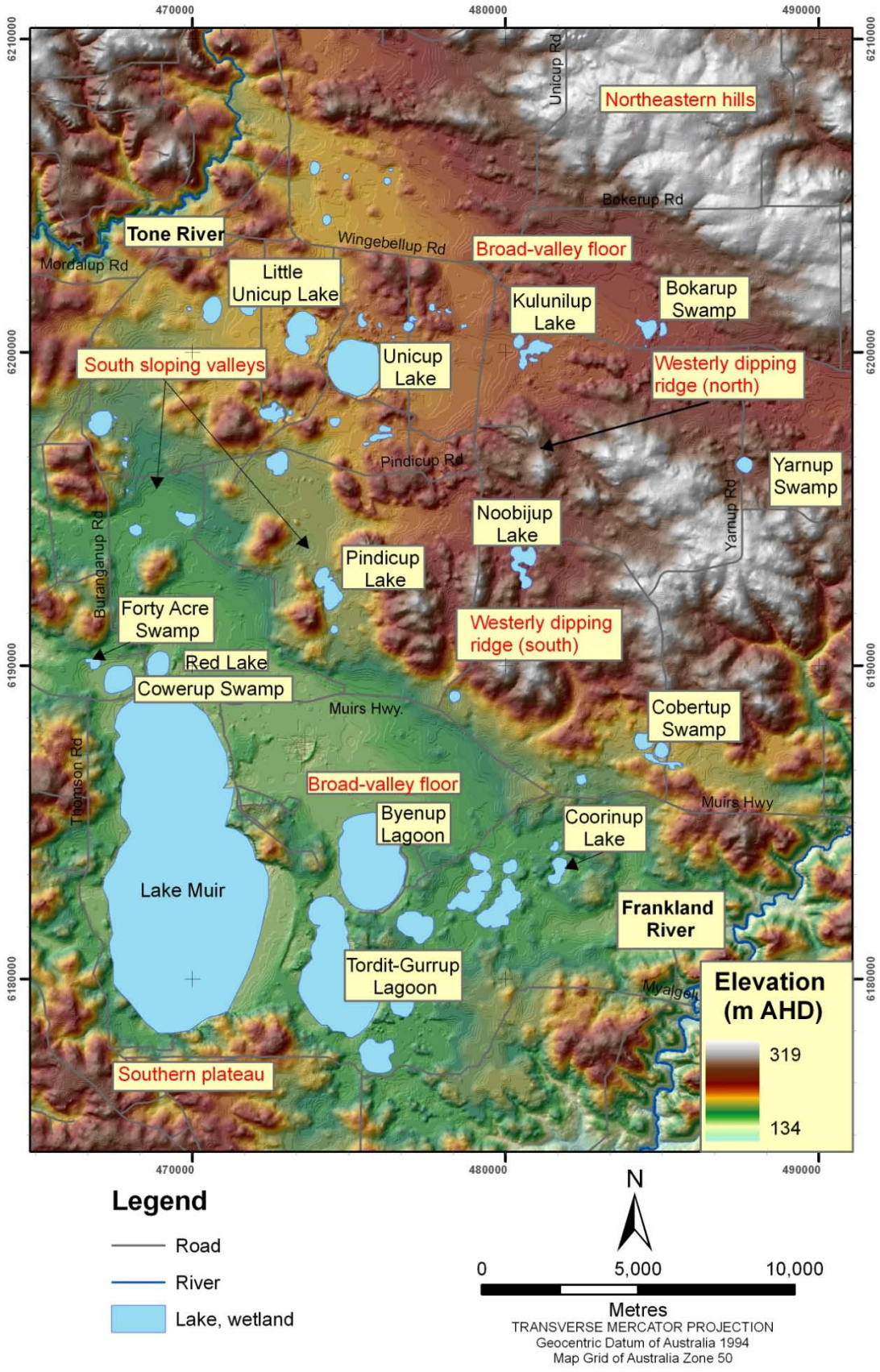

Figure 3–1 Geomorphology of the study area showing the major roads, lakes and main geomorphic features.

study area extend eastward from Lake Muir with elevations between 175 to 180 m AHD. Extensive areas are water logged making access difficult in winter.

Two of the three valleys in the study area slope southward and connect the northern part of the study area to the southern section. Buranganup Road marks the western flank of the largest valley, with the eastern flank being marked by a line of small hills west of Pindicup Lake (Figure 3–1). This line of hills separate the two valleys with the second valley being about 2 km across near Unicup Lake and narrowing to 1 km at Pindicup Lake. Near Muirs Hwy. the two valleys open up to become the poorly drained flats in the south of the study area. The third valley is narrow and slopes westward (270–200 m AHD) starting just east of Noobijup Lake (Figure 3–1). This valley is confined by the two westerly sloping ridges that divide the study area into its northern and southern parts.

3.3 CLIMATE

The climate is temperate with warm dry summers and cool wet winters. At Manjimup the Bureau of Meteorology has recorded average daily minimum temperatures that ranges from 6.4 to 13.3 ºC and average maximum temperatures from 14.3 to 27.1 ºC, with similar values to those recorded at Mt Barker (Figure 1–1). North-eastwards across the region the mean annual rainfall decreases from 900 to 700 mm. The mean annual pan evaporation (class A) is about 1400 mm. Regional climate stations are listed (Table 3-1).

Groundwater is reliant on rainfall for recharge. Across the southwest of Western Australia the rainfall pattern has changed in recent times. The Indian Ocean Climate Initiative Panel (2002) showed that not only has the winter rainfall across the southwest generally declined by 15 to 20% since the mid-1970s, but also that the rainfall pattern has changed, with less rain in early winter (May–June) and more rain in late winter (August–October).

Table 3-1 Bureau of Meteorology climate stations showing which stations have the longest record and availability of rainfall or evaporation.

Station no.	*Name*	*Easting* (m MGA)*	*Northing* (m MGA)*	*Start*	*Rainfall (Mean Annual mm)*	*Evaporation (mean daily mm)*
9843	Frankland Vineyards	499384	6188867	1975	595	3.9
9573	Manjimup	409258	6209596	1915	1009	not available
9581	Mount Barker	558699	6230732	1886	729	not available
9592	Pemberton	412116	6187776	1941	1194	3.1

* Zone 50

Little mention is made of summer rainfall except to acknowledge that major summer events in the southwest since 1970 are more frequent, but the cause of this is not conclusive (Climate Note 6/05, 15 August 2005). On land cropped with annual winter pasture, the consequence of more frequent summer events is increased recharge to groundwater.

Work by Nicholls et al. (no date) for the Indian Ocean Climate Initiative Panel addressed rainfall in Manjimup and showed that the number of extreme rainfall events had declined as well as total rainfall. Between May and October during the 1950s Manjimup typically received 150 mm from heavy rain days, whist by the 1970s the heavy rain days had decreased to about 50 mm.

In the study area, readings commenced in 1898 at the Lake Muir (9568) rainfall station but ceased in 1968, just prior to the annual rainfall decrease in the 1970s (Figure 1–1; Table 3-2). Other stations (Table 3-2) in the study area had much shorter life spans, that of Mordalup being 17 years and Kelvin Bank 8 years. Bokerup (Figure 1–1) is currently open, but readings commenced only in 1959. Bangalup (9506), just east of the study area, is the closest functioning climate station with long term rainfall records (Figure 1–1; Table 3-2).

Table 3-2 Local rainfall stations within or near the study area.

Station no	*Name*	*Easting* (m MGA)*	*Northing* (m MGA)*	*Start*	*End*	*In study area*
9568	Lake Muir	464819	6180484	1898	1968	yes
9718	Mordalup	464728	6204513	1900	1917	yes
9951	Kelvin Bank	461644	6202561	1974	1982	yes
9673	Bokerup	488647	6209995	1959		yes
9506	Bangalup	492368	6185970	1920		no

* Zone 50

Bangalup (9506) has a long term average annual rainfall of 742 mm. Plotting the annual rainfall as a moving 5-year average shows an above average rainfall between the 1920s and 1950s and below average rainfall since the 1970s (Figure 3–2). This is consistent with the general decline in rainfall noted by the Indian Ocean Climate Initiative Panel (2002).

Wetting or drying trends can be seen using the accumulation monthly residual rainfall (AMRR) as described by Ferdowsian et al. (2001):

$$\mathrm{AMRR}_t = \sum_{i=1}^{t} (M_{ij} - \overline{M_j}) \qquad (3.1)$$

where M_{ij} is the rainfall (mm) in the month i which corresponds to the j^{th} month of the year; $\overline{M_j}$ is the mean monthly rainfall (mm) for the j^{th} month of the year; and t is number of months since the start of records.

The study area has experienced what would have been classified as wet years between the 1920s and 1950s with an upward trending AMRR. The AMRR then flattened before commencing a downward or drying trend (Figure 3–3). The study area is currently experiencing a drying trend which commenced in the 1970s (Figure 3–3).

Concern about changing rainfall pattern led to work by CSIRO and the Australian Bureau of Meteorology (2007) predicting future changes in rainfall. They predicted that by 2030 the mean annual rainfall in the southwest of Australia will decrease between 2 and 5%, with the winter rainfall decreasing a further 10%.

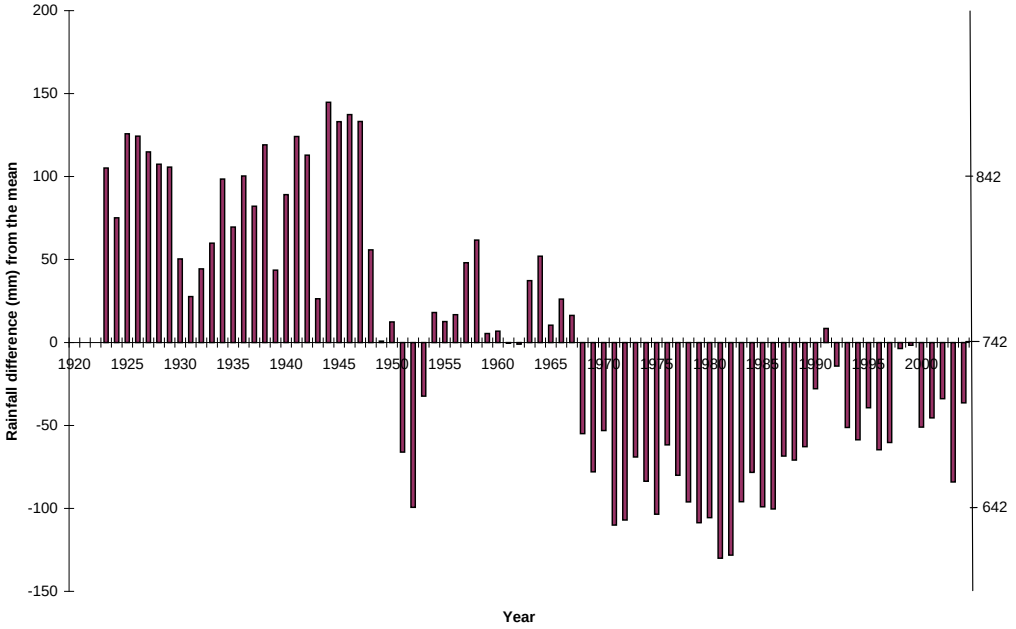

Figure 3–2 Average annual rainfall (5 year moving average) relative to the mean for Bangalup climatic station (9506).

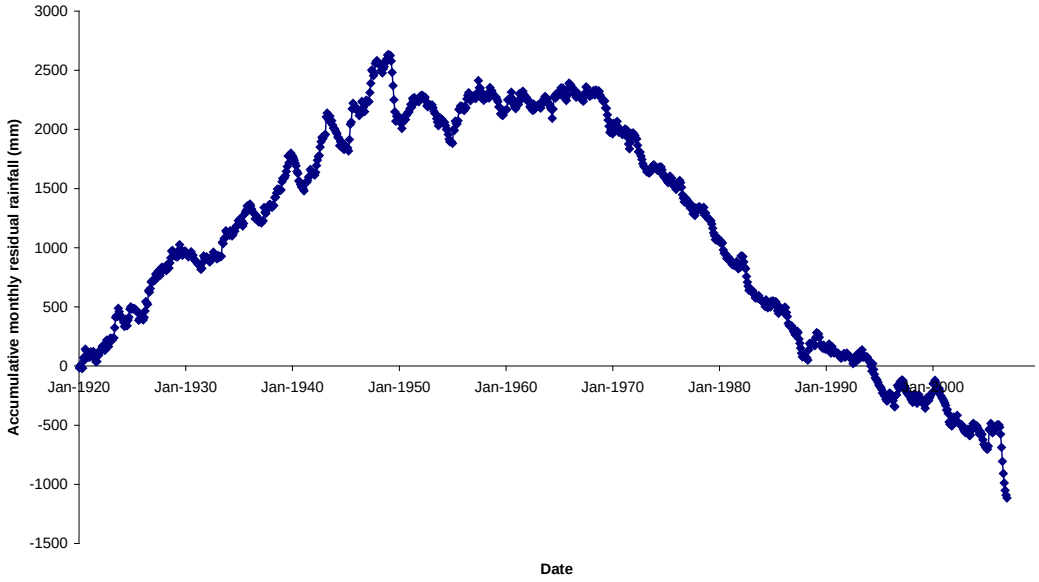

Figure 3–3 The accumulated monthly residual rainfall for Bangalup (9506) showing that the study area experienced a wetting period from the 1920s to the 1950s and has been in a drying phase since the 1970s.

3.4 SURFACE WATER

The study area is internally draining, with two main rivers skirting its edges the Tone River in the northwest and the Frankland River in the southeast (Figure 1–1 and Figure 3–1). Surface water catchments have been defined by the Western Australian Water and Rivers Commission (Smith, 2003) but are currently in the process of being redefined based on improved topographic information and fieldwork (R. Hearn *pers. comm.*). The study area is characterised by many poorly defined drainage lines that terminate in swampy depressions. These streams only flow in the winter or after heavy summer rain. Being indistinct, the direction of flow along many of the drainage lines is readily determined only when surface water is flowing.

Numerous lakes have formed: where the flats abut the elevated hill or plateau such as Lake Muir; in valleys between dissected hills such as Cobertup Swamp; and along the poorly drained flats such as Kulunilup Lake and Bokarup Swamp (Figure 3–1). The wetlands, swamps, and seasonally wet flats are found in 13 Nature Reserves (Gibson and Keighery, 1999) with Lake Muir the largest wetland covering 40.8 km^2. Lake Muir and many other wetlands are terminal drainage basins.

The wetlands in this study are classified according to the lake substrate. The lake floor substrate is either: organic-poor clays and sands (Lake Muir, Unicup Lake); organic-rich peat (Yarnup Swamp, Kulunilup Lake); or a mixture of both (Tordit-Gurrup Lagoon). Alternative classifications have been used by other workers to reflect properties such as water quality and level. However, these are changing with the changing rainfall pattern (Figure 3–2 and Figure 3–3) and land use.

Monitoring of six wetlands (Lake Muir, Lake Unicup, Byenup Lagoon, Poorginup Lagoon, Tordit-Gurrup Lagoon and Yarnup Swamp) commenced in 1977, originally every two months but in later years only in September and November (R. Hearn *pers. comm.*). Measurements comprised lake water depth, salinity (TDS) and pH. In 2006. weekly monitoring of Bokarup Swamp, Kulunilup Lake, Unicup Lake, Little Unicup Lake, and Yarnup Swamp commenced with additional wetlands added in 2007. Other water quality monitoring projects are detailed in Storey (1998).

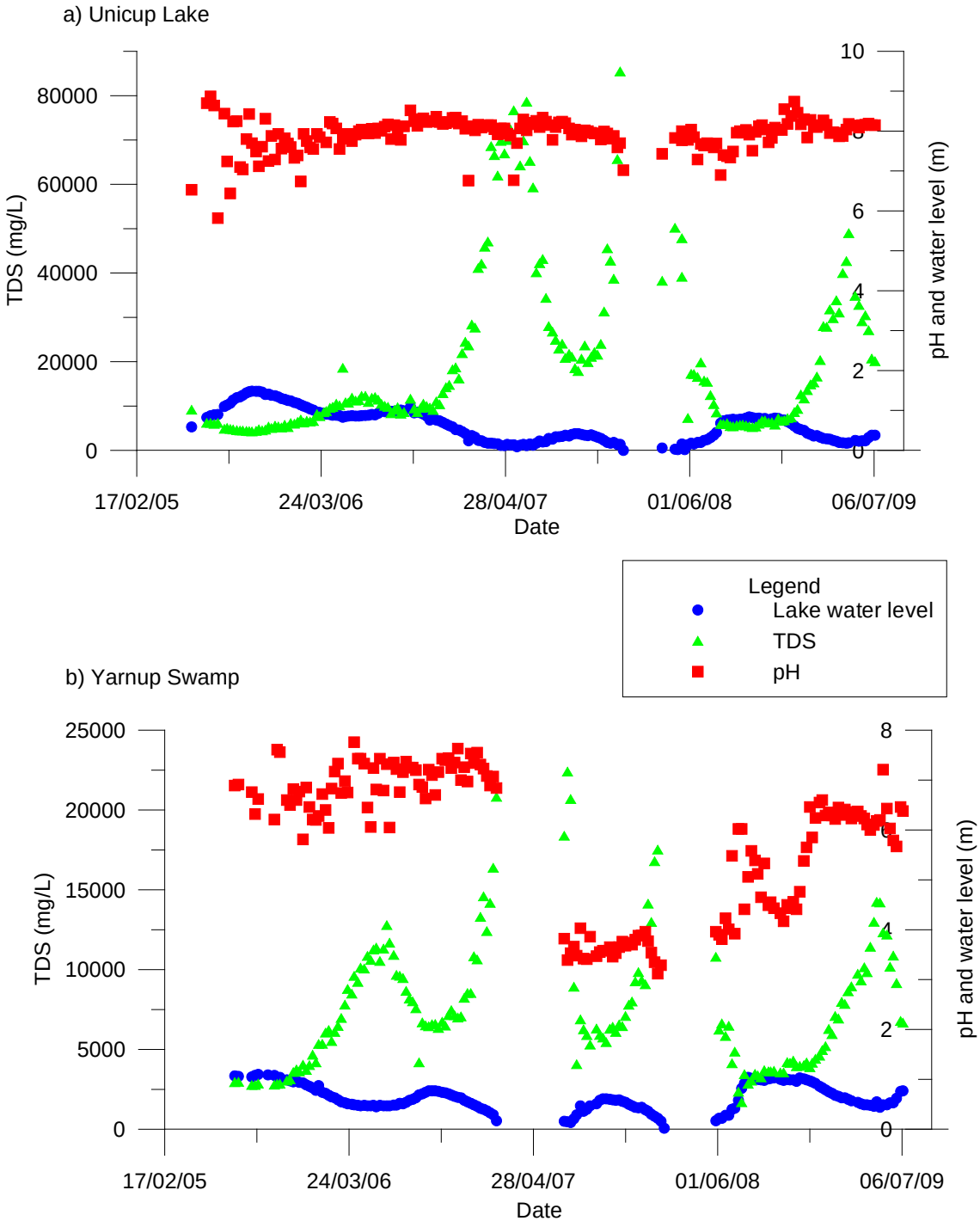

Figure 3–4 Comparison between a) Unicup Lake (inorganic clay substrate) and b) Yarnup Swamp (peat substrate) showing the variation in pH, depth and salinity. The pHs in Unicup Lake are maintained at near neutral whereas the pH value in Yarnup Swamp falls after the lake dried out in summer and autumn of 2007.

Many permanent wetlands exist in the study area and include Kulunilup Lake, Yarnup Swamp, Byenup Lagoon and Tordit-Gurrup Lagoon. However, Unicup Lake (Figure 3–4(a)), Bokarup Swamp and Noobijup Lake are permanent wetlands that are now drying in summer. The drying trend within wetlands is a response to both the particularly low rainfall of the last few years and the below average rainfall since the 1970s (Figure 3–2 and Figure 3–3). Lake Muir has always been a seasonal lake, often dry in autumn. The maximum depth for surface water, recorded since 1978, was 1.3 m in November 1988. The water quality in the wetlands ranges from brackish to saline. The salinity is quite variable from year to year and is dependent on local rainfall and surface water inflow.

Unicup Lake had a significant increase in salinity between 2005 and 2007 (Figure 3–4a). In 2005 and most of 2006 the lake water had a salinity of about 10 000 mg/L. During the dry summer and autumn months (January to May) of 2007 evaporation concentrated the salinity to just below 80 000 mg/L. During the wet winter months (June to August 2007), direct rainfall and surface water inflow lowered this to about 20 000 mg/L (Figure 3–4(a)).

The pH now falls in the peat wetlands that are now dry in summer, as exemplified by Yarnup Swamp (Figure 3–4(b)). Prior to the summer of 2006–2007, the pH was between 5.81 and 7.71. On re-flooding in 2007, the pH fell to between 3.39 and 4.07, with water depths ranging from 0.13 to 0.61 m. The pH regained its 2005–2006 values by 2009. Other peat wetlands with low pH in 2007 are Noobijup Lake, Bokarup Swamp, Cobertup Swamp (North), Cowerup Swamp and Kulunilup Lake. In comparison, Unicup Lake (Figure 3–4a) and Little Unicup Lake (wetlands with clay and sandy substrates) had pH > 6, even following re-flooding if they dried in summer.

3.5 SOIL AND LANDSCAPE

The study area has been mapped as the Warren–Denmark Southland soil–landscape zone (Stuart-Street and Scholz, *in prep*; van Gool et al., 2005) with 5 regional soil–landscape systems (Table 3-3). The Warren–Denmark Southland Zone falls from north to south across a series of indistinct steps or benches. This zone has formed on granitic and gneissic rocks of the Yilgarn Craton and the Albany–Fraser Orogen.

The majority of the study area is classified as Unicup System (Figure 3–5) which is poorly drained flats with lakes and low dunes. The undulating low hills to the northeast and the ridges that divide the area in half are mapped as Frankland Hills. In the southwest is the Manjimup Plateau and in the southeast the Perup Plateau. Both are described as lateritic plateau with broad swampy depressions. The Wilgarup Valleys follow the Tone and Frankland Rivers and are classified as major valleys.

Soils in the study area are sandy to loamy gravels and duplex sandy gravels. Deep sands are associated with the Manjimup Plateau and Unicup Systems. Wet soils are associated with the broad swampy depressions of the Manjimup and Perup Plateaus and poorly drained flats of the Unicup System.

Table 3-3 Soil–landscape description as described by Stuart-Street and Scholz (*in prep*).

System	Landform	Soil	Vegetation	Soil pH (area %)		
				5.6–6.0	6.0–6.5	6.5–8.0
Frankland Hills	Undulating low hills and rises	Loamy gravels, duplex sandy gravels, deep sandy gravels and grey deep sandy duplexes	Jarrah-marri-wandoo forest and woodland	29	2	68
Manjimup Plateau	Lateritic plateau with broad swampy depressions	Sandy gravel, loamy gravel, non-saline wet soil and deep sand	Jarrah-marri forest and woodland	37	0	63
Perup Plateau	Lateritic plateau with broad swampy depressions	Sandy gravel, loamy gravel, and wet soil (sometimes saline)	Jarrah-marri-wandoo forest and woodland	28	1	71
Unicup	Poorly drained flats with lakes and low dunes	Pale deep sand and wet soils (sometimes saline) and grey sandy duplex	Banksia-paperbark scrub and jarrah-marri woodland	61	14	23
Wilgarup Valleys	Major valleys	Loamy gravel, sandy gravel, loamy earth, stony soil and loamy duplex	Marri-jarrah-wandoo forest and woodland	18	9	70

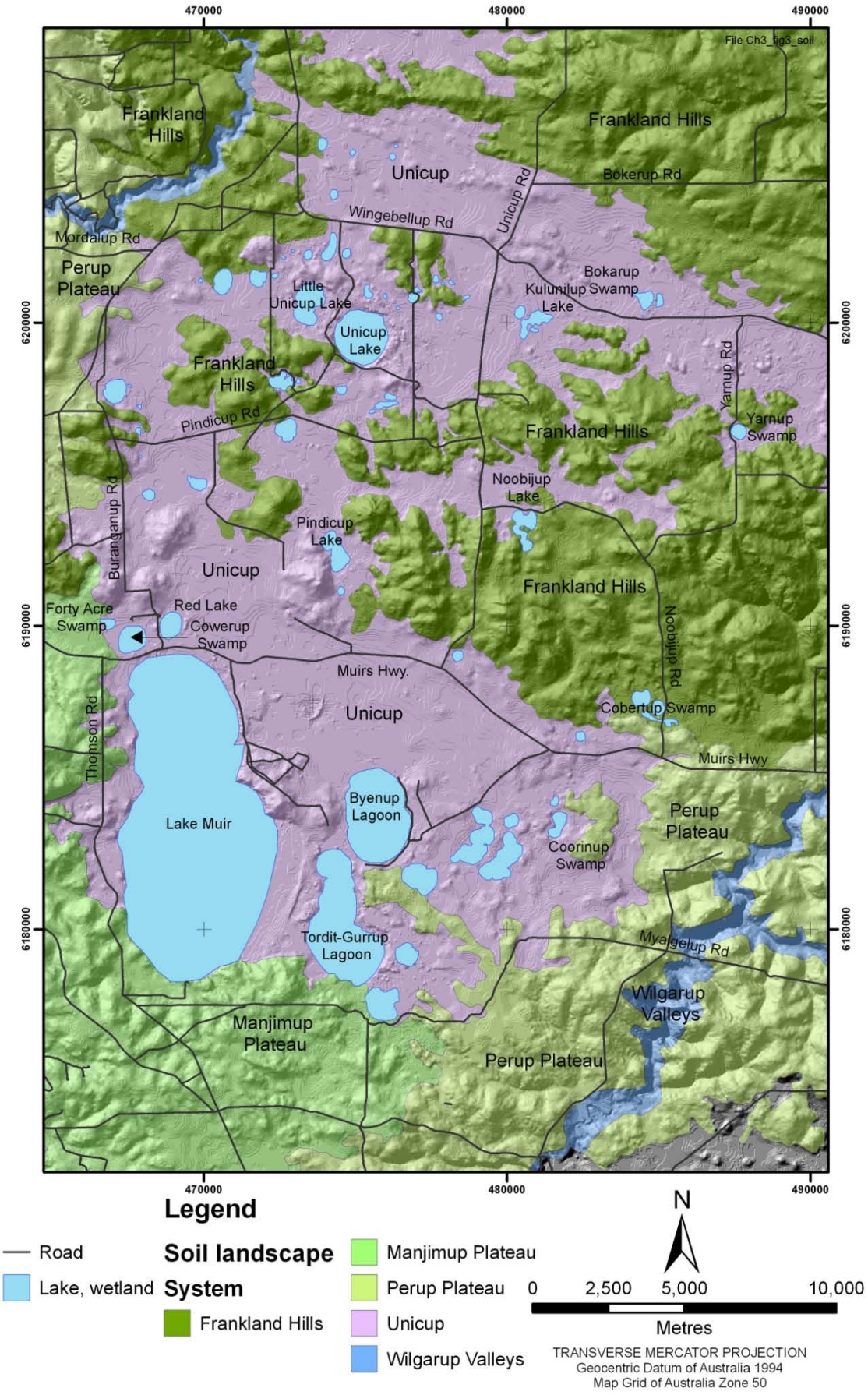

Figure 3–5 Mapped soil and landscape systems.

The landscape system mapping recorded pH of soils between depths of 0.5 and 0.8 m. For all except the Unicup System over 50% of the area within a particular system was classified as neutral (pH 6.5–8.0). In the Unicup System 61% was classified as moderately acid with pH between 5.6 and 6.0 (Table 3-3).

3.6 VEGETATION

At a regional scale the area is predominately located within the Kwornicup and Jingalup vegetation systems which are described as poorly drained swampy plains and lateritic uplands with dissected water courses, respectively (Beard, 1981). The area comprises medium forest or woodlands and low woodlands. The medium forest and woodlands consist of jarrah (*Eucalyptus marginata*), marri (*Corymbia calophylla*), yate (*E. occidentalis*), *E. decipiens* and wandoo (*E. wandoo*). Low woodlands contain closed forest of paperbark (*Melaleuca spp*.) scrubland, tea tree thickets (*Melaleuca spp*. and *Kunzea spp*.), sedgelands and reed swamps.

Detailed mapping by Gibson and Keighery (1999) of 9 Nature Reserves found more than 30 different structural vegetation units. Mapping of all 13 Nature Reserves identified a total of 976 taxa (862 were native and 114 were introduced) of which 3 species are on the Declared Rare Flora list and 33 taxa are on the DEC Priority Flora list.

3.7 CLEARING HISTORY

Aboriginal people lived in the area for thousands of years, but it is European land management that has shaped the landscape seen today. Farming initially was grazing on native grasses. Extensive clearing of the study area during the 1950s and 60s was undertaken to allow intensive grazing and cropping to develop. In the 1990s, timber plantations were established to help combat land salinisation.

Europeans settled the area in the 1850s. The main European explorers were the official survey expeditions and those seeking land suitable for stock grazing. In 1852, Gregory, a government surveyor, travelled extensively through the Warren district and traversed the Tone River (Berry, 1987). In the same year, Thomas and Robert Muir travelled near

Lake Muir seeking land for their stock. This first wave of settlers mainly grazed stock on the native grasses in the timbered country (Berry, 1987).

Major land clearing commenced after World War II with the introduction of efficient land clearing machinery. The main farming was sheep grazing on subterranean clover pastures. This farming system remained unchanged till the mid-1990s when timber plantations for pulpwood production were encouraged.

Published data on clearing within the study area only deal with the northern section. By 1988, 46% (104 km^2 out of 227 km^2) had been cleared (Smith et al., 2005) for agricultural purposes. Landsat TM scenes for the northern section (above the 6187500 mN) of the study area were reviewed up to 2003 to determine where cleared land had been placed under timber plantations (Smith et al., 2005). Plantations can be first identified when they are about 3 years old from the Landsat TM scenes. By 2003 an area of about 37.5 km^2 had been replanted with plantation timber, with 1.7 km^2 having been harvested (Table 3-4).

Table 3-4 History of timber plantations showing the area of land planted and harvested since 1990 in the north of the study area (Smith et al., 2005).

Year	Planting (km^2)	Harvesting (km^2)
1990–1996	4.3	Nil
1998	0.2	< 0.1
1999	2.7	< 0.1
2000	5.4	< 0.1
2002	11.9	1.6
2003	12.9	Not available
Total	37.5	1.7

3.8 SALINISATION

Land and water salinisation is extensive in the southwest of Western Australia. The process is well documented in the literature and is briefly outlined here. Clearing of native deep-rooted vegetation has changed the water balance by reducing evapotranspiration and interception of soil water by plants. Recharge to the groundwater has increased and consequently the watertable has risen. Salts stored in the unsaturated zone are dissolved as the groundwater rises. Once the watertable is within 2 m of the ground surface, the groundwater can be evaporated back to the atmosphere leaving the salts behind in the ground (Nulsen, 1981). Saline groundwater within the root zone of trees causes distress and eventually death. Once the groundwater reaches the surface it is discharged onto the surface forming scalds or into the local streams and eventually lakes and swamps.

Major land clearing contributing to land and water salinisation commenced just after WWII when the study area was experiencing a period of above average rainfall (Figure 3–2 and Figure 3–3). Land clearing decreased after the introduction of clearing control legislation in 1978 (Smith et al., 2005) which coincided with the period of declining rainfall (Figure 3–2 and Figure 3–3). An absence of records relating to groundwater means that the rate of groundwater rise or decline in the study area is not known.

Although groundwater levels have not been monitored, the effects of land salinisation have been noted during various investigations (Department of Environment and Conservation, *in prep*; Gibson and Keighery, 1999; Storey, 1998). Salinisation is threatening vegetation health and lake water quality.

4 Methodology

4.1 INTRODUCTION

This chapter focuses on data acquisition and the selection of the geochemical model used in this study. The data acquisition is divided into 5 sections. The first describes the drilling and construction techniques of the bore network. The next two sections describe the geological data acquired and the groundwater sampling techniques employed in this study, while the fourth section explains analytical methods. The fifth section focuses on data quality and verification of chemical results.

4.2 BORE NETWORK

Three groundwater bore networks have been constructed in the study area since the 1990s. The Western Australian Department of Water (formally Water and Rivers Commission) maintains 7 bores which were constructed to assist the hydrogeological mapping of the Pemberton Irwin Inlet Sheet SI5010-14 (De Silva, 2000; Panasiewicz et al., 1997). These bores have the prefix PM for 'Pemberton mapping' (Figure 4–1; Appendix 3). The other two networks are maintained by the Western Australian Department of Environment and Conservation (DEC). The older of the two was constructed between 1990 and 2001 to understand groundwater quality and flow at a local scale. These bores, with the prefix EMU ('early Muir–Unicup'), form 4 main clusters and are mainly on private land (Appendix 3).

Since 2002, DEC has changed its focus from understanding groundwater at a local scale to understanding groundwater at a catchment scale. Bores were constructed at 71 sites between 2003 and 2006 and these bores have the prefix MU for 'Muir–Unicup' (Figure 4–1; Appendix 3). Some sites have a single bore while others have 2 or more bores. At sites with only one bore, the Site ID and Bore ID are identical. The initial bore at each site was drilled to basement. If additional bores were drilled a suffix of D, S, I, or A was used (Table 4-1). The suffix D was given to the initial bore drilled to basement. Shallow and intermediate bores were given the suffix S

and I, respectively. Suffix A was given to bores drilled in 2006. The MU bores are predominantly located on DEC reserves or Crown Land adjacent to the roads.

Table 4-1 Labelling protocol for MU bores showing the relationship of the different prefixes.

Site ID	Bore ID	Number of bores at site	Bore depth (relative)
MU34	MU34	only1	to basement
MU42	MU42D	more than 1	to basement
MU42	MU42S	more than 1	shallow
MU42	MU42I	more than 1	intermediate
MU42	MU42A	more than 1	variable

4.2.1 Drilling techniques

The majority of bores were drilled using an air-core technique, with 3 bores drilled using the wire-line diamond-core drilling technique. The rock cuttings, obtained during air-core drilling, were removed by injection of compressed air into the hole. The compressed air forces rock cuttings to move up the inside of the hollow drill rods thus, preventing strata contamination. The cuttings were retained in a cyclone during drilling of a 1 m interval. This drilling method produces an averaged sample of the strata over the 1 m interval. A disadvantage of the method is that textural information, such as sedimentary structure, is often obscured.

Sedimentary structure was better preserved in cores obtained using the wire-line technique. Core, of nominal diameter 83.1 mm, was removed using a split-barrel core sampler. The sampler allows the core to be placed into core trays with minimal disturbance. Core loss can be problematic when drilling through zones of contrasting competence such as densely packed clay overlying loosely packed coarse-grained sand. As the sediment in the study area is weakly consolidated to unconsolidated, core loss was anticipated. In areas of unconsolidated core, the size of the split-barrel core sampler was reduced to a 45.1 mm diameter and a free falling hammer used. The hammer was dropped repeatedly until the split-barrel core sampler had penetrated 0.5 m, then the core was retrieved.

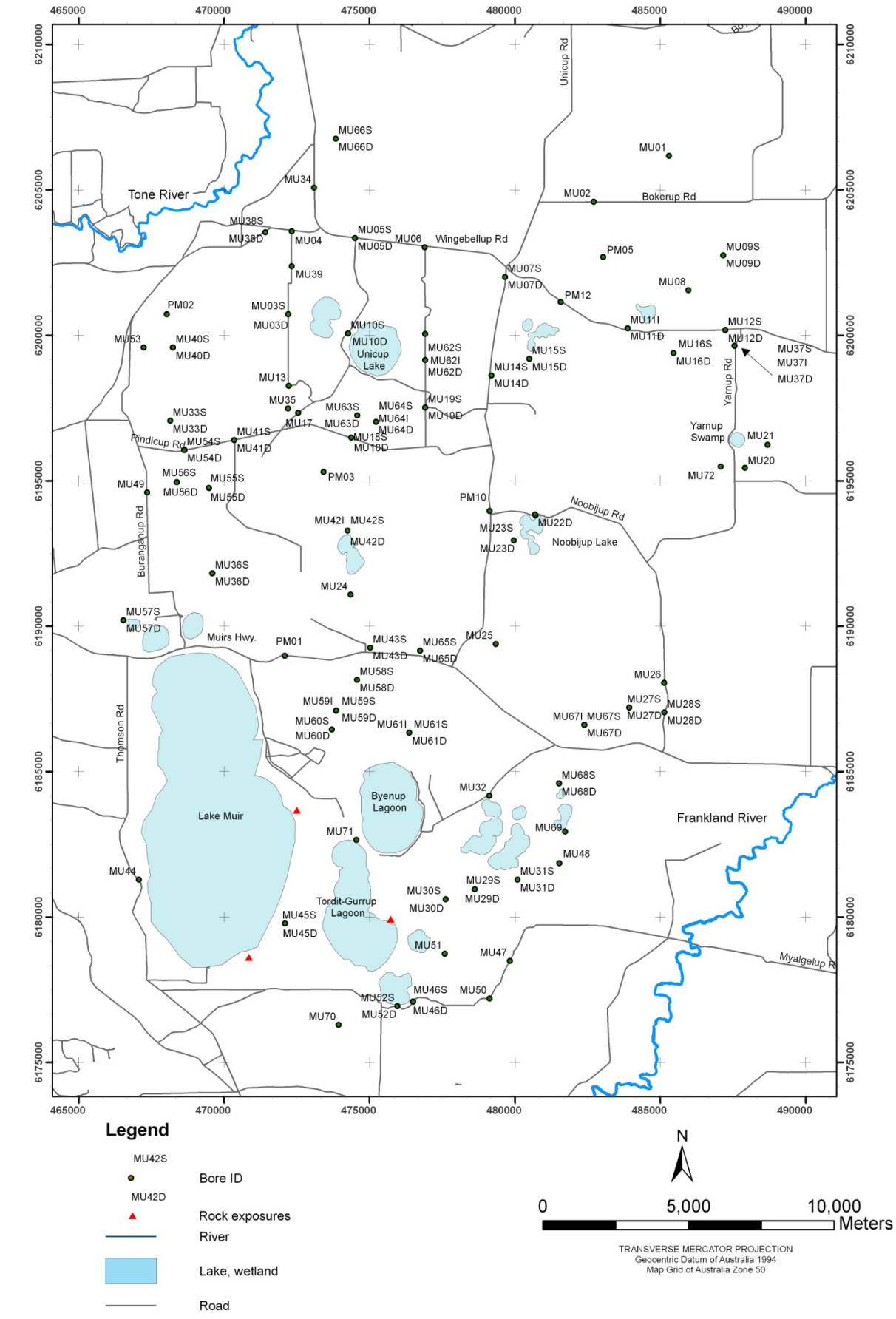

Figure 4–1 Location of bore sites.

4.2.2 Construction techniques

Full details of the bore construction are available for the individual PM bores (Panasiewicz et al., 1997), and the MU bores (New et al., *in prep*). A summary of the construction methods is given below.

The PM and MU bores were cased with 50 mm PVC pipe and a 0.4 mm slotted screen placed at a selected depth. The screen length varied from 2 to 9 m with most being 3 to 6 m in length. The bore annulus was packed with gravel from the base of the slotted casing to a height of 1 to 2 m above the slots. Above the gravel pack the annulus was then sealed with 5 m of grout before being backfilled to surface. Some shallow bores were gravel packed to near surface. All bores were sealed at surface and locked headworks constructed. A valve was fitted if the hydraulic head was above surface.

Documentation on the EMU network was limited, but where possible the bore construction was identified. Most of EMU bores were cased with 50 mm PVC pipe, but a few were cased with 40 mm PVC pipe. The length of the screened interval varied and the annulus fill was not documented. To prevent groundwater spillage onto the ground surface, headworks were constructed for bores that had hydraulic heads above ground surface. Information from these bores cannot be used in isolation but, with care, can be used in conjunction with information from the MU bores.

4.3 GEOLOGICAL DATA ACQUISITION

Regolith units were mapped as part of this study. This included reviewing of the geological descriptions from previous drilling programs (EMU and PM bores) and the current MU bores. Additional work was conducted, namely:

- petrographic descriptions (MU bores) using optical microscopy, X-Ray Diffraction (XRD), and Scanning Electron Microscopy (SEM) coupled with energy dispersive x-ray microanalysis;
- mapping rock outcrops and exposures; and
- reviewing the geophysical surveys.

4.3.1 Petrographic descriptions

The geological descriptions were missing for many EMU bores and, when present were of variable quality. Interpreted lithology was available for PM bores (Panasiewicz et al., 1997). Rock-chips from the MU bores were originally characterised by the field geologist in terms of grain morphology, mineralogy, colour, and sedimentary structure (Field Geologists' Manual, 1989; Munsell Color, 2000; Tucket, 1982). At the time of drilling a 30 cm^3 sample for each metre interval was collected and stored in chip trays for future reference.

This study has re-assessed the initial field descriptions from the 30 cm^3 reference sample. Previous petrographic descriptions for the MU bores were augmented using optical microscopy. Emphasis was placed on interpretation of the depositional environment from grain morphology, mineralogy, colour, and sedimentary structure. This information enabled regolith units to be assigned.

The grain morphology included grain size, rounding and degree of sorting. The grain sizes were classified based on the Wentworth scale (Field Geologists' Manual, 1989) as listed in Table 4-2. The Wentworth scale allowed the gravel, sand, and silt groups to be subdivided based on the grain size (Field Geologists' Manual, 1989). This study has retained the sand group subdivisions of very-coarse grained sand through to very-fine grained sand, but not subdivisions for the gravels or silts (Table 4-2). The small size of rock-chip sample stored as reference material precluded the use of hydrometer to approximate clay sizes. Estimated ratios of clay, silt and sand have been used to give a lithological classification (Figure 4–2). The lithological classification (Figure 4–2) was based on Picard's method as described in Tucket (1982). The sediments in the study area are weakly consolidated to unconsolidated, therefore the terms sandstone, siltstone, claystone and mudstone have been changed to sand, silt, clay and mud. By removing the term 'stone' these classifications can be used to describe weathered basement rock.

Table 4-2 Wentworth scale used in this study.

Group	Grain size		Size class
	from (mm)	to (mm)	
Gravel	> 2.00		Gravel
	1.00	2.00	Very-coarse grained sand
	0.50	1.00	Coarse grained sand
Sand	0.25	0.5	Medium grained sand
	0.125	0.25	Fine sand
	0.0625	0.125	Very-fine grained sand
Silt	0.0039	0.0625	Silt
Clay	< 0.0039		Clay

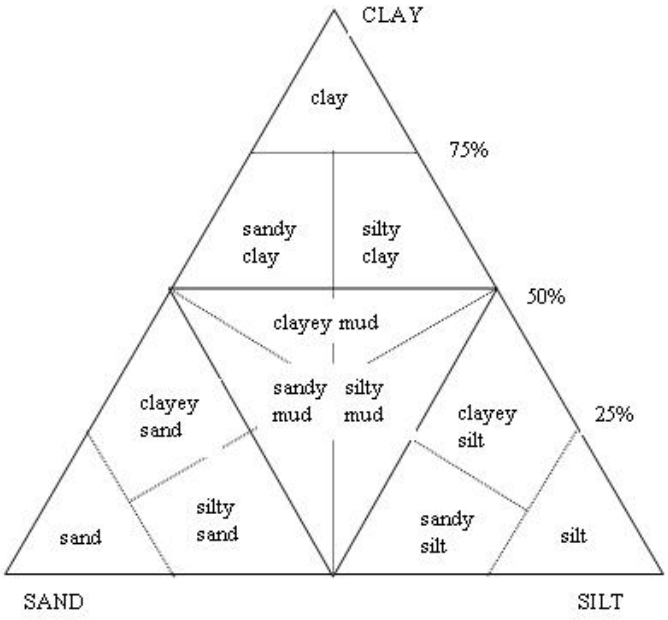

Figure 4–2 Rock classification used to obtain a lithological description (after Picard's method as described in Tucket (1982)).

The grain roundness was grouped into 6 classes:- very angular, angular, sub-angular, sub-rounded, rounded, well-rounded (Field Geologists' Manual, 1989; Reineck and Singh, 1980; Tucket, 1982). The degree of roundness is often used to help interpret the depositional environment (Reineck and Singh, 1980). The general assumption is that with increasing abrasion during transport grains become more spherical. However, Reineck and Singh (1980) noted that many factors need to be considered when using this assumption, such as original mineral composition of the grain and external forces acting on the grain. In this study the importance of grain roundness becomes evident when defining regolith units and their boundaries.

Sorting gives an indication of the energy level at which the sediment was deposited. Energy levels were classified broadly as high or low. High energy environments tended to be characterised by coarser-grained, better sorted sediments than the low energy environments which have sediments that are finer-grained and poorly-sorted (Reineck and Singh, 1980).

Fine-scale sedimentary structure was destroyed during air-core drilling, but coarse structure was often discernable if the unit was very thickly bedded (> 1 m). Cycles of graded bedding were evident in the sediment. Upper and lower contacts of the regolith were generally identifiable to within a metre, but the contact between sediment and weathered basement rock was more difficult to determine if both were clay dominated.

Munsell colour designation was recorded at the time of drilling.

4.3.2 Field oxidation test for sulfides

Rock-chips were tested for the presence of sulfide using the two-part field procedure of Hey et al. (2000). A representative regolith sample was split into two 5 gm samples, and a 1:5 paste made. Sample 1 was made with 1 part regolith and 5 parts deionised water, and the paste pH recorded as pH_F. Sample 2 was made with 1 part regolith and 5 parts 30% hydrogen peroxide with pH adjusted to between 4.5 and 5.5 with sodium hydroxide. Reaction of the hydrogen peroxide with sulfide causes a bubbling reaction and lowering of the pH according to the formula (Ahern et al., 2003):

$$FeS_2 + {}^{15}\!/_{2}\, H_2O_2 \rightarrow Fe(OH)_3 + 4H_2O + 2SO_4^{2-} + 4H^+ \qquad (4.1)$$

The pH of sample 2 was recorded as pH_{FOX} once the above reaction was complete.

The initial pH_F will give an indication of sulfides if they have started to oxidise with a pH < 4 indicating possible sulfides and between 4 and 5.5 indicating a strongly acid soil. The final pH_{FOX} gives an indication of sulfides being present. A pH_{FOX} of < 3 strongly indicates the presence of sulfides; between 3 and 4 is a borderline result; and between 4 and 5 is indeterminable.

Interferences include carbonate, organic matter and manganese (Hey et al., 2000). Carbonate, such as calcite and calcite shell material can influence the final pH_{FOX}. Initially the pH will drop as the hydrogen peroxide reacts with the sulfide, as described in equation (4.1), but H^+ ions will react with the carbonate raising the pH value and masking the presence of sulfide.

Organic matter, such as peat and decaying vegetation, will oxidise in the presence of hydrogen peroxide and may lower the measured pH_{FOX} value. Resulting pH may be between 3 and 4 but this is a borderline result and again sulfides may or may not be present.

Manganese compounds will react violently with hydrogen peroxide.

The test was performed on unconsolidated rock-chips from a selection of bores at the time of drilling. As the aim was to identify possible sulfides at the watertable, rock-chips retrieved from depths of 1 to 10 m were tested. In addition, rock-chips collected at one metre intervals over the remaining sections in two bores (MU42D and MU46D) were tested. However, these rock-chips where about 2 years old and deterioration was evident.

Indicator sticks for pH, covering the range 1 to 14, were used to measure pH at time of air-core drilling. A calibrated pH meter (WTW pH 330i) was used for samples from bores MU42D and MU46D in January 2006 and all wire-line diamond core in April–May of that year.

4.3.3 Mineral identification

Initial mineral identification made in the field was checked using optical microscopy and Scanning Electron Microscopy or X-Ray Diffraction (XRD).

4.3.3.1 Scanning Electron Microscopy

Scanning Electron Microscopy was conducted at the CSIRO Electron Beam and XRD Laboratory in Kensington, Western Australia using a Philips XL40 controlled pressure Scanning Electron Microscope with energy dispersive X-ray microanalysis (EDAX). Scanning Electron Microscopy with EDAX enables elements to be determined in solid materials. Mineral samples were attached to a glass slide with double-sided carbon tape. Element identification and quantification was made using energy dispersive x-ray microanalysis (EDAX). Mineral identification was made using the MinIdent for Windows database.

4.3.3.2 X-Ray Diffraction

X-Ray Diffraction (XRD) is a rapid analytical technique that identifies and provides a qualitative estimate of the minerals present. Dry powdered samples (Table 4-3) were analysed at the CSIRO Electron Beam and XRD Laboratory in Kensington using a Philip® X'Pert MPD instrument. Samples of crystalline basement rock were prepared by staff at the XRD laboratory. Regolith samples were pulverised using a tungsten carbide swing mill. Mineral identification was made by comparing the obtained diffraction data against the X-Ray Diffraction Table by the XRD laboratory staff. Mineral abundances in wt % were estimated using Siroquant version 3 software.

4.3.4 Total extraction of major and trace elements

Selected samples (Table 4-3) were prepared and analysed at Actlabs Pacific Pty Ltd in Cloverdale for a suite of 65 major and trace elements. Total acid digestion using HF, $HClO_4$, HNO_3 and HCl was employed and trace elements were determined by Inductively Coupled Plasma–Mass Spectrometry (ICP-MS) and Inductively Coupled Plasma–Atomic Emission Spectrometry (ICP-AES). Some trace minerals may not be totally dissolved, such as Al-oxides, zircon, monazite, sphene, gahnite, chromite, magnetite, barite, cassiterite, ilmenite and rutile. Most other silicates will be dissolved, but there may be some loss of Si, As, Sb and Cr.

Table 4-3 List of samples analysed by XRD and chemical extraction with their associated stratigraphic unit and lithology (results listed in the Appendix 4), X indicates that sample was analysed.

Sample ID	Depth (m BGL)	Stratigraphic unit	Lithology	XRD	Total and exchangeable extraction
MU09-27	27	Granitoid rock	Crystalline basement rock	X	
MU10-4.75	4.75	Werillup Formation	Clay		X
MU10-5.1	5.1	Werillup Formation	Sandy clay (at watertable)	X	X
MU12-5.4	5.4	Pallinup Formation	Fine-grained quartz sand	X	X
MU12-10	10	Pallinup Formation	Fine-grained quartz sand		X
MU12-49	49	Granitoid rock	Crystalline basement rock	X	
MU32-18	18	Granitoid rock	Crystalline basement rock	X	
MU42-23.5	23.5	Werillup Formation	Coarse grained quartz sand	X	X
MU42-29	29	Werillup Formation	Coarse grained quartz sand	X	X
MU42-31.4	31.4	Werillup Formation	Carbonaceous clay	X	X
MU46-21.45	21.45	Werillup Formation	Carbonaceous sandy silt	X	X
MU46-45.5	45.5	Weathered basement rock	Weathered basement rock	X	X
MU52-2.35	2.35	Recent sediment	Silty clay		X
Yarnup Creek	0.1	Recent sediment	Sandy silt		X

4.3.5 Selective extraction of trace elements

Selective extraction of readily exchangeable elements were performed at the Wet Chemical Laboratory CSIRO (Kensington). The elements were extracted from 5 g pulverised regolith samples (Table 4-3) using a solution of 1M ammonium acetate at pH 5 and 25 °C (Gray, 1999). The samples were placed on a shaker for 6 hours then centrifuged (4000 rpm) for 15 minutes and the supernatant decanted. A suite of 65 major and trace elements were determined in the extracted solution by ICP-MS and ICP-AES by Actlabs Pacific Pty Ltd in Cloverdale.

4.3.6 Airborne geophysical survey

An airborne geophysical survey was flown in May 1998 by Agraria-World Geoscience. The survey was flown east to west (90–270°) at a line spacing of 150 m and a flying height of 60 m. The north south tie lines (0–180°) were flown 1500 m apart. Measurements were collected for magnetic and radiometric interpretations, and the development of a digital terrain model. The initial data were processed by Agraria Limited and presented in an unpublished report (Chakravartula and Street, 2000).

For use in this study the digital magnetic data were re-processed by Mr Paul Wilkes of the Department of Exploration Geophysics at Curtin University of Technology. Depths to magnetic basement were obtained using the Euler homogeneity equation as outlined by Thompson (1982) and used to construct a topographic map for the Eocene.

4.3.7 Field Mapping

The study area has considerable dense jarrah–marri forest cover. Extensive development of ferricrete further conceals the underlying geology. Field mapping was restricted by the lack of rock exposures. These include natural rock outcrop and rock exposures in road cuttings and the walls of farm dams. Rock exposures were also found in new plantations where the ferricrete had been ripped to allow tree planting.

4.4 GROUNDWATER DATA ACQUISITION

4.4.1 Field measurements

Physical groundwater parameters were measured in the field to elucidate horizontal and vertical groundwater flows. The depth to standing water (SWL), electrical conductivity (EC), temperature (T) and pH were initially measured when the bores were developed. Methods are described in section (4.4.2.1) and summarised in Table 4-4. Field measurements were also taken routinely twice yearly by the DEC staff (Table 4-4) before the start of, and at the end of, the winter rains in late May and late October, respectively. Capacitance water-level loggers were trialled with the aim of recording the water level response to rainfall events. The loggers required weekly checking and cleaning as iron fouled the probe. After reviewing the logger readings it was decided that the readings were unreliable.

Depth to standing water was measured prior to disturbance of the water column. An electrical depth meter was used for the initial reading (at the time of sampling for chemical analysis) and a fox whistle used for the twice yearly measurements. The saline nature of the water often caused interference problems with the electrical tape.

The depth to groundwater was recorded and converted to Australian Height Datum (AHD) to facilitate comparison of levels across the study area. Following the convention for groundwater, water levels below ground level were recorded as positive readings and water levels above ground were documented as negative depths.

The uncompensated EC, T and pH were recorded for three separately bailed samples after discarding the first sample. A stainless steel bailer was lowered to the slotted interval to collect the water sample. The uncompensated EC in millisiemens per centimetre (mS/cm) and T in degree Celsius (°C) were measured using a WTW pH/Cond 340i set. The pH was measured using a pH probe (WTW pH/Cond 340i) which was calibrated daily using pH 7 and pH 4 buffer solutions.

4.4.2 Sampling of groundwater

Groundwater samples were collected in two main sampling programs. The first, in summer of 2005, sampled 58 bores. The second program during the summer of 2006/2007 sampled 81 bores and at Lake Muir, groundwater from 3 pits dug on the lake floor to a depth of approximately 1 m deep. Treatment of the sample from

collection to analysis is listed in Table 4-5. Problems encountered with the anion analysis during the first program resulted in modifications of the method of storage during the second program (Table 4-5).

4.4.2.1 Abstraction

Groundwater sampling was is aimed at getting fresh formation water without changing the chemical or physical properties related to it. Aeration of groundwater while purging the bore can affect measurement of certain parameters. To prevent aeration, the groundwater was abstracted at the same rate as the bore refilled, i.e. the hydraulic head within the bore did not fall significantly during purging. Most of the bores were purged using a peristaltic pump and a suction pump was used for the deep, low-flow bores. Pump hoses were decontaminated between bores using a solution of Decon 90.

In this study the high yielding bores had 3 casing volumes abstracted prior to sample collection. The low yielding bores were purged until 3 consecutive stable reading for EC and pH were obtained. The minimum time to obtain 3 consecutive reading would be 45 minutes.

Electrical conductivity, T and pH readings were taken 15 minutes apart during pumping. The parameters were measured as groundwater was passed through a flow-through cell. Prior to collecting the water sample, redox and dissolved oxygen were measured using a WTW pH 330i redox probe and WTW Multimeter 340i dissolved O_2 probe, respectively. Pump type used, pumping rate, and changes in water level were recorded during groundwater abstraction at each bore.

4.4.2.2 Collection method

Groundwater collection was dependent on the analyte required. Samples were analysed for alkalinity, major cations and anions, and trace metals. This required 3 separate samples per bore to be collected from each bore. All sample bottles were labelled with program name, bore ID, date and collection details such as filtered or unfiltered, acidified or un-acidified. Sample bottles were rinsed with the sample which was then discarded.

Table 4-4 Collection method and equipment used to collect the field parameters used in this study.

Field parameter	Summer 2005 and 2006/2007 programs				Twice yearly sampling		
	Bore treatment	Collection method	Measurement instrument	Frequency	Bore treatment	Collection method	Measurement instrument
Standing water level			Electrical tape	15 minutes*	Nil		Fox whistle
pH	Pumped	Flow-through cell	WTW pH 330i set	15 minutes	Nil	Bailed	WTW pH/Cond 340i set
Electrical conductivity[#]	Pumped	Flow-through cell	WTW LF 230 set	15 minutes	Nil	Bailed	WTW pH/Cond 340i set
Temperature	Pumped	Flow-through cell	WTW LF 230 set	15 minutes	Nil	Bailed	WTW pH/Cond 340i set
Redox	Pumped	Flow-through cell	WTW pH 330i	Prior to sampling	–	–	–
Dissolved oxygen	Pumped	Flow-through cell	WTW multimeter 340i set		–	–	–
Alkalinity (HCO_3^-, CO_2)	Pumped	125 ml bottle	Titrated	Once off	–	–	–

uncompensated, * or more frequently if required, – not applicable

Table 4-5 Method of sample collection and perseveration used for the groundwater sampling programs in 2005 and 2006/2007.

	Summer 2005 program					Summer 2006/2007 program				
	Bore treatment	Bottle (ml)	Filtered (0.1 µm)	Acidified (nitric acid)	Transport	Bore treatment	Bottle (ml)	Filtered (0.1 µm)	Acidified (nitric acid)	Transport
Anions (Cl^-, SO_4^{2-}, Br^-)	Pumped	125	Yes	No	Frozen	Pumped	125	Yes	No	Refrigerated
Cations (Na^+, K^+, Ca^{2+}, Mg^{2+}) and trace metals	Pumped	250	Yes	Yes	Refrigerated	Pumped	250	Yes	Yes	Refrigerated

A new 125 ml polythene bottle was used to collect samples for field determinations of alkalinity. The bottle was filled to the top and capped.

Groundwaters for major cation, anion and trace metal determinations were filtered using a 0.1 μm nominal pore size membrane filter (Supor®-100) to minimise the content of colloidal oxyhydroxides and clay (Kennedy et al., 1974). For anion determinations, a 125 ml polythene bottle was filled and a gap left to allow for water expansion when frozen. A 250 ml polythene bottle containing Aristar* grade HNO_3 (69%) at 100 μL per 100 ml of sample was filled for cation and trace metal work. On the day of collection the bottles were refrigerated, prior to the 125 ml bottle being frozen that evening. The water samples were frozen as there was going to be a several month delay between collection and analysis. No samples were frozen in the summer 2006/2007 program.

4.5 ANALYTICAL TECHNIQUES

4.5.1 Alkalinity Titration

Alkalinity determination by titrations should be done within one day of sample collection (American Public Health Association, 1999). Therefore, the water samples were titrated in the field using a Schilling burette and 0.01M HCl titrant. A 25 ml sample was titrated to pH 4.3.

Alkalinity (mg/L $CaCO_3$) was calculated as:

$$\frac{\text{Volume (ml HCl)} \times \text{Concentration (M HCl)} \times 50000}{\text{Volume of inital sample}} \qquad (4.2)$$

and was reported as 'the alkalinity to pH 4.3 = __ in mg/L $CaCO_3$' (American Public Health Association, 1999).

4.5.2 Ion chromatographic analysis

Determinations for anions (Cl^-, SO_4^{2-}, F^-, Br^-) were performed by high performance ion chromatography (HPIC) at the CSIRO Laboratory at Kensington using an Metrohm (Ltd) modular ion chromatograph. The analysis of major anions would ideally have been done on the filtered and non-acidified groundwater sample.

However, storage problems with these samples during the summer 2005 program required that the analysis be done on the filtered acidified sample in July 2006 (Table 4-6) and as such the NO_3^- determinations have not been included in the results. The storage problems were traced back to freezing of the sample. Saline groundwater freezes at lower temperatures than pure H_2O. As the saline groundwater initially freezes pure ice forms, leaving the ions to concentrate in the unfrozen portion. Leakage of this concentrated unfrozen portion resulted in the loss of ions. On defrosting the ion concentrate of the whole sample is less than that of the sample when initially collected. This dilution was evident when the analyses data were validated.

In this study, a Metrohm METROSEP A Supp 5 250/4.0 separator column was used with an eluent of 3.2 mM Na_2CO_3 and 1.0 mM $NaHCO_3$ at a flow rate of 0.7 ml/min. The column used was calibrated to determine Cl^- concentrations up to 500 mg/L and SO_4^{2-} concentrations up to 75 mg/L.

4.5.3 Inductively Coupled Plasma–Mass Spectrometry (ICP–MS)

Trace element determinations (Au, Ag, As, Ba, Be, Bi, Cd, Ce, Cs, Dy, Er, Eu, Ga, Gd, Ge, Hf, Hg, Ho, In, La, Li, Lu, Mo, Nb, Nd, Pb, Pd, Pr, Pt, Rb, Re, Sb, Se, Sm, Sn, Sr, Ta, Tb, Te, Th, Tl, Tm, U, W, Y, Yb, Zr) by Inductively Coupled Plasma–Mass Spectrometry (ICP–MS) were conducted at Ultra Trace Analytical Laboratories in Canning Vale using a Perkin–Elmer Elan 6000ICP Mass Spectrometer using a Babington nebuliser.

Jarvis and Jarvis (1992) and Jarvis et al.(1992) categorised analytical interferences occurring in ICP–MS analysis into 3 groups: those resulting from the presence of polyatomic ions; doubly charged ions; and refractory oxides. Polyatomic ions form in the plasma from two or more atomic species such as ArO^+ and ArH^+. Other polyatomic ions include S from H_2SO_4 or Cl from HCl or $HClO_4$ which form combinations of $ArCl^+$, ClO^+ and ArS^+. The potential formation of these polyatomic ions constrains what acid can be used to stabilises groundwater samples. Nitric acid was used. Typical interferences by polyatomic ions are $^{40}Ar^{32}S^+$ on ^{72}Ge, $^{32}S^{16}O^+$ on ^{48}Ti and $^{40}Ar^{35}Cl^+$ on ^{75}As. Arsenic has no isotope that is free from interference. Therefore, in samples with significant Cl levels As determinations may be compromised.

Most of the ions which form in the plasma are singly charged (M^+), but elements with a second ionisation energy lower than 16 eV (first ionisation energy of Ar) will form doubly charged ions. The scale of measurement of mass is m/z or amu for a singly charged ion. If an element forms a doubly charged ion (M^{2+}) the signal is seen at a mass to charge ratio of two i.e. half the mass of the parent ion. Under normal operating conditions the production of doubly charged ions is small (Jarvis et al., 1992).

Formation of oxide species (MO^+) in the plasma may result from incomplete dissociation or recombination. These species occur 16, 17 or 18 amu above the parent ion (Jarvis and Jarvis, 1992). Examples of oxide formation are MnO^+ and FeO^+ (Jarvis et al., 1992).

According to Jarvis and Jarvis (1992) despite the range of possible spectroscopic interferences few actually cause problems.

4.5.4 Inductively Coupled Plasma– Atomic Emission Spectrometers (ICP–AES)

Major and trace element determinations (Co, Cu, Ni, Sc, Zn, Al, B, Ca, Cr, Fe, K, Mg, Mn, Na, P, S, Si, Ti, V) by Inductively Coupled Plasma–Atomic Emission Spectrometry were performed by Ultra Trace Analytical Laboratories using a Perkin–Elmer, Optima 3000ICP ICP Spectrometer.

Inductively Coupled Plasma–Atomic Emission Spectrometer (ICP–AES) uses the principle of viewing the appropriate region in the Ar plasma tail flame to determine the atomic and ionic emission lines of elements. Excited electrons emit energy at a given wavelength which is particular to its chemical character. Each element emits energy at multiple wavelengths but in this analytical technique it is most common to select a single wavelength for a given element.

Table 4-6 Summary of analysis history for the summer 2005 program.

Laboratory	*Analyte*	*Sampling method*					*Analysis method*				
		Collection	*Analysis*	*Filtered*	*Holding*	*Acidified*	*Method*	*Instrument*	*Column*	*Eluent*	*Time*
CSIRO	Cl^-, SO_4^{2-}, F^-, Br^-	March 2005	July 2005	Yes	-4 °C	No	IC	Metrohm	METROSEP A Supp 5 250/4.0	3.2 mM Na_2CO_3, 1.0 mM $NaHCO_3$	42
	Cl^-, SO_4^{2-}, F^-, Br^-	March 2005	June 2006	Yes	22 °C*	Yes	IC	Metrohm	METROSEP A Supp 5 250/4.0	3.2 mM Na_2CO_3, 1.0 mM $NaHCO_3$	42
Ultra Trace Analytical Laboratories	Various	March 2005	June 2005	Yes	22 °C*	Yes	ICP-AES	Perkin–Elmer, Optima 3000ICP ICP Spectrometer			
	Various	March 2005	June 2005	Yes	22 °C*	Yes	ICP-MS	Perkin–Elmer Elan 6000ICP Mass Spectrometer			

* Sample refrigerated in field, but held at 22 ºC in laboratory

Table 4-7 Summary of analysis history for the summer 2006–2007 program.

Laboratory	*Analyte*	*Sampling method*					*Analysis method*				
		Collection	*Analysis*	*Filtered*	*Holding*	*Acidified*	*Method*	*Instrument*	*Column*	*Eluent*	*Time*
CSIRO	Cl^-, SO_4^{2-}, F^-, Br^-	November 2006–May 2007	December 2006–June 2007	Yes	22 °C*	No	IC	Metrohm	METROSEP A Supp 5 250/4.0	3.2 mM Na_2CO_3, 1.0 mM $NaHCO_3$	42
Ultra Trace Analytical Laboratories	Various	November 2006–May 2007	December 2006–June 2007	Yes	22 °C*	Yes	ICP-AES	Perkin–Elmer, Optima 3000ICP ICP Spectrometer			
	Various	November 2006–May 2007	December 2006–June 2007	Yes	22 °C*	Yes	ICP-MS	Perkin–Elmer Elan 6000ICP Mass Spectrometer			

* Sample refrigerated in field, but held at 22 ºC in laboratory

These emissions are measured using an optical spectrometer and the intensity of the energy emitted is proportional to the concentration of the element in the analysed sample. Very high temperatures in the ICP ensure more efficient atomisation than techniques that use lower temperature flames such as atomic absorption spectrometry (AAS) (Jarvis and Jarvis, 1992).

The main types of spectral interferences with this technique are line coincidence, wing overlaps and continuum interferences. According to Jarvis and Jarvis (1992) interferences can be avoided or minimised by various techniques employed by the laboratory.

4.6 QUALITY CONTROL AND DATA VALIDATION

4.6.1 Statistical methods

The quality of the analyses were checked using general descriptive statistics. The method reproducibility or between-run precision was determined using mean ($\bar{x}$), standard deviation (σ), relative standard deviation (RSD), and confidence interval (CI). The repeatability or within-in run precision was determined using relative percent difference (RPD).

Mean ($\bar{x}$) was calculated as:

$$\bar{x} = \frac{\sum_{i=1}^{n} x_i}{n} \qquad (4.3)$$

where x is the value of the sample measurement, and n is the number of samples.

The standard deviation (σ) was calculated as:

$$\sigma = \sqrt{\frac{\Sigma(x - \bar{x})^2}{n-1}} \qquad (4.4)$$

The relative standard deviation (RSD) was calculated as:

$$\text{RSD} = 100 \times \frac{\sigma}{\bar{x}} \qquad (4.5)$$

and was reported as %.

Table 4-8 Reproducibility for the chloride standard.

Standard name	M7 100	M7 80	M7 60	M7 40	M7 20	M7 10
Nominal value (mg/L)	500	400	300	200	100	50
$\bar{x}$	501.69	391.17	308.75	203.97	99.40	48.35
σ	3.22	4.42	4.61	2.45	1.13	1.31
CI (95%)	2.16	4.09	4.27	2.26	1.05	1.21
RSD (%)	0.64	1.13	1.49	1.20	1.14	2.71
n	11	7	7	7	7	7

Table 4-9 Reproducibility for the sulfate standard.

Standard name	M7 100	M7 80	M7 60	M7 40	M7 20	M7 10
Nominal value (mg/L)	75	60	45	30	15	7.5
$\bar{x}$	75.90	58.87	45.39	29.93	14.79	8.09
σ	0.70	1.12	0.54	0.36	0.14	0.20
CI (95%)	0.44	0.94	0.45	0.30	0.12	0.17
RSD (%)	0.92	1.91	1.18	1.20	0.98	2.44
n	12	8	8	8	8	8

Table 4-10 Reproducibility for the bromide standard.

Standard name	M7 100	M7 80	M7 60	M7 40	M7 20	M7 10
Nominal value (mg/L)	2	1.6	1.2	0.8	0.4	0.2
$\bar{x}$	2.01	1.53	1.19	0.78	0.39	0.22
σ	0.08	0.04	0.03	0.04	0.02	0.01
CI (95%)	0.05	0.03	0.03	0.04	0.01	0.01
RSD (%)	4.20	2.45	2.73	5.62	4.31	5.35
n	13	8	8	8	8	8

Table 4-11 Reproducibility for the fluoride standard.

Standard name	M7 100	M7 80	M7 60	M7 40	M7 20	M7 10
Nominal value (mg/L)	0.3	0.24	0.18	0.12	0.06	0.03
$\bar{x}$	0.29	0.24	0.19	0.13	0.07	0.04
σ	0.05	0.01	0.01	0.01	0.02	0.01
CI (95%)	0.03	0.01	0.01	0.01	0.01	0.01
RSD (%)	16.32	5.43	6.07	9.97	21.05	33.07
n	13	7	8	8	8	8

The confidence interval (CI) around the mean was calculated as:

$$\bar{x} \pm t\left(\frac{\sigma}{\sqrt{n}}\right) \qquad (4.6)$$

where *t* is dependent on both the degrees of freedom (n-1) and the degree of confidence required.

The relative percent difference (RPD) (American Public Health Association, 1999) was calculated according to:

$$\text{RPD} = \frac{\text{sample result - duplicate result}}{(\text{sample result} + \text{duplicate result}) \div 2} \times 100 \qquad (4.7)$$

and was reported as %.

4.6.2 Reproducibility

Standard solutions, used to calibrate the Metrohm (Ltd) modular IC, were used to check the method reproducibility or between-run precision. The standard solutions used at CSIRO's Wet Chemical Laboratory were made in-house. The Cl^- and SO_4^{2-} exhibited the best reproducibility compared to Br^- and F^-.

The RSD (equation (4.5)) for Cl^- value ranged from 0.64 to 2.71% (Table 4-8) with the highest value being for the 50 mg/L sample. Similar values were found for the sulfate uncertainty with RSD ranging from 0.92 to 2.44% (Table 4-9). The bromide measurement uncertainty ranged from 2.45 to 5.62% (Table 4-10). The fluoride measurement uncertainty ranges from about 5% to over 33% (Table 4-11). In this

study, the results for Br^- were used with care, but the fluoride values were not acceptable and have not been used.

4.6.3 Repeatability

To check the uniformity of the samples, duplicates were collected in the field and analysed. The within-run precision or repeatability was checked using samples that were split at the time of analysis and were referred to as laboratory duplicates.

Field duplicates were collected to check that the sample result could be repeated. They were taken immediately after the initial sample and were subjected to the same filtering, preservation, holding and analysis methods. A field duplicate was collected from every 7th bore with a total of 19 field duplicates in total. The duplicates were submitted to the same laboratory in which the analysis was conducted.

The RPD for the anions are listed in Table 4-12. The RPD for: Cl^- range from -2.42 to 1.72; SO_4^{2-} from -1.05 to 4.81; and Br^- from -12.21 to 3.18%. Two of the Br^- are > 5% (MU10D and MU14S) otherwise the remaining 17 are < ± 3.18%. The cations had RPD values of less than 5% with most values < ± 3% (Table 4-13).

To check the reproducibility at CSIRO Wet Chemical Laboratory determinations every 5th sample was split. The replicate sample was analysed either directly after the initial sample or at the end of the sample run. A total of 31 replicate samples for anions were run at CSIRO (Table 4-14). A total of 14 laboratory replicates were analysed for cations (Table 4-15) and trace metals at Ultra Trace Pty Ltd.

Table 4-12 Repeatability for the anion field duplicates (diluted samples) with the RPD values >± 5% highlighted in grey. Anion values in mg/L.

	Dilution	*Chloride*		*RPD*	*Sulfate*		*RPD*	*Bromide*		*RPD*
	factor	*1*	*2*	*%*	*1*	*2*	*%*	*1*	*2*	*%*
MU02	20	265.99	266.42	-0.16	15.63	15.69	-0.41	0.65	0.64	0.78
MU02	12	457.99	459.05	-0.23	26.29	26.28	0.01	1.52	1.52	0.13
MU04	8	219.94	218.98	0.44	19.80	19.80	-0.01	0.57	0.56	1.07
MU10D	10	68.64	69.62	-1.43				0.10	0.11	-12.21
MU14S	15	180.39	177.31	1.72	26.53	26.66	-0.51	0.46	0.51	-10.42
MU24	20	205.03	203.98	0.52	28.05	28.02	0.11	0.48	0.46	3.18
MU34	8	239.78	239.86	-0.04	18.68	18.70	-0.12	0.56	0.57	-0.71
MU37D	15	186.73	188.71	-1.05	45.60	46.10	-1.08	0.47	0.48	-2.34
MU39	15	368.84	376.41	-2.03	21.50	21.57	-0.33	0.86	0.88	-1.84
MU48D	30	435.04	435.50	-0.11	45.27	45.19	0.17	0.77	0.76	0.39
MU55D	9	250.95	251.68	-0.29	24.38	24.37	0.03	0.53	0.53	0.19
MU59I	25	525.02	527.28	-0.43	57.99	58.62	-1.07	0.90	0.92	-1.32
MU61D	50	407.96	403.12	1.19	14.57	14.41	1.11	0.75	0.74	1.47
MU64D	15	191.45	196.14	-2.42	15.32	14.60	4.81	0.43	0.43	1.63
MU64I	9	256.04	256.64	-0.24	19.40	19.43	-0.18	0.63	0.63	-0.48
MU66D	8	239.38	240.88	-0.63	22.91	22.85	0.25	0.53	0.54	-1.50
MU68S	4	238.53	237.53	0.42	18.04	18.09	-0.27	0.59	0.58	1.53
PM04	7	229.27	228.77	0.22	31.49	31.71	-0.71	0.57	0.56	0.71
PM12	25	241.49	241.65	-0.07				0.66	0.66	0.61

Table 4-13 Repeatability for the cation field duplicates with cation values in mg/L.

Bore ID	*Calcium*		*RPD*	*Potassium*		*RPD*	*Magnesium*		*RPD*	*Sodium*		*RPD*
	1	*2*	*%*	*1*	*2*	*%*	*1*	*2*	*%*	*1*	*2*	*%*
MU02	338	338	0.00	2.4	2.4	0.00	969	970	-0.10	1900	1900	0.00
MU04	41.3	40.9	0.97	16.2	16.1	0.62	166	167	-0.60	990	964	2.66
MU10D	26.1	26.6	-1.90	15.8	16	-1.26	46.9	47.5	-1.27	454	453	0.22
MU14S	72.5	72.2	0.41	18.9	18.8	0.53	232	228	1.74	1510	1510	0.00
MU24	110	109	0.91	39.7	39.5	0.51	332	325	2.13	2700	2730	-1.10
MU34	109	110	-0.91	11	11.2	-1.80	139	138	0.72	1070	1080	-0.93
MU37D	235	233	0.85	22.1	21.9	0.91	258	256	0.78	1580	1560	1.27
MU39	33.6	33.6	0.00	5.5	5.5	0.00	417	412	1.21	3130	3240	-3.45
MU48	1230	1230	0.00	24	24	0.00	1330	1340	-0.75	5850	5980	-2.20
MU55D	107	106	0.94	8.5	8.5	0.00	245	241	1.65	1140	1130	0.88
MU59I	973	964	0.93	72.5	71.5	1.39	1140	1130	0.88	6810	6630	2.68
MU61D	4930	4820	2.26	39.5	39.5	0.00	1770	1790	-1.12	5450	5560	-2.00
MU64D	214	209	2.36	14.6	14.8	-1.36	244	244	0.00	1510	1520	-0.66
MU64I	51.1	51.5	-0.78	11	11.3	-2.69	197	200	-1.51	1300	1320	-1.53
MU66D	75.8	75.8	0.00	5.9	5.9	0.00	163	163	0.00	1030	1040	-0.97
MU68S	32.1	31.8	0.94	4.1	4	2.47	101	98.8	2.20	467	462	1.08
PM04	65.5	65.2	0.46	10.4	10.4	0.00	131	131	0.00	939	929	1.07
PM12	203	203	0.00	17	17	0.00	553	564	-1.97	3300	3270	0.91

Table 4-14 Repeatability for the anion laboratory duplicates with the RPD values >± 5% highlighted in grey. Anion values in mg/L.

	Dilution	*Chloride*		*RPD*	*Sulfate*		*RPD*	*Bromide*		*RPD*
	factor	*1*	*2*	*%*	*1*	*2*	*%*	*1*	*2*	*%*
MU07S	30	209.12	212.26	-1.49	34.49	35.00	-1.48	0.60	0.61	-2.64
MU11I	15	148.98	148.60	0.25	26.93	26.99	-0.24	0.42	0.44	-4.20
MU12A	15	245.41	243.43	0.81	26.85	26.80	0.19	0.68	0.73	-7.06
MU13	10	225.37	224.04	0.59	13.98	13.68	2.16	0.64	0.58	9.94
MU14S	15	180.39	175.86	2.54	26.53	26.55	-0.10	0.46	0.47	-2.60
MU22S	15	411.21	410.57	0.16	35.68	35.51	0.46	0.62	0.60	2.95
MU23D	25	191.42	192.32	-0.47	22.74	22.83	-0.40	0.44	0.43	0.92
MU29S	30	296.76	295.30	0.49	22.98	22.81	0.72	0.73	0.72	0.97
MU30D	35				20.01	20.07	-0.33	0.85	0.85	-0.59
MU30S	10	79.74	80.03	-0.37	9.68	9.96	-2.87	0.22	0.22	-2.73
MU31D	30	342.85	345.16	-0.67	18.73	18.63	0.53	0.66	0.68	-2.38
MU32	15	252.92	255.79	-1.13	24.81	25.20	-1.57	1.014	0.98	3.41
MU32	10	389.13	389.60	-0.12	40.52	40.44	0.20	0.99	1.01	-2.80
MU35	20	287.79	292.18	-1.51	29.57	29.55	0.08	0.58	0.58	1.03
MU36D	10	169.37	169.08	0.17	11.60	11.52	0.68	0.31	0.34	-10.40
MU38D	10	28.88	29.25	-1.27						
MU40S	35	251.03	249.29	0.69	25.95	25.90	0.20	0.47	0.48	-1.26
MU41S	10	113.08	114.28	-1.06	9.05	9.12	-0.79	0.30	0.30	-1.68
MU43S	10	225.80	225.82	-0.01	13.49	13.79	-2.26	0.57	0.57	0.70
MU49	7	206.74	207.56	-0.40	12.60	12.53	0.59	0.33	0.33	1.21
MU52S	15	211.94	210.54	0.66	10.81	10.38	4.00	0.49	0.49	0.00
MU59D	60	529.98	530.10	-0.02	53.87	53.58	0.54	0.90	0.89	0.67
MU62S	6	204.90	205.80	-0.44	10.30	9.78	5.18	0.45	0.47	-3.68
MU66S	9	267.48	267.21	0.10	22.00	21.13	4.05	0.58	0.62	-6.68
MU67D	8	279.34	276.65	0.97	11.26	10.85	3.74	0.72	0.76	-4.59
MU67S	8	214.85	212.75	0.98	12.74	12.20	4.33	0.54	0.57	-4.33
MU69	30	485.66	482.88	0.57	20.13	20.00	0.66	0.89	0.86	3.19
MU71	5	182.80	179.68	1.72	13.88	13.69	1.35	0.31	0.32	-2.86
MU72	12	421.09	421.01	0.02	28.88	28.87	0.04	1.45	1.46	-0.48
PM01	40	308.90	313.27	-1.41	21.70	21.40	1.42	0.53	0.54	-1.31
PM02	20	208.42	212.39	-1.89	13.18	13.17	0.08	0.51	0.50	0.99
PM02	10	443.91	440.50	0.77	26.79	26.88	-0.35	1.46	1.48	-1.16

Table 4-15 Repeatability for the cation laboratory duplicates with cation values in mg/L.

Bore ID	*Calcium*		*RPD*	*Potassium*		*RPD*	*Magnesium*		*RPD*	*Sodium*		*RPD*
	1	*2*	*%*	*1*	*2*	*%*	*1*	*2*	*%*	*1*	*2*	*%*
MU02	338	335	0.89	2.4	2.4	0.00	969	955	1.46	1900	1870	1.59
MU09S	190	189	0.53	12.5	12.5	0.00	647	641	0.93	2430	2410	0.83
MU12S	14.3	14.5	-1.39	10.4	10.3	0.97	55.5	56.6	-1.96	618	623	-0.81
MU14S	72.5	72.3	0.28	18.9	19	-0.53	232	230	0.87	1510	1520	-0.66
MU23D	303	300	1.00	23.5	24	-2.11	396	392	1.02	2550	2550	0.00
MU36S	34.2	34	0.59	4.5	4.6	-2.20	84.2	83.8	0.48	586	589	-0.51
MU39	33.6	33.2	1.20	5.5	5.5	0.00	417	412	1.21	3130	3200	-2.21
MU45D	688	706	-2.58	418	420	-0.48	3970	4100	-3.22	28000	28000	0.00
MU58S	771	766	0.65	5.5	5.5	0.00	1290	1290	0.00	6010	6200	-3.11
MU67D	507	503	0.79	14.1	13.8	2.15	33.6	32.8	2.41	922	910	1.31
MU69	171	172	-0.58	76	76.5	-0.66	919	924	-0.54	7950	8050	-1.25
MU70	209	217	-3.76	24.8	24.9	-0.40	511	511	0.00	1960	1960	0.00
MU71	8.3	8.2	1.21	16.1	15.9	1.25	21.6	21.2	1.87	760	760	0.00
PM03	44.5	45.1	-1.34	9.4	9.6	-2.11	132	133	-0.75	901	928	-2.95

The RPD for the anions are listed in Table 4-14. Again, the greatest variability is seen in the Br^- analyses (-10.40 to 9.94%.) with 27 of the 31 samples having a variability < 5%. The RPD for the Cl^- ranges from -1.89 to 2.54, SO_4^{2-} from -2.87 to 5.18%.

4.6.4 Data validation

The accuracy of the water analyses was estimated using the charge balance method which is also referred to as the anion-cation balance (American Public Health Association, 1999; Appelo and Postma, 2005; Freeze and Cherry, 1979). Water is electrically neutral. Therefore, the sum of the positive ionic charges should equal the sum of the negative ionic charges. The charge balance equation is based on the percentage difference defined as:

$$\%difference = 100 \times \frac{\sum cations - \sum anions}{\sum cations + \sum anions} \qquad (4.8)$$

where cations and anions are expressed in meq/L (American Public Health Association, 1999).

Generally, the major cations and anions are used to calculate equation (4.8). Freeze and Cherry (1979) suggested the major ions should include Na^+, Mg^+, Ca^+, Cl, HCO_3^- and SO_4^{2-} whereas Appelo and Postma (2005) also included K^+ and NO_3^-. Errors within ± 5% are considered acceptable.

The initial data validation in July 2005 indicated problems with the results. The anion-cation balance showed that only 12 samples of the 57 had an acceptable balance of ± 5%. Resolving this issue involved checking of initial work such as the quality of chromatograms and sample dilution technique; additional research of the literature. As part of the process, groundwater samples were reanalysed using techniques such as spiking of samples. Sample leakage as discussed in section 4.5.2 when freezing was finally identified as the cause of low anion values.

Final data validation on samples showed that 90% of the 140 samples had electron balance ± 5% with the maximum error being 13%. Of these 15 samples 10 had errors between 5 and 6%. All charge balances are listed in Appendix 4 Table 5.

4.7 GROUNDWATER MODELING

Saturation indices were calculated using PHREEQC software. The program is designed to perform a wide variety of low-temperature aqueous geochemical calculations in natural or polluted water (Parkhurst and Appelo, 1999). PHREEQC uses ion-association and Debye-Hückel expression to account for the non ideal behaviour of the solution.

For aqueous solutes, the standard state is defined as an ideal solution with solute concentration of 1 mol/Kg H_2O = 1 modal (Appelo and Postma, 2005). Groundwater is not an ideal solution. To correct for the non ideal behaviour of groundwater an activity coefficient (γ_i) is applied. The activity coefficient is calculated using the Debye-Hückel theory and the ionic strength (*I*) (Appelo and Postma, 2005):

$$I = 1/2 \sum (m_i / m_i^{o} \times z_i^2) \equiv 1/2 \sum m_i \times z_i^2 \qquad (4.9)$$

where m_i is the molality (mol/kg H_2O), m_i^0 is the standard state and z_i is the charge of the ion *i*. For water with an $I < 0.1$, the Debye-Hückel equation defines the activity coefficient (γ_i) as:

$$\mathrm{Log}\gamma_i = -\frac{Az_i^2\sqrt{I}}{1 + B\overset{\circ}{a}_i\sqrt{I}} \qquad (4.10)$$

where *A* and *B* are temperature dependent constants. At 25°C A = 0.5085 and B = 0.3285X10^{10}/m. The empirical ion-size parameter is $\overset{\circ}{a}_i$.

The Davies equation is used by PHREEQC to overcome the problems with higher ionic strength water. This equation is a modified Debye-Hückel equation (Parkhurst and Appelo, 1999):

$$\mathrm{Log}\gamma_i = -Az_i^2\left(\frac{\sqrt{I}}{1+\sqrt{I}} - 0.3I\right) \qquad (4.11)$$

The Davies equation is applicable up to ionic strengths of 0.5 (Appelo and Postma, 2005). Over 90% of the groundwater analysed in the study had ionic strengths of 0.5 or less. Thus PHREEQC has been used.

5 Geology

5.1 INTRODUCTION

The main focus of this chapter is the landform evolution since in the study area since the commencement of sea-floor spreading between Australia and Antarctica in the Eocene. The chapter will include a discussion of the lithostratigraphy, the lateral and the vertical extent of regolith materials, and the depositional and erosional environments. The local geology will then be placed within context of the regional geology. The regolith units will be identified as they are important to both the movement and hydrochemical evolution of groundwater within the study area. Boreholes referred to in this chapter can be found on Figure 4–1.

The study area is situated mainly on the Proterozoic Albany–Fraser Orogen near the boundary between the Proterozoic Albany–Fraser Orogen and the Archaean Yilgarn Craton (Figure 5–1 and Figure 5–2). It is predominantly underlain by quartzo-feldspathic gneisses, mainly derived from granitoid rocks of the Biranup and Nornalup complexes (Myers, 1990) of the Albany–Fraser Orogen. In its northeast part, it is underlain by granitic rocks of the Archaean Yilgarn Craton (Wilde and Walker, 1984).

Late Eocene sediments of the Werillup and Pallinup Formations overlie basement to form the onshore margin of the Eucla Basin (Clarke et al., 2003; Hocking, 1990). The sediments are poorly exposed being covered by extensive ferricrete and thin alluvium and colluvium. Consequently, their distribution within the study area is poorly understood and is currently based upon historical coal exploration and regional mapping (Dampier Mining Company Limited, 1981; De Silva, 2004; Wilde and Walker, 1984). Distinct depositional facies have been recognised for the Werillup and Pallinup Formations in the Eucla Basin (Clarke et al., 2003; Gammon et al., 2000a; Holdgate and Clarke, 2000), but not within the study area. The lack of detailed geological information within the study area reflects the regional scale of past mapping programs.

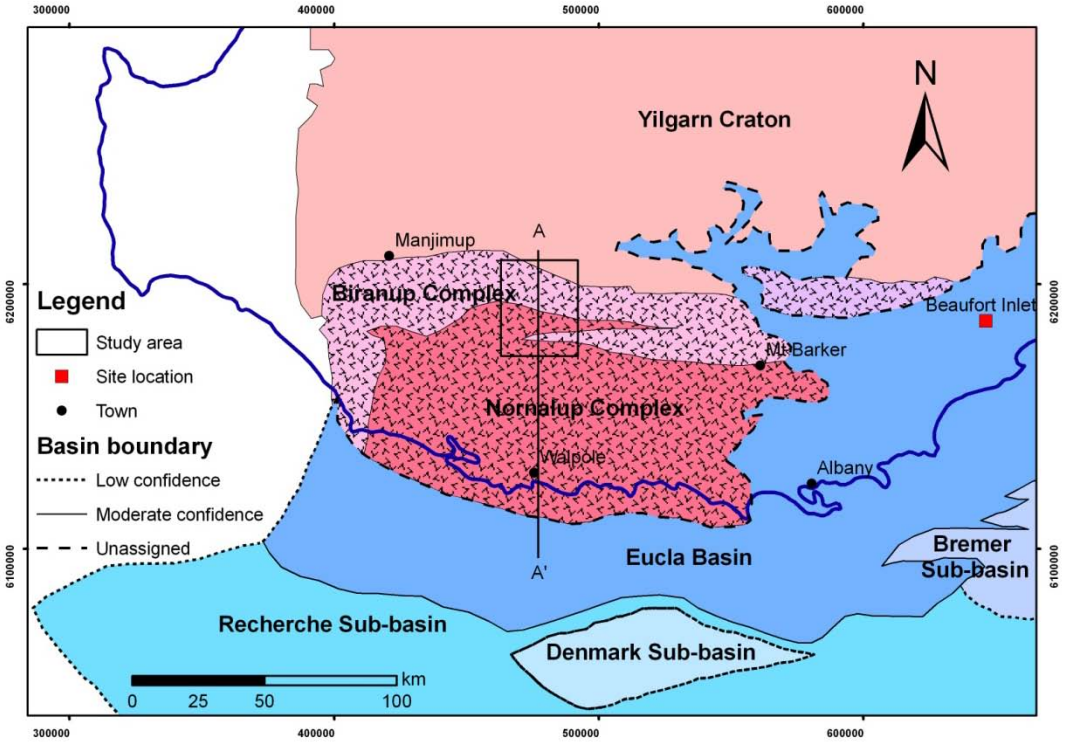

Figure 5–1 Regional geological setting after Bradshaw et al. (2003) and Myers (1990). See Figure 5–2 for section A–A'.

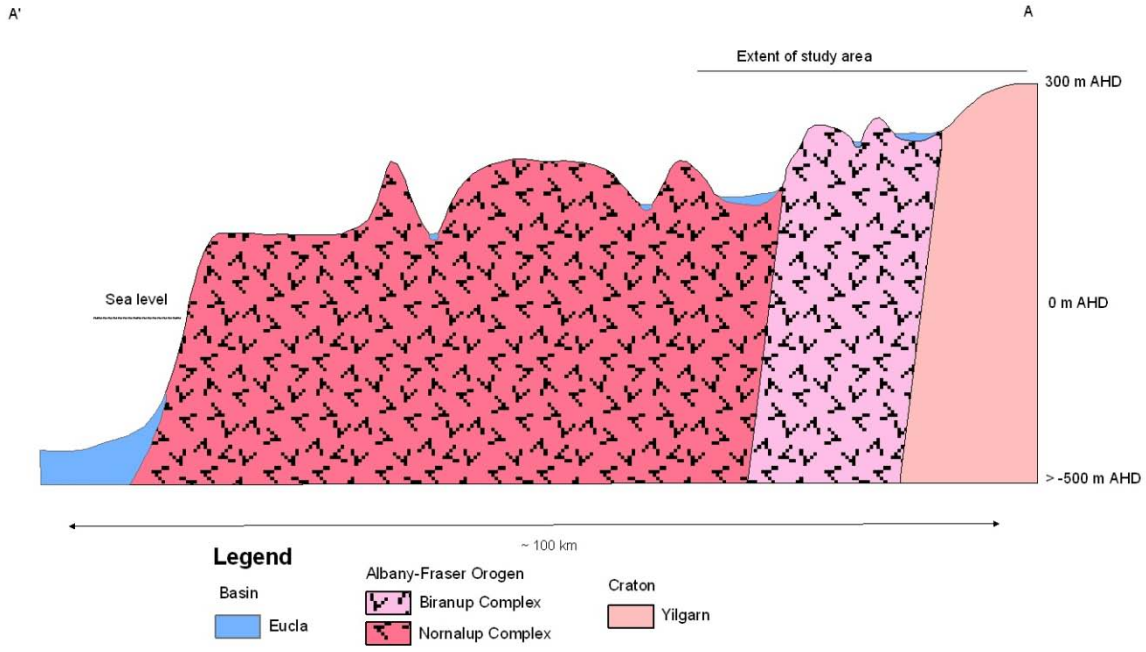

Figure 5–2 Diagrammatic section showing the relationship of the hard rock provinces and sedimentary basin (see Figure 5–1 for section line).

Extensive work has been undertaken on palaeochannels on the Yilgarn Craton (Clarke, 1993; 1994; de Broekert and Sandiford, 2005; Johnson et al., 1999) as the sediments within these channels contain significant resources of gold, uranium and groundwater. The work of de Broekert and Sandiford (2005), combined with that on tectonic setting (Norvick and Smith, 2001; Veevers, 2000), geology (Bradshaw, 2006; Clarke et al., 1996; 2003; Gammon and James, 2001; Gammon et al., 2000a; Li et al., 2003), and the evolution of the south-west river systems (Beard, 1999), has been used in the present study to give the regional setting to the late Eocene deposits in the study area.

5.2 TERMINOLOGY

5.2.1 Palaeochannel deposits

The term palaeochannel deposit has been problematic for many years. After comparison with modern rivers such as the Amazon and Mississippi Rivers, Schumm (1977) concluded that the documented palaeochannel deposits are most likely to be sediment deposited in a shifting and aggrading river channel over time. To clarify the landscape in which the deposits were laid down, de Broekert and Sandiford (2005) used the term inset-valley to reflect a valley that has been incised into an older valley on the Yilgarn Craton.

In this thesis the term palaeochannel has been retained as it is the term most commonly used to describe the subcrop of Eocene sediments in depressions eroded in basement rocks of the region, However, it is recognised that the palaeochannel sediments consist of both fluvial sediments and marine sediments infilling the late Eocene valleys.

5.2.2 Regolith units

Regolith is defined as (Eggleton, 2001)

The entire unconsolidated or secondary recemented cover that overlies more coherent bedrock, that has been formed by weathering, erosion, transport and/or deposition of older material.

A regolith unit

is a subdivision of the regolith, generally mappable.

Depositional facies analysis would allow examination of the fluvial and marine sediments , but is limited when dealing with the weathered basement. Whereas, regolith science allows all units to be described including the fluvial and marine sediments. Regolith terminology is used in this study.

5.3 REGIONAL SETTING

Current understanding of the tectonic evolution in the southwest margin of Australia since its separation from Antarctica is based on work by the Geological Survey of Western Australia (1990) and more recently, results of the international Deep Sea Drilling Program.

5.3.1 Australian-Antarctic separation

The separation of southern Australia from Antarctica has been divided into 3 tectonic phases (Norvick and Smith, 2001) (Figure 5-3). The first phase from Late Jurassic to Cretaceous was characterised by rifting. The second phase characterised by basin development commenced in the Cenomanian and involved sea-floor spreading from the early Campanian (~83.5 Ma). The third phase commenced at about 45 Ma during the Lutetain (middle Eocene) and extends to today. It is characterised by the final separation of Australia and Antarctica and collapse of the continental margin with widespread marine transgressions.

Sedimentation in the Bight Basin commenced off southern Australia (Bradshaw et al., 2003) during the first (rifting) phase. The Bight Basin contains several sub-basins including the Denmark, Recherche and Bremer Sub-basins (Figure 5–1). Sediments (8000 m thick) of the Bremer Sub-basin were deposited in ancient rivers and lakes during the Late Jurassic and Early Cretaceous (Bradshaw, 2006) (Figure 5–3). West of this sub-basin is the little known Denmark Sub-basin (Figure 5–1 and Figure 5–3) containing 2000 m of inferred Mesozoic age sediments unconformably overlain by 500 m of Cenozoic sediments (Bradshaw et al., 2003).

At the end of the first phase, the continental crust off south-western Australia started to thin (Norvick and Smith, 2001) enabling sea-floor spreading to commence in phase two. The rate of sea-floor spreading was about 0.8 cm/yr (Li et al., 2003). The sea between Australia and Antarctica was restricted as a connection remained through Tasmania (Muller et al., 2000).

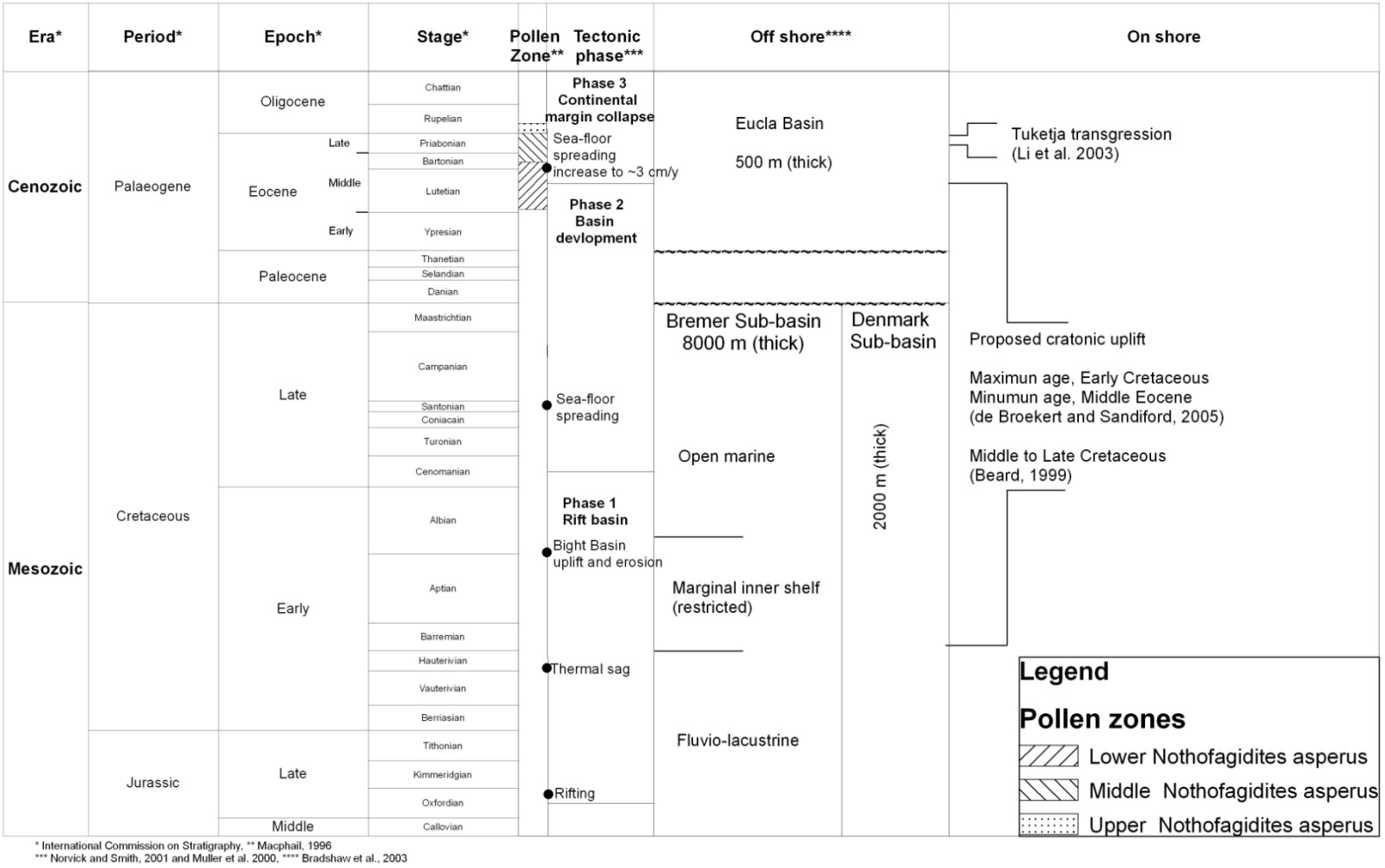

Figure 5–3 Summary of main geological and tectonic events as Australia separated from Antarctica.

During the third phase, the rate of sea-floor spreading increased to about 3 cm/yr (Li et al., 2003; Veevers, 2000) and was accompanied by rapid thermal subsidence producing a marine transgression along much of Australia's continental margin (Norvick and Smith, 2001). Results of the Tuketja transgression which occurred in the Eucla Basin in the late Eocene (Norvick and Smith, 2001) are evident in the study area. Antarctica had separated by about 35 Ma (late Eocene) but the Circum-Antarctic currents were not fully established until the late Oligocene (~25 Ma) (Norvick and Smith, 2001).

5.3.2 River systems

The source of the sedimentary deposits of the Bremer, Denmark and Recherche Sub-basins was probably the Yilgarn Craton. Apatite fission track thermochronology suggests that the topographic surface of southwestern Australia was very different in the Cretaceous than today. In the Early Cretaceous (130 Ma) the elevation of the land surface to the north and possibly west of the study area is estimated to have been between 600 and 1800 m above sea level (Kohn et al., 2002). By the Late Cretaceous elevations were reduced to between 0 and 600 m.

Regional drainage during the Cretaceous is thought to have been towards the south to southeast (Beard, 1999; de Broekert and Sandiford, 2005; Exon et al., 2005). De Broekert and Sandiford (2005) suggested that drainage flowed from the eastern Yilgarn Craton across the Eucla Basin into the Eyre and Recherche Sub-basins of the Mesozoic Bight Basin. Beard (1999) postulated that the now west flowing Yilgarn River flowed south from the Yilgarn Craton across the Albany–Fraser Orogen into the rift zone between Australia and Antarctica until uplift of the Yilgarn Craton in the Middle to Late Cretaceous (Figure 5–3).

There has been limited work on the drainage systems in the southwest corner of Western Australia, but Beard (1999) noted that there are no obvious gaps in the watershed between the southern boundary of the Blackwood River catchment and the northern catchment boundaries of the Warren and Frankland Rivers (Figure 1–1). This would suggest that the Warren and Frankland Rivers formed as a result of uplift of the Yilgarn Craton and flowed predominately south.

De Broekert and Sandiford (2005) also proposed that an uplift event played a major role in the creation of inset-valleys on the Yilgarn Craton. They placed the time of uplift between Early Cretaceous and early middle Eocene, with the maximum age based on the incision of inset-valleys into Early Cretaceous sediments and the minimum age based on the presence of siliciclastic sand of possibly early middle Eocene age in the Eyre Sub-basin. Clarke (1994) contended that uplift north of the Jarrahwood axis must have occurred prior to the Jurassic and that some rivers prior to the uplift flowed north. If the inferred Mesozoic age for the sediments of the Denmark Sub-basin (Bradshaw et al., 2003) is correct, then the rivers would have been flowing south during the Mesozoic within the vicinity of southwest coast of Australia.

5.3.3 Tuketja transgression

Acceleration of the sea-floor spreading rate around 43 Ma coincided with basin subsidence rates of 300 m/10^6 yr 100 km offshore and between 30–50 m/10^6 yr near shore (Li et al., 2003). The Tuketja transgression is placed between about 34.65 and 37.1 Ma during the late Eocene (Li et al., 2003).

The transgression contributed to the in-filling of inset-valleys in the mid to late Eocene (Clarke et al., 2003; de Broekert and Sandiford, 2005). During the transgression the clastic and organic rich sediments of the Werillup Formation were deposited in a fluvial environment prior to the deposition of the spicular marine sediment of the Pallinup Formation (Clarke et al., 2003).

5.4 AGE CORRELATION WITH THE WERILLUP FORMATION

Pollen analysis has confirmed that sediments within the study area contain assemblages consistent with the Upper *Nothofagidites asperus* palynomorph zone (Figure 5–3), and therefore can be correlated with the Werillup Formation as defined by Clark et al. (2003). No formal palynostratigraphic framework has been constructed for the Eocene sediments of Western Australia. Previous work by Stover and Partridge (1982) on pollen assemblages from the Werillup Formation has dated the sediments as late Middle to early late Eocene using a zonation scheme developed for the Gippsland Basin in eastern Australia. Milne (2003) cautioned that Western Australian Tertiary pollen assemblages do not correlate well with eastern Australian

Gippsland Basin zonation, as index species from several zones occur together. However, assemblages from the Murray Basin reported by Macphail (1996) are similar to the Western Australian assemblages. The age assessments given by Milne (2003) follow the zonation of Macphail (1996).

Table 5-1 Age and correlation (based on zonation of Macphail, 1996) for the Werillup Formation in the study area as determined by Milne (2003).

Bore hole ID	Sample depth (m)	Provisional age	Palynomorph zone
MU14D	22–23	Late Eocene–earliest Oligocene	?Middle *N. asperus* Zone Equivalent to Upper *N. asperus* Zone Equivalent
MU14D	26–27	Late Eocene	Middle *N. asperus* Zone Equivalent
MU14D	29–30	Late Eocene	Middle *N. asperus* Zone Equivalent

Pollen analysis (Milne, 2003) of three samples from bore MU14D has placed the sediments into two palynomorph zones (Table 5-1). A palynomorph assemblage equivalent to Middle *N. asperus* Zone Equivalent has been identified from depths 26 to 27 m and 29 to 30 m. The suggested age for this zone is late Eocene. The palynomorph assemblage extends from ?Middle *N. asperus* Zone Equivalent to Upper *N. asperus* Zone Equivalent at depth 22 to 23 m. This assemblage has been given a provisional age of late Eocene to earliest Oligocene.

5.5 PREVIOUS WORK ON THE WERILLUP AND PALLINUP FORMATIONS

5.5.1 Regional studies

The Werillup Formation is described as consisting predominately of fluvial sediments comprising a channel sand facies with a flood plain facies (Clarke et al., 2003; Holdgate and Clarke, 2000). The channel sediments contain an upward-fining succession of basal gravel and sand grading into silt and then clay. In contrast, the flood plain lithology consists of massive silty kaolinitic clays with thin bands of lignite. The lignites thin towards the upper reaches of the palaeo-valleys.

The Pallinup Formation has been described as a shallow marine sequence of sediments deposited under low energy conditions in a warm sea of normal salinity (Gammon et al., 2000b). In the Eucla Basin, these sediments grade from sponge-rich

facies to muddy spiculites and spiculitic mudstones interpreted as having formed within protected shoreface environments and low energy offshore environments, respectively. Calcareous fossils are rare in these facies, but where present have been interpreted as forming in an open-shelf environment (Gammon and James, 2001). About 50 km inland of the present coastline, this marine sequence abutted a late Eocene palaeo-escarpment (Gammon and James, 2001). The Pallinup Formation is also preserved along river systems (Gammon and James, 2001; Gammon et al., 2000a).

The Pallinup Formation has been subdivided into 5 units: the informal units 1 to 4; and the Fitzgerald Member (Gammon et al., 2000b). According to Gammon et al. (2000b) units 1 and 2 are transgressive; whereas the finest grained units 3 and 4 coincided with peak relative sea-level and maximum flooding; and the Fitzgerald Member is regressive. The informal units 1 and 2, are basal sandstone units with unit 1 being a medium grained sandstone and unit 2 a fine grained sandstone (Gammon et al., 2000a). Unit 2 contains up to 20% sponge spicules but the spicules are absent from some beds. Units 3 and 4 are a spiculitic mudstone with up to 30% of sponge spicules.

5.5.2 The study area

Late Eocene sediments identified within the study area were considered to form part of the Plantagenet Group infilling old drainage channels (Dampier Mining Company Limited, 1981; Wilde and Walker, 1984). More recent work has suggested locations for the palaeochannels (Chakravartula and Street, 2000; De Silva, 2000; Smith, 1997; 2003). It was proposed by De Silva (2000) that at least three palaeochannels exist within the study area: the Unicup; the Noobijup; and the Lake Muir palaeochannels (Figure 5–4). The Unicup and Noobijup palaeochannels trend west to east and the Lake Muir palaeochannel northwest to southeast. The sediments within the channels consist of plastic clay, carbonaceous clay, silt and sand of the Werillup Formation. The location of the palaeochannels was based on limited exploration drilling for coal (LM bores) and groundwater (PM bores). The work by De Silva (2000, 2004) indicated that the thickness of the sediments ranged from: 39 to > 42 m for the Unicup palaeochannel; 37 to 73 m for the Noobijup palaeochannel; and 37 to 46 m for the Lake Muir palaeochannel.

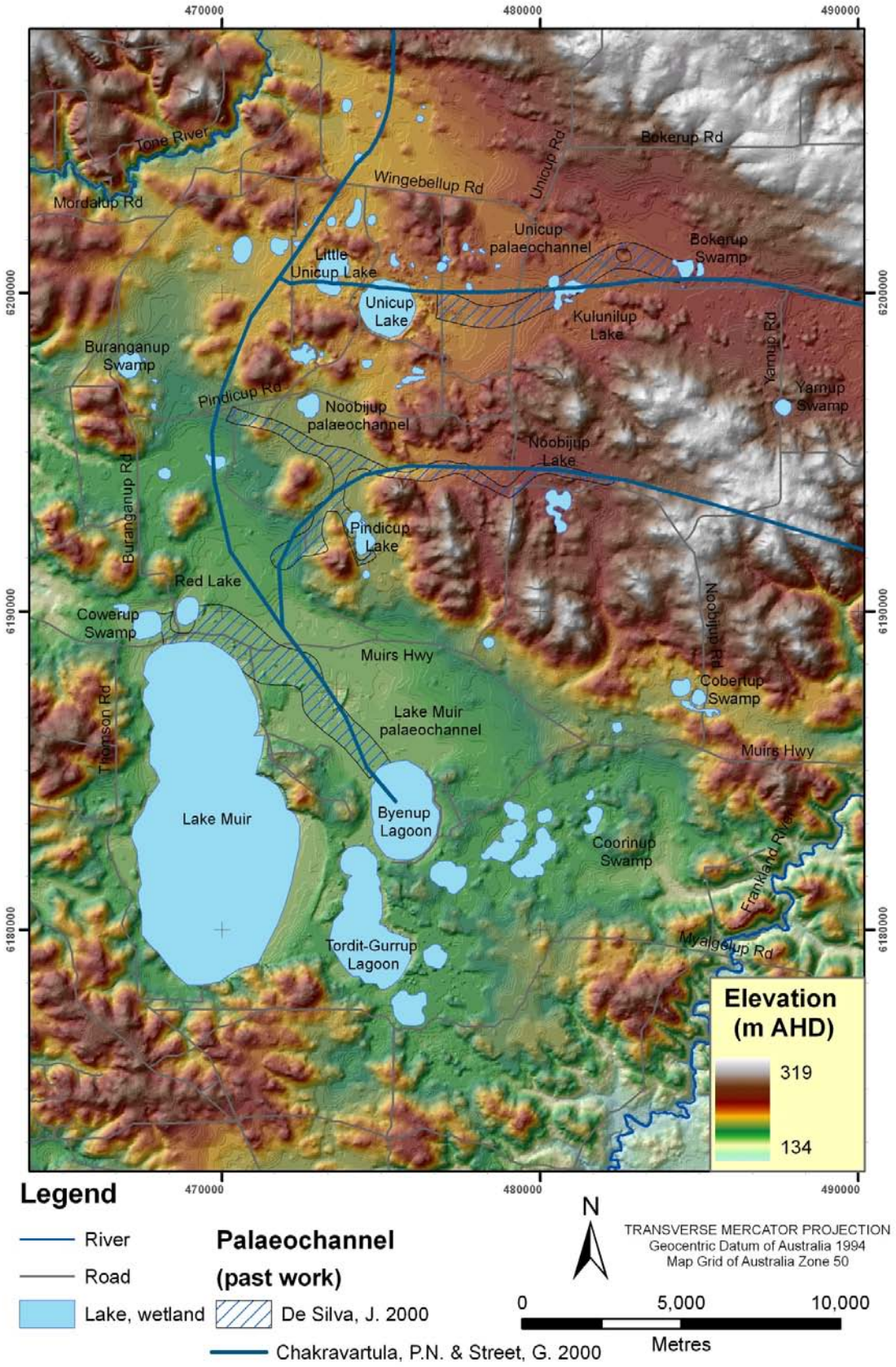

Figure 5–4 Position of the palaeochannels based on the work by Chakravartula and Street (2000) and De Silvia (2000, 2004).

The Pallinup Formation was not identified within the study area (De Silva, 2000; 2004; Panasiewicz et al., 1997; Wilde and Walker, 1984). However, Smith (2003) noted that sponge spicules had been recorded from one borehole (PM10) and consequently included the Pallinup Formation in his discussion on sedimentary aquifers.

Airborne geophysical investigations including magnetic and radiometric surveys were flown over the study area in 1998. Chakravartula and Street (2000) were unable to delineate the Eocene sediments with confidence using the magnetic data. They mapped palaeochannels but did not present the geophysical evidence used in their identification. Two palaeochannels mapped by Chakravartula and Street (2000) flow west and follow a similar path to the Unicup and Noobijup palaeochannels (Figure 5–4). These join a north to south flowing channel located west of Unicup Lake and to the northeast of Lake Muir flowing under the Byenup Lagoon. Chakravartula and Street (2000) produced a detailed map of faults within the study area from the geophysical data. Most major faults are orientated west and northwest, with the minor faulting being both northwest and northeast (Chakravartula and Street, 2000).

5.6 LITHOSTRATIGRAPHY OF THE STUDY AREA

Regolith within the study area consists of weathered basement rocks and sediments (Figure 5–5). The Werillup Formation is preserved in ancient valleys where it unconformably overlies either fresh or weathered basement rock. The Pallinup Formation, identified in this study, conformably overlies the Werillup Formation. A ferricrete is found throughout the study area and in places has features that indicate transport. The ferricrete overlies the late Eocene sediments of the Pallinup Formation. Where the Pallinup Formation is absent, the ferricrete lies on top of weathered basement rock. Quaternary sediments mostly overlie the ferricrete, but also lie directly upon the Werillup Formation where the Pallinup Formation has been eroded. Weathered basement rock is found throughout the study area.

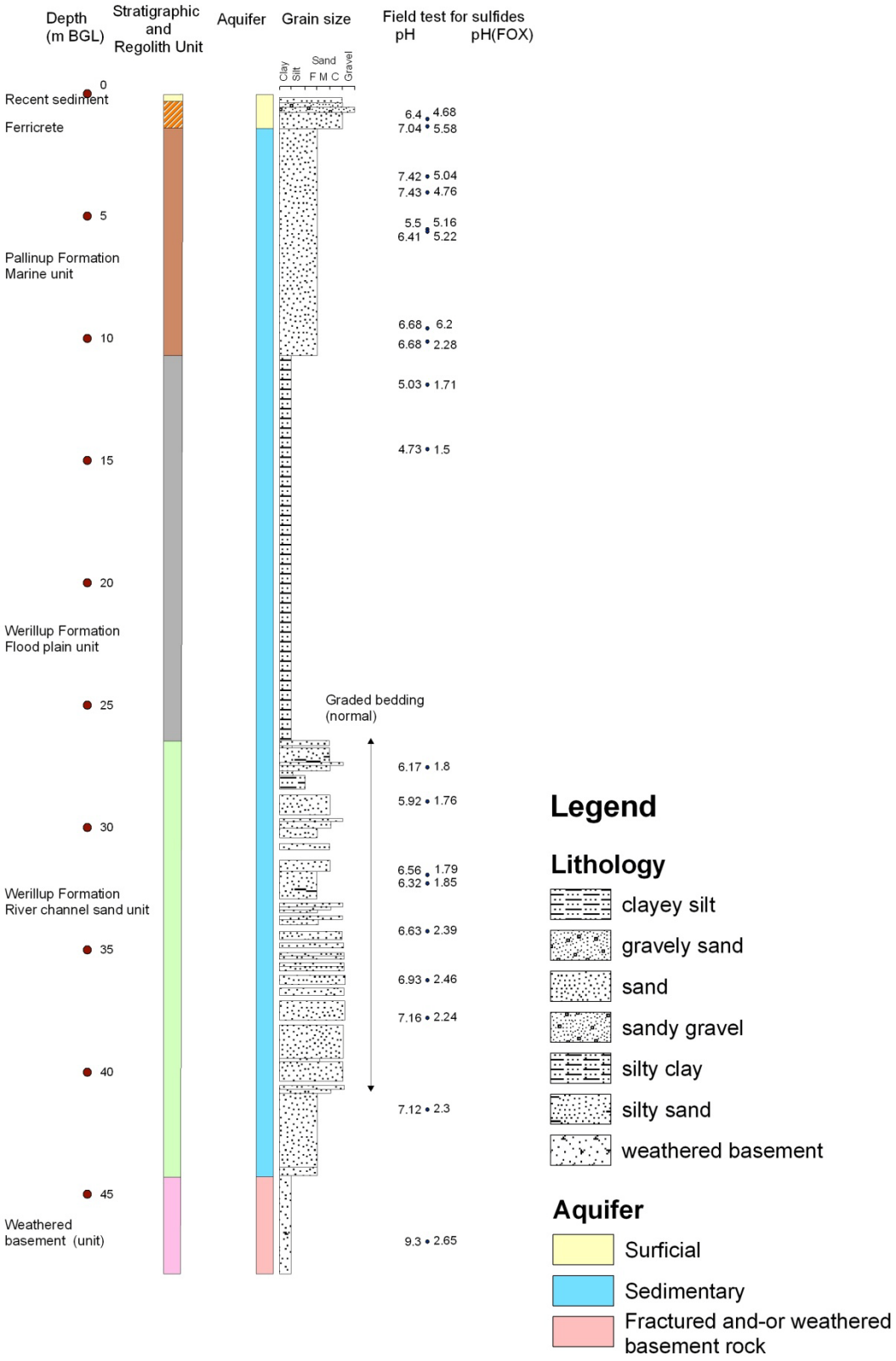

Figure 5–5 Lithologic log of borehole MU12A showing relationship of regolith units to the stratigraphic units and aquifers.

5.6.1 Weathered basement rock

Crystalline rocks are extensively weathered in the study area. The weathered mantle extends from the low lying hills in the northeast, over the two ridges in the centre of the study area, to the plateau along the southern edge of the study area. It is also present under the broad-valley floors and plains.

It is either covered by ferricrete or sediments, and is exposed only in some road cuttings and dam walls. In the low lying areas, the weathering is of variable thickness, ranging from 1 to 43 m, but is generally less than 20 m. Greater thicknesses recorded in bores MU46D and MU49 are associated with fault zones. On the hills, limited drilling suggests that thickness of the weathered basement rock varies from less than 5 m (MU50) to about 22 m (MU01).

Various classification schemes have been proposed to describe the weathering profiles (Anand and Paine, 2002; Anand et al., 1989; Eggleton, 2001; Nahon and Tardy, 1992) and are summarised in Figure 5–6. Directly above the fresh rock is saprock in which less than 20% of the weatherable minerals are altered. Up profile, the saprock grades into saprolite which has over 20% of the weatherable materials altered, but the parent rock remains identifiable. This zone is termed coarse-grained saprolite by Nahon and Tardy (1992). The plasmic (clay) or arenose (sandy) zone has lost the fabric of the parent rock (Anand and Paine, 2002) and is referred to as fine-grained saprolite by Nahon and Tardy (1992) (Figure 5–6). Above the plasmic or arenose zone is the mottled zone and then the ferricrete. The zonation of Nahon and Tardy (1992) has been adopted in the present study.

Weathered basement rock in the study area comprise clay to gravely sand and has an extensive range of colours, dominated by greenish grey through to white. The sandy and gravely sections (equivalent of coarse-grained saprolite) are generally found above the fresh rock, and grade into silts and clays of the fine-grained saprolite. The mottled zone within the weathered rock tends to be developed only where the weathered profile is capped by the ferricrete. Not all zones may be present within the profile. In the study area, the weathered rock found on the hills generally exhibits the complete profile, while only the saprolitic zones are found under the thick sediment profile in the valleys.

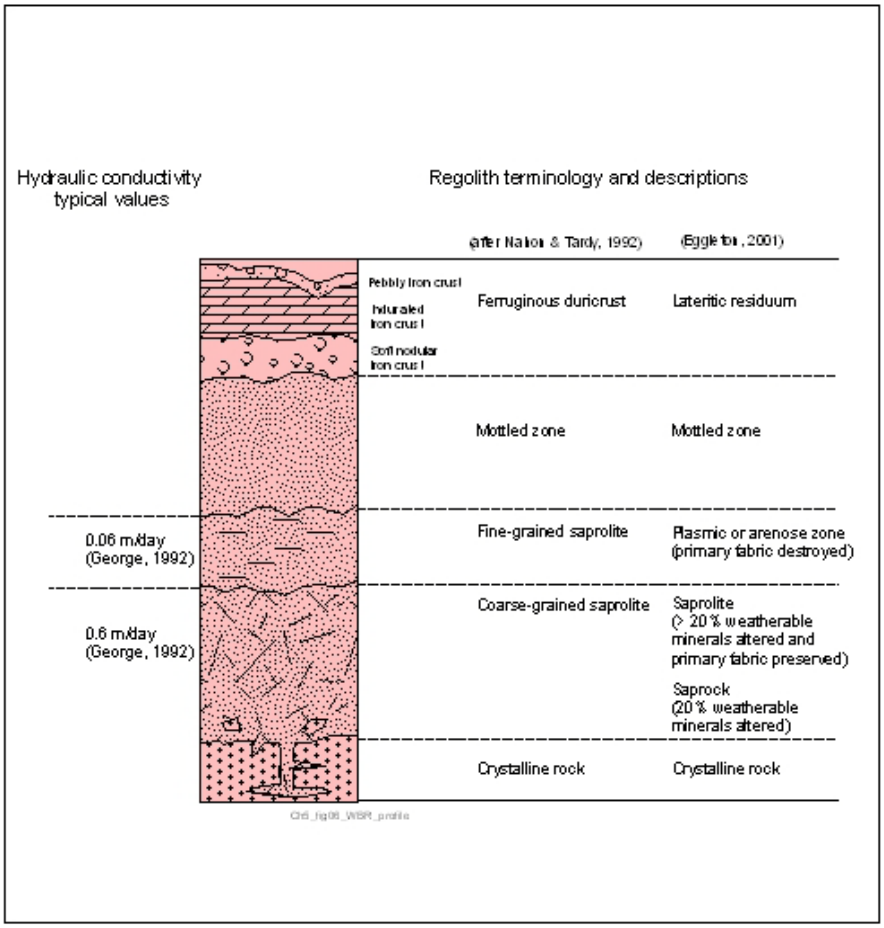

Figure 5–6 Theoretical profile of weathered crystalline rock showing the regolith classifications of Nahon and Tardy (1992) and Eggleton (2001), and typical hydraulic conductivity values for the weathered material from George (1992).

Minerals identified in the weathered basement rock are typical of weathered granite and granitic gneiss. The main minerals identified by XRD were plagioclase feldspar, microcline, mica, quartz and kaolinite (Appendix 4 Table 1). The major plagioclase feldspar was albite. Biotite and muscovite were the major micas present in the weathered materials.

Regolith sample MU46–45.5 comprise 0.7 wt% Ca and 0.15 wt% Na. Albite is the only plagioclase feldspar identified by XRD thus an alternative mineral is required to account for the Ca value. In the south of the study area minor quantities of carbonate mineral have been identified by XRD. These are huntite and siderite with Mg

substitution. Huntite typically occurs in fault zones as an alteration or weathering product of dolomite- and magnesite-bearing rocks (Deer et al., 1966). Siderite commonly occurs in bedded sedimentary rocks and is also known to occur as a hydrothermal mineral in metallic veins. Directly west of the study area paragneiss has been identified and compared to the carbonaceous metasediments of the Broken Hill Inlier (BHP Minerals Pty. Ltd, 2000). Elsewhere in the Biranup Complex (Figure 5–1) metasedimentary rocks are documented, but these are mainly quartzite (Myers, 1990). Further work would be needed to determine if the gneiss present in the study area was also of sedimentary origin in addition to the granitic gneiss mapped by Wilde and Walker (1984).

Minor rutile and zircon were identified in weathered materials by XRD.

5.6.2 Werillup Formation

Subcrop of the Werillup Formation sediments in the study area is confined to the valleys present during the Eocene. Two regolith units have been identified within the Werillup Formation in the present study: the flood plain regolith unit and the channel sand regolith unit (Figure 5–5). These two units are consistent with the findings of Clarke et al. (2003) elsewhere.

5.6.2.1 Flood plain regolith unit

The flood plain unit contains dark-grey to black clays, silts and sandy silts that are carbonaceous, and fine- to coarse-grained quartz sands (Figure 5–5). The thickness of this unit varies with thickness of more than 20 m found in boreholes MU11D, MU37D, MU12D, MU04, MU33D and MU59D and is up to 32 m (borehole MU59D).

The sediments are either carbonaceous clays and silts interbedded with fine- to coarse-grained quartz sands, or thick beds of carbonaceous clay through to carbonaceous sandy silts. The bedding thickness of carbonaceous clayey silt in borehole MU12A (Figure 5–5) and carbonaceous sandy silt in borehole MU46A is over 10 m, but in borehole MU42A is generally less than 0.5 m with many beds being between 0.1 to 0.2 m. The drilling techniques used in this study have obscured many of the bedding contacts, but where preserved there is a sharp bedding contact between quartz sands and underlying clays or clayey silts. Graded bedding is seen

with sands fining upward to clays (Figure 5–5). Quartz sands are poorly- to moderately-sorted, fine- to coarse-grained, with grains being angular to subangular.

The main minerals present other than quartz, are albite, kaolinite and minor gibbsite.

Samples MU42–31 and MU46–21 contained 0.16 and 0.23 wt% Ca, respectively. XRD analyses did not identity calcium minerals in these samples suggesting that small quantities of Ca are present in solid solution in albite rich plagioclase or adsorbed onto clays.

Wood fragments are common throughout the flood plain sediments, with the structure of the original woody tissue frequently preserved. The fragments have undergone varying degrees of compaction and have been classified as lignite by previous workers (Dampier Mining Company Limited, 1981). The sediments contain a rich and moderately diverse pollen assemblage. The major taxa identified are Cryptogam spores (ferns and mosses), Gymnosperms (conifers), *Haloragacidites harrisii* (Casuarinaceae), *Milfordia* spp. (Restionaceae), *Malvacipollis* spp. (Euphorbiaceae: *Austrobuxus*) *Myrtaceidites* spp. (Myrtaceae), *Nothofagidites* spp. (Nothofagus), *Proteacidites* spp. (Proteaceae) and other angiosperms (Milne, 2003).

5.6.2.2 River channel sand regolith unit

The river channel sand unit consists of upward-fining cycles of silts and quartz-rich sands and gravels. These sediments are light grey, generally poorly-sorted, and contain angular to rounded quartz grains ranging in size from silt- to gravel-size (Table 4-2). The coarse-grained sands and gravels are mostly subangular to subrounded with the finer clasts being subrounded to rounded.

The total thickness of quartz sands and silts intersected by drilling was > 65 m (borehole MU63D). The upwardly fining cycles are generally 2 to 3 m in thickness but cycles greater than 5 m have been logged with a 12 m thick cycle intersected in borehole MU03D.

In some boreholes the subangular quartz grains occur in a grey clay matrix. The thickness of beds with the clay matrix is: 1–5 m in boreholes MU46, MU56, MU61 and MU66; 12–13 m in boreholes MU64; 26 m in MU63; and 50 m in MU55D.

Borehole MU64 has 2 zones separated by 6 m of light grey quartz sand not associated with the grey clay matrix.

A dark mineral associated with the quartz sands was identified by SEM – EDAX as ilmenite.

5.6.3 Pallinup Formation

The Pallinup Formation was identified in this study and is mostly confined to the northeast of the study area under the broad-valley floor on which Kulunilup Lake and Bokarup Swamp are located, and in the Pindicup Creek Valley between the two westerly sloping ridges (Figure 3–1). In the west of the study area, the Pallinup Formation has been identified in borehole MU41D. This formation overlies the Werillup Formation except in borehole MU08 where it sits on weathered basement rock.

Sediments of the Pallinup Formation consist of light-grey, well-sorted quartz sand in a silt matrix (Figure 5–5). The sand ranges in grain-size from 0.05 to 0.25 mm. Quartz grains are sub-rounded to well-rounded. The thickness of this unit ranges from 2 m where intercepted in borehole MU41D to 14 m in borehole MU23D. It is about 8 m under the Kulunilup Lake area and 13 to 14 m near Noobijup Lake.

Siliceous sponge spicules are associated with this unit. The spicules (? megasclere) are broken and mostly 1 mm in length but range up to 2 mm. They account for 1 to 5% of the sample. Spicules are absent from the more silty samples (borehole MU12D). They have not been identified to class level in this study, but the classes Demospongiae and Hexactinelida have been identified in the Pallinup Formation on the southern coast of Western Australia (Gammon et al., 2000b).

5.6.4 Recent sediments

Recent sediments consist of sands, clays and gravels that generally overlie the ferricrete (Figure 5–5), but also may lie directly upon weathered basement rock and are between 2 and 34 m thick. They have been deposited in a variety of environments with wind-blown sand dunes occurring in the southeast corner of Lake Muir, east side of Unicup Lake and abutting the west side of hills near borehole MU42. Lacustrine sediments are widespread on the broad-valley floors and wetlands in the north and south of the study area.

Halite, gypsum and jarosite have been identified in these sediments by SEM – EDAX. Halite forms a crust on the dried surface of Lake Muir associated with gypsum. The cubic crystals are about 70 µm across.

Gypsum has been identified in borehole MU48, and as a salt crust on the surface of Lake Muir. The gypsum crystals (borehole MU48) are up to 3 cm long, 1.5 cm wide and 0.5 cm thick. They are associated with a reddish grey to light reddish brown cemented, medium-grained, poorly-sorted, sand at depths between 2 and 4 m. The gypsum crust on Lake Muir comprises very fine crystal plates aggregated in the 'desert rose' pattern (Figure 5–7).

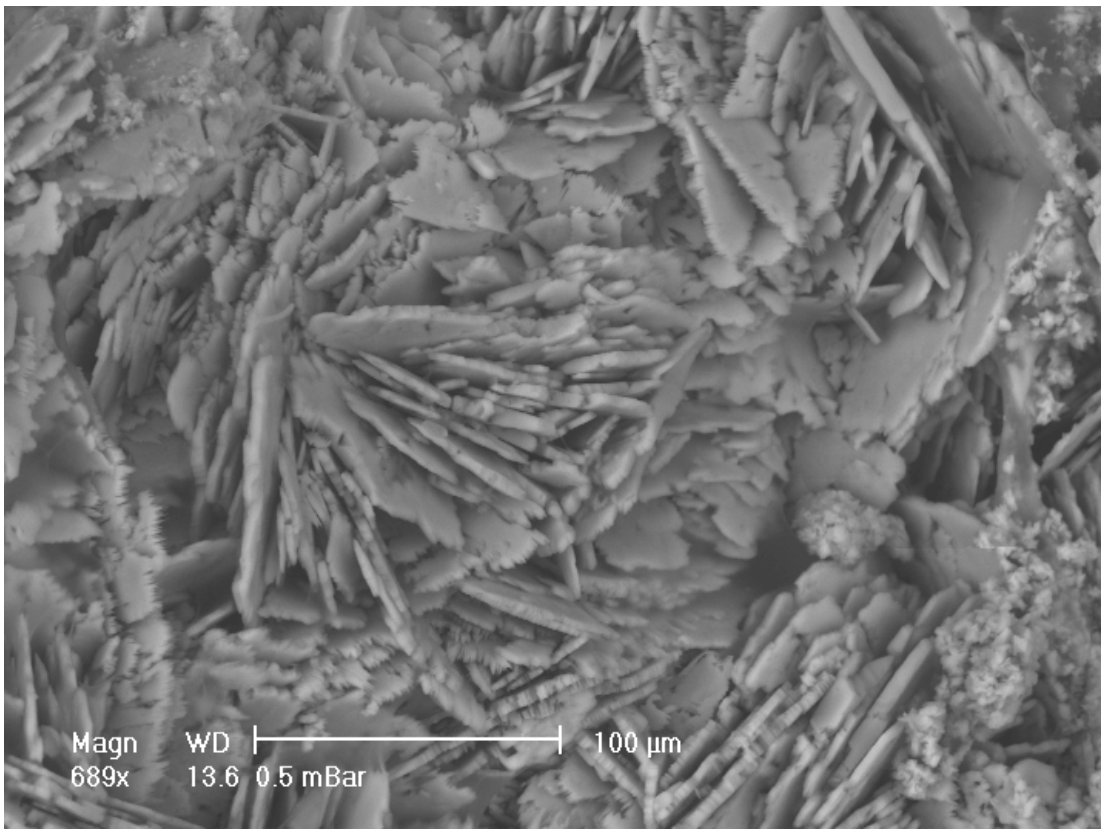

Figure 5–7 Scanning electron micrograph of gypsum crust on Lake Muir.

The fine crust was not visible during the initial visit to the lake on 16/01/07 when light rain had fallen the previous day. The fine crust was present on the subsequent visit two days later (18/01/07) on both the dried organic mat and directly upon the sediments of the dried lake floor.

Jarosite and natrojarosite were identified forming a crust on the banks of Tordit-Gurrup Lagoon near the location of the rock outcrop on Figure 4–1. The crust

formed directly down slope of a groundwater seep that was active at the end of summer in 2008. A 1:5 paste of the crust had a pH value of 2.5. Sodium substitution for K was evident from the SEM – EDAX analysis.

5.7 LANDSCAPE EVOLUTION — LATE EOCENE

5.7.1 Basement rock surface topography

Two basement topographic surfaces for the late Eocene have been modelled using:

- the depth to fresh basement rock recorded from the drilling project; and
- the depth to magnetic basement from the geophysical survey.

The data, when gridded, has enabled 2D contour maps and 3D rendered surfaces to be created. A common elevation datum (m AHD) has been used to allow comparison between the two modelled surfaces.

Table 5-2 Summary of the grid line geometry used to interpolate regular spaced XYZ points by Kriging.

Data source	Minimum (m MGA)	Maximum (m MGA)	Cell (m)	# of lines	Length (m)
Drilled depth to fresh basement rock	465 000	490 000	250	101	25 000
	6 175 000	6 208 000	250	133	33 000
Interpreted depth to magnetic basement	465 000	490 000	50	501	25 000
	6 175 000	6 208 000	50	661	33 000

Kriging, was used to interpolate regular spaced XYZ points from irregularly spaced XYZ points (Table 5-2). The optimum spacing between grid coordinates depends on the number of actual sample points in a given area. The grid spacing was based on the following formula (Hengl, 2006):

$$p = 0.0791\sqrt{\frac{A}{N}} \qquad (5.1)$$

where p is the grid resolution in m, A is the area in m^2 and N is the number of sample points. The value 0.0791 is derived from cartographic concepts and can range from 0.1 to 0.05 (Hengl, 2006).

5.7.1.1 Model 1

The DEC drilling project sited most of the 71 deep bores on the broad-valley floors. Of these, MU46D, MU47 and MU49 were not considered in the interpretation as they intersected fault zones and did not reach fresh basement rock. Only a few bores were sited on the hills and ridges. To enable the topographic model to reflect these hills and ridges, an estimated depth of 20 m along the hills and ridges was applied. This depth to basement rock was based on limited bore information in this terrain which is between 5 and 22 m BGL to basement. The grid resolution was determined on the 68 known depths to fresh basement rock which covered an area of 825 000 000 m^2. Using equation (5.1), the grid resolution would be 270 m. However, it could be as low as 170 m if a factor of 0.05 was used. For ease of data manipulation a regular grid with a cell size of 250 x 250 m was created for the depth to basement model (Table 5-2). The difference between predicted and actual depths to basement show an increased scatter at greater depths (Figure 5–8).

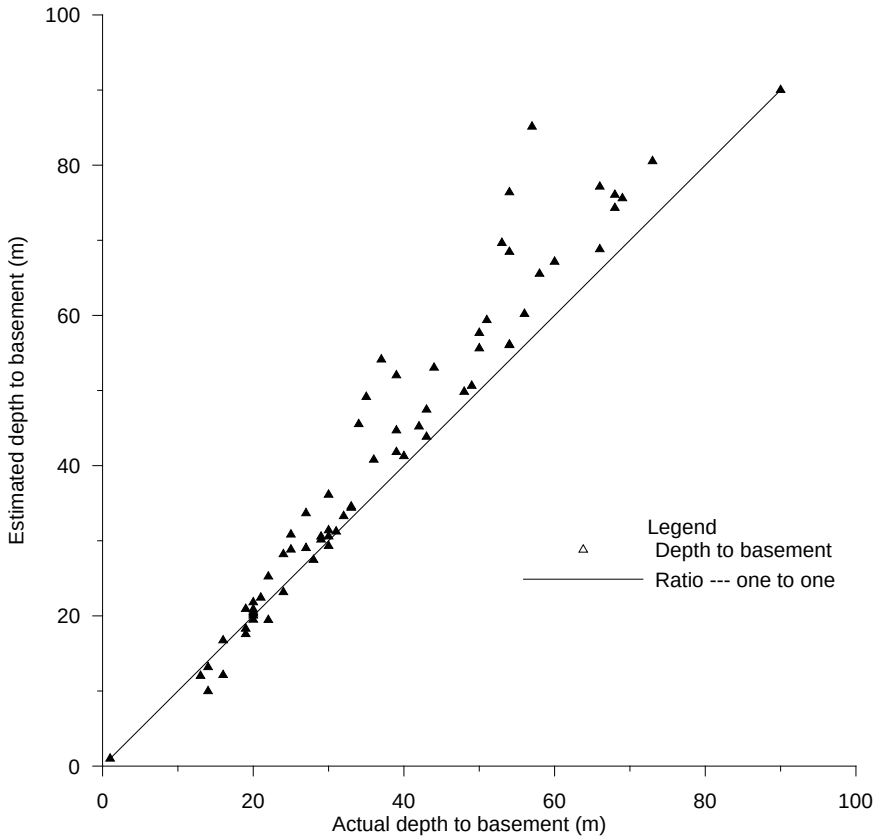

Figure 5–8 Model 1 — Comparison between predicted depths and actual depths to basement rock (m AHD).

5.7.1.2 Model 2

Estimated depths to magnetic basement were determined by Mr. Paul Wilkes (Department of Exploration Geophysics, Curtin University of Technology) by reprocessing the airborne magnetic data using the Euler homogeneity equation as outlined by Thompson (1982). The initial depth to basement data was supplied in ASCII text format by Mr. Paul Wilkes. All subsequent verification, interpretation, manipulation and modelling of the data was done as part of this study.

The Euler homogeneity equation when applied to a potential field helps to determine the source location and depth of anomalies within the potential field data. These anomalies can then be contoured to show the subsurface geometry. The Euler homogeneity equation, when taking into account a background level of the potential field can be written as (Thompson, 1982):

$$(x - x_0)\frac{\partial M}{\partial x} + (y - y_0)\frac{\partial M}{\partial y} + (z - z_0)\frac{\partial M}{\partial z} = N(B - M) \qquad (5.2)$$

where M is the observed field at location (x, y, z) caused by a magnetic source at location (x_0, y_0, z_0), B is the background level of the observed field, and N is the degree of homogeneity or the interpreted structural index. The structural index is a measure of the rate of change with distance of a field (Reid et al., 1990). This equation was applied using a structural index of 0.5 to produce an estimated depth to magnetic basement.

Thompson (1982) stressed that this method does not produce a geological model and that interpretation of the profile is left to the user. The estimated depths to the magnetic basement will include the depth to granitic or gneissic rock and depth of steeply dipping structures such as faults and dykes. On reviewing the estimated depths, they ranged from -37.9 to 205.5 m. The estimated depths were compared to borehole information, rock outcrop and regional faults (Myers, 1990) to help distinguish between the crystalline basement rock surface and steeply dipping faults or dykes. The actual depth to basement rock is generally less than 80 m (Table 5-3). Depths greater that 80 m are known to exist, but are associated with extensive thickness of weathered basement rock in fault zones such as recorded in borehole MU46A.

Table 5-3 The depth to fresh basement rock showing the number of boreholes within each interval.

Depth to fresh basement rock between (m BGL)	*Number of bores within each interval*	*Number of bores (Cumulative frequency %)*
5–15	6	8.2
15.1–20	9	20.5
20.1–30	16	42.4
30.1–40	12	58.9
40.1–50	10	72.6
50.1–80	18	97.3
> 80	2	100

The initial validation involved plotting a histogram of the 1591 points (Table 5-4) which showed 15% of the points to be greater than 80 m depth. Spatially these points exhibited two trends: west to west-northwest; and northeast. The westerly trending points approximate the regional faulting in the study area. The northeast trending points are likely to reflect localised faulting. These points were interpreted to represent faults and removed from the data set. The remaining 1353 XYZ data points were gridded (Table 5-2) and contoured to produce a geometric surface representative of the basement rock surface. A grid resolution of 50 m was used.

Agreement between the estimated depth to basement and actual depth (Figure 5–9) was poor with a linear trend of $y= 0.177x + 30.623$ and $R^2 = 0.0236$. The poor correlation suggests that the underlying structure is influencing this modelled surface even though the depths > 80 m were removed. However, under Lake Muir and east of the lake, the predicted topographic surface produced trends that are worth investigating.

Table 5-4 Depth to basement rock generated by the Euler homogeneity equation, showing that 15% of the points are > 80 m BGL, significantly greater than the 2.7% actual depths known to be > 80 m BGL.

*Depth to fresh basement rock between (m BLG)**	*Number of points within each interval*	*Number of points (Cumulative frequency %)*
< -20	12	0.75
-19.9 to -10	40	3.27
-9.9 to -5	30	5.16
-4.9 to 0	52	8.43
0.1 to 20	306	27.67
20.1 to 60	688	70.94
60.1 to 80	224	85.03
> 80	238	100.00

* negative values above ground level

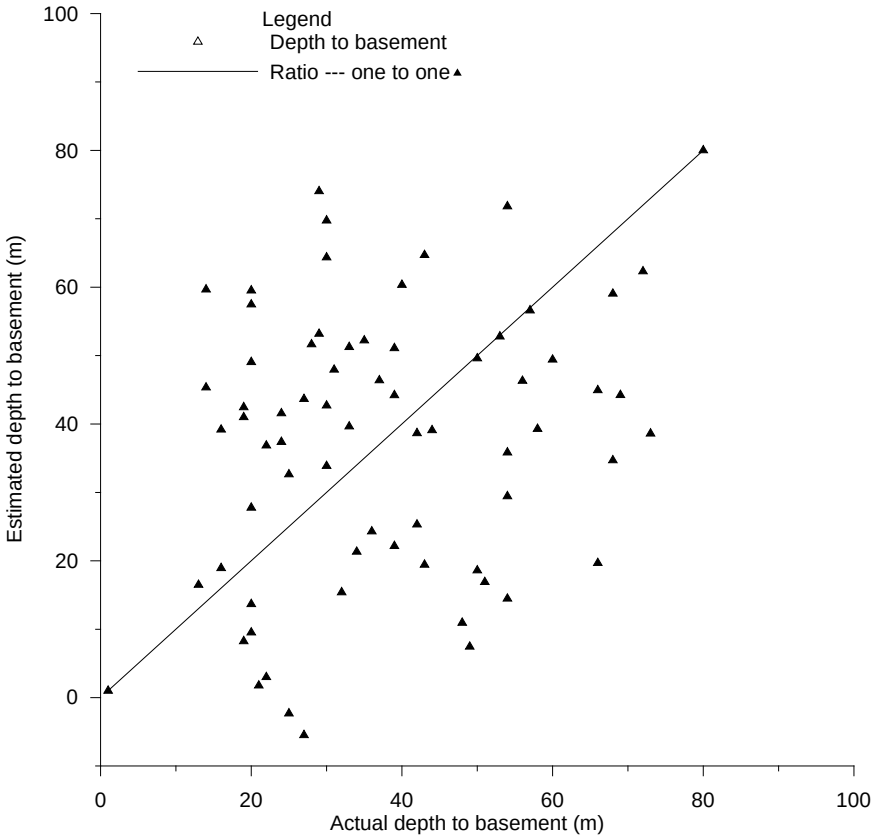

Figure 5–9 Model 2 — Comparison between depths predicted from the geophysical data and actual depths to basement (m AHD).

5.7.1.3 Model interpretation

The location of possible palaeovalleys was inferred from the predicted fresh basement rock elevations (model 1) and depth to magnetic basement (model 2). The results of both models 1 and 2 indicate the presence of 2 main palaeovalley systems, whereas model 2 suggests the presence of a third palaeovalley system (Figure 5–10 and Figure 5–11). The jaggedness of the modelled 3D topographic surface reflects the limits of the modelling software. Nevertheless, the rendered 3D surfaces suggest there was more topographic relief during the late Eocene than today. The topographic relief inferred by model 2 (Figure 5–11) is intensely dissected when compared to model 1 and the current topographic relief (Figure 3–1). The inferred palaeovalleys in model 2 tend to be steeper and narrower than those inferred in model 1.

To facilitate comparison, the palaeovalleys inferred from both models 1 and 2 have been labelled palaeovalleys 1 and 2, while the additional valley inferred from model 2 is labelled palaeovalley 3 (Figure 5–10 and Figure 5–11). The palaeovalleys have been further subdivide into smaller segments and labelled for the ease of discussion. Thus palaeovalley 1, segment A is referred to as palaeovalley 1A as seen in Figure 5–10; Figure 5–12 and Table 5-5. The model interpretation includes comparisons with known depths to fresh basement rock (Figure 5–12), geological cross sections (Figure 5–13; Figure 5–14; Figure 5–15; and Figure 5–16) and is summarised in Table 5-5.

Inferred palaeovalley 1, segments A to C

Both models suggest the presence of a palaeovalley system in the north of the study area (Figure 5–10 and Figure 5–11), but the interpretation regarding the length and directions of some segments within the system differ between the models.

Model 1 indicates that segment 1A is located beneath the current broad-valley floor on which Bokarup Swamp and Kulunilup Lake are located (Figure 5–12) It narrows to the southeast and is confined by the hills in the northeast (Figure 5–12 and Figure 5–14) and the westerly sloping ridge in the south (Figure 5–16). The inferred

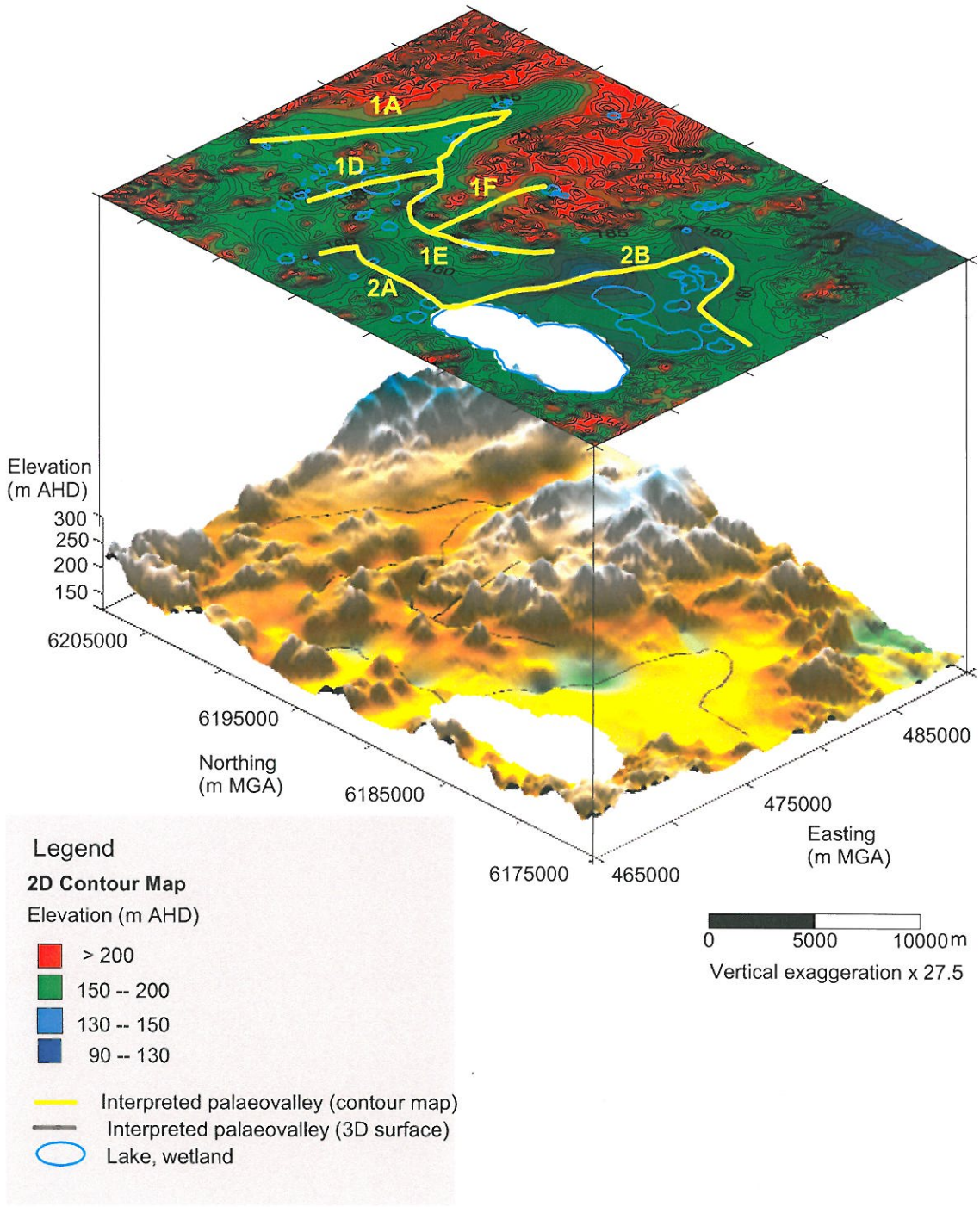

Figure 5–10 Fresh basement rock topography as a 2D contour and 3D rendered surface for model 1 based on drilling data showing the location of the interpreted palaeovalleys.

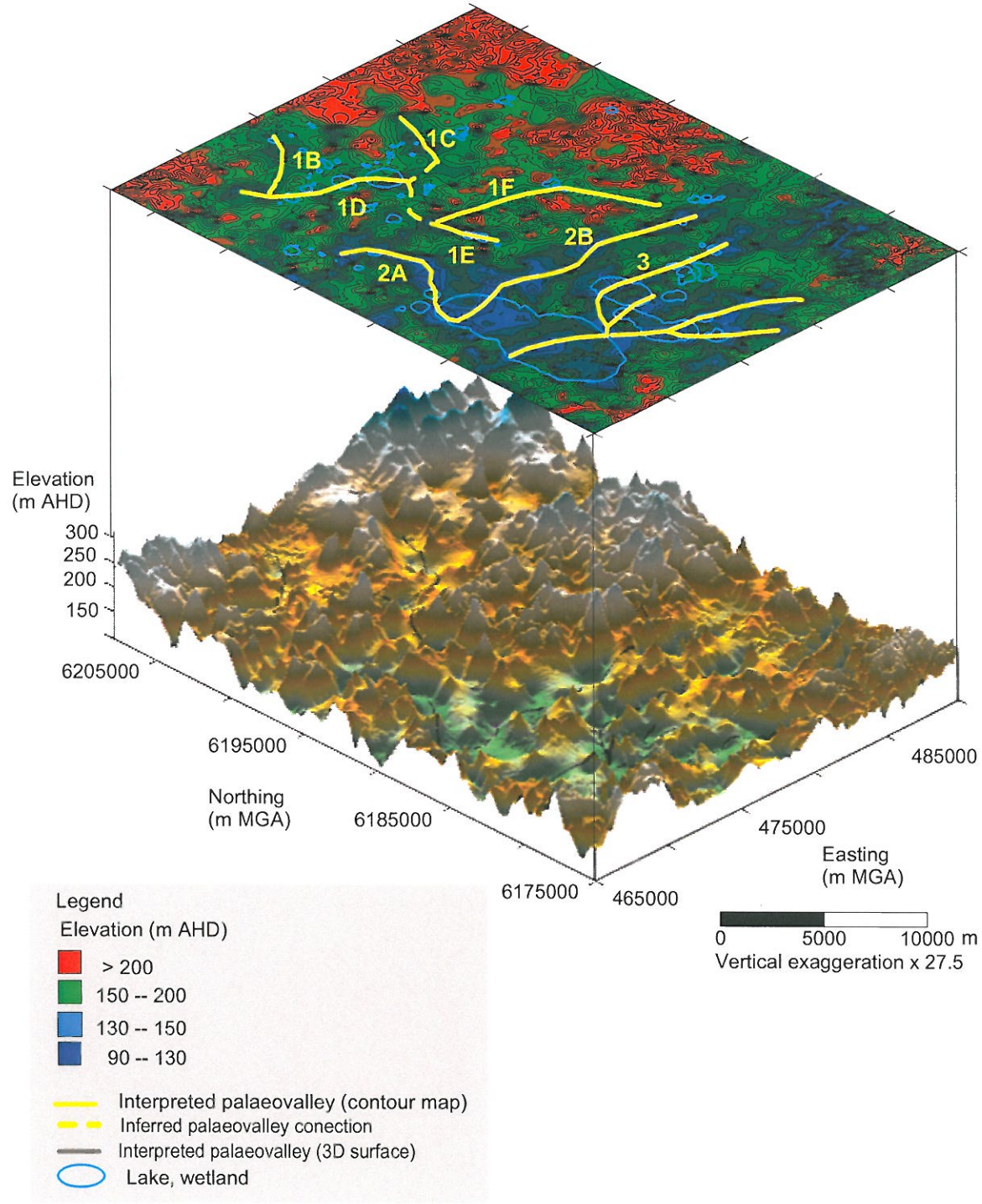

Figure 5–11 Fresh basement rock topography as a 2D contour and 3D rendered surface for model 2 based on Euler homogeneity equation showing the location of the interpreted palaeovalleys.

Table 5-5 Comparison of fresh basement rock topography models with geological cross sections 6 200 000, 6 197 500 mN and sections 474 200, 480 000 mE and the known depths to fresh basement rock.

Interpreted palaeovalley	*Segment*	*Model 1*	*Model 2*	*Geological cross section*	*Actual fresh basement rock elevations (m AHD)*	*Comment*
1	1A	*x*	—	6 200 000 mN 6 197 500 mN 480 000 mE	152–181	broad-flat palaeovalley
	1B	?	*x*	?		located under known weathered basement rock and near bore MU66D which intersected a fault
	1C	?	*x*	?		possible
	1D	*x*	*x*	6 200 000 mN 474 200 mE	133–146	palaeovalley
	1E	*x*	*x*	6 197 500 mN 474 200 mE	125–147	palaeovalley, no defined connection between sections A and B with geophysics
	1F	*x*	*x*	480 000 mE	136–171	steep sided palaeovalley
2	2A	*x*	*x*	6 197 500 mN	128–153	palaeovalley
	2B	*x*	*x*	474 200 mE	117–121	palaeovalley
	southern arm	*x*	—		148–158	? palaeovalley
3		—	*x*			possible palaeovalley

x indicates the interpreted palaeovalley segment is present in the model
— indicates the interpreted palaeovalley is not present
? indicates questionable

palaeovalley (segment 1A) is about 6 km wide in cross section (Figure 5–10 and Figure 5–16) and has been infilled with at least 52 m of sediment. Actual elevation of the fresh basement rock surface is between 152 and 181 m AHD (Figure 5–10; Figure 5–12; Table 5-5).

Model 2 places a different interpretation on the northern segments of the inferred palaeovalley 1. It shows two smaller segments labelled 1B and 1C on Figure 5–11 that are separated by a ridge running southwest. There is no defined connection with segment 1B and segment 1D. The northern end of segment 1B is located near a fault zone that was intersected in borehole MU66D. Segment 1B slopes southwest under low hills interpreted from the surface geology to be weathered basement rock, therefore the segment is most likely to follow a northeast trending lineation as identified by Chakravartula and Street (2000). Segment 1C has steep sides at the head of the valley in the north but opens into a broader palaeovalley about 4 km across. An inferred connection between segments 1C and 1D is seen on Figure 5–11.

The location of segment 1A interpreted from model 1 (Figure 5–10) is preferred to the location of segments 1B and 1C interpreted by model 2 (Figure 5–11). Oblique-sections through the palaeovalley 1A are evident in sections 480 000 mE and 6 200 000 mN (Figure 5–13 and Figure 5–16). Confidence in the direction of inferred palaeovalley 1B predicted by model 2 is low especially since segment 1B starts near a know fault and extends beneath a hill of weathered basement rock. The direction of segments 1B and 1C are more likely to reflect northeast structural lineations (Chakravartula and Street, 2000) rather than the actual Eocene topographic surface.

Inferred palaeovalley 1, segments D to F

Segment 1A in model 1 is inferred to have been incised by the valley segment 1D labelled on Figure 5–10 which extends under Little Unicup and Unicup Lakes (Figure 5–12) before turning to the south (segment 1E) (Figure 5–12; Figure 5–14; Figure 5–15). The elevation of fresh basement rock in the vicinity of segment 1D is between 133 and 146 m AHD, lower than that of segment 1A in model 1 (Table 5-5). The interpreted south arm (segment 1E) is located beneath the current small valley in

which Pindicup Lake is situated (Figure 5–12 and Figure 5–15). The fresh basement rock elevation is at 125 m AHD just north of Pindicup Lake (Figure 5–12 and Figure 5–15) and has been infilled with at least 51 m of sediment (Panasiewicz et al., 1997). The palaeovalley is steep sided and between 1.5 to 2 km across.

Model 2 also inferred segments 1D and 1E, which are labelled on Figure 5–11. Segment 1D (model 2) extends further northwest than the same segment in model 1 The northwest extension continues under a rise of weathered basement rock (Figure 5–12) and is thus not supported by current surface geology. A join between segments 1D and 1E is not evident in model 2 (Figure 5–11). Borehole data, however, indicates a connection between segments 1D and 1E thus the inferred connection is shown in Figure 5–11.

Both models 1 and 2 infer a west sloping segment (1F) that is located under the current west sloping valley between the two westerly sloping ridges (Figure 5–10; Figure 5–11; Figure 5–12; Figure 5–16). Segment 1F is about 1.5 to 2.5 km across and the fresh basement rock elevation decreases from 171 to 136 m AHD (Figure 5–12; Table 5-5).

Model 2 suggests segment 1F extends under the modern valley before heading southeast under Noobijup Lake (Figure 5–12). There is no borehole data to confirm this, although the current ridge is dissected by a narrow valley (Figure 5–12).

Inferred palaeovalley 2, segments A and B

Models 1 and 2 suggest the presence of a south dipping palaeovalley (segment 2A) in the west of the study area, which turns to the east near Lake Muir (segment 2B) (Figure 5–10 and Figure 5–11). The palaeovalley 2A runs parallel to Buranganup Road (Figure 5–12). The fresh basement rock elevation is between 153 and 128 m AHD along segment 2A, decreasing to between 121 and 117 m AHD in segment 2B (Figure 5–12). Segment 2B is evident on section 474 200 mE (Figure 5–15) as a narrow valley. Model 1 has interpreted segment 2B to swing south near Coorinup Swamp (Figure 5–12). This southern extension coincides with sediments of the Werillup Formation between 8 and 12 m thick. The Werillup Formation sediments are suggestive of low energy deposition within a river system. The fresh

basement rock elevations between 154 and 146 m AHD are higher than the main channel in segment 2B. An alternative explanation for southern extension of valley segment 2B is discussed in relation to palaeovalley 3.

Inferred palaeovalley 3

Model 1 has not progressed the understanding of the palaeovalleys under the southern section of Lake Muir and to the east, under Byenup Lagoon and Tordit-Gurrup Lagoon. Model 2, on the other hand, has suggested that a connected series of palaeovalleys are located in the south of the study area. Two palaeovalley segments join in the vicinity of Tordit-Gurrup Lagoon to form one valley which runs beneath Lake Muir (Figure 5–11 and Figure 5–12). This valley is joined by two northern tributaries with the junction located near the eastern edge of Lake Muir (Figure 5–12).

The two northern tributary valleys are located north and south of a bore that intersected shallow fresh basement rock at 162 m AHD (Figure 5–12). Department of Agriculture Western Australia tried unsuccessfully to establish bores to fresh basement rock around Byenup Lagoon. According to the driller's notes, the bores collapsed due to unconsolidated sands or 'turkey nesting sand'. This suggests the possible presence of palaeovalley-fill in the area and fresh basement rock at 162 m AHD may represent a ridge between the two palaeovalleys.

To the east the interpreted palaeovalley under the southern part of Tordit-Gurrup Lagoon bifurcates into a northern and southern segments (Figure 5–11 and Figure 5–12). The existence of the northern segment is not supported by the stratigraphy. The fresh basement rock elevation is between 161 and 163 m AHD (Figure 5–12) and at these sites the Werillup Formation was not identified. However, as seen on section 474 200 mE (Figure 5–15) palaeovalley segment 2B was intersected by bore MU59D located between bores MU60D and MU58D. The distance between bores MU60D and MU58D is approximately 2 km and a narrow palaeovalley, such as palaeovalley 2B, could easily be missed by exploratory drilling. Therefore, it is possible that similar narrow palaeovalleys have been missed elsewhere in the study area.

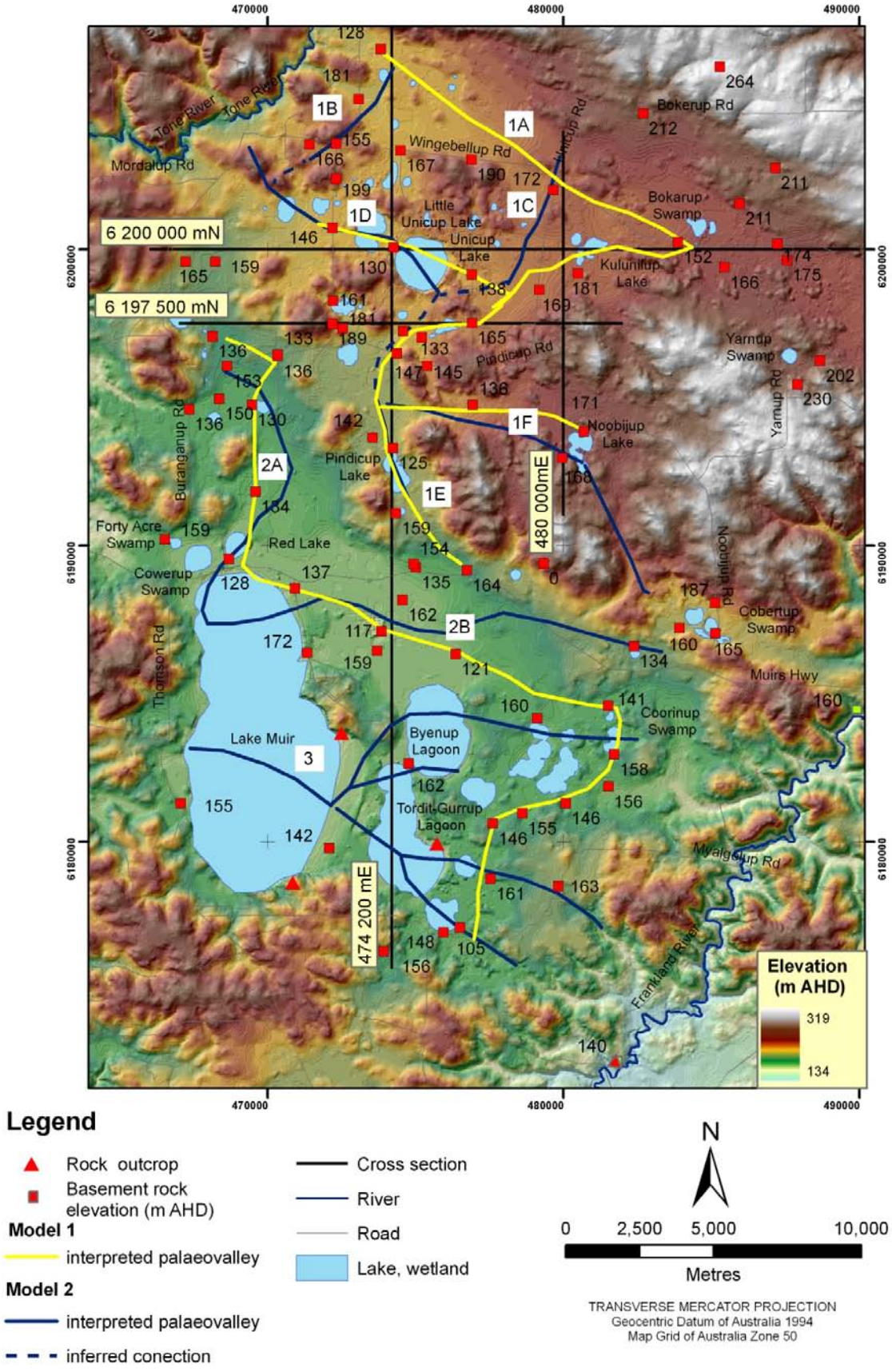

Figure 5–12 The location of the interpreted palaeovalleys from the two models in relation to the know depths to fresh basement rock.

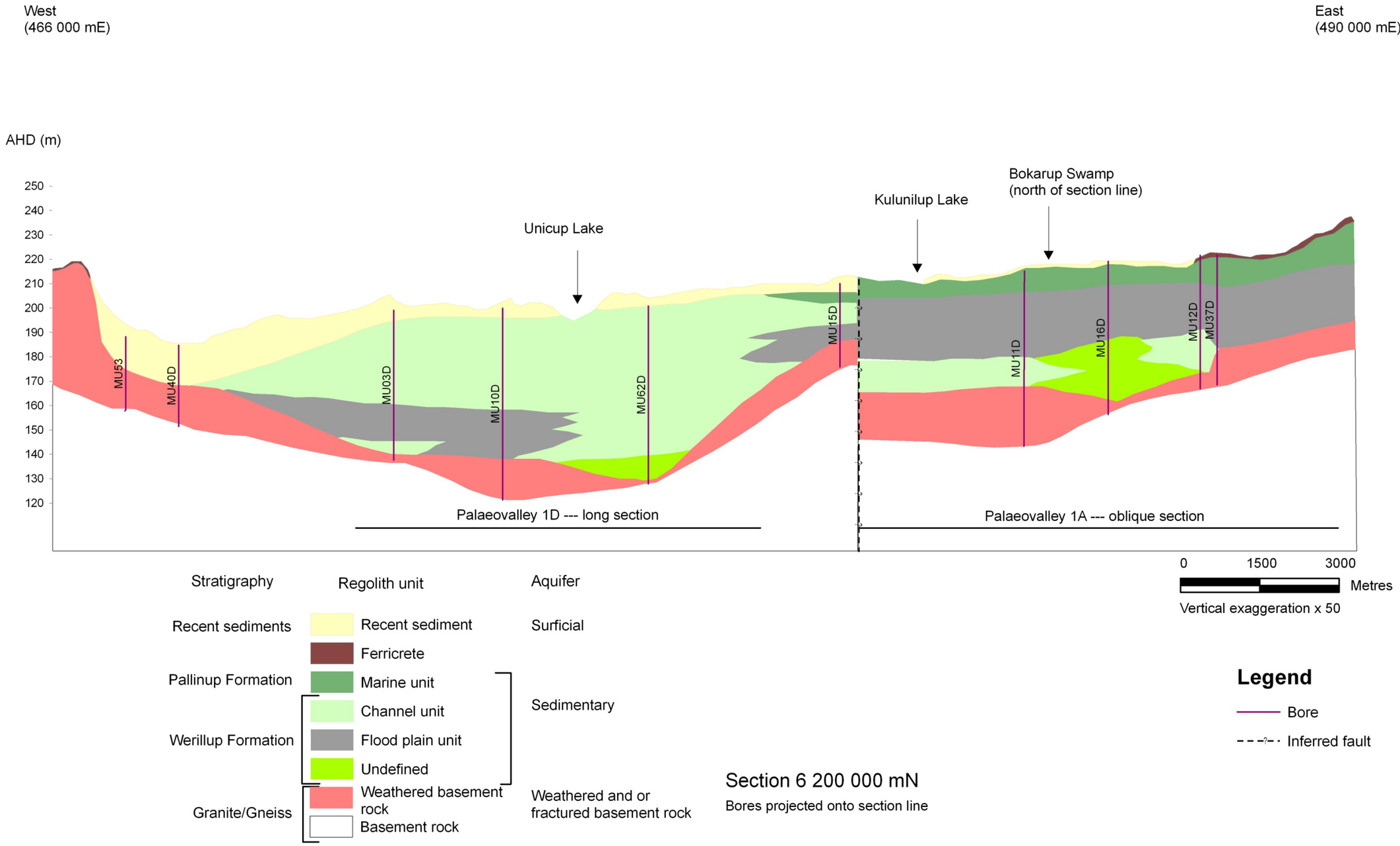

Figure 5–13 Section 6 200 000 mN showing the stratigraphic profile of the valley fill sediments in the north of the study area.

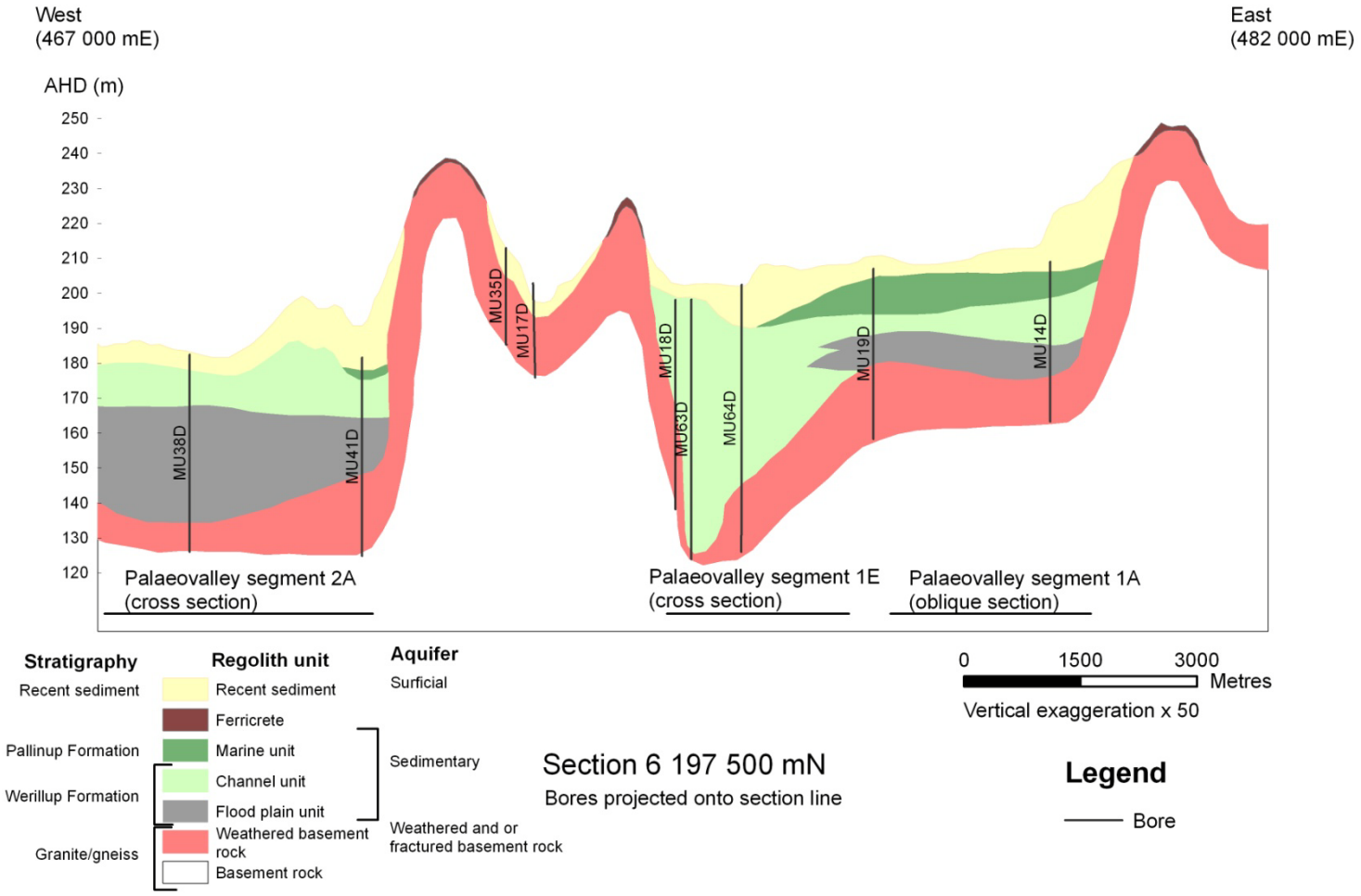

Figure 5–14 Section 6 197 500 mN showing the stratigraphic profile of the valley fill sediments separated by hills of weathered basement rock.

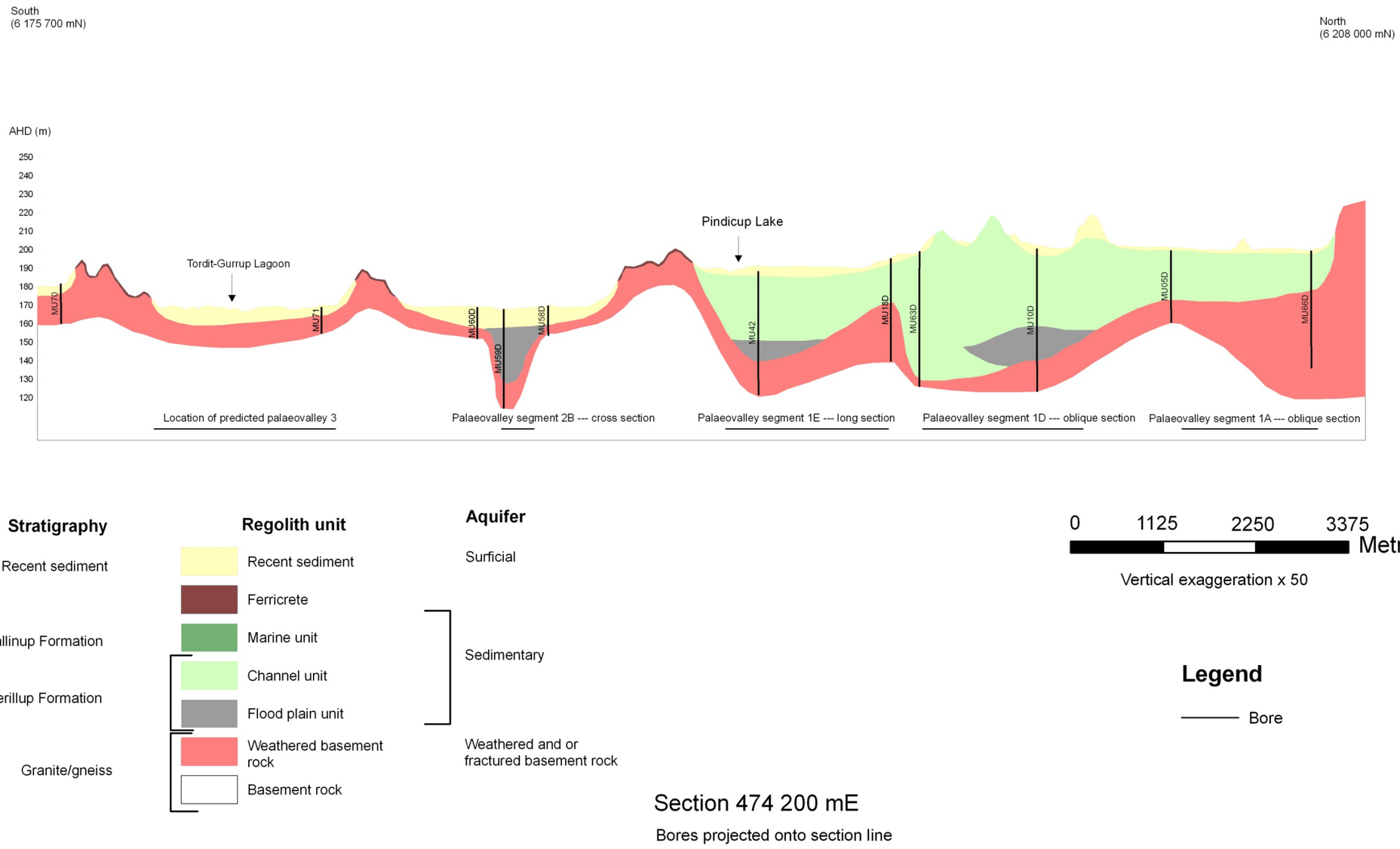

Figure 5–15 Section 474 200 mE showing the stratigraphic profile of the valley fill sediments in the north of the study area and the reduced thickness of valley fill sediments in the south of the study area.

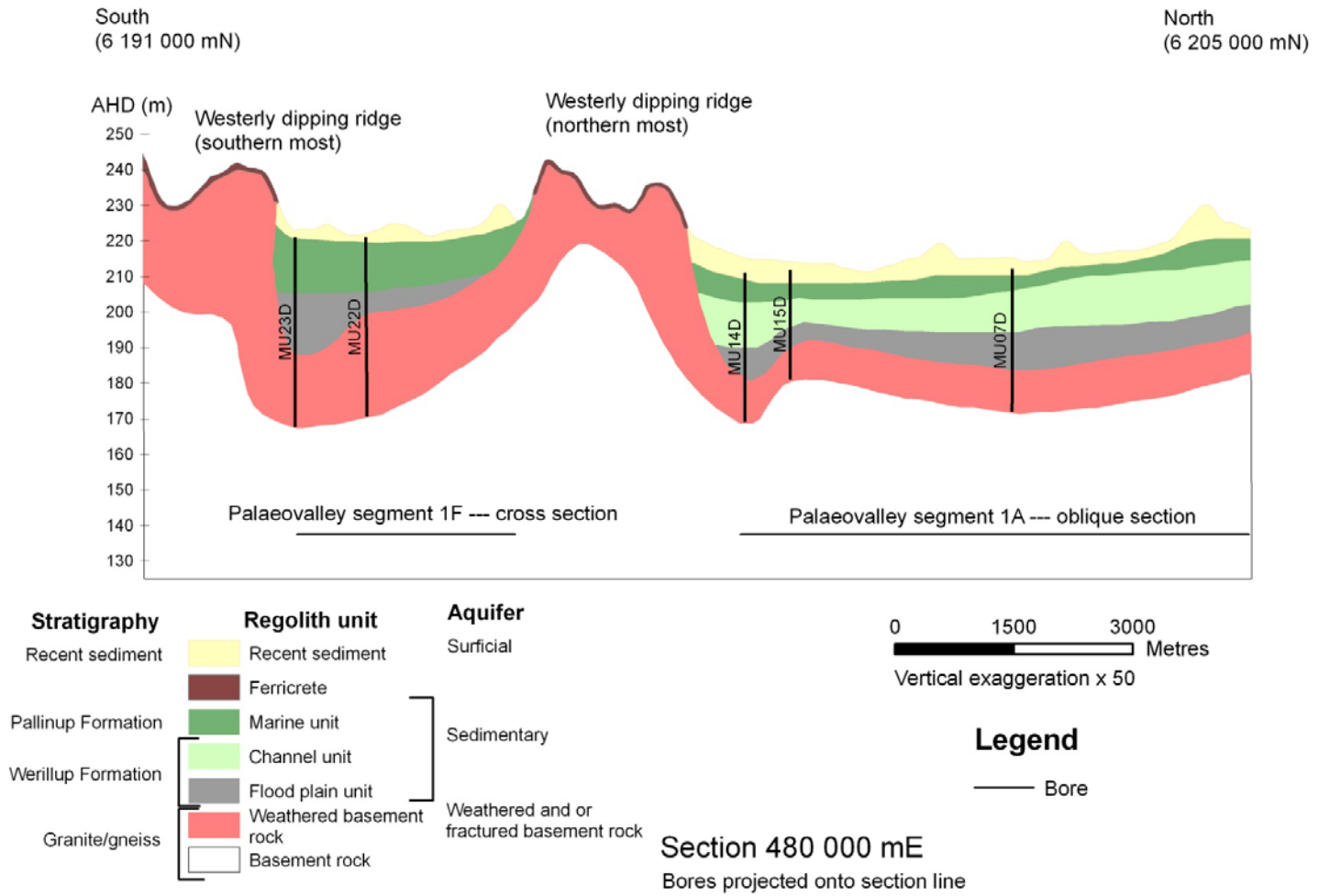

Figure 5–16 Section 480 000 mE showing the stratigraphic profile of the valley fill sediments separated by the westerly sloping ridges located in the centre of the study area.

The most southern arm of palaeovalley 3 may be a valley and/or an expression of geological structure. This segment may represent a palaeovalley as bores MU46A, MU46D and MU52D intersected the Werillup Formation, but mainly the flood plain regolith unit (9 to 13 m) with only 2 to 3 m of the channel sand regolith unit being intersected in MU46A. This inferred segment of the palaeovalley is also coincidental with a major lineament evident from the magnetic survey (Chakravartula and Street, 2000). This fault zone was intersected in bores MU46D and MU46A.

There are no boreholes to confirm the presence of a palaeovalley beneath Lake Muir, but basement rock is relatively close to the surface with rock outcrops on the east edge of Lake Muir, the southern edge of Lake Muir and the eastern edge of Tordit-Gurrup Lagoon (Figure 5–12).

If the palaeovalley 3 inferred from model 2 runs roughly east then the Werillup Formation identified in bores MU68D, MU29D to MU31D may either represent part of the inferred palaeovalley 3 or the southern extension of valley segment 2B interpreted by model 1 (Figure 4–1; Figure 5–12 and Figure 5–17). Currently there is insufficient information to resolve the basement rock topography in this section of the study area.

5.7.2 Fluvial depositional environment

Fluvial sediments were deposited during the late Eocene as the continental margin collapsed (Li et al., 2003; Norvick and Smith, 2001) (Figure 5–3). In the study area the fluvial deposits of the Werillup Formation that infilled palaeovalleys consisted of quartz dominated sand (preserved as the channel sand regolith unit), and carbonaceous clays and silts (preserved as the flood plain regolith unit). The thickness and distribution of these two regolith units enables the deposition environment to be elucidated.

Sediments of the Werillup Formation were deposited initially by a river confined to the palaeovalley segment 1D (Figure 5–13). The base of this channel is currently at about 130 to 138 m AHD and is at least 14 m below the lowest known point of the palaeovalley 1A interpreted from model 1 (Figure 5–13 and Table 5-5). The channel sand regolith unit is up to 65 m thick within palaeovalley 1D. The coarse-grained sand suggests that this section of the river had reasonably high water flows. Work

by Hjulström (1939) cited in Ritter et al. (1995) investigated movement of particles in relation to mean velocity (water flow). The Hjulström curve gives an indication of the energy flows and grains-sizes in relation to erosion, transportation and deposition. For deposition of upward fining quartz dominated beds, ranging from coarse-grained through to fine-grained sands, the flow velocities would have decreased from the order of 15 cm/sec to 2 cm/sec.

Once palaeovalley 1D had been infilled level to the base of palaeovalley 1A (model 1) the river could migrate across this broad palaeovalley floor. In palaeovalley 1A, the flood plain regolith unit is thickest in the east near Bokarup Swamp with between 22 and 25 m intersected (Figure 5–13). This thickness decreases to the west of Kulunilup Lake with a thickness of between 5 to 10 m being recorded. The climate during the late Eocene is documented as wet and humid in southwestern Australia (Quilty, 1994). Under these conditions, the flood plain would have been thickly vegetated. The flood plain regolith unit would have accumulated as overbank deposits on a flat, poorly drained, flood plain with very low water flows, and even stagnant conditions. Normally under sub-aerial conditions dead plant tissue decays rapidly. Thus, the preservation of carbonaceous material suggests a swampy environment with stagnant oxygen-deficient water. For these materials to accumulate, the subsidence rate needs to be similar to the deposition rate (Reineck and Singh, 1980). To determine the rate of subsidence, detailed palynological analysis of the cores would be needed to obtain an age, but considering the poorly constrained nature of palynological zonation for Western Australia in the Eocene and Oligocene a concise age may not be possible.

Rapidly shifting meandering channels or braided streams tend to inhibit the development of flood plain deposits (Reineck and Singh, 1980) and this is evident towards the centre of the palaeovalleys. Thin sands beds between 0.1 and 0.5 m were overlain by thin carbonaceous clay beds of similar thickness in bore MU42A.

Valley segment 2A contains thick sequences of sand coated with clay. A clay coating on the quartz grains was noted in many of the bores, but prior to bore MU55D being drilled the clay coatings were interpreted as contamination from carbonaceous clay caught in the cyclone during drilling. However, no discrete units of carbonaceous clays were intersected in bore MU55D which had 55 m of upward-

fining quartz-dominated sand with fine carbonaceous clay coatings to the grains. The presence of the clay on the quartz grains is interpreted in this study as the result of the river channel eroding beds or lenses of carbonaceous clay prior to deposition of the quartz sand. For the clay coating to be preserved during deposition in a high energy river environment the zone of erosion would need to be close to the zone of deposition.

Regional mapping by Wilde and Walker (1984) suggest two possible exits for a palaeoriver channel in the south of the study area. One possible exit for the river is an eastward extension to palaeovalley 2B (model 1), between two hills of weathered basement rock rather than the segment turning south (Figure 5–12). There is no borehole data to confirm this. The second possible exit coincides with palaeovalley 3 (Figure 5–11). Under Tordit-Gurrup Lagoon the interpreted palaeovalley bifurcates into a northern and southern arm. The northern arm coincides with mapped Eocene sediments (Wilde and Walker, 1984). However, the shallow basement rock at 161 and 163 m AHD, is overlain by recent sediments (Figure 5–12). No sediments of late Eocene age were identified.

Supporting the palaeoriver exiting the south of the study area are documented sediments similar to the sediments of the Werillup Formation about 30 km southeast of the study area (De Silva, 2000; Panasiewicz et al., 1997) However, additional work is required to resolve where the palaeoriver may have exited the study area in the south.

5.7.3 Marine depositional environment

The sediments are well sorted and range between 0.25 mm and ~0.1 mm in grain size indicating a high-energy marine environment such as occurring on beaches with wave action, shoals, and tidal channels or inlets. The grain size and amount of sponge spicules in the rocks of the Pallinup Formation in the study area suggest that they are equivalent to unit 2 as defined by Gammon et al. (2000a) which represents a rising sea-level. The absence of unit 3 within the study area suggest that the Pallinup Formation was deposited close to the maximum extent of the Tuketja transgression.

5.8 LANDSCAPE EVOLUTION — POST LATE EOCENE

Lineaments have been extensively mapped from the geophysical magnetic data but the lineament generations or age have not been interpreted (Chakravartula and Street, 2000). Extensive faulting would have initially occurred between 1300 Ma and 1000 Ma as the South Australian Craton collided with the Western Australian Craton (Yilgarn and Pilbara Cratons) forming the Albany–Fraser Orogen (Myers et al., 1996). Faulting or reactivation of the faults would have occurred during the separation of Australia from Antarctica. Faulting was still occurring after the development of the ferricrete of the Pallinup Formation. The faulting initially caused an erosional environment that is evident in the south of the study area, but then changed to depositional when the southern edge of the study area was uplifted to create the closed internal drainage basin of today.

5.8.1 Fluvial–marine contact

The nature of the fluvial-marine contact between the Werillup and Pallinup Formations gives an indication of the processes occurring along the continental margin. The stratigraphic contact between the Werillup and Pallinup Formations, in the study area, currently ranges in elevation from 180 (MU41D) to 226 m AHD (MU09D). This is a vertical difference of 46 m over a horizontal distance of 18 km giving a gradient of 0.0025. This gradient is similar to that of the same stratigraphic contact north of Albany in the Eucla Basin (Smith, 1997). Assuming the Pallinup Formation was laid down on a land surface that had a gradient of 0.0025 it would be expected that the thickness of this formation (in the study area) would be between 49 m to 56 m. However, the preserved thickness of Pallinup Formation in the study area suggests that the original gradient was much shallower.

The maximum recorded thickness of Pallinup Formation is 48 m at the Beaufort Inlet (Gammon et al., 2000a) about 160 km east from the study area (Figure 5–1). This suggest that the marine sediments were deposited on a surface with a gradient of about 0.00024 which is more in line with the mean gradient for delta plains of modern rivers (Syvitski et al., 2005). Subsidence of the Eucla Basin occurred in the Early Miocene (Cope, 1975) and this would account for the steepening of the fluvial–marine contact gradient evident today.

5.8.2 Faulting and erosion

The timing of faulting that post dates deposition of the Pallinup Formation is based on the presence of *in situ* ferricrete (on Pallinup Formation) in the northeast of the study area (Figure 5–13). However, using ferricrete as a stratigraphic marker can be problematic (Taylor and Shirtliff, 2003) and needs to be supported by other geological evidence such as the relative level of the stratigraphic contact between the Werillup and Pallinup Formations. The ferricrete associated with the Pallinup Formation to the west of Kulunilup Lake has either been transported or eroded away. The main interval of ferricrete formation in Western Australia was at the beginning of the Oligocene (Quilty, 1994). However, Anand and Paine (2002) extended the period of ferricrete formation into the Miocene. The age of ferricrete formation suggests that the faulting and erosion occurred during or since the Miocene.

Fault movement post deposition of the Pallinup Formation is evident from comparison of the relative levels of the stratigraphic contact between the Werillup and Pallinup Formations. South of Bokarup Swamp the marine base is between 209 and 211 m AHD in boreholes MU11D, MU16D, MU12D and MU37D and the intercepted thickness of marine sediments is 9 to 12 m (Figure 5–13). To the southwest of Kulunilup Swamp the base is at 204 m AHD with only 4 m of marine sediment preserved in borehole MU15D (Figure 5–13).

The preservation of the marine sequence with *in situ* ferricrete in boreholes MU12D and MU37D suggests that the thickness of this sequence was originally about 12 m (Figure 5–13). No Pallinup Formation has been identified in the south of the study area (Figure 5–17). This suggests that at least 12 m of sediment has been eroded. However, it is likely that greater than 12 m of sediment has been eroded as the Werillup Formation also decreases in thickness to between 8 and 19 m in the south of the study area (Figure 5–17) and is absent from boreholes MU58D, MU60D, and MU71 (Figure 5–15). Basement rock is close to surface and is exposed east of Lake Muir and Tordit-Gurrup Lagoon and south of Lake Muir (Figure 5–17).

The Pallinup Formation is also preserved in the narrow west sloping valley in which Noobijup Lake is situated. Thirteen to 14 m is preserved and overlain by 1 to 2 m of recent sediment. At 206 m AHD the stratigraphic contact between the Pallinup and Werillup Formations is 2 to 4 m higher than the contact directly to the north in

boreholes MU14D and MU15D (Figure 5–16). Down slope of borehole MU22D 9 m is preserved in borehole PM10 (Figure 4–1) with the base at 203 m AHD. This is overlain by 5 m of recent sediments (Panasiewicz et al., 1997). This suggests that erosion has been followed by deposition. Erosion was most probably induced by faulting and this is supported by the changing level of the stratigraphic contact between the fluvial and marine sequence.

5.8.3 Uplift and deposition

Timing of the change from erosion to deposition in the study area is not clear. The ferricrete on the weathered basement rock south of Lake Muir suggest that these hills were present when the Werillup and Pallinup Formations were deposited. The Werillup Formation has been identified outside the study area about 30 to 35 km southeast of Lake Muir (De Silva, 2000; Panasiewicz et al., 1997) suggesting that the original river exited the study area from the south. The change from an eroding environment to one of deposition could have taken place by uplifting the southern boundary and/or a change in climate from a wet to a much drier climate where the river flows decrease and eventually stop.

Uplift along the southern and eastern boundary is indicated by the elevations of fresh basement rock. The current Frankland River is at about 160 m AHD near the Muirs Hwy., decreasing in the south to about 140 m (Figure 5–12). These elevations are well above the fresh basement rock elevations of 117 m AHD in borehole MU59D and 121 m in borehole MU61D which intersect palaeovalley 2B (Table 5-5 and Figure 5–12).

In southwestern Australia, climate from the Late Miocene to recent is poorly documented, however it is generally recognised that the climate has became progressively drier (Anand and Paine, 2002; Quilty, 1994). A drier climate may result in reduced surface water flow and this would help contribute to the change from erosion to deposition.

5.8.4 Current lateral extent of Werillup and Pallinup Formations

The lateral extent of the combined Werillup and Pallinup Formations have been mapped using the drilling information, and the limited rock exposures (Figure 5–17). The margin of the subcrop of the Werillup and Pallinup Formations is covered by

either recent sediments or ferricrete and in places there is insufficient information to infer the boundary position. Additional geological information is needed to constrain the boundary in the northeast. The eastern boundary has not been established for the sediments of the late Eocene in the west dipping valley that contains Noobijup Lake.

In the southern half of the study area, the late Eocene sediments have not been identified under Lake Muir although geophysical data indicate that buried valleys may occur under and to the east of Lake Muir (Figure 5–11). The Werillup Formation east of Lake Muir is generally thin and discontinuous. Granitic and gneissic rock outcrop indicate that the basement is close to surface in this area. In the south of the study area, additional work is required to enable the lateral boundary of the Eocene sediments to be placed with confidence.

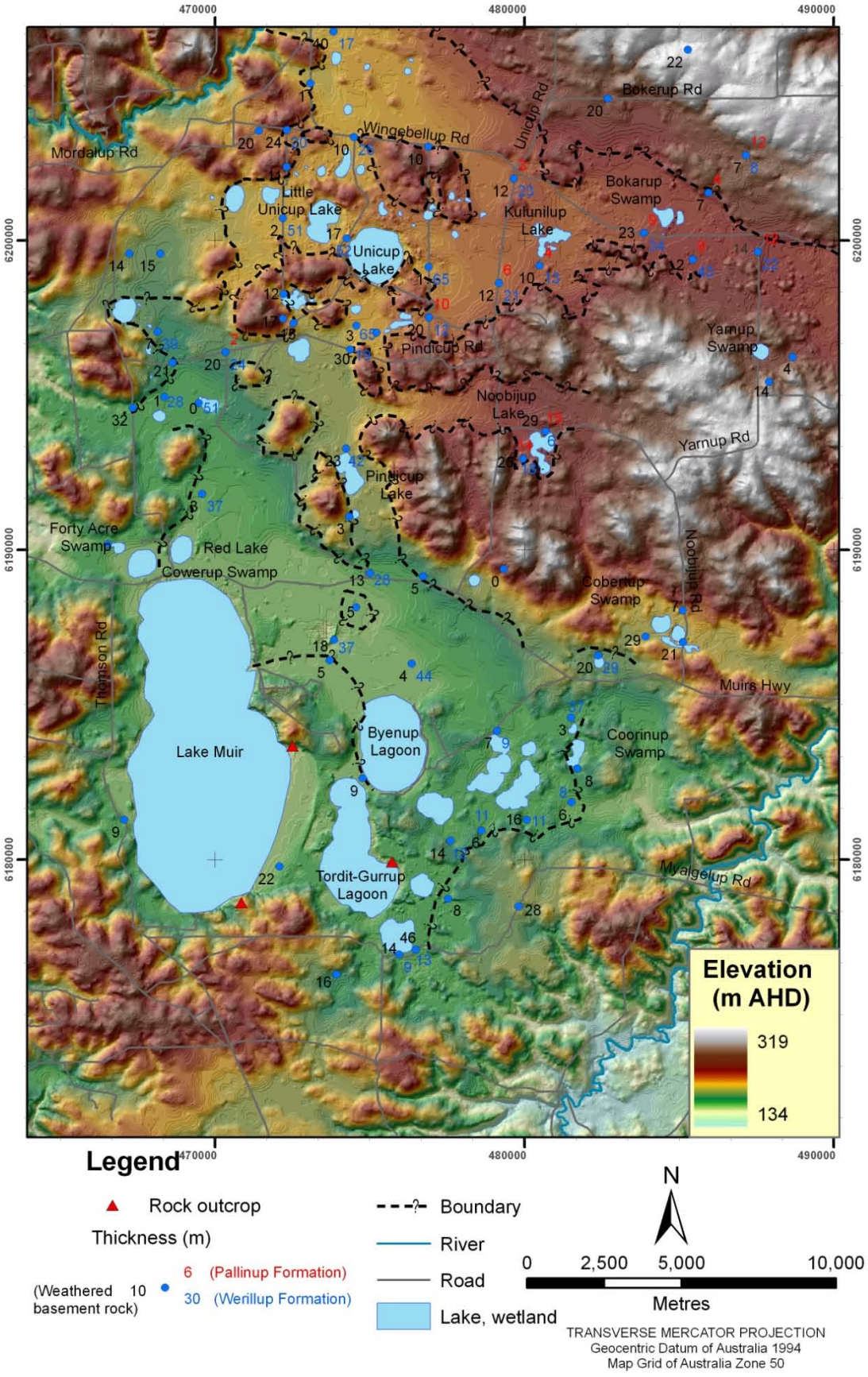

Figure 5–17 Lateral extent of late Eocene sediments.

6 Hydrogeology

6.1 INTRODUCTION

Groundwater in the study area is present in three distinct hydrogeological settings:

- the fractured and weathered basement rocks of the Yilgarn–Southwest Province;
- the fractured and weathered basement rocks of the Albany–Fraser Province; and
- the sediments of the Eucla Basin which overlie the basement rocks.

Regional hydrogeology mapping (De Silva, 2000; 2004) recognised three distinct aquifers in the study area and proposed three palaeochannels (Figure 5–4):

- the surficial aquifer;
- the sedimentary aquifer; and
- the fractured and/or weathered basement rock aquifer.

The hydrogeology of the study area was summarised (Smith, 2003) prior to the 2003 groundwater investigation program. This summary recognised that the 2003 groundwater investigation program would increase and refine our knowledge of groundwater flows and quality in the study area.

The main focus of this chapter is the detailed hydrogeology of the study area derived during this research project. The chapter provides information on the physical properties of the groundwater, groundwater flows, and the interactions between groundwater and the aquifer media that control water salinity in the area. The PM and MU bores referred to in this chapter are shown on Figure 4–1.

6.2 AQUIFERS

6.2.1 Surficial aquifer

The surficial aquifer is comprised of recent Cenozoic alluvial, colluvial, lacustrine sediments and transported ferricrete that overlie both the sediments of late Eocene

age (Figure 5–5) and weathered basement rock. These sediments are found mainly on the broad-valley floors and at the base of hill slopes. They are generally absent from the crest of hills and where ferricrete is exposed *in situ*. Consisting of clay, sand and gravel, the aquifer is between 2 to 34 m thick with the greatest thickness found at the base of hill slopes above weathered basement rock. The aquifer is generally thicker in the south of the study area, as uplift of the southern margin resulted in a depositional environment in this area.

The sediments form an unconfined aquifer with the depth to water varying from 0 to 6 m, but most commonly between 1 and 3 m BGL.

6.2.2 Sedimentary aquifer

The sedimentary aquifer is composed of sediments correlated with the Werillup and Pallinup Formations (including the *in situ* ferricrete of the Pallinup Formation) which are part of the on-shore Eucla Basin and overlie the fractured and/or weathered basement rock aquifer (Figure 5–5). The sedimentary aquifer is confined where overlain by sediments of the surficial aquifer, but elsewhere in the study area is unconfined.

The margin of the sedimentary aquifer is concealed by ferricrete or sediments of the surficial aquifer. The extent of the aquifer (Figure 5–17) has been inferred in the present study from field mapping and the study of rock chips from drill holes (see section 5.8.4).

The aquifer is present beneath the flat to gently-sloping land surface that forms the floor of the modern broad-valleys (Figure 5–17). Thickness of this aquifer (Table 6-1) is variable, ranging from 4 m in bore MU08 to > 65 m in bore MU63D (Figure 4–1). It is thinnest where it abuts the flanks of the valleys or low hills (Figure 5–13 to Figure 5–16). Thickness increases away from the valley flanks and is generally between 30 and 40 m near Kulunilup Lake. It has a variable thickness around Unicup Lake from about 20 m in bore MU04 to between 50 and 65 m in bores MU03D, MU10D, MU62D, MU63D and MU64D (Figure 4–1).

The sedimentary aquifer is poorly defined in the southern part of the study area where erosion, since the formation of the ferricrete, has removed the Pallinup Formation. The Werillup Formation, where present, is generally thin. The aquifer has not been identified in bores MU58D and MU60D (Figure 4–1) north and south

respectively of bore MU59D which has intersected one of the thickest sections (37 m) of the aquifer in the south (Figure 5–15). Similar thickness is seen further east with 44 m in bore MU61 and 37 m in bore MU68 (Figure 4–1). The aquifer thins significantly east of Tordit-Gurrup Lagoon, with thicknesses between 8 m and 12 m in bores MU29, MU30, MU31 and MU48 (Figure 4–1). Further work is needed to determine the thickness of the regolith and depth to basement rock if the extent of the aquifer in the south is to be more precisely defined.

Table 6-1 Maximum and minimum thickness of the sedimentary aquifer at various locations within the study area.

Location	Thickness (m) (minimum)	Bore ID	Thickness (m) (maximum)	Bore ID
North of Bokarup Swamp	4	MU08	12	MU09
Surrounding Kulunilup Lake	17	MU15D	43	MU11D
Surrounding Unicup Lake	20	MU04	> 65	MU63D
Valley containing Noobijup Lake	20	MU22D	34	PM10
East of Lake Muir	8	MU48	44	MU61D

The aquifer consists of three regolith units: the channels sands, the flood plain and the shallow marine units. The channel sand regolith unit consists of normally-graded beds containing poorly sorted, fine- to coarse-grained, subangular to subrounded quartz-dominated sand with minor clay. The channel sand unit intersected by drilling is between 4 m and > 65 m thick in bores MU29D and MU63D, respectively (Figure 4–1). It is found both above and below the flood plain unit.

The flood plain regolith unit consists of interbedded, dark grey to black, carbonaceous clays, carbonaceous silts and medium- to coarse-grained quartz sand. The thickness of the unit is variable, ranging from 3 m in bore MU67D to 66 m in bore LM7 (Dampier Mining Company Limited, 1981).

The shallow marine regolith unit consists of well sorted, fine-grained quartz sand with some clay. This unit, where preserved near Bokarup Swamp, Kulunilup Lake and Noobijup Lake, is generally between 8 to 10 m thick, but ranges between 2 m in bore MU41D and 14 m in bore MU22D.

6.2.3 Fractured and/or weathered basement rock aquifer

The fractured and/or weathered basement rock aquifer (defined by Smith (2003)) (abbreviated to weathered basement rock (WBR) aquifer) is laterally extensive in the study area (Figure 5–13 to Figure 5–16) and is confined to semi-confined. The weathered profile is developed over fresh granite and gneiss (Figure 5–5 and Figure 5–6) and ranges in thickness from about 1 m in bores MU34 and MU56D to > 46 m in bore MU46A. Regional shear zones are known in the study area. Under the broad-valley floors the aquifer is overlain by either the sedimentary or surficial aquifers (Figure 5–13 to Figure 5–16). It is normally the only aquifer present on the slopes and crests of hills where it is capped by *in situ* ferricrete.

Most of the bores sited in the fractured and/or weathered basement rock aquifer are screen within the weathered profile and thus term fractured and/or weathered basement rock aquifer has been abbreviated to weathered basement rock (WBR) aquifer.

6.3 PHYSICAL PROPERTIES OF THE GROUNDWATER

6.3.1 Total Dissolved Solids

Total Dissolved Solids (TDS) in the groundwater of the study area increase from north to south with a minimum of 210 mg/L in bore MU19S to a maximum 95 300 mg/L in bore MU45D (Figure 6–1). According to the classification by the Australian Water Resources Council (1988) less than 21% of the groundwater is fresh or brackish, with the remainder being saline (Table 6-2).

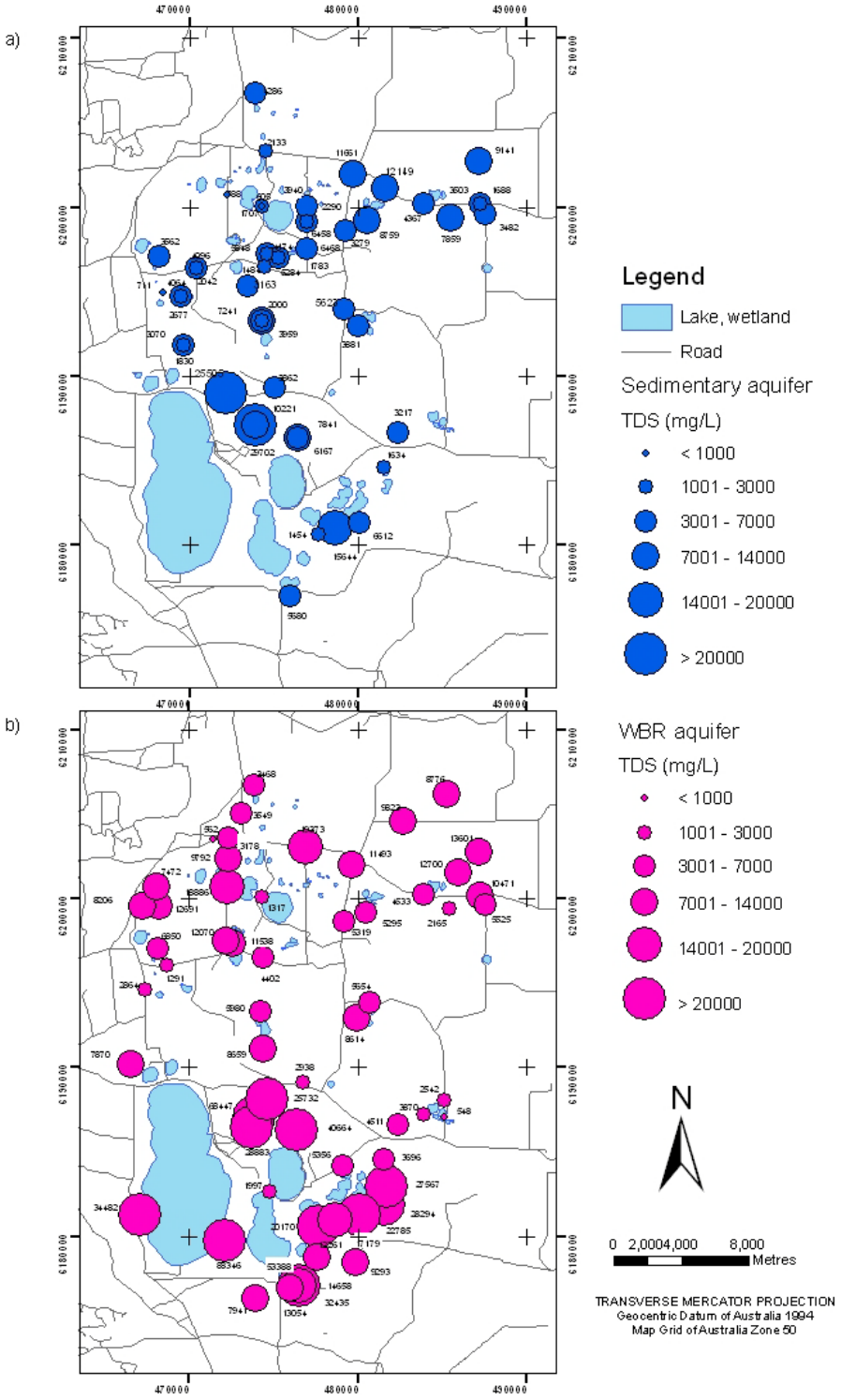

Figure 6–1 TDS of groundwater across the study area showing the increase from north to south a) sedimentary aquifer, b) WBR aquifer.

Table 6-2 Groundwater quality classifications (Australian Water Resources Council, 1988) giving the % of bores within each TDS grouping and the cumulative % showing that 21% of the bores have groundwater that is fresh to brackish and the remaining bores having saline groundwater.

TDS (mg/L)	%	Cumulative %	Classification
134–1000	7	8	fresh to brackish
1001–3000	14	21	brackish
3001–7000	30	51	saline
7001–14000	33	84	saline
14001–20 000	5	89	saline
> 20 000	11	100	saline

6.3.1.1 TDS – variability

Groundwater quality varies substantially in the study area. Rainfall distribution, lithology, landscape position and geological structure are the main factors that contribute to the variability.

TDS shows an increase from north to south within all aquifers (Figure 6–1). Across the surficial aquifer (16 bores) groundwater TDS ranges from about 500 mg/L to > 35 000 mg/L. The groundwater in the sedimentary aquifer shows a steep gradient in TDS increasing to the south. In the north the TDS is up to 10 000 mg/L, whereas, east of Lake Muir the values rise abruptly to 30 000 mg/L TDS. The greatest change in TDS is recorded in the WBR aquifer, with values of 3000 to 12 000 mg/L in the north and up to about 95 300 mg/L in the south just east of Lake Muir.

In the south of the study area the groundwater can change from brackish to highly saline over short vertical distances. For instance, bore MU30S contains brackish water with TDS of 1200 mg/L at 7.5 m depth (base of screen), whereas at 33 m depth was 24 700 mg/L (MU30D) when recorded in May 2006. The TDS may also decrease vertically downhole as seen in various bores listed in Table 6-3.

The WBR aquifer has generally higher TDS than the overlying sedimentary aquifer (Figure 6–2). In bores MU46S, MU46I and MU46D TDS value increases from 16 750 mg/L at 20 m (sedimentary aquifer) to 35 000 mg/L at 41 m (WBR aquifer) and 65 000 mg/L at 65 m at its base. In the sedimentary aquifer TDS increases from about 2000 mg/L at 4 to 6 m to between 6000 and 7000 mg/L at depths greater than 45 m in bores MU62, MU63 and MU64.

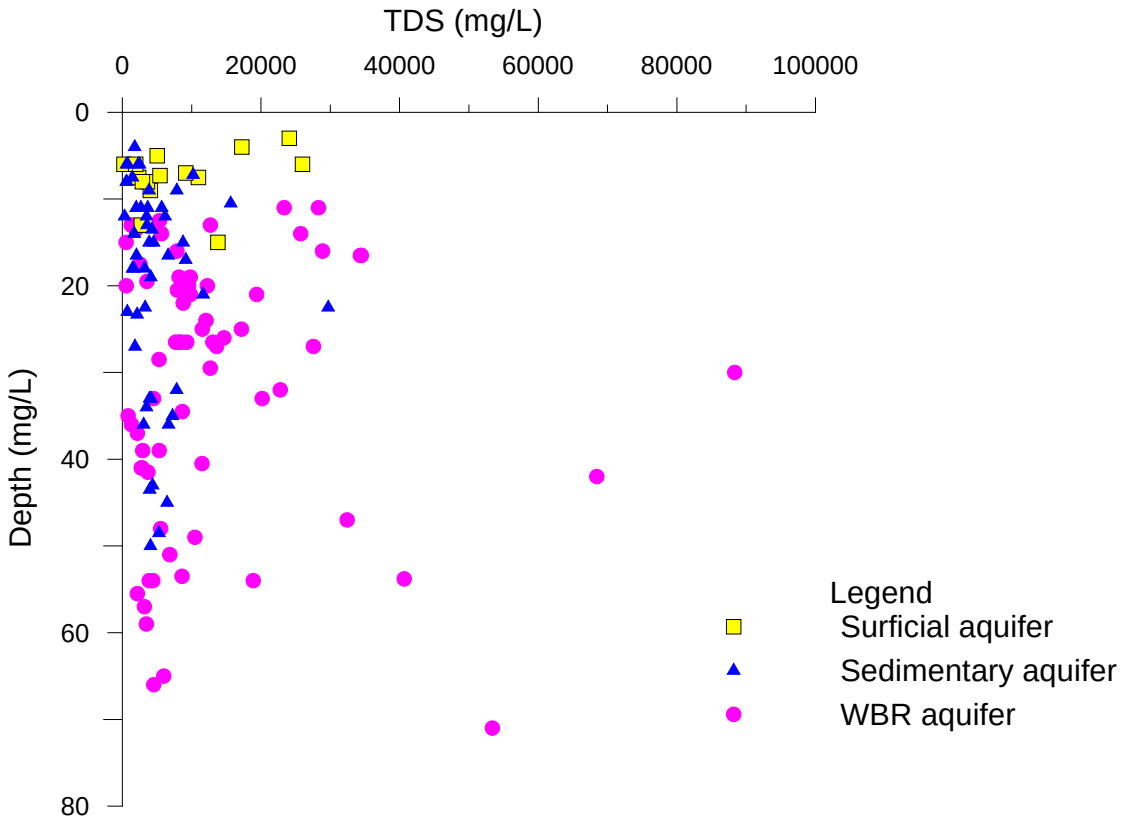

Figure 6–2 Variation of groundwater TDS with depth showing a broad scatter of TDS values in all aquifers.

6.3.1.2 Rainfall and evapo-concentration

Rainfall directly recharges the surficial aquifer, and the sedimentary aquifer where it is unconfined. The groundwater is generally fresh to brackish where recharged by rainfall and the watertable is at depths greater than 2 m in summer. The hydraulic heads at sites

MU62 and MU63 show a downward vertically gradient. The watertable is at depths greater than 2 m in summer and the TDS is about 2500 mg/L.

Where the watertable is within 2 m of surface in the summer months, groundwater discharge is by evaporation with the salts precipitating within the regolith profile (Nulsen, 1981). Concentration of salts is evident under Lake Muir which has a watertable within 1 m of lake floor. The TDS at the watertable is between 34 080 and 77 840 mg/L. On the broad-valley floors evapo-concentration has resulted in the surficial aquifer having TDS values that are classified as brackish to saline as recorded in bore MU15A with a TDS of 22 250 mg/L (Table 6-3).

Table 6-3 Bores showing a decrease in TDS of groundwater with depth.

Bore ID	Depth (m BGL)	TDS (mg/L)	Aquifer at screen	Date
MU15A	4	22 250	Surficial	31/10/2006
MU15S	15	10 350	Sedimentary	31/10/2006
MU15D	20.5	6200	Weathered basement rock	31/10/2006
MU16S	9	7550	Sedimentary	11/05/2006
MU16D	55.5	2500	Weathered basement rock	11/05/2006
MU22S	7.5	12 300	Surficial	11/05/2006
MU22D	14	7950	Sedimentary and weathered basement rock	11/05/2006
MU54S	8	3350	Sedimentary	9/05/2006
MU54D	13	2000	Weathered basement rock	9/05/2006

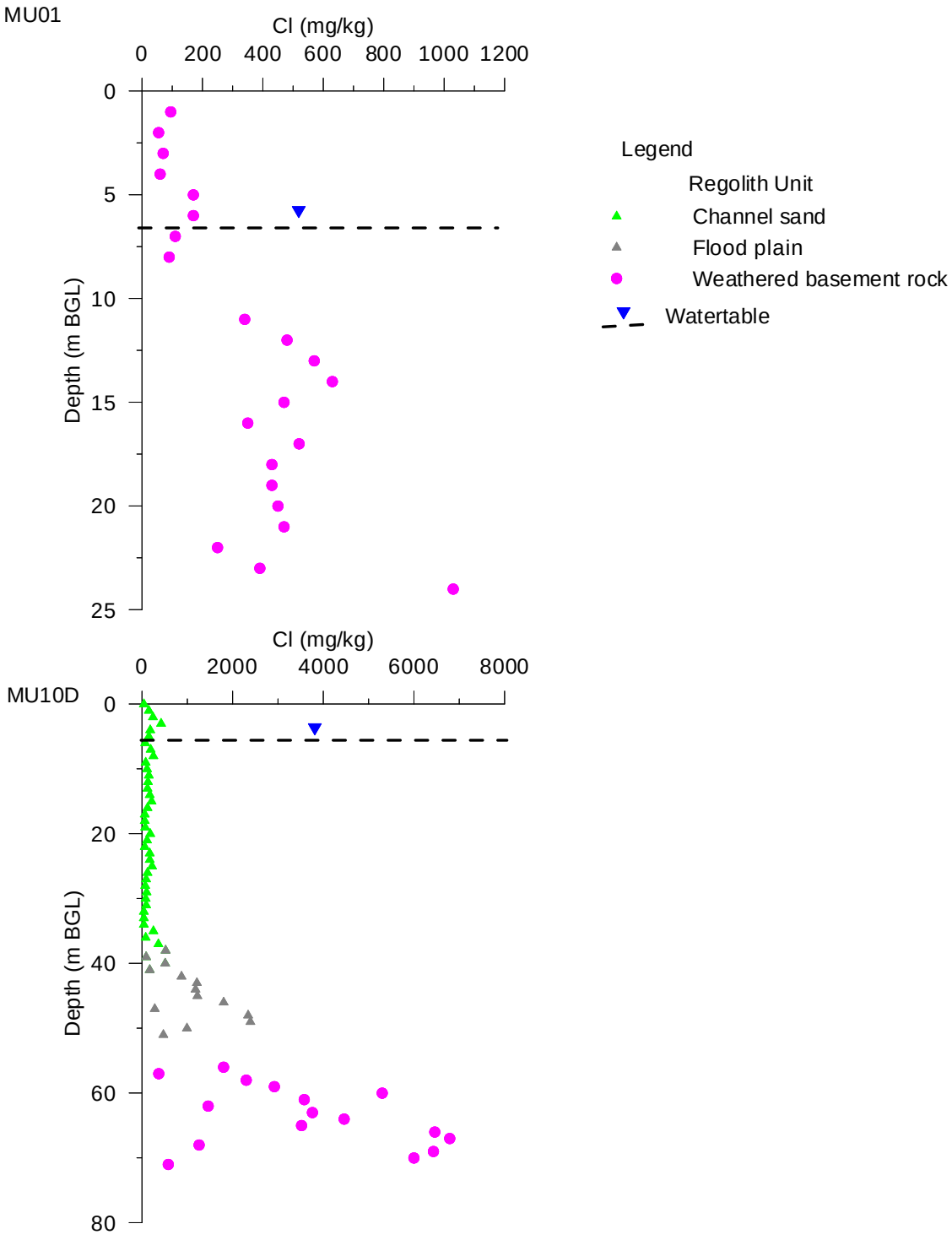

Figure 6–3 Dissolved chloride concentrations derived from rock chips recovered from a) MU01 b) MU10D.

6.3.1.3 Landscape position

Two regolith profiles were selected to assess the influence of landscape position on groundwater TDS. Bore MU01 is located on the upper slope, whereas MU10D is sited on the valley floor. Chloride solute concentrations from regolith water extracts were measured from rock chip samples according to the method described by Johnston et al. (1982). Regolith water extracts were made by adding a fixed volume of distilled water to 25 g of regolith sample (after oven drying), shaken for one hour and the chloride concentration measured on the solution extract. Bore MU10D intersected the sediments of the Werillup Formation and the chloride solute concentrations (at metre intervals) showed a distinct difference between the two regolith units (Figure 6–3).

The channel sand regolith unit had chloride values ranging from 40 to 420 mg/kg. In contrast, the chloride values obtained from the sediments of the flood plain regolith unit ranged from 90 to 2390 mg/kg. The lower values probably reflect where layers of quartz-dominated sand were interbedded with organic clays and silts of the flood plain unit.

The WBR aquifer is either the sole aquifer on the upper slopes of hills or is overlain by the sedimentary aquifer (Figure 5–13 to Figure 5–16). The regolith water extracts from bore MU01 (sited on the northeast hills) had chloride solute concentrations that initially increase down hole (Figure 6–3(b)). Between 1 to 14 m depth the chloride values increased from 55 to 620 mg/kg. Below this the chloride values were scattered between 250 and 520 mg/kg, whereas a value of 1030 mg/kg was noted at the deepest recorded depth of 24 m BGL (Figure 6–3(b)). The increase in chloride solute concentrations in this bore are similar to the 'monotonic' vertical chloride values described within the Manjimup Wood Chip licence area about 30 km northwest (Johnston, 1987). As with the Manjimup Wood Chip licence area this type of profile is associated with upper slopes in the study area .

In contrast, MU10D is sited on a broad-valley floor where the WBR aquifer is overlain by the sedimentary aquifer. The chloride solute concentrations obtained from regolith water extracts at bore MU10D ranged from 370 to 6790 mg/kg with most being more than 1000 mg/kg (Figure 6–3(a)). The chloride solute concentrations show a distinct

variation related to lithology within the Werillup Formation. The channel sand regolith unit has chloride concentrations less than 1000 mg/kg whereas the flood plain unit has values greater than 1000 mg/kg. The weathered basement rock material indicates that position in the landscape is also important, with the chloride solute concentration being greater at the base of the valley compared to the upper slopes (Figure 6–3).

6.3.1.4 Geological structure

Groundwater TDS of 30 000 mg/L in the south of the study area is very high considering average annual rainfall of between 700 and 900 mm. The Tone River catchment, north of the study area, has groundwater TDS values from 1000 to 20 000 mg/L and averages 10 000 mg/L (Smith et al., 2005). About 30 km to the south of the study area the groundwater in bore PM06 has 17 000 mg/L TDS (Panasiewicz et al., 1997).

The magnitude of the groundwater TDS (up to 95 300 mg/L) in the study area is indicative of an internally draining groundwater basin. If very saline groundwater from the southern part of the study area was discharging into the Frankland River and mixing with the river water a rise in TDS along this stretch may be evident. The TDS of surface water along the Frankland River was measured on the 26th March 2007 to identify whether groundwater exits the study area by this route. There was no apparent rise in TDS with values ranging from 9850 to 15 550 mg/L, similar to the river water north of Muirs Hwy. (Table 6-4).

Uplift since the Miocene has elevated the plateau in the south of the study area and created a barrier to groundwater flow. This is evident by the lack of saline groundwater discharge into the Frankland River and the high groundwater TDS values east of Lake Muir. This plateau has created an internally draining groundwater basin.

Table 6-4 TDS recorded along the Frankland River on 26th March 2007. Discharge sites of highly saline water are not evident.

Easting (MGA)	Northing (MGA)	TDS (mg/L)	Comments
486059	6179087	11 500	Low flow
481463	6172294	13 300	pool
481388	6172342	14 950	
482446	6173450	15 000	
482499	6173549	15 550	Long pool
488613	6182689	15 100	Long pool
489193	6182546	14 250	Low flow
491231	6184929	9840	Long pool
501380	6198214	14 400	North of Muirs Hwy

6.3.2 Temperature

Groundwater temperature varied from 14.3 to 26.7°C between 2004 and 2007, with a majority of measurements being between 16 and 19°C.

6.3.3 Hydraulic head

Depths to standing water level were measured on a regular basis to determine hydraulic heads. In fresh water environments the hydraulic head is often assumed to be the height of the water column relative to a fixed datum such as AHD. However, from equation (6.1) it can be seen that the hydraulic head calculation includes density and acceleration due to gravity (Freeze and Cherry, 1979):

$$h = z + \frac{p}{\rho g} \qquad (6.1)$$

where h is the hydraulic head (m), z is the elevation above a reference datum (m), p is fluid pressure (N/m^2), ρ is the fluid density (kg/m^3) and g is the acceleration due to gravity (m/s^2). The fluid pressure, p, is defined as (Freeze and Cherry, 1979):

$$p = \rho g h_p \qquad (6.2)$$

where h_p is the pressure head (m). In the field, h_p is measured as the height (m) of the water column from a set point such as the screen interval. If g and ρ are constant, equation (6.2) can be substituted into equation (6.1) and the hydraulic head becomes:

$$h = z + h_p \qquad (6.3)$$

In the study area, g can be considered a constant, but the groundwater density will vary. Water density is affected by dissolved solids, dissolved gases, water compressibility and temperature (Oberlander, 1989). Oberlander (1989) investigated the significance of these components on density. Compressibility and geothermal gradients became important at depths greater than 200 m and 300 m, respectively. In the study area, the deepest bore is 80 m. Therefore, the most important variable on water density is TDS, the value of which varies significantly (Figure 6–1).

6.3.3.1 Density determinations

Groundwater density can be calculated using an empirical formula if the salinity (S) in g/kg is known. For TDS up to about 7000 mg/L, S is approximately equal to TDS value/1000 (McCutcheon et al., 1992). However, in the present study 49% of the groundwater sampled had values greater than 7000 mg/L (Table 6-2). Therefore, TDS cannot be used to determine salinity precisely. Salinity (g/kg) can be calculated from electrical conductivity using equations (6.4) and (6.5) (McCutcheon et al., 1992):

$$S = a_0 + a_1 R_T^{1/2} + a_2 R_T + a_3 R_T^{3/2} + a_4 R_T^2 + a_5 R_T^{5/2} + \Delta S \qquad (6.4)$$

$$\Delta S = \frac{T - 15}{1 + 0.0162(T - 15)}(b_0 + b_1 R_T^{1/2} + b_2 R_T + b_3 R_T^{3/2} + b_4 R_T^2 + b_5 R_T^{5/2}) \qquad (6.5)$$

where R_T is the ratio of electrical conductivity to the conductivity of seawater at 35 g/kg (~50 mS/cm), T is temperature in °C, the empirical coefficients

for a_i are:

$a_0 = 0.008$, $a_1 = -0.1692$, $a_2 = 25.3851$, $a_3 = 14.0941$, $a_4 = -7.0261$, $a_5 = 2.7081$

and for b_i are:

$b_0 = 0.0005$, $b_1 = -0.0056$, $b_2 = -0.0066$, $b_3 = -0.0375$, $b_4 = 0.0636$, $b_5 = -0.0144$.

Using salinity, groundwater density can be calculated using the following empirical formula (McCutcheon et al., 1992):

$$\rho_g = \rho_o + AS + BS^{3/2} + CS^2 \qquad (6.6)$$

where ρ_g is the density of groundwater (kg/m^3), ρ_o is density of pure water (kg/m^3) as a function of temperature, T is temperature (°C), S is salinity (g/kg) and

$$A = 8.24493\times10^{-1} - 4.0899\times10^{-3}T + 7.6438\times10^{-5}T^2 - 8.2467\times10^{-7}T^3 + 5.3675\times10^{-9}T^4$$

$$B = -5.724\times10^{-3} + 1.0227\times10^{-4}T - 1.6546\times10^{-6}T^2$$

$$C = 4.8314\times10^{-4}$$

The density of pure water is obtained using Thiessen-Scheel-Diesselhorst equation (6.7)

$$\rho_0 = 1000[1 - \frac{(T + 288.9414)}{508929.2(T + 68.12963)}(T - 3.9863)^2] \qquad (6.7)$$

Groundwater densities calculated across the study area range from 1.00 to 1.08 g/cm^3.

6.4 GROUNDWATER MOVEMENT

Groundwater flow in the study area has both lateral and vertical components. Lateral groundwater flow takes place in local or intermediate flow systems. The terms 'local' and 'intermediate' are not specific but provide a qualitative framework (Freeze and Cherry, 1979). In the present study, local flow systems are considered to be shallow and follow the topographic slope, originating close to the local surface-water divide and discharging to the nearest drainage. Local flows are found within the WBR aquifer where it is exposed on the hills and ridges. The intermediate flow systems are deeper than the local flows and are present in the sedimentary aquifer and the underlying WBR aquifer.

Determining the vertical component of the groundwater flow enables aquifer interactions to be evaluated. Comparison of hydraulic heads within individual aquifers indicates the direction of potential groundwater movement between aquifers and enables areas of potential recharge and discharge within the study area to be identified.

6.4.1 Water level classification

Measured water levels indicate the elevation of the potentiometric surface at a specific depth in a confined aquifer or the elevation of the watertable in an unconfined aquifer (Freeze and Cherry, 1979). In this study, the bores have been coded according to the aquifer across which the screens are set. The watertable is determined by the water levels in 15 bores. The potentiometric surface for the sedimentary aquifer and the WBR aquifer was defined by water levels in 43 and 42 bores, respectively. The screens are set across the boundary of the two aquifers in 29 bores.

6.4.2 Variable density corrections

To enable groundwater of differing density to be compared, Lusczynski (1961) developed the concept of the fresh-water pressure head (h_f) and environmental pressure head (h_e). The fresh-water pressure head allows horizontal gradients to be determined, whereas the environmental pressure head enables vertical gradients to be compared.

6.4.2.1 Fresh-water pressure head

In a saline aquifer, the water level in a bore represents the pressure required to balance the pressure exerted by groundwater in the aquifer at the level of the screens. The pressure exerted is defined by equation (6.2). If the groundwater in the bore was fresh, to exert the same pressure at the level of the screens, the height of the water within the column would change according to:

$$\rho_p g h_p = \rho_f g h_f \qquad (6.8)$$

$$\text{or} \qquad h_f = (\rho_p/\rho_f) h_p \qquad (6.9)$$

where h_f is the fresh-water pressure head, ρ_p is the density of the water at the screens and ρ_f is a reference density which in this study is the fresh-water density. By converting the pressure head to fresh-water pressure head (equation (6.9)) the horizontal groundwater gradient within the study area can be determined.

When using fresh-water pressure heads to the determine horizontal gradient it is important to consider that lateral variation in density can affect flow direction (Oberlander, 1989). A significant error in flow direction can occur in areas that have a low hydraulic gradient (Alkalali and Rostron, 2003). In the study area, the hydraulic

gradient is generally greater than 0.7 m/km. Consequently, this source error in flow direction is not considered an issue. In the sedimentary and WBR aquifers the fresh-water pressure heads for October 2006 were used to determine horizontal groundwater flow direction.

6.4.2.2 Environmental heads

The environmental pressure heads need to be calculated to determine the vertical groundwater flow gradient. Within a saline aquifer the vertical water column will be of varying density. The environmental pressure head is defined by Lusczynski (1961) as 'the water of constant or variable density occurring in the environment along a vertical [line] between that point [screen] and the top of the zone of saturation'. This head is calculated using:

$$\rho_f h_e = \rho_p h_p - Z_i(\rho_p - \rho_a) - Z_r(\rho_a - \rho_f) \qquad (6.10)$$

where Z_i is the depth (m AHD) at which the water pressure is measured or the depth to the screen interval, Z_r is the depth datum (m AHD) such as ground level, ρ_a is the average density over the interval, and h_e is the environmental pressure head. From these parameters the vertical groundwater flow gradient can be determined.

6.4.3 Horizontal groundwater flow

6.4.3.1 Watertable

The watertable has not been contoured, but the levels suggest that it generally slopes southward with fresh-water pressure heads ranging from 209 m AHD (bore MU15A) in the north to 172 m (bore MU45) in the south of the study area. The watertable will locally be influenced by the northeast hills, westerly sloping ridges and the elevated plateau that bounds the southern end of the study area.

6.4.3.2 Local flows in the WBR aquifer

Groundwater flow within the WBR aquifer is characterised by local and intermediate flow systems. The local flow system generally follows the topographic slope, originating close to the local surface-water divide and discharging at the nearest

drainage. Localised flows are found within the elevated hills in the northeast, the westerly sloping ridges and the plateau in the south (Figure 3–1 and Figure 6–4).

Local groundwater flows associated with the northeast hills are predominantly south to southwest toward Bokarup Swamp, Kulunilup Lake and Unicup Lake. The fresh-water pressure head decreases from 281 m AHD (bore MU01) to 231 m AHD (bore MU02) over a distance of about 3000 m.

The topographic relief is more dissected within the two westerly sloping ridges. The northernmost ridge contains numerous hills separated by short north draining valleys. Along the southernmost ridge the hills are more pronounced and are separated by south draining valleys. The local flows are more complex along these two ridges, but essentially follow the topographic relief.

Groundwater flow near the plateau in the south will also follow the topographic relief towards Lake Muir and the poorly drained flats on which Tordit–Gurrup Lagoon is located. Other areas where groundwater movement is likely to be influenced by local topographic highs are southwest of Unicup Lake, Yarnup Swamp and Cobertup Swamp (Figure 3–1 and Figure 6–4).

6.4.3.3 Intermediate flows in the sedimentary and WBR aquifers

The direction of lateral groundwater flow in an isotropic aquifer is generally considered to be perpendicular to the lines of equal potentiometric pressure (Freeze and Cherry, 1979). The sedimentary and WBR aquifers are anisotropic. Factors such as the magnitude and direction of the hydraulic gradient (after correction for density); magnitude and direction of structural gradient; and differences between the reference density and the ambient groundwater density can affect groundwater flow directions (Alkalali and Rostron, 2003). The driving force ratio (DFR) was derived by Davies, (1987) and sited in Alkalali and Rostron (2003) to measure the possible degree of influence these factors have on groundwater flow according to:

$$DFR = \frac{\Delta\rho}{\rho_f}\frac{\nabla E}{\nabla h_f} \qquad (6.11)$$

where h_f is the fresh-water head calculated at a reference density ρ_f, E is the elevation of the base of the aquifer, and $\Delta\rho$ is the difference in density between the reference and the formation water density. *DFR* values greater than 0.5 are considered significant and corrections to the groundwater flow need to be considered. The *DFR* values for the sedimentary and WBR aquifers ranged from 0.017 to 0.048, well below 0.5. Thus the lateral groundwater flows have been developed from the fresh-water pressure heads even though the aquifers are anisotropic.

The calculated flows in the sedimentary and WBR aquifers were similar and thus are discussed together. Groundwater flow appears strongly influenced by the topographic rises within the study area creating several zones in which the flow direction is reversed and groundwater convergence occurs. Many of the lakes in the study area are associated with such zones of groundwater convergence.

East of Bokarup Swamp, bores MU12D and MU37D are sited on a topographic saddle at 222 m AHD. The presence of a groundwater divide to the east of bore MU37D cannot be confirmed by the available hydraulic head data (Figure 6–4). Under the broad-valley floor, west of Bokarup Swamp the groundwater flow is influenced by the northeast hills and the northernmost westerly sloping ridge. Convergence of the southwest and northwest groundwater flows is roughly aligned with the line of lakes from Kulunilup Lake to Unicup Lake (Figure 6–4).

In the northwest, groundwater flows into the Tone River (west of bore MU66D) through a narrow valley about 1 km across (Figure 4–1 and Figure 6–4). The southern flank of this valley forms a gentle topographic rise that prevents groundwater flowing south to the Tone River from the broad-valley floor.

In the valley east of Buranganup Road, groundwater flows to the southwest. Hills of weathered basement rock block the flow resulting in the formation of a small chain of lakes just north of Pindicup Road and Buranganup Road junction (Figure 6–4). West of bore MU49 a topographic saddle is evident (Figure 4–1 and Figure 6–4), but a groundwater divide cannot be confirmed on available hydraulic head data. Towards the south of this valley the groundwater flows to the southwest under the northern part of Lake Muir.

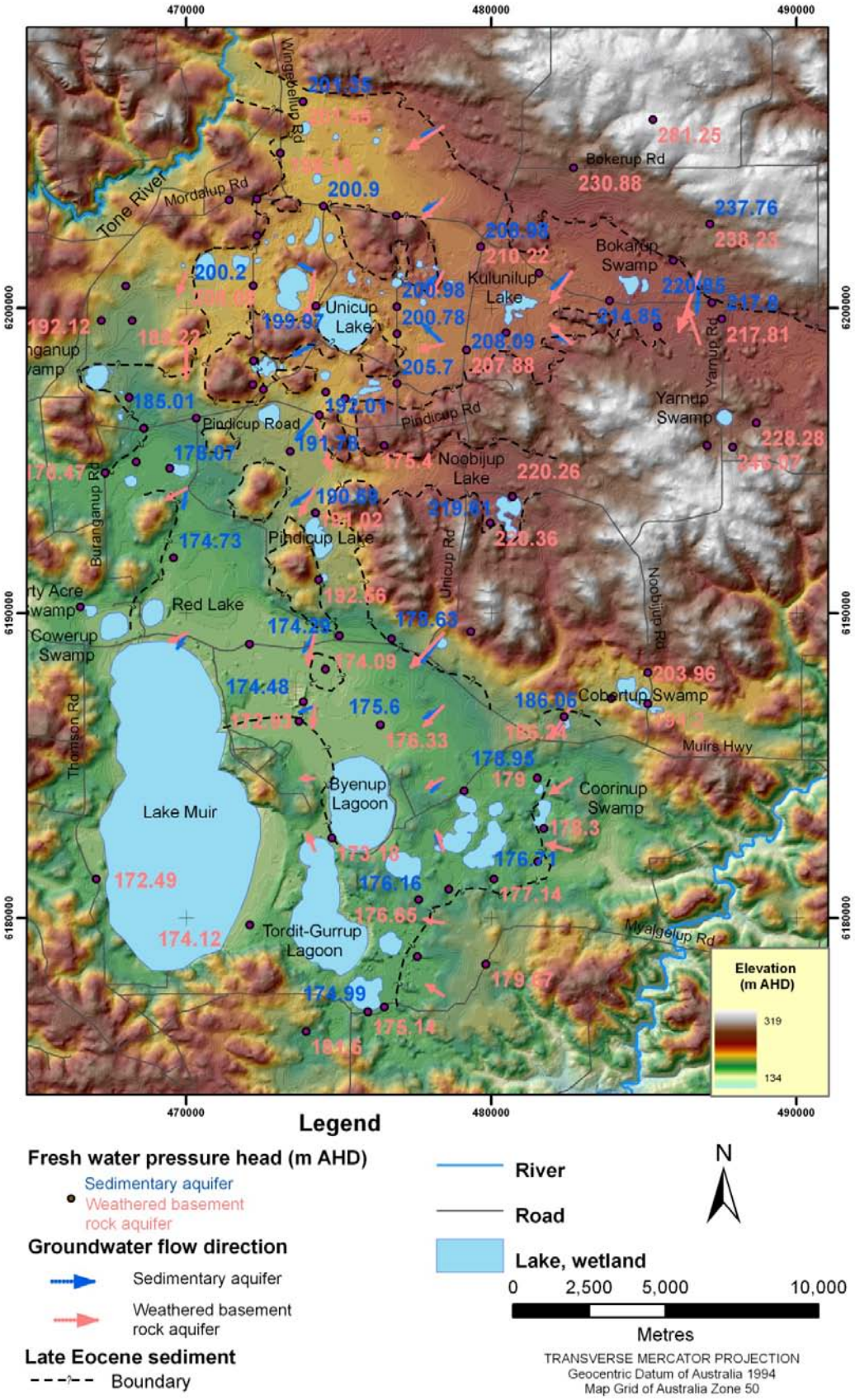

Figure 6–4 Groundwater flow directions derived from the fresh-water pressure heads in October 2006 for the sedimentary and the WBR aquifers.

In the south, groundwater flow is influenced by the southernmost westerly sloping ridge and the southern plateau. Near Muirs Hwy. the groundwater flow is to the southwest. The fresh-water pressure heads near the southern plateau indicate that groundwater flow has changed from southwest to northwest in the WBR aquifer (Figure 6–4). The southwest and northwest flows converge under Lake Muir and Byenup Lagoon.

The groundwater flows generally westward in the valley between the two westerly sloping ridges.

6.4.3.4 Hydraulic gradient

The hydraulic gradient is influenced by both topography and lithology. In the north, the topographic influence is evident in the WBR aquifer with a hydraulic gradient of 5.9 m/km near Bokarup Swamp (Figure 6–4). The hydraulic gradient decreases to between 1.5 and 2 m/km under Kulunilup Lake. The gentle gradient of the basement topography (Figure 5–13 to Figure 5–16), combined with the thick sequences of flood plain regolith unit (Figure 5–13), have reduced the groundwater flow. Thick sequences of quartz sand (bores MU63 and MU64) allow the groundwater to move more freely south of Unicup Lake where the hydraulic gradient has increased significantly to 7.1 m/km in the sedimentary aquifer.

In the south of the study area, the hydraulic gradient of the WBR and sedimentary aquifers are similar at 2.9 and 2.6 m/km, respectively. They decrease to 1.3 and 0.71 m/km respectively, under the poorly-drained flats to the east of Byenup Lagoon.

6.4.4 Aquifer interactions

The difference in the environmental pressure heads between two bores screened at different depths at the same site allows the potential gradient in the vertical direction to be determined between these two points. If the shallow bore has an environmental pressure head greater than that of the deeper bore, groundwater flow at that site is potentially downwards. Potential upward groundwater flow is present where the hydraulic head for the deep bore is greater than that of the shallow bore.

To account for the density differences in the groundwater column the environmental pressure heads in the present study were determined using equation (6.10) and the difference between the heads calculated according to:

$$\Delta h_e = h_{eS} - h_{eD} \qquad (6.12)$$

where h_{eS} is the depth of the environmental pressure head (m AHD) for the shallow bore and h_{eD} is the environmental pressure head (m AHD) for the deep bore.

Where the difference between the environmental pressure heads was ± 0.1 m, the groundwater was considered to have no net upward or downward flow. If the environmental pressure head difference was positive (> 0.1 m) recharge from the upper aquifers to the lower aquifers was occurring, whereas potential groundwater movement was upward if the vertical difference was negative (< -0.1 m).

6.4.4.1 Seasonal response

All three aquifers respond to the seasonal variation in rainfall (Figure 6–5). The weekly environmental pressure head at sites MU15 and MU10 are shown in Figure 6–5. As field EC was not recorded on a weekly basis, the EC recorded in May 2007 was used in equations (6.4) and (6.5). There is a general increase in the depth to the water level through the dry summer and autumn months (December to May) and a decrease during the wet winter and spring months (June to November). The response in the surficial aquifer is greater than that in the sedimentary and WBR aquifers with a particularly rapid rise of the watertable over a four week period around August (Figure 6–5(a)).

The sedimentary and WBR aquifers, while having different environmental pressure heads, respond similarly to the seasonal conditions (Figure 6–5). The magnitude of the response is more subdued in the WBR aquifer (bore MU15D) with the maximum difference in the environmental pressure head being 0.42 m compared to 0.64 m in the sedimentary aquifer (bore MU15S) (Figure 6–5(a)).

Seasonal water level response is also evident at site MU10 (Figure 6–5(b)). The screens in bore MU10D straddled two aquifers therefore the heads do not reflect the individual aquifers. Water levels in the bores MU10I and MU10D reflect the seasonal variation but do not respond quickly to rainfall events as seen in the shallowest bore MU10S.

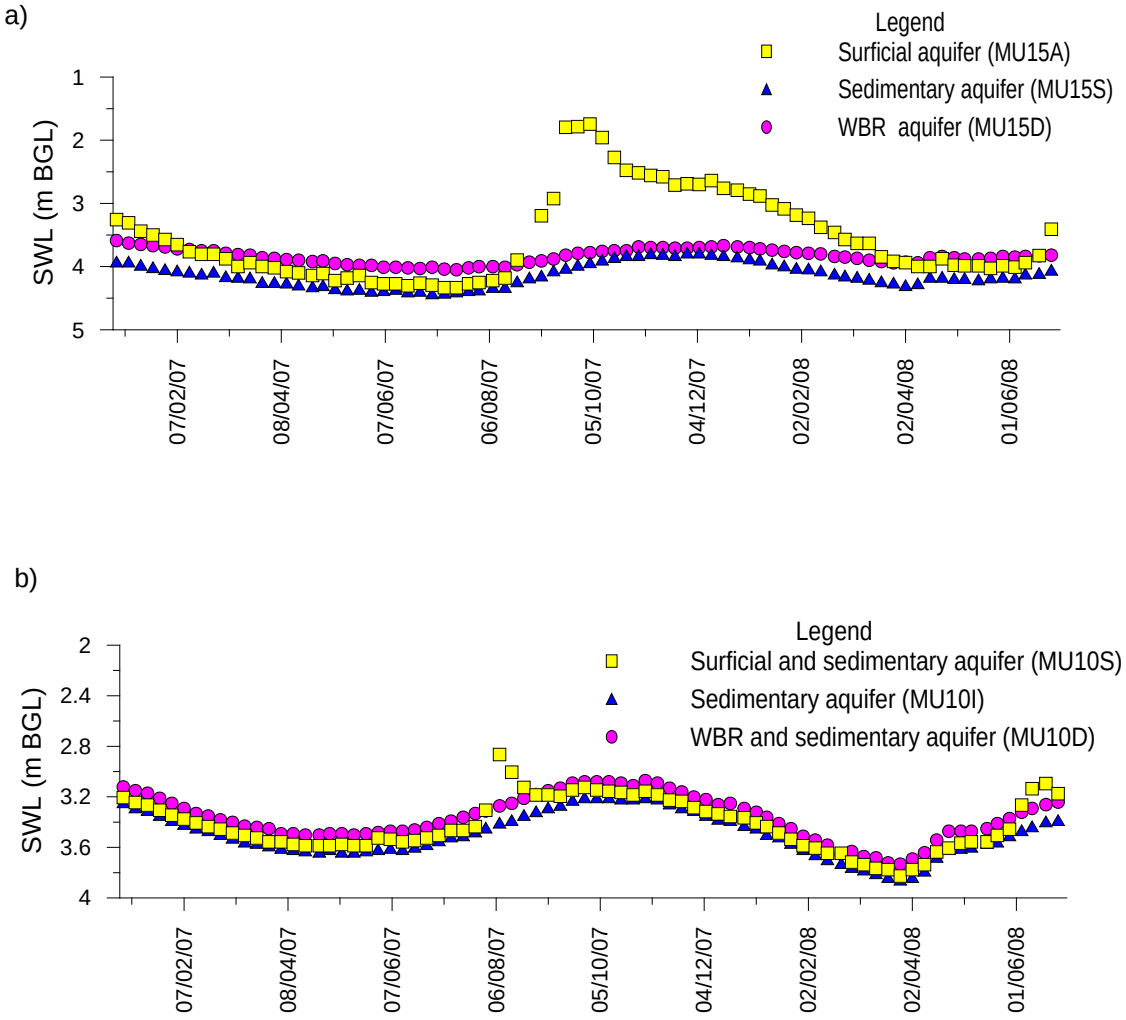

Figure 6–5 Seasonal groundwater response to recharge (water depth corrected for density) a) bores MU15A, MU15S and MU15D; b) bores MU10S, MU10I and MU10D.

6.4.4.2 Downward groundwater pressure

Recharge from the surficial aquifer into the underlying aquifers is indicated where the difference in the environmental pressure heads is positive (equation (6.12)). Bores with a difference in environmental pressure head greater than 0.5 m (bores MU62S and MU62D; MU63S and MU63D; MU64S and MU64D) were generally associated with the channel sand regolith unit near Unicup Lake. Bores MU62D, MU63D and MU64D intersected between 39 and 65 m of the channel sand regolith unit in which the poorly-sorted quartz sands and gravels allow groundwater to move freely. In the south of the study area environmental pressure head differences greater than 0.1 m are seen in bores

MU54S and MU54D, MU57S and MU57D, MU60S and MU60D. These bores are associated with weathered basement rock overlain by recent sediments.

6.4.4.3 Upward groundwater pressure

Potential leakage from the WBR aquifer into the sedimentary aquifer or potential groundwater discharge is indicated where the difference in the environmental pressure heads is negative (equation (6.12)) and is seen in Figure 6–5(a). Environmental pressure head differences < -0.1 are coincidental with the areas of convergent groundwater flows. These areas are evident on the poorly draining flats under Bokarup Swamp and Kulunilup Lake in the north and east of Byenup Lagoon in the south. In the vicinity of Yarnup Swamp the hydraulic head is above ground level (Figure 6–6).

6.4.5 Hydraulic conductivity

Hydraulic conductivity (K) is a measure of the rate at which fluid will move through an area of porous medium according to:

$$K = \frac{k\rho g}{\mu} \qquad (6.13)$$

where k is intrinsic permeability, ρ is fluid density, μ is the fluid viscosity, and g is gravity. Hydraulic conductivity can be determined in the field by means of a 'slug test', in which the time taken for the water level in a bore to recover after the removal of a set volume of water is measured. Such testing to determine hydraulic conductivity was not undertaken in this study, and calculated estimates of hydraulic conductivity were obtained for the lithologies encountered in this study and compared to published values for similar lithologies elsewhere.

Figure 6–6 Artesian flow at Yarnup Swamp (photo).

Hazen developed an empirical relationship between effective grain size and hydraulic conductivity (Freeze and Cherry, 1979):

$$K = Ad_{10}^2 \qquad (6.14)$$

where d_{10} is the grain-size diameter at which 10% by weight of the particles are finer and 90% are coarser. K is in cm/s, d_{10} in mm, and the coefficient A is 1.

In the present study grain-size diameters of 0.002, 0.034 and 1.03 mm were assigned to the clay, silt and sand lithologies, respectively, from the field logs. Using equation (6.14) an estimate of K was obtained for the Pallinup Formation, Werillup Formation and weathered basement rock at each bore site. The geometric mean was then used to obtain an estimated hydraulic conductivity for each aquifer.

Previous work within the Yilgarn Craton has found that the coarse-grained saprolite zone (Figure 5–6) has typical hydraulic conductivity between 0.6 and 0.75 m/day

(Clarke et al., 2000; George, 1992). The values for the fined-grained saprolite are between 0.06 and 0.09 m/day (Clarke et al., 2000; George, 1992). Peck and Williamson (1987) obtained values for the coarse-grained saprolite that were significantly lower (0.0098 m/day). Much lower values of hydraulic conductivity reported by Peck and Williamson (1987) may have resulted from the drilling technique used (Clarke et al., 2000).

In the present study, a hydraulic conductivity of 0.6 m/day was derived for the weathered basement rock in the study area, similar to the measured hydraulic conductivity value obtained by Clarke et al. (2000) and George (1992) for the coarse-grained saprolite of the Yilgarn Craton.

The hydraulic conductivity derived for the Werillup Formation in the study area is about 10 m/day. Measured hydraulic conductivity for the Werillup Formation elsewhere is between 6 to 10 m/day (Reynolds and Marimuthu, 2007).

The hydraulic conductivity derived for the Pallinup Formation in this study of 1 m/d is greater than the values of 0.1 to 0.5 m/day measured elsewhere (Reynolds and Marimuthu, 2007). This apparent discrepancy may be explained by the Pallinup Formation sediments tested by Reynolds and Marimuthu (2007) having been cemented, whereas those in the study area are only weakly lithified.

6.4.6 Groundwater recharge and discharge

In this study, groundwater recharge was estimated using the chloride mass balance method as defined by Wood and Sanford (1995) and documented in Bazuhair and Wood (1996). The equation is:

$$q = (P)(Cl_{wap})/Cl_{gw} \qquad (6.15)$$

where q is the recharge flux, P is the average annual precipitation, Cl_{wap} is the weight-average chloride concentration in precipitation and Cl_{gw} is the chloride concentration in the groundwater.

Rainfall in this region contains about 10 mg/L of Cl (Hingston and Gailitis, 1976). The rainfall decreases from 900 to 700 mm across the study area thus a value of 800 mm was used for P. The groundwater dissolved chloride concentrations range from 100 to

48 500 mg/L with an average of 5600 mg/L. This gives an estimate of 1.4 mm/year recharge or about 0.2% of annual rainfall (Table 6-5). Work immediately north of the study area found that just under 1% of the annual rainfall was returned to the groundwater as recharge (*pers comm*. G Mauger). Thus an estimate of 0.2% may be too low. The estimate of 0.2% is increased to 0.35% of rainfall if the median Cl concentration of the groundwater is used (Table 6-5).

The groundwater dissolved chloride concentrations differ significantly between the north and south. Again using the chloride mass balance approach indicates that there is greater recharge in the north of the study area than the south. Additional work is needed to refine the estimates of groundwater recharge. Currently there are too few SWL records for the recharge to be estimated using hydrographs, but the current field data program is collecting these data.

Table 6-5 Recharge as percentage of rainfall using the chloride mass balance approach as detailed in Bazuhair and Wood (1996).

Study area	Average Cl (mg/L)	Recharge (mm/year)	Percentage of rainfall
Between 6 210 000 and 6 175 000 mN	5600	1.4	0.2
Between 6 210 000 and 6 190 000 mN	3400	2.3	0.3
Between 6 190 000 and 6 175 000 mN	9300	0.9	0.1
	Median Cl (mg/L)	Recharge (mm/year)	Percentage of rainfall
Between 6 210 000 and 6 175 000 mN	2800	2.8	0.35
Between 6 210 000 and 6 190 000 mN	2400	3.2	0.4
Between 6 190 000 and 6 175 000 mN	4300	1.9	0.2

Minor groundwater discharge from the study area is by groundwater flow into the Tone River west of bore MU66D (Figure 4–1 and Figure 6–4). Otherwise groundwater discharge is via evaporation from Lake Muir and the ground surface where the watertable is within 2 m.

Groundwater flows into the Tone River through the narrow valley that connects the study area directly with the river. The annual discharge into the Tone River can be estimated using the Darcy equation:

$$Q = -Kia \qquad (6.16)$$

where K is the hydraulic conductivity (m/day), i is the hydraulic gradient (m/m) and a is the cross-sectional area (m^2).

At bore MU66D there is a 20 m thickness of sediments described as the channel sand regolith unit and 40 m of weathered basement rock. The hydraulic gradient for the sedimentary aquifer is 2.2 m/km (2.2×10^{-3} m/m), and cross-sectional area across the neck of the narrow valley west of bore MU66D is 2×10^4 m^2 (width 1000 m and depth of sedimentary aquifer 20 m). The hydraulic conductivity is 10 m/day. The WBR aquifer has a hydraulic gradient of 4.1×10^{-3} m/m and saturated hydraulic conductivity of 0.6 m/day. The cross sectional area is assumed to be 4×10^4 m^2. The total loss is estimated to be 1.95×10^5 m^3/y (Table 6-6).

Table 6-6 Estimation of annual groundwater discharge to Tone River.

	Sedimentary aquifer	WBR aquifer
K (m/day)	10	0.6
i (m/m)	2.2×10^{-3}	4.1×10^{-3}
a (m^2)	2×10^4	40×10^4
Q (m^3/day)	440	98
Q (m^3/y)	1.6×10^5	0.35×10^5

Information on local evaporation is needed to estimate groundwater discharge from Lake Muir. Tyler et al. (1997) compared several methods of determining groundwater evaporation and salt flux from a dry lake: Class A evaporation pan; microlysimeters; Bowen ratio energy budget; eddy correlation method; and soil chloride profiling as developed by Allison and Barnes (1985). They found good agreement between evaporation estimates using microlysimeters and the eddy correlation method.

Problems were encountered in the soil chloride profile method — it could not be applied to coarse-grained wind-blown sediment. Evaporation rates determined from the Class A evaporation pan were several orders of magnitude larger than the measured evaporation from the playa surface. Since the only evaporation data for Lake Muir are from a Class A evaporation pan at the climatic station at Frankland Vineyards (BOM no. 9843), water balance estimates for Lake Muir have not been attempted in the present study.

7 Hydrogeochemistry

7.1 INTRODUCTION

Groundwaters of southwestern Australia are dominated by chloride and sodium ions (Gray, 2001; Mann, 1983; McArthur et al., 1991; 1989) reflecting the original marine aerosol signature (Hingston and Gailitis, 1976). The regional mapping, including the study area, identified a Na–Cl type groundwater (Panasiewicz et al., 1997), but no detailed work has been done on the hydrogeochemistry for the study area prior to the present investigation.

Groundwater with low pH has been noted in the study area since 1997 (Panasiewicz et al., 1997; Smith et al., 2005; Smith, 2003) and a preliminary investigation revealed that groundwater in the north of the study area had a positive Net Acidity and low pH (Smith et al., 2004). Groundwater with a positive Net Acidity at near neutral pH was not identified prior to this PhD study. The potential mechanisms for groundwater acidity and/or alkalinity are varied and complex. The measurement of groundwater alkalinity has been standardised and is reproducible (American Public Health Association, 1999), but the same cannot be said for acidity determinations (American Public Health Association, 1999; Hedin, 2006; Hedin et al., 1994; Kirby and Cravotta III, 2005a; 2005b).

The focus of this chapter is the detailed hydrogeochemistry of the study area. Potential geochemical interactions between the aquifers and groundwater will be addressed when examining the different hydrochemical facies present. Boreholes referred to in this chapter can be found on Figure 4–1.

7.2 HYDROCHEMICAL FACIES

The concept of hydrochemical facies enables the characterisation of water bodies on the basis of differences in their chemical composition. The facies can be identified visually by plotting the major cations and anions (as meq%) on a Piper plot (Figure

7–1). When waters of the study area are plotted, major anions most often indicate a chloride type water (Cl > 50%) with some points plotting in the sulfate dominant (SO_4 > 50%) field. The cations are mostly sodium + potassium dominant (Na + K > 50%). A few water compositions plot near the centre of the cation triangle, with Na (Na + K), Ca and Mg each being less than 50%, showing these groundwaters have no dominant cation type.

Three types of groundwater are evident (Figure 7–1). The majority of the groundwaters have Cl^- and Na^+ (+ K^+) as the major ions and are referred to in this study as Na–Cl type waters. A second group has Cl^- as the dominant anion but no single dominant cation, although Na^+ and Ca^{2+} both exceed Mg^{2+}. This group is referred to as Ca–Na–Cl type water. The third groundwater type has sulfate as the dominant anion and is referred to as the Na–Mg–SO_4 type water.

Each hydrochemical facies has a well-defined distribution within the study area. The Na–Cl groundwater type is found in all aquifers, whereas the Ca–Na–Cl type is restricted to the WBR aquifer to the east of Lake Muir and the Na–Mg–SO_4 type is of minor extent under Forty Acre Swamp (Figure 3–1).

7.3 GEOCHEMICAL CHARACTERISTICS

7.3.1 Field measurements

7.3.1.1 pH

Groundwater pH was measured in the field during sample collection and thereafter twice yearly. Values ranged from 2.95 (bore MU15S May 2005) to 9.85 (bore MU49 May 2004), with the majority (~ 85%) being between 5 and 7. Low pH values (< 5) recorded in the north of the study area are mostly in groundwater from the sedimentary aquifer within 37 m of ground surface (Figure 7–2(a)). Occasional low pH was noted in the surficial and WBR aquifers.

Work by Cooperative Research Centre for Landscape Environments and Mineral Exploration (CRC LEME) showed the groundwater pH values in southwestern Australia to have a bi-modal distribution with median pH values of 6.6 and 3.6

(Shand and Degens, 2008). The groundwater in the study area does not show bi-modal distribution (Figure 7–2(a)) and has a median pH of 5.98.

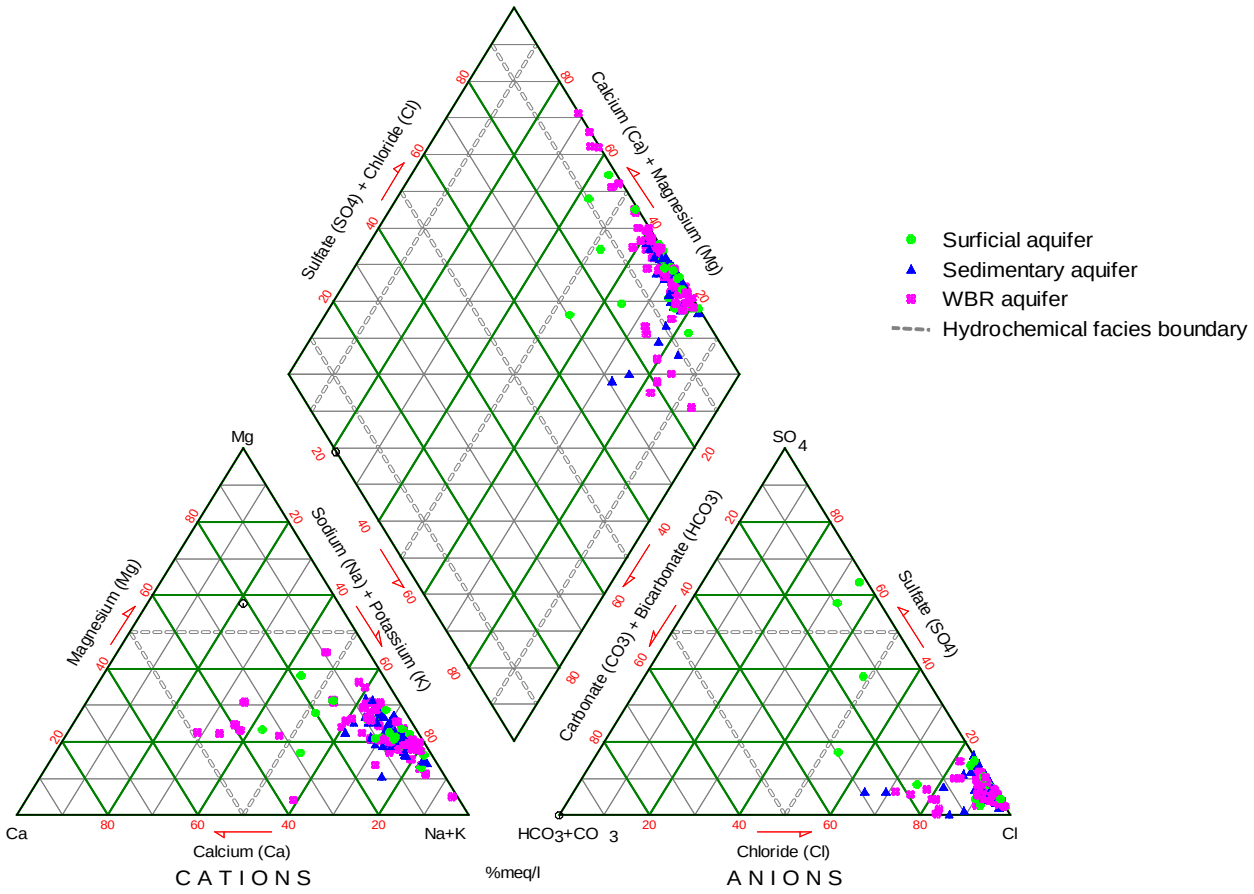

Figure 7–1 Hydrochemical facies showing the three types of groundwater present in the study area.

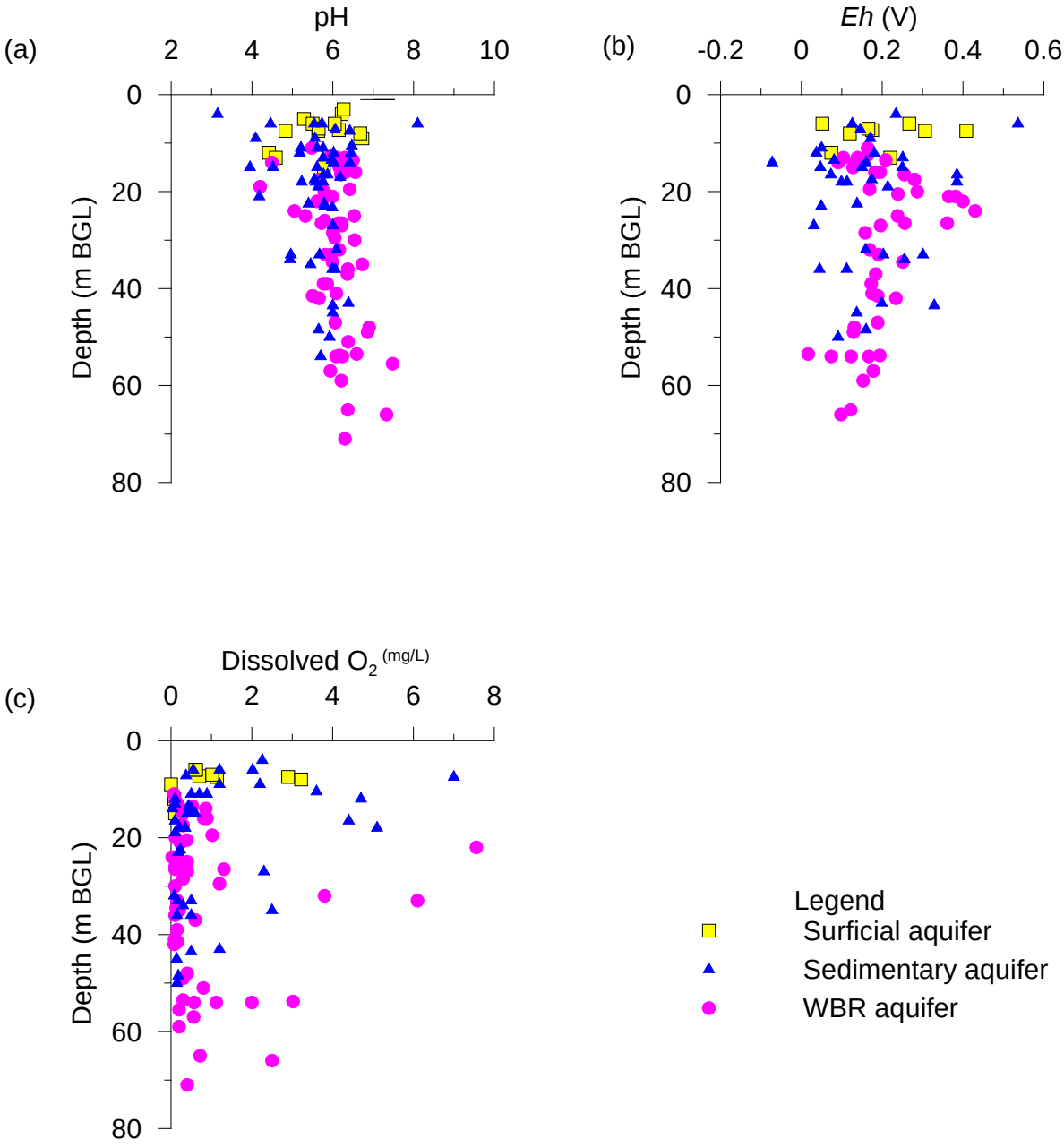

Figure 7–2 Field results measured using a flow-through cell at time of water sampling – a) pH; b) *Eh*; and c) dissolved O_2.

7.3.1.2 Eh

Groundwater *Eh* is influenced by various redox reactions (Lindberg and Runnells, 1984) and thus *Eh* gives a general indication of redox conditions. In groundwater the elements that undergo redox reactions are usually found in low concentrations and the slow chemical kinetics of some redox reactions lead to the lack of internal equilibrium (Christensen et al., 2000).

Eh was measured using an *Eh* probe located in a flow-through cell. Values recorded from the groundwater were between -0.07 and 0.54 V (Figure 7–2(b)) and plot within the transition zone between oxygenated surface water and reduced groundwater (Appelo and Postma, 2005).

7.3.1.3 Dissolved O_2

Dissolved O_2 was measured using a probe located in a flow-through cell, giving an indication of the aerobic or anaerobic condition. The majority of measurements revealed dissolved O_2 concentrations to be less than 1 mg/L (Figure 7–2(c)). Concentrations between 0.5 and 1 mg/L indicate anaerobic conditions (Christensen et al., 2000).

7.3.2 Major ions and trace elements

Work in the 1950s developed a sequence for the major anion evolution in groundwater (Chebotarev, 1955 sited in Freeze and Cherry 1979). As groundwater moves along its flow path the change in major anion normally is as follows:

$$HCO_3^- \rightarrow HCO_3^- + SO_4^{2-} \rightarrow SO_4^{2-} + HCO_3^- \rightarrow SO_4^{2-} + Cl^- \rightarrow Cl^- + SO_4^{2-} \rightarrow Cl^-$$

With increasing age the anion dominance evolves from HCO_3^- to Cl^- and is accompanied by an increase in TDS. However, the anions in southwestern Australia groundwater have a marine aerosol signature (Hingston and Gailitis, 1976) thus Cl^- is the dominant anion even in very fresh groundwater. Chloride generally behaves as a conservative ion in groundwater (Davis et al., 1998) and, not being a significant constituent in silicate rocks, it is not involved in weathering (Freeze and Cherry, 1979). Thus the ion to chloride ratio should reflect the ion to chloride ratio for

seawater and any change in ion ratios relative to seawater will give an indication of geochemical process. Major ions (in mg/L) are plotted against the Cl^- in Figure 7–3 to illustrate changes in ion concentrations. The dilution-evaporation line for seawater is shown to indicate enrichment or depletion relative to seawater.

7.3.2.1 Sodium

The extent to which the Na^+ concentration deviates from the dilution-evaporation line for seawater is evident by plotting the Na^+/Cl^- weight ratio against Cl^- concentration (Figure 7–3(b)). The Na^+/Cl^- ratios are scattered around the seawater weight ratio of 0.55. As Cl^- concentrations increase there is a general trend for waters to show depletion of Na^+ as indicated by the waters that have a Na^+/Cl^- ratio less than the seawater weight ratio of 0.55. Exceptions to this are the groundwaters under Lake Muir and at bores MU44, MU45D and MU59D (Figure 4–1) where the groundwater plots close to the seawater ratio of 0.55 at concentrations > 17 000 mg/L Cl^-. Minor Na^+ enrichment is apparent over a range of Cl^- concentrations (Figure 7–3 (a–b)), but the greatest enrichment is at concentrations < 955 mg/L Cl^- (~2000 mg/L TDS). Depletion of Na^+ is evident in all aquifers.

7.3.2.2 Calcium and Magnesium

Calcium ion and Mg^{2+} concentrations commonly show enrichment in relation to the seawater dilution-evaporation line (Figure 7–3 (c–d)) although there is occasional minor depletion. Groundwater in the WBR aquifer shows the greatest enrichment for both ions. The Ca^{2+} enrichment is evident at both low and high Cl^- concentrations. The Mg^{2+} enrichment (not associated with the lakes) is most apparent above 700 to 800 mg/L Cl^- concentration.

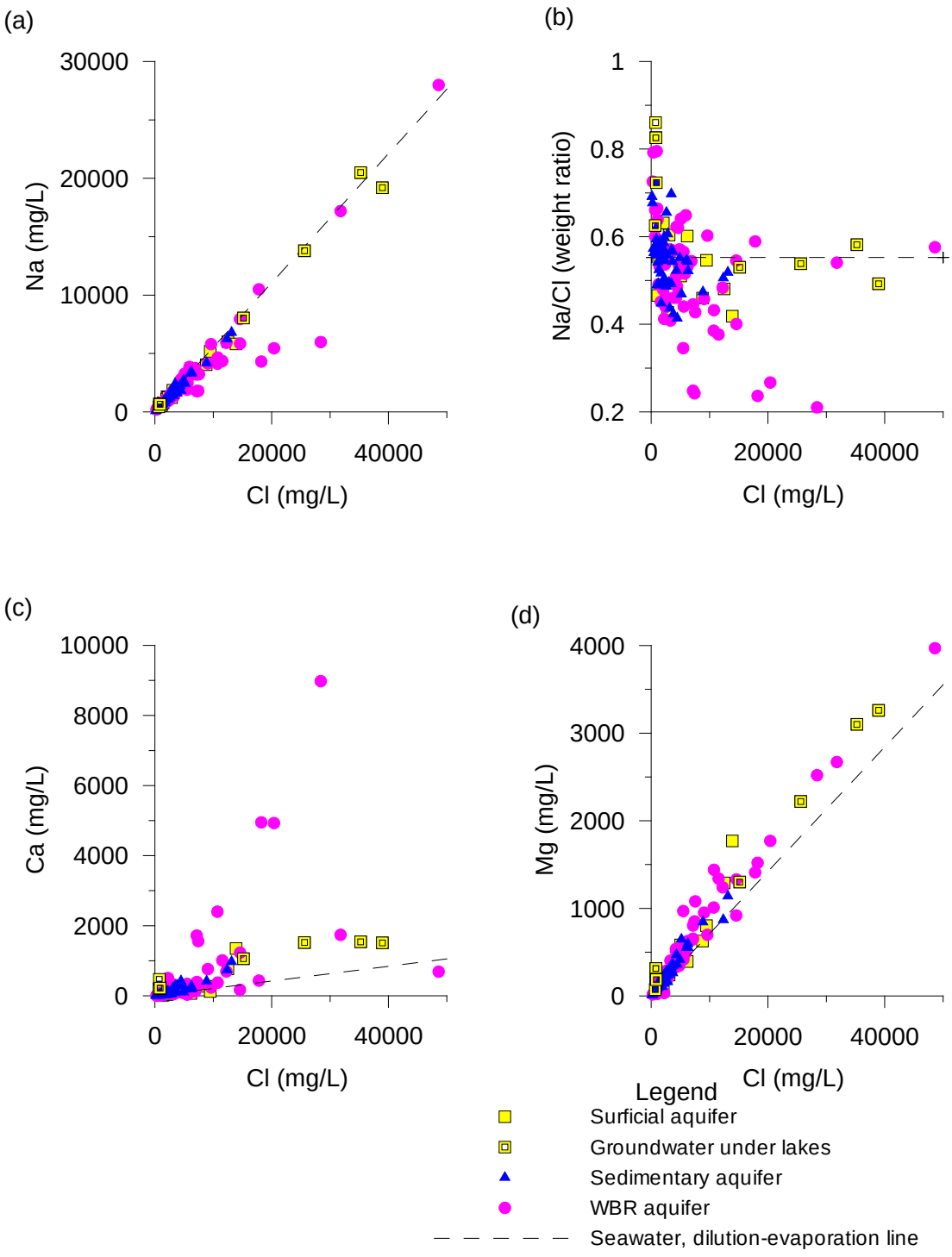

Figure 7–3 (a–d) Major ion concentration plotted against the concentration of Cl^-, the dashed line represents the dilution-evaporation line for seawater.

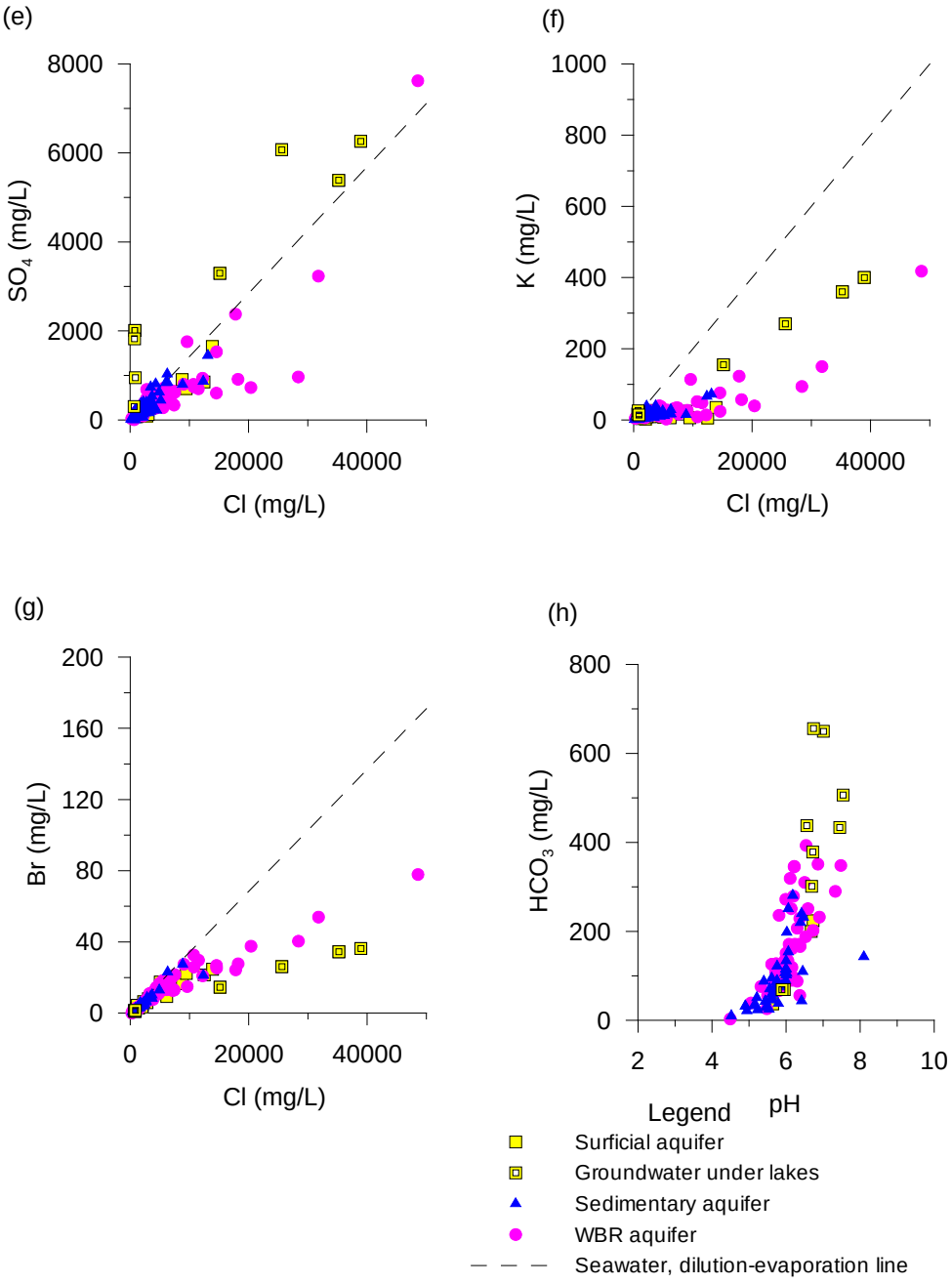

Figure 7–3 (e–h) Major ion concentration plotted against the concentration of Cl^-, and HCO_3^- concentration plotted against pH, the dashed line represents the dilution-evaporation line for seawater.

7.3.2.3 Potassium

Groundwater from all 3 aquifers is depleted in K^+ relative to seawater dilution-evaporation line (Figure 7–3(f)). This is consistent with groundwater throughout the Yilgarn Craton (McArthur et al., 1991).

7.3.2.4 Bromide

The concentration of Br^- is depleted with respect to the Cl^- concentration (Figure 7–3(g)). Like Cl^-, Br^- is considered a conservative ion in groundwater (Davis et al., 1998) and therefore the concentration of both ions should plot along the seawater dilution-evaporation line. Wildfires and peat swamps are documented as causing bromide depletion. Whereas, precipitation and dissolution of halite are known to alter the Cl^-/ Br^- ratios (Davis et al., 1998).

Methyl bromide (CH_3Br), a major species causing the depletion of the stratospheric ozone is known to be emitted from wild fires, along with CH_3Cl (Mano and Andreae, 1994). Extratropical forest biomass emits 0.0032 ± 0.0012 g of CH_3Br per kg of dry matter burnt compared to 0.050 ± 0.032 g of CH_3Cl per kg of dry matter burnt (Andreae and Merlet, 2001). This gives a Cl^-/Br^- (weight) ratio of 13 and suggests that relatively more Br^- may be lost during wildfires than Cl^-. Wildfires are a natural part of the forest ecosystem in Western Australia.

Peat swamps are known to act as a sink for Br^-. Zaccone et al. (2008) found that Br^- accumulated in the humic acid fraction of the peat. There are many peat swamps in the study area and, therefore, Br^- may not behave conservatively in the groundwater.

The precipitation and dissolution of halite will affect the Cl^-/ Br^- ratios under Lake Muir. As halite is precipitated the residual brine is enriched in Br^-. Whereas, the dissolution of halite will enrich the brine with Cl^-. Precipitation and dissolution of halite has been observed on the lake floor of Lake Muir. The apparent depletion of Br^- at the watertable is likely to be influenced by the precipitation and dissolution of

halite. In the present study Br^- has not been used to examine the interactions between groundwater and the aquifer media.

7.3.2.5 Bicarbonate ion

The concentration of HCO_3^- decreased with decreasing pH (Figure 7–3 (h)) and is absent at pH below 4.5.

7.3.2.6 Sulfate

Groundwater sulfate concentration ranged from 3 to 7621 mg/L. Most of the groundwater was depleted in SO_4^{2-} with respect to seawater evaporation-dilution line, except for groundwater under Lake Muir and Forty Ace Swamp which had a relative excess of SO_4^{2-} (Figure 7–3(e)). Depletion of SO_4^{2-} with respect to seawater evaporation-dilution line was recorded in all 3 aquifers.

Total sulfur, recalculated as sulfate was compared to sulfate for water samples analysed in 2007. Total sulfur equalled the measured sulfate up to about 600 mg/L (Figure 7–4). The measured SO_4^{2-} is less than the recalculated total sulfur values > 600 mg/L indicating that low concentrations of other aqueous sulfur species may be present.

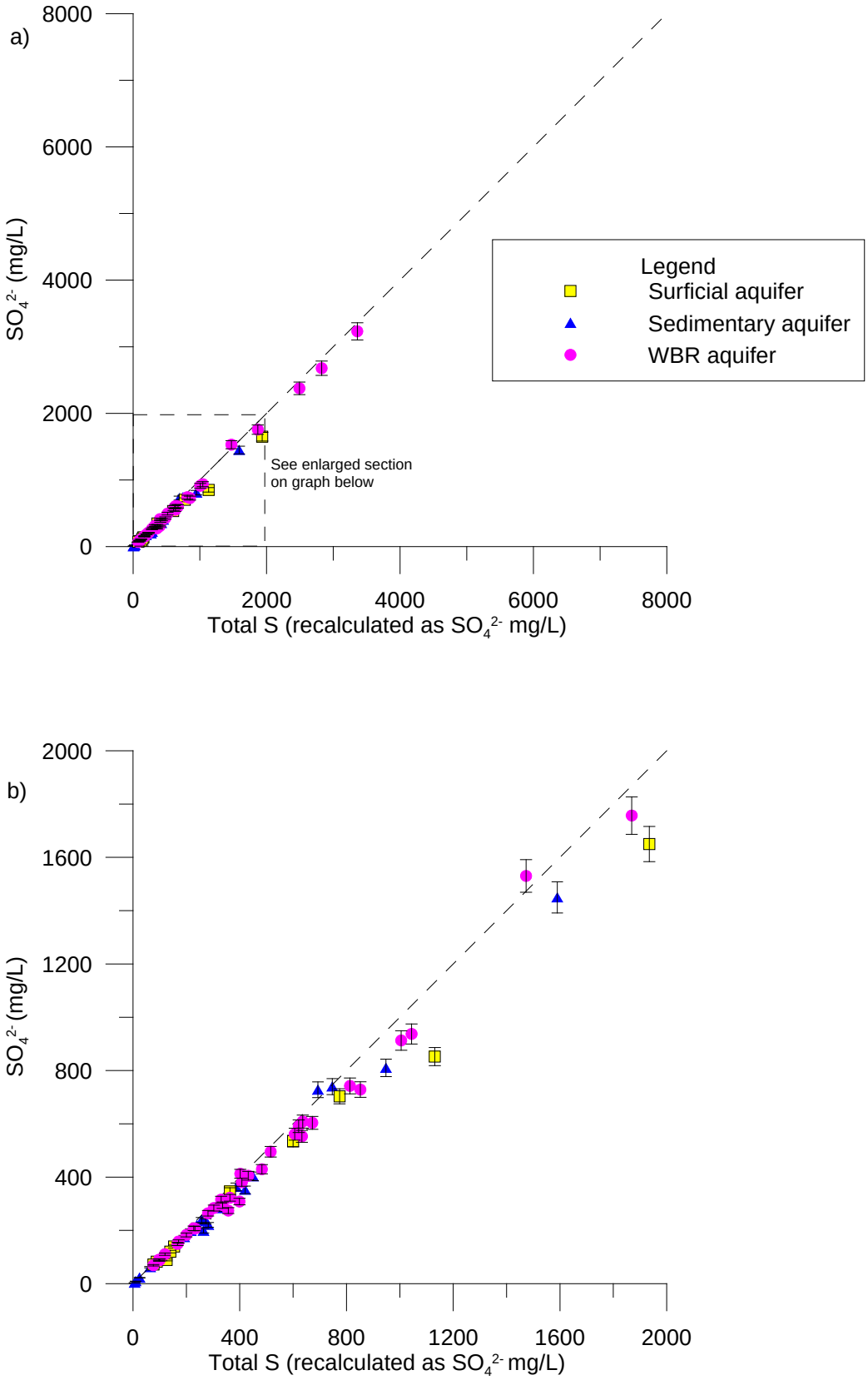

Figure 7–4 a) Comparison of measured SO_4^{2-} and total sulfur (recalculated as SO_4^{2-}) determined in 2007. B) Enlargement of measured SO_4^{2-} and total sulfur (recalculated as SO_4^{2-}) for values < 2000 mg/L. The error bars are ± 5% and dashed line assumes a ratio of 1.

7.3.2.7 Iron

Dissolved $Fe_{(Total)}$ is ubiquitous in the groundwater (Figure 7–5(a)), with the concentration in all but one sample being above the detection limit of 0.1 mg/L. Eighty one percent of groundwater samples contained $Fe_{(Total)}$ concentrations > 1 mg/L with 50% containing > 10 mg/L. Water within both the sedimentary and WBR aquifers had similar dissolved $Fe_{(Total)}$ concentrations, with maxima of 142 mg/L in the sedimentary aquifer and 109 mg/L in the WBR aquifer. The surficial aquifer had concentrations raging from < 1 mg/L to 31.1 mg/L. The greatest dissolved $Fe_{(Total)}$ concentrations are found in waters with pH ~ 6.

7.3.2.8 Aluminium

Of the 122 groundwater samples analysed 72 had Al concentrations above detection level, ranging from 0.01 mg/L to 15.1 mg/L. Of these, a majority had concentrations below 1 mg/L. There was an increase in the dissolved Al concentrations below pH 4.5 (Figure 7–5(b)). The highest concentrations were associated with the sedimentary aquifer.

7.3.2.9 Manganese

Virtually all analysed groundwater samples had levels of Mn above the detection level of 0.01 mg/L with 30% having concentrations > 1 mg/L, and a maximum of 12.5 mg/L (Figure 7–5(c)). The greatest scatter of Mn concentration was associated with the WBR aquifer, whilst the least scatter was recorded in the sedimentary aquifer.

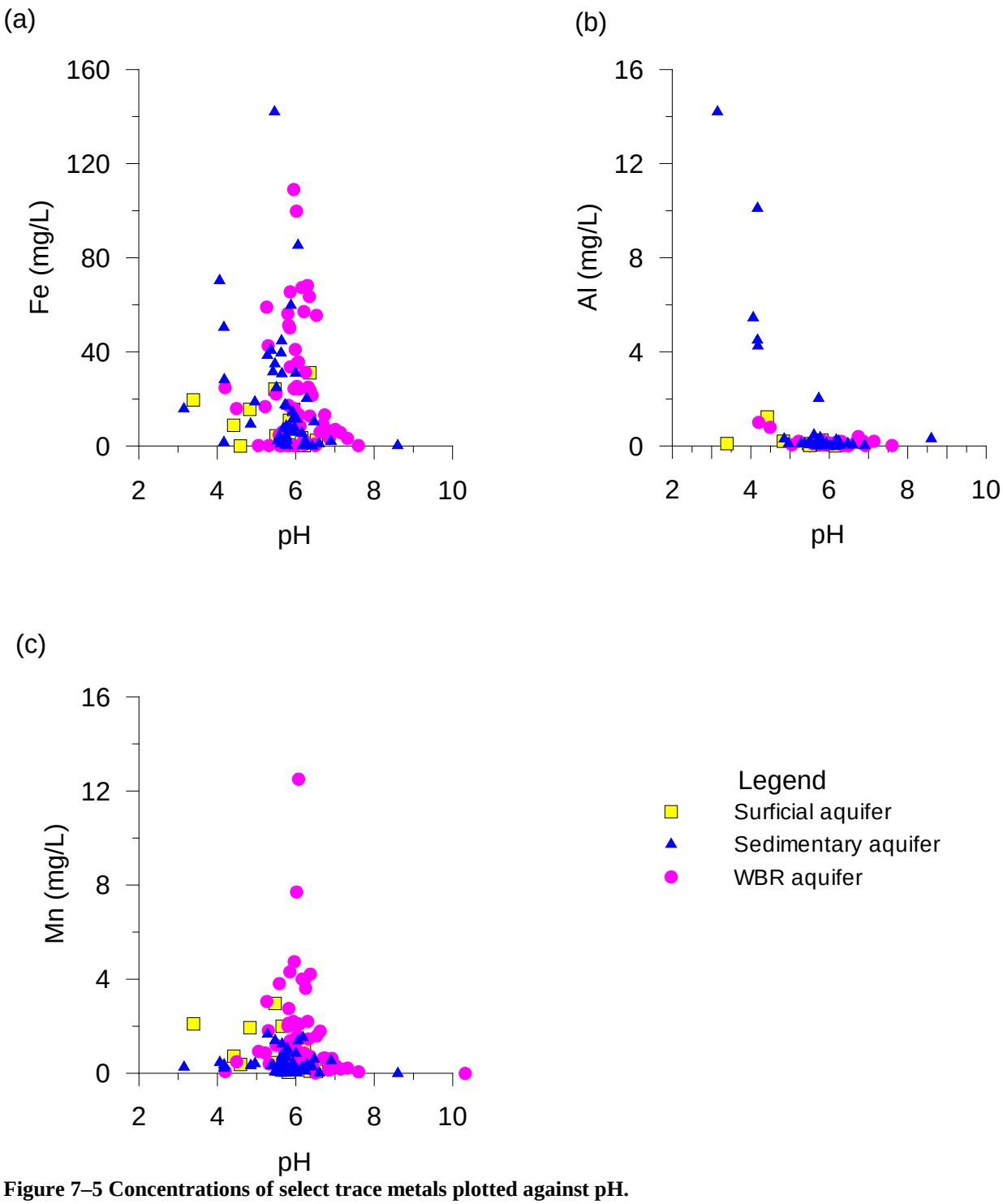

Figure 7–5 Concentrations of select trace metals plotted against pH.

7.3.3 Minerals

7.3.3.1 Ferric hydroxysulfates

Jarosite ($KFe_3^{3+}(SO_4)_2(OH)_6$) and/or natrojarosite ($NaFe_3(SO_4)_2(OH)_6$) have been identified from groundwater seeps near rock outcrop on the lake edge of Tordit-Gurrup Lagoon (Figure 4–1) by SEM – EDAX. The precipitate crust had a 1:5 paste pH 2.5 (03/04/08), whereas the weekly lake water pH values ranged from 7.83 to 8.78 in 2008.

7.3.3.2 Pyrite

Sulfides are extensive in the rocks within the study area. In the sedimentary aquifer, pyrite (FeS_2) is found in both the channel sand and the flood plain regolith units. Pyrite with a grain size of ~5 μm has been identified (using SEM – EDAX) in the quartz dominated channel sands. Coarse-grained pyrite found in the flood plain regolith unit was identifiable by optical microscopy. Pyrite is more extensive in the flood plain unit with these materials containing visible pyrite up to 3%. An inorganic sulfide content of between 0.6 and 1.2 wt % was determined in samples MU46-21.45 and MU42-31.4 respectively, from the flood plain regolith unit. In the weathered basement, pyrite is the main accessory mineral with up to 3% pyrite visible in drill rock chips. Inorganic sulfide of 1.6 wt % was determined in regolith sample MU46-45.5.

7.3.3.3 Iron oxides

Iron oxides present in ferricrete are widespread throughout the study area. This crust is either exposed on surface or covered by a veneer of recent colluvial and alluvial material. Iron oxides are also present as fine orange coatings on sand grains at depth.

7.3.3.4 Evaporite minerals

Gypsum and halite have been noted in the study area. A gypsum crust ($CaSO_4.2H_2O$) was identified by SEM – EDAX on the surface of Lake Muir and as distinct crystals (up to 3 cm length) in near surface sediments of bore MU48

(Figure 4–1). Gypsum is the first sulfate evaporite mineral to be precipitated (Alpers et al., 1992). After gypsum the next sulfate mineral to be precipitated depends on the water chemistry (Spencer, 2000). In water of marine origin, gypsum may alter to anhydrite ($CaSO_4$) just prior to the initiation of halite precipitation according to:

$$Ca^{2+} + SO_4^{2-} + 2H_2O \rightarrow CaSO_4 \cdot 2H_2O \rightarrow CaSO_4 + 2H_2O \qquad (7.1)$$

Halite has been identified by SEM – EDAX as salt crystals on the surface of Lake Muir during the summer months. The crystals are very fine up to 50 μm in size. Salt crusts are also visible at groundwater discharge sites during the summer months.

7.3.4 Saturation indices

The calculation of saturation indices (SI) enables the degree of mineral saturation in water to be assessed. Values of SI for specific minerals were computed from the groundwater solution compositions using PHREEQC software. If the SI for a mineral is zero (± 0.2 for a major element mineral and ± 1 for minor element mineral) the groundwater is considered as being in equilibrium with that mineral. For SI values less than zero the groundwater is undersaturated with respect to that mineral and if present the mineral may dissolve. SI values greater than zero indicates that the groundwater is oversaturated with the mineral, and the mineral may be precipitated from the groundwater.

The SI for calcite, siderite, kaolinite, alunite and jarosite in the water samples have been plotted against pH in Figure 7–6 (a–e)). Most of the groundwater is undersaturated with respect to calcite (Figure 7–6(a)). Waters in equilibrium or oversaturated with respect to calcite are confined to the WBR aquifer and groundwater under Lake Muir and Forty Acre Swamp. A greater number of waters are in equilibrium with respect to siderite, but a majority of waters are undersaturated (Figure 7–6(b)).

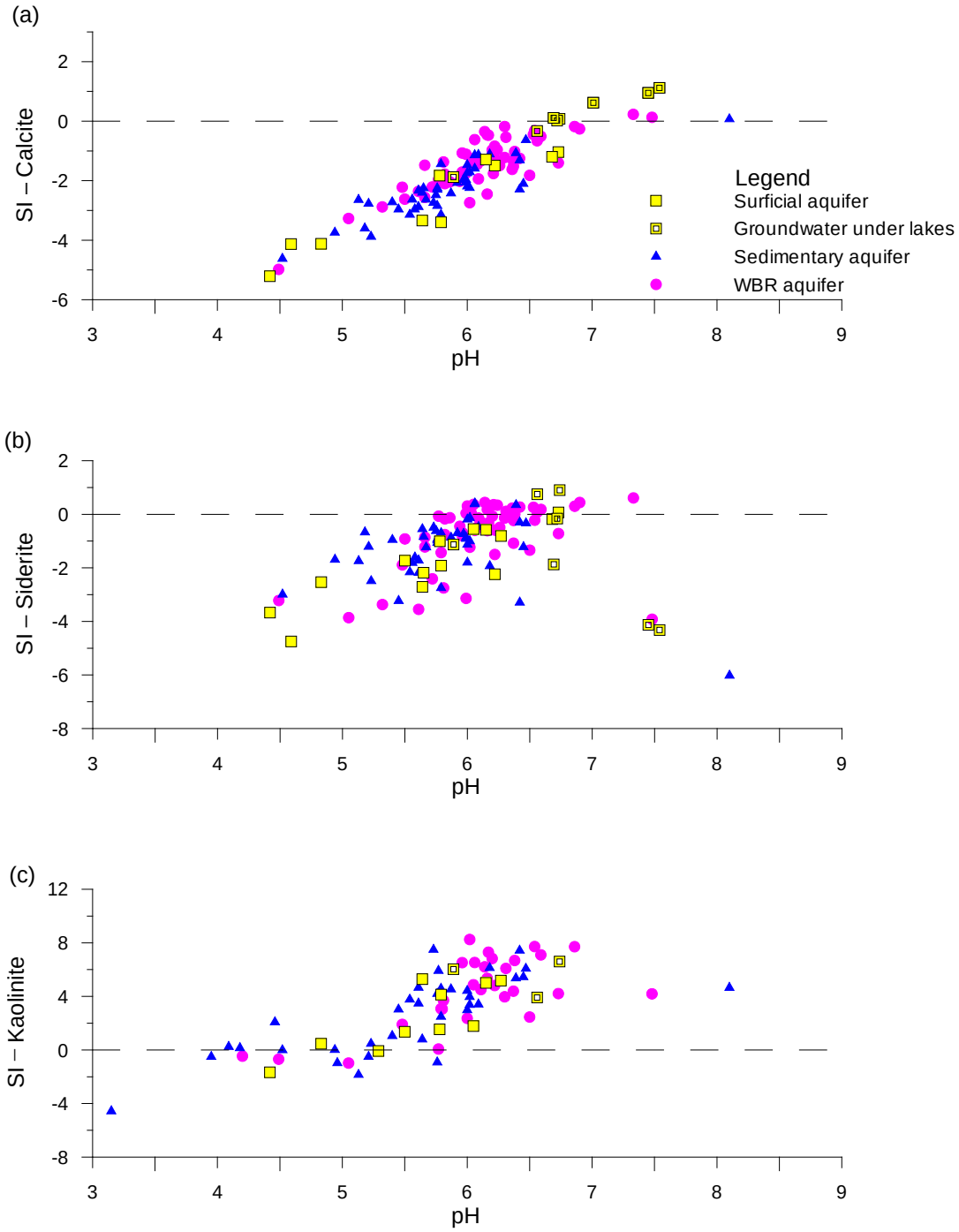

Figure 7–6 (a-c) SI for select minerals related to pH.

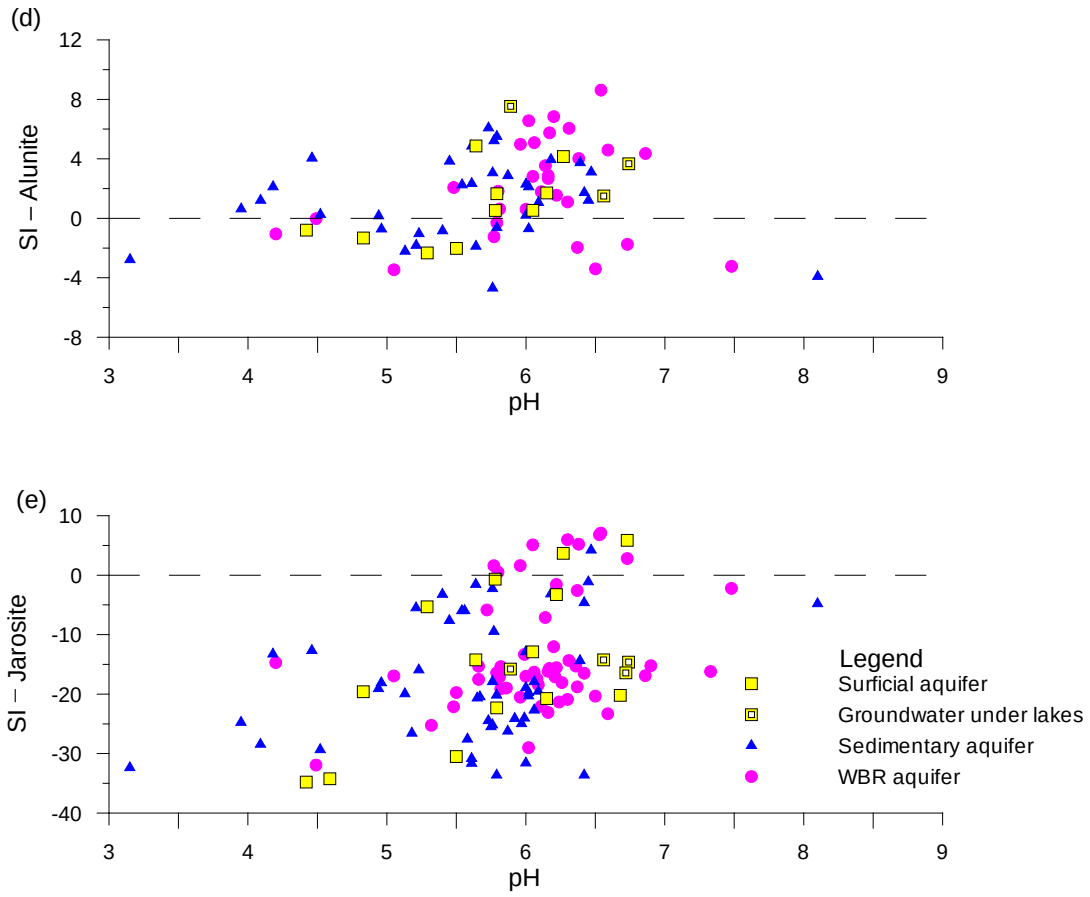

Figure 7–6 (d–e) con. SI for select minerals related to pH.

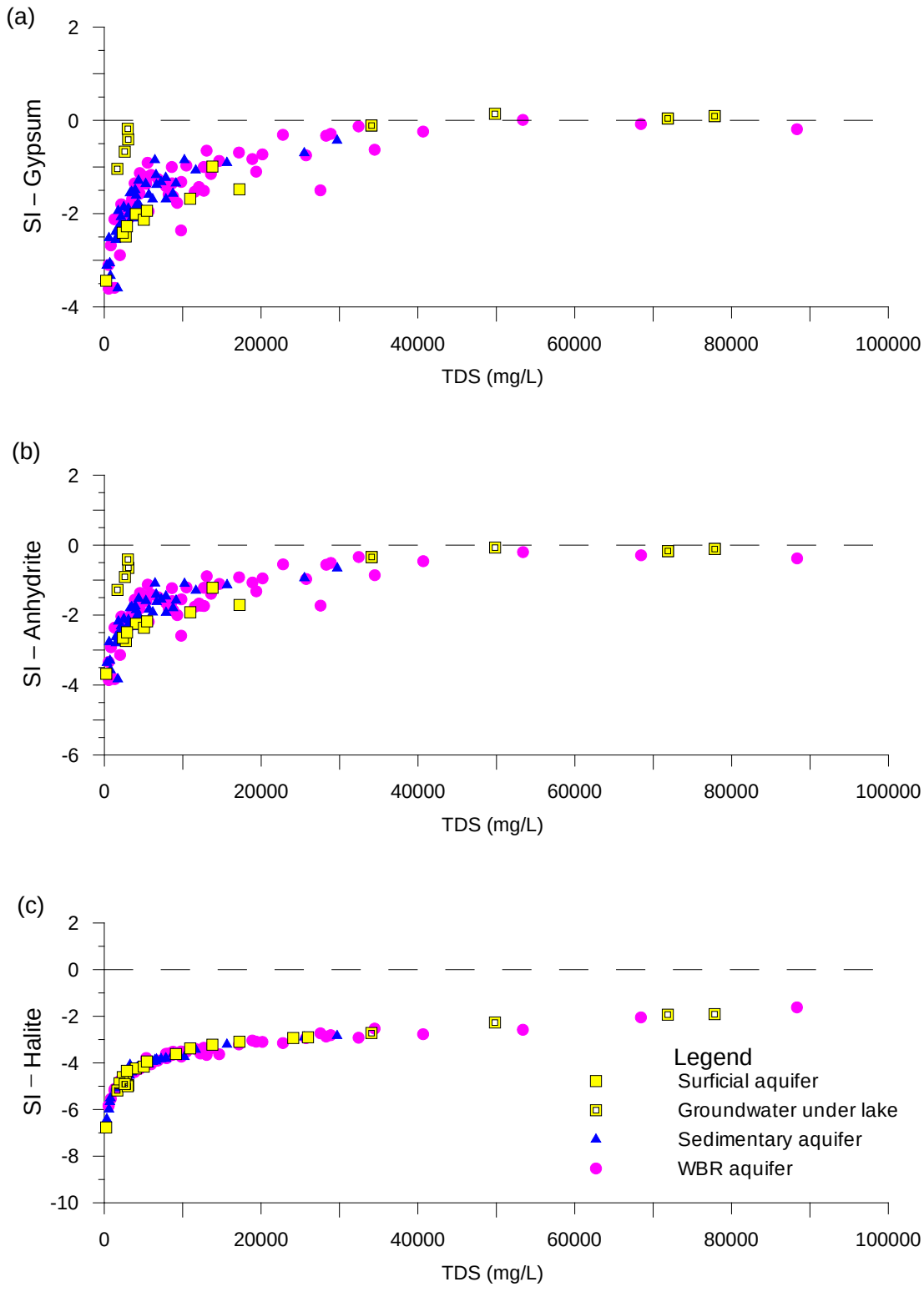

Figure 7–7 (a-c) SI for select minerals related to TDS.

The SI indicates that a majority of the waters are oversaturated with respect to kaolinite (Figure 7–6(c)), returning to saturation then undersaturation as the pH decreases. Groundwaters are mostly in equilibrium or oversaturated with respect to alunite, but undersaturated with respect to jarosite (Figure 7–6(d–e)). However, it is unlikely that alunite or jarosite will be present at pH > 3. While they have been documented at pH > 3 they are generally not stable at these pH values (Brown, 1971; Stoffregen et al., 2000).

The SI for gypsum, anhydrite and halite have been plotted against TDS (Figure 7–7). The groundwater is in equilibrium with gypsum at TDS > 20 000 mg/L (Figure 7–7 (a)) and also is in equilibrium with anhydrite at TDS > 30 000 mg/L. Although halite has been identified, the SI of the groundwater at this location is undersaturated with respect to halite (SI < -1.6) (Figure 7–7(c)). Drying of the lake sediment enables halite to form once halite saturation is reached.

7.4 NA–CL TYPE WATER

The majority of the groundwater sampled in the study area can be classified as a Na–Cl type water. Variation in major ions with respect to the ion/chloride seawater ratio suggest that processes, such as weathering of the regolith and crystalline basement, ion exchange, mineral precipitation, evapo-concentration and redox reactions, have played a part in the groundwater evolution within the study area.

7.4.1 Sodium and calcium enrichment

There is minor enrichment in the solute concentration of Na^+ and significant enrichment in the Ca^{2+} solute concentration relative to the seawater dilution-evaporation line. Garrels and Mackenzie (1967) suggest that groundwater moving through a silicate-dominated crystalline rock aquifer should trend towards a Na–Ca–HCO_3 type water with the Na and Ca composition reflecting the rock's plagioclase feldspar mineralogy.

Groundwater in the study area moves through the weathered granitic gneiss. Kaolinite and minor gibbsite have been identified by XRD. Kaolinite is the

weathering product of many silicate minerals including feldspars, biotite and chlorite.

Calcium and Na^+ concentrations in the groundwater samples have been plotted on a silicate stability diagram (Figure 7–8). Albite is the major plagioclase feldspar identified in the gneiss. Thus the choice of stability diagram is for Na-dominated silicates and their weathering products (Figure 7–8). The incongruent dissolution reactions of albite to kaolinite ($Al_2Si_5O_5(OH)_2$), and to gibbsite ($Al(OH)_3$), and kaolinite to montmorillonite are given below:

$$2Na(AlSi_3)O_8 + 2H^+ + 9H_2O \rightarrow Al_2Si_5O_5(OH)_2 + 2Na^+ + 4H_4SiO_4 \qquad (7.2)$$

$$Na(AlSi_3)O_8 + H^+ + 7H_2O \rightarrow Al(OH)_3 + Na^+ + 3H_4SiO_4 \qquad (7.3)$$

$$Na(AlSi_3)O_8 + Mg^{2+} + 4H_2O \rightarrow 2Na_{0.5}(Al_{1.5}Mg_{0.5})Si_4O_{10}(OH)_2 + 2Na^+ + H_4SiO_4 \qquad (7.4)$$

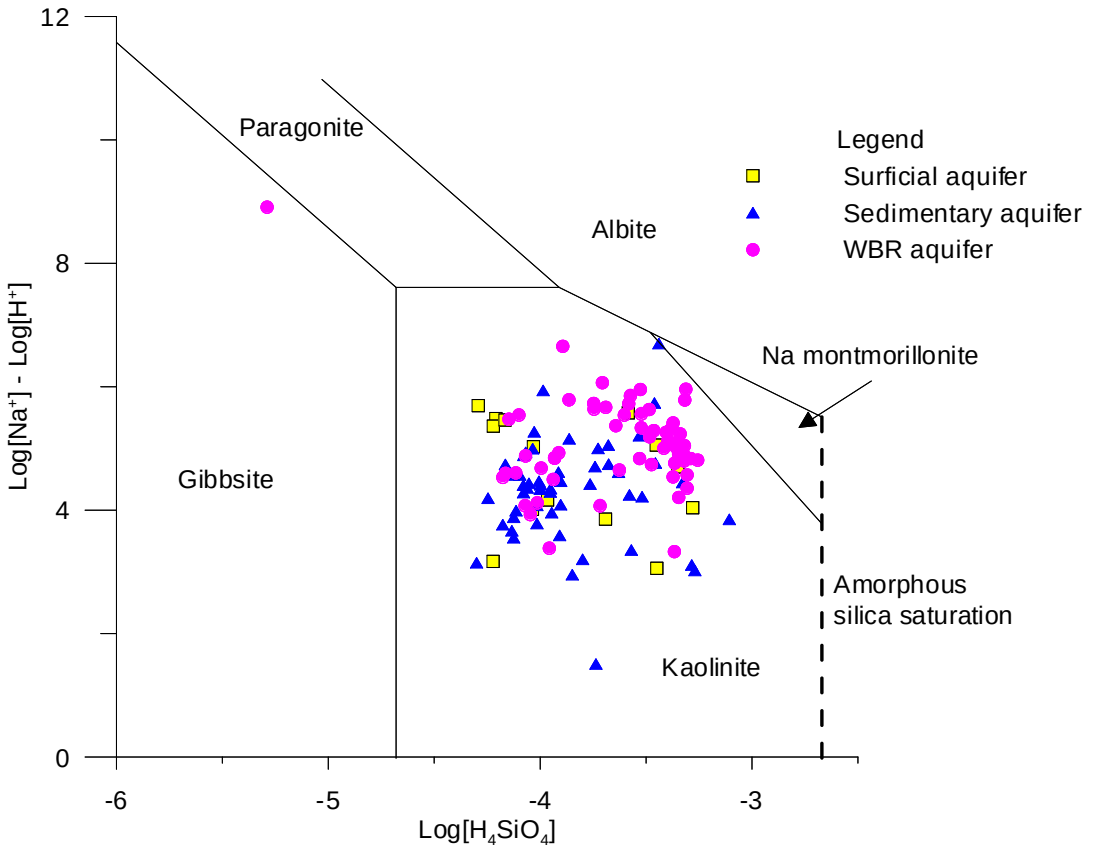

Figure 7–8 Composition of groundwater samples plotted on the stability diagram of anorthite and its possible weathering products at 25°C and 1 bar pressure. The figure shows a stability field for an idealized Na montmorillonite.

The H_4SiO_4 values for the samples were calculated using PHREEQC. The stability limits for albite, kaolinite, gibbsite and montmorillonite have been calculated from equations given by Faure (1998) and Langmuir (1997). The groundwater samples plot predominately within the kaolinite field (Figure 7–8), consistent with kaolinite being the major clay present. One sample plotted (bore MU67D) in the gibbsite stability field and minor gibbsite has been identified by XRD (Appendix 4 Table1). Gibbsite is an extreme product of silicate weathering (reaction (7.3)) and if weathering continues Al-hydroxy complexes will be released. The dissociation of gibbsite into aqueous Al-hydroxy complexes is pH dependant. The amphoteric nature of aluminium results in the aluminium solubility increasing below pH 4.5 and above pH 7, whereas at near neutral pH the total dissolved Al^{3+} concentration is low (Appelo and Postma, 2005). The pH of the groundwater in bore MU67D is 10.32 thus this point plotted in the gibbsite stability field.

According to Garrels and Mackenzie's (1967) model for hydrochemical evolution in igneous and high-grade metamorphic crystalline rock terrains, weathering of albite should produce a groundwater enriched in Na^+ showing only minor Ca^{2+} enrichment. The groundwater weight ratios of Na^+/Cl^- (Figure 7–3(b)) plot above and below the seawater weight ratio of 0.55 indicating both enrichment and depletion of the Na^+ is occurring in the study area with depletion being dominant. In all three aquifers groundwater enrichment of Na^+ is evident between concentrations of 142 and 9623 mg/L Cl. Groundwater depletion of Na^+ starts at relatively low concentrations of Cl^- (954 mg/L), with the Na^+/Cl^- weight ratios being mostly between 0.55 and 0.4. Weathering of albite would account for the minor Na^+ enrichment in groundwater, but the depletion of Na^+ indicates that other chemical process are occurring.

Aqueous concentrations of Ca^{2+} by contrast are enriched in all bar one sample compared to the seawater dilution-evaporation line, with enrichment evident in all three aquifers. If the calcium enrichment was solely due to chemical weathering of plagioclase feldspar, the plagioclase feldspar should be more calcium rich than albite. However, Ca-rich plagioclase feldspars such as anorthite or bytownite have not been identified. Other process such as cation exchange (discussed below) better explain the increased solute concentration of Ca^{2+}.

7.4.2 Calcium and magnesium enrichment with sodium depletion

Enrichment of Ca^{2+} and Mg^{2+} and depletion of Na^{+} in groundwater can be explained by cation exchange (section 2.7.2). Cation exchange is related to the total solute concentration and aquifer media. With increasing total solute concentration, the exchange coefficient for $K_{Na\backslash Ca}$ needs to be maintained (equation (2.39)). This is achieved by decreasing the concentration of the adsorbed Ca^{2+} and increasing the solute concentration of Ca^{2+}. Likewise the absorbed Na^{+} increases and the solute concentration of Na^{+} decreases. As the groundwater solute concentration increase the regolith material will adsorb Na^{+} and release Ca^{2+} or Mg^{2+} to the groundwater thus maintaining the exchange coefficient for $K_{Na\backslash Ca}$ and $K_{Na/Mg}$.

The exchangeable elements were selectively extracted from various regolith units using 1M ammonium acetate at pH 5 (Appendix 4 Table 3). The elements extracted suggest that the flood plain regolith unit is a major source of exchangeable Ca and Mg. At pH 5 there was 1097 mg/kg Ca and 275 mg/kg Mg readily exchangeable Ca and Mg in the carbonaceous clays and silts of the flood plain regolith unit (sample MU46-21.45). Not surprisingly the quartz dominated sands (sample MU42-29) and siliceous marine sands (sample MU12-10) had low concentrations of exchangeable Ca and Mg. Sample MU42-29 had only 115 mg/kg readily exchangeable Ca and sample MU12-10 had 43 mg/kg readily exchangeable Ca and 41 mg/kg of Mg.

Increase in dissolved concentration of Mg^{2+} starts at about 800 mg/L Cl whereas Ca^{2+} enrichment occurs at much lower Cl^{-} values (142 mg/L bore MU05S). At Cl^{-} concentrations of between 700 and 955 the increase in Mg^{2+} concentrations coincides with decrease in Na^{+} concentrations relative to the seawater dilution-evaporation line supporting cation exchange as a factor in the groundwater evolution.

7.4.3 Calcite

The first major chemical divide in the EJH model (section 2.7.3, Figure 2–3 and Figure 2–4) is the precipitation of calcite (Eugster and Jones, 1979). Approximately 80% of the groundwaters in the study area are undersaturated with respect to calcite (SI < -0.5; Figure 7–6(a)) including all from the surficial aquifer. Soil mapping (Stuart-Street and Scholz, *in prep*; van Gool et al., 2005) tend to support the groundwater SI with respect of calcite with 75% of the Unicup System having a soil

pH < 6.5 (Figure 3–5; Table 3-3). With such pH, the soils are unlikely to be buffered by calcite.

The waters under Lake Muir are saturated to oversaturated with respect to calcite. Otherwise waters with SI values > -0.5 are associated with the WBR aquifer at bores MU11D, MU12D, MU16D in the north of the study area. The sedimentary aquifer is oversaturated with respect to calcite at bore MU10S.

7.4.4 Sulfate, calcium and gypsum

Gypsum is a common evaporite mineral precipitated in closed basins containing brines (Eugster and Hardie, 1978; Eugster and Jones, 1979; Hardie and Eugster, 1970). In alkaline poor water, gypsum is the mineral precipitated at the second chemical divide in the EJH model (Figure 2–3 and Figure 2–4) (Eugster and Jones, 1979). Alkaline poor water is defined by the molar concentration of Mg^{2+} and Ca^{2+} exceeding HCO_3^- (Drever, 1997). In the study area the concentration of Mg^{2+} and Ca^{2+} exceeds HCO_3^- in a majority of the groundwater samples.

A gypsum crust has been identified on the floor of Lake Muir and gypsum crystals were observed in near surface sediments of bore MU48 to the east of the lake. The SI values support gypsum formation at TDS > 20 000 mg/L (Figure 7–7(a)). Sulfate enrichment is associated with the groundwater beneath Lake Muir. Dissolution of the gypsum crust occurs with rainfall and surface water flow onto the lake floor. Dissolution of gypsum creates a SO_4^{2-} and Ca^{2+}-rich water that infiltrates down to the watertable. The Ca^{2+} is utilised by the lake biota to produce shells which are evident throughout the lake profile and the groundwater becomes locally enriched with SO_4^{2-}.

Gypsum formation may account for some of the sulfate depletion in the south of the study area but it does not account for the sulfate depletion in the north of the study area where TDS values are generally < 20 000 mg/L (Figure 6–1).

7.5 GROUNDWATER ACIDITY AND ALKALINITY IN NA-CL TYPE WATER

The Total Acidity component of the groundwater can be calculated using equation (2.26). Total Acidity values are up to 255 mg/L $CaCO_3$ equivalent.

The components that make up the groundwater acidity are the concentration of H^+ and the metals ions Fe, Al and Mn in solution. Oxidation and hydrolysis of metal ions such as the oxidation of Fe^{2+} and precipitation of ferric oxyhydroxides release H^+ ions (equation 1.1). Dissolved $Fe_{(Total)}$ is the major metal ion within the groundwater and thus is the predominant metal ion contributing to groundwater acidity (Figure 7–5). The concentration of Mn ions in groundwater is less than 12.5 mg/L with 70% of analysed samples containing < 1 mg/L. Dissolved Al ions contribute to the groundwater acidity only at low pH values of < ~4. Where Al was detected in solution, the concentrations were normally < 1 mg/L, although values up to 15.1 mg/L have been measured.

Total Alkalinity (by titration) is assumed to be derived from $HCO_3^- + CO_3^{2-}$. At pH < 10.3 the major carbonate species is HCO_3^- (Figure 2–1). The groundwater concentration of HCO_3^- decreases with decreasing pH (Figure 7–3(h)).

To obtain the Net Acidity, the Total Acidity was subtracted from the Total Alkalinity. A positive Net Acidity (Total Acidity > Total Alkalinity) is evident in both the sedimentary and WBR aquifers (Figure 7–9). In the sedimentary aquifer groundwater with a positive Net Acidity is found in the north of the study area and between the two westerly sloping ridges. In the south of the study area, groundwater in the sedimentary aquifer has a negative Net Acidity (Total Alkalinity > Total Acidity). Most of the groundwater associated with the WBR aquifer has a negative Net Acidity but samples with a positive Net Acidity were found mostly in the north of the study area (Figure 7–9).

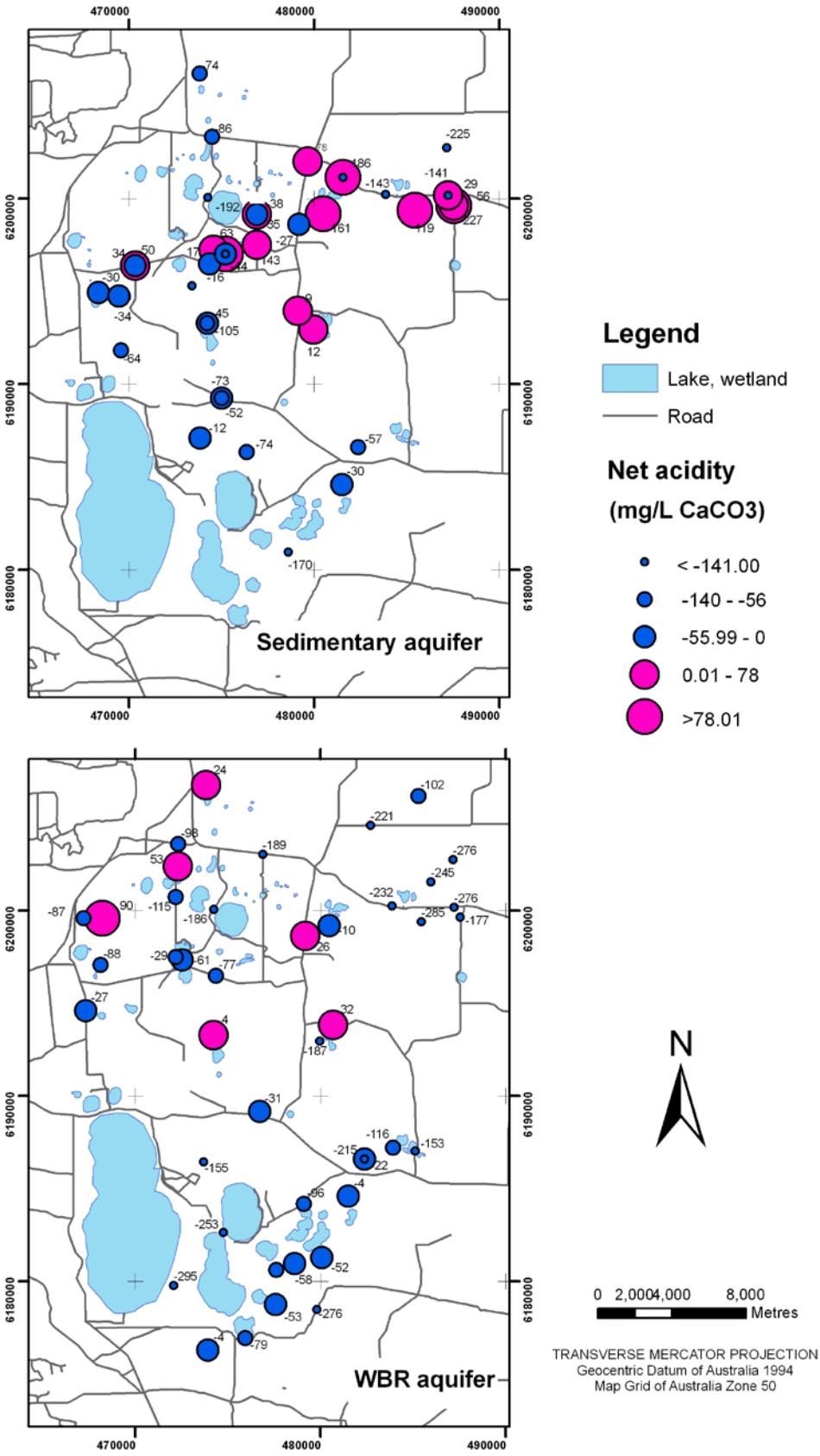

Figure 7–9 Variation in Net Acidity associated with groundwater in the sedimentary and WBR aquifers.

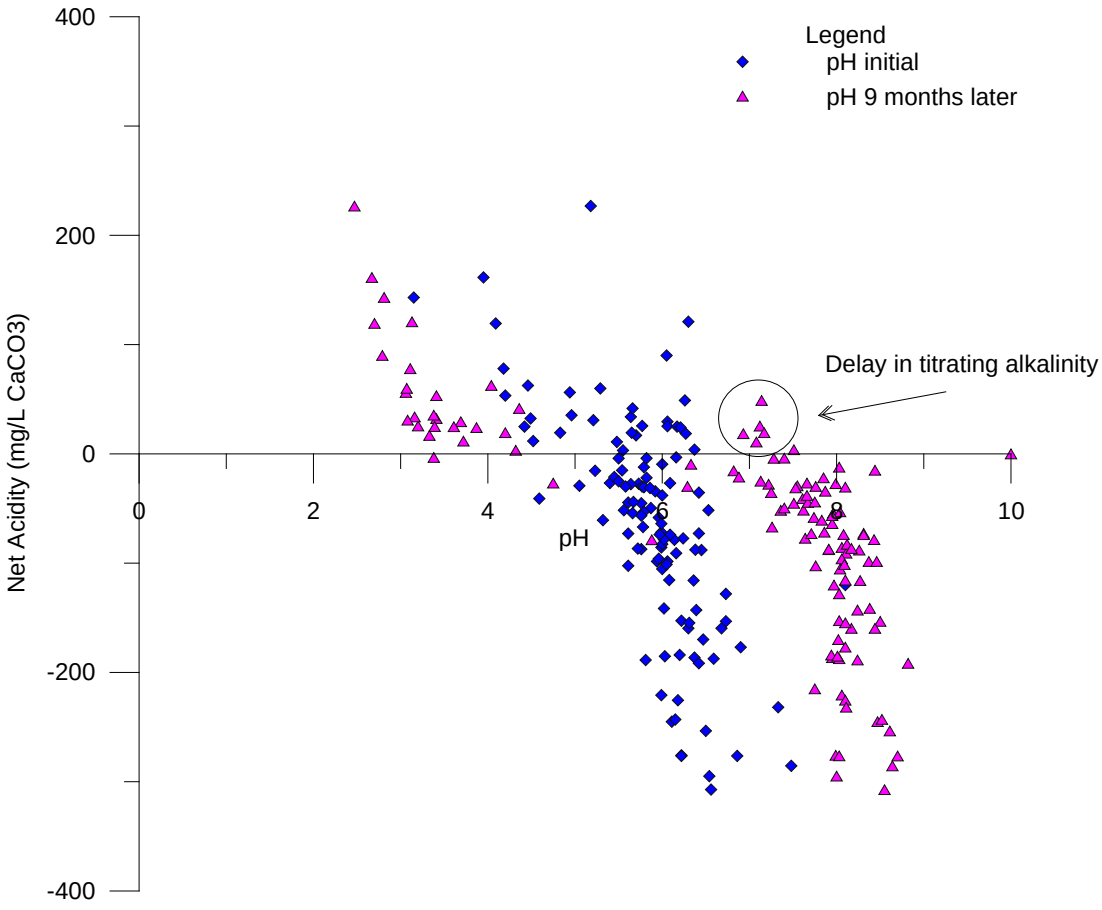

Figure 7–10 Initial groundwater field pH and pH of initial sample after 9 to 12 months showing that the pH of waters with a positive Net Acidity decreases, whereas the pH of waters with a negative Net Acidity increases. Groundwater with pH between 5.5 and 6.3 can have either a positive or negative Net Acidity.

Plotting the Net Acidity against pH measured in the field shows that groundwaters in the study area with pH values between 5.5 and 6.3 can have either a positive or negative Net Acidity (Figure 7–10). When the pH was re-measured on the initial sample 9 to 12 months later the pH had decreased for samples with a positive Net Acidity, whereas the pH has increased for the groundwater samples with a negative Net Acidity (Figure 7–10). Exceptions to this are groundwater samples from bores where there was a delay in titrating the samples. The precipitation of ferric oxyhydroxides according to equation (1.1) and the release of H^+ ions would reduce the measured alkalinity (Figure 7–10).

The decrease in pH for samples with a Net Acidity is consistent with the finding of Kirby and Cravotta III (2005a, 2005b) in their review of the theoretical and practical aspects of acidification.

7.5.1 Sulfur and iron geochemistry

7.5.1.1 Sulfate reduction

The groundwater in the study area plots in the SO_4^{2-} field on the *Eh*–pH diagram for thermodynamically stable aqueous species in the S–O_2–H_2O system at 25°C and for total sulfur = 10^{-2} mole/kg (SO_4^{2-} ~960 mg/L) (Figure 7–11). The boundary position for S^0 and SO_4^{2-} stability is dependent on the total concentration of sulfur (Langmuir, 1997). Groundwater sulfur concentrations in the present study ranged from 1.25 to 2530 mg/L with 15% having the total sulfur < 10^{-3} mole/kg and 74% between 10^{-2} and 10^{-3} mole/kg total sulfur. The groundwaters still plot within the within the SO_4^{2-} field, despite the boundary change between the fields of S^0 and SO_4^{2-} caused by assuming a total sulfur of 10^{-3} mole/kg. The relations of the *Eh*–pH diagram suggest that H_2S will not be stable under the prevailing groundwater conditions.

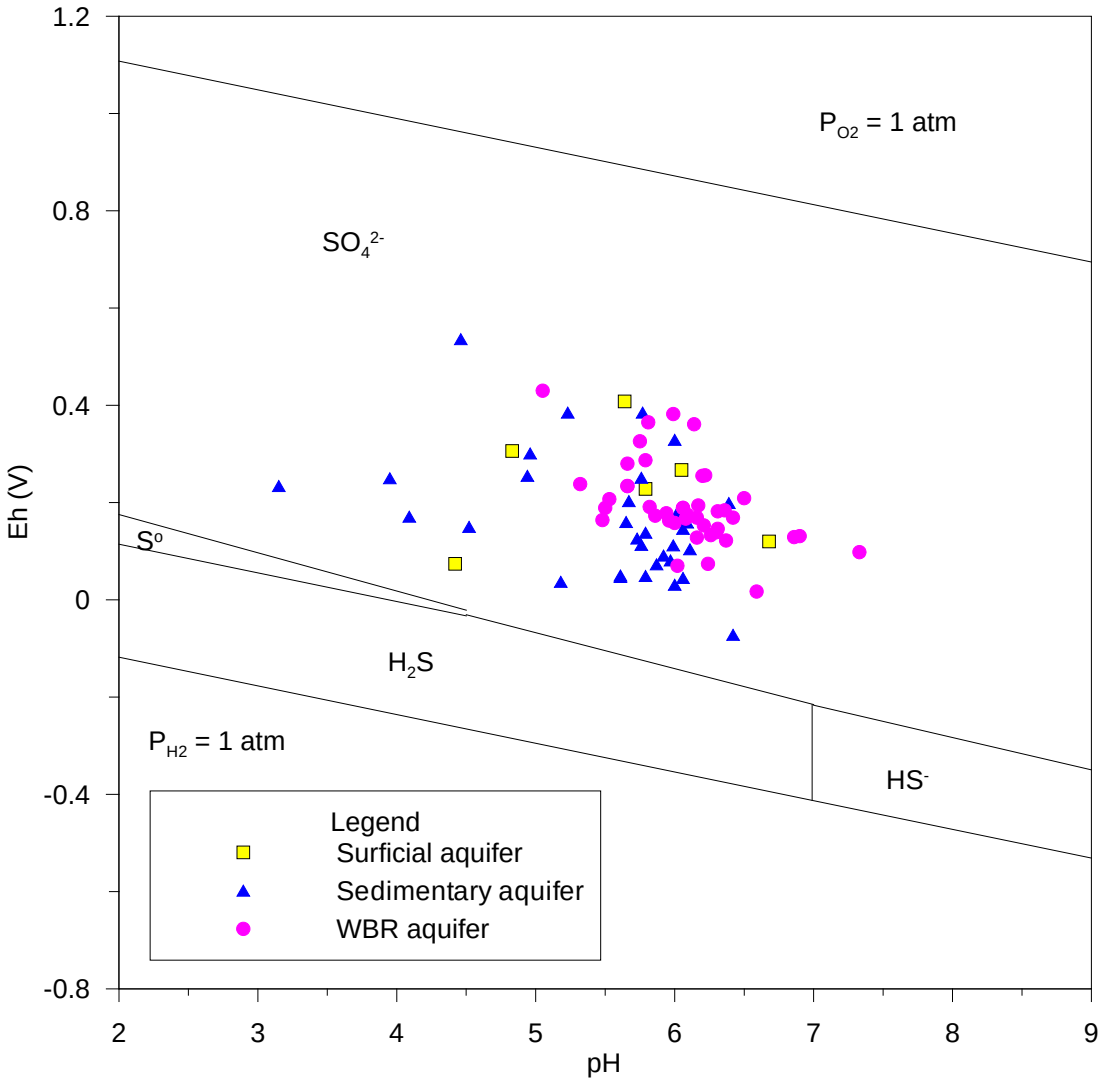

Figure 7–11 *Eh*–pH diagram for the S–O_2–H_2O system at 25°C assuming ΣS = 10^{-2} mole/L.

However, comparison of the measured SO_4^{2-} concentration with the total sulfur concentration recalculated as SO_4^{2-} (Figure 7–4), suggests that an additional sulfur species is present in some groundwater samples. The most stable sulfur species based on the thermodynamic data (Langmuir, 1997) is likely to be hydrogen sulfide (H_2S) or the hydrogen sulfide ion (HS^-):

$$H_2S = H^+ + HS^- \qquad (\log K_1 = -6.99) \qquad (7.4)$$

$$HS^- = H^+ + S^{2-} \qquad (\log K_2 = -12.44 \text{ to } -18.5) \qquad (7.5)$$

It is unlikely to be S^{2-} (reaction (7.5)). The second dissociation constant (log K_2) has a range from −12.44 to −18.5 (Langmuir, 1997), but is generally considered to be about −18 (Rickard and Morse, 2005). With a log K_2 of about −18 the aqueous sulfide ion has no significant activity in natural aqueous systems (Rickard and Morse, 2005).

Sulfide species have not been analysed for, but the characteristic 'rotten egg' smell of hydrogen sulfide has been noted when logging drill rock chips and during purging of bores. The 'rotten egg' smell has been noted for all three aquifers and is suggestive of low concentrations of hydrogen sulfide being present. Hydrogen sulfide is a product of dissimilatory sulfate reduction that requires anaerobic bacteria to respire using sulfate as the terminal electron acceptor according to (Appelo and Postma, 2005):

$$SO_4^{2-} + 2C_{organic} + 2H_2O \rightarrow H_2S + 2HCO_3^- \qquad (7.6)$$

The sulfate reducing bacteria (SRB) fall into two groups: heterotrophic SRB and autotrophic SRB. Heterotrophic SRB use organic compounds as the electron donor, while autotrophic SRB use H_2/CO_2 as the electron donor (Ehrlich, 2002).

The charge of sulfur in sulfate is +6 and in hydrogen sulfide is -2 thus the reduction of sulfate to hydrogen sulfide requires the transfer of 8 electrons. There is general agreement that sulfate is initially reduced to sulfite (SO_3^{2-}), but the reaction by which further reduction of SO_3^{2-} to sulfide takes place are not agreed upon and is probably a multistep process involving other sulfur intermediates (Ehrlich, 2002).

One step that has been recognised is the disproportionation of thiosulfate ($S_2O_3^{2-}$) (Ehrlich, 2002; Fossing and Jorgensen, 1990; Jorgensen, 1990a; 1990b; Jorgensen and Bak, 1991). Disproportionation is where an element is both oxidised and reduced in the same reaction (Brown and LeMay, 1977). The disproportionation of thiosulfate to SO_4^{2-} and HS^- is described by the reaction (Ehrlich, 2002):

$$S_2O_3^{2-} + H_2O \rightarrow HS^- + SO_4^{2-} + H^+ \qquad (7.7)$$

Disproportionation of thiosulfate to hydrogen sulfide and sulfate has been documented in freshwater sediments and marine sediments (Jorgensen, 1990a; 1990b) and while not investigated in the present study, warrants additional work. Other work that is relevant to the study area involves the extent of possible sulfate reduction in oxidised zones.

Sulfate reduction is generally considered to occur under anaerobic conditions within the reduced zone (Figure 2–5) (Dolla et al., 2006; Ehrlich, 2002) but increasingly sulfate reduction is being documented in oxidised zones (*Eh* > 0 V) and even in oxic zones (Dolla et al., 2006; Jorgensen, 1990a; 1990b). Under these conditions oxygen is reduced, but there is currently no evidence for bacterial growth. This suggest that oxygen reduction by sulfate reducing bacteria is a protective mechanism against the effect of oxygen rather than a means of deriving energy (Dolla et al., 2006). This might be an important mechanism for sulfate reducing bacteria in groundwater near the watertable since seasonal falls in the watertable will turn anoxic zones into transiently oxic zones.

7.5.1.2 Fe(III) reduction

Iron in solution is the major metal contributing to acidity. The groundwater within the study area plots in the Fe^{2+} field on the *Eh*–pH diagram for the thermodynamically stable species in the Fe–O_2–H_2O–S system at 25ºC (Figure 7–12). The field solution boundaries are drawn for an activity of dissolved Fe species of 10^{-6} mole/L and $\sum S=10^{-2}$ mole/L. Dissolved Fe has been identified in groundwater from all three aquifers with values ranging from < 1 to 142 mg/L and high values are found both in the north and south of the study area (Figure 7–13).

There are two sources of soluble iron in the study area. One is from chemical weathering of iron minerals such as biotite identified in the weathered basement rock. It is difficult to quantify how much of the dissolved iron is from this source. The second source is the extensive ferricrete within the study area. A major source of iron in groundwater is from the redox cycling of Fe involving biotic reduction of ferric oxyhydroxides (Kappler and Straub, 2005). While not quantified, the

extensive ferricrete in the study area is likely to contribute significant quantity of dissolved Fe to the groundwater.

Although microbial reduction of Fe(III) was documented back as long ago as the 19th century, the process of abiotic reduction of Fe(III) was considered more important until the 1980s. The ability of microorganisms that could obtained energy for growth by the complete oxidation of organic matter to carbon dioxide and to use Fe(III) and Mn(IV) as the sole electron acceptor has become evident since the 1980s. This has led to numerous laboratory studies aimed at understanding the process of Fe(III) reduction at near neutral pH and in nonsulfidogenic environments. While individual factors that contribute to the reduction process are known, the complex interaction between these factors is poorly understood (Roden and Urrutia, 2002).

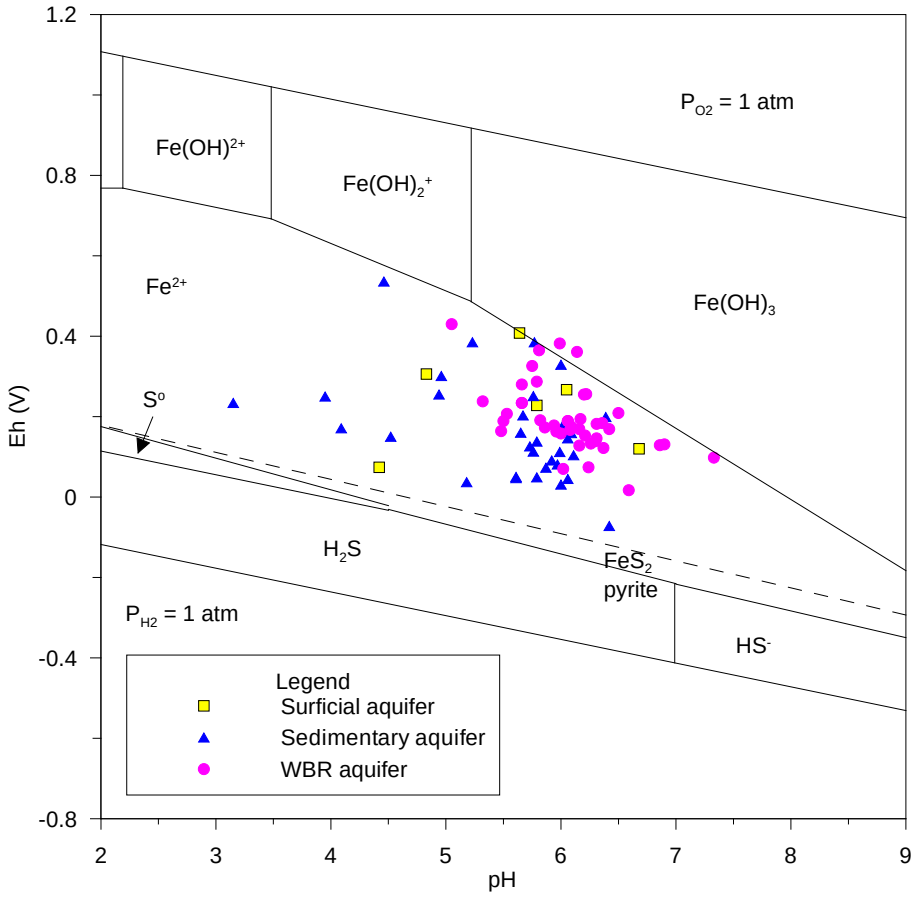

Figure 7–12 *Eh*–pH diagram for the Fe–O–H_2O system at 25°C. Field boundaries are drawn for an activity of dissolved Fe species of 10^{-6} mole/L and $\Sigma S = 10^{-2}$ mole/L. Dashed line is the upper boundary for pyrite stability.

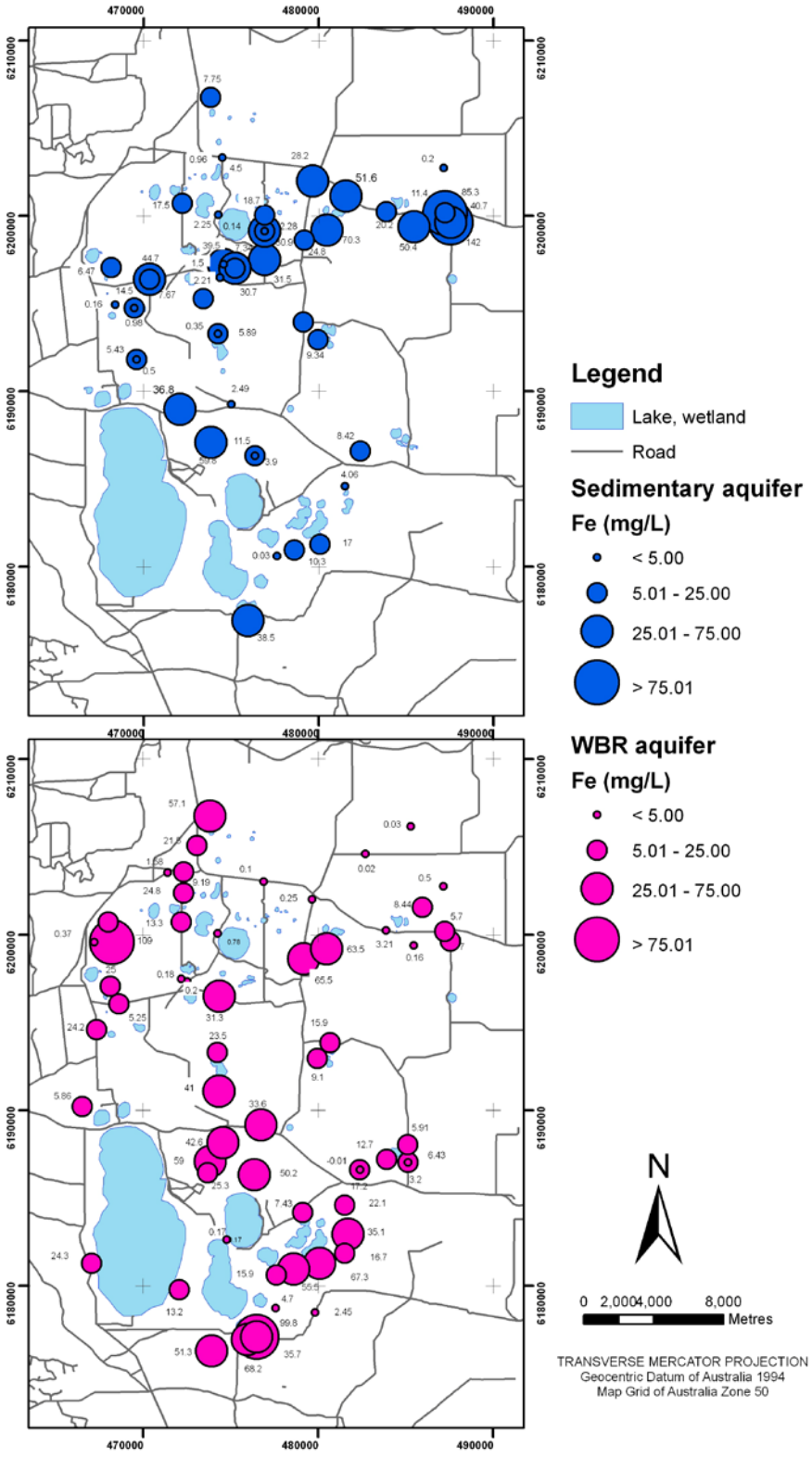

Figure 7–13 Spatial variation of dissolved Fe($_{total}$) in the groundwater from the sedimentary and WBR aquifers.

In many laboratory studies, amorphous Fe(III) oxide, such as ferrihydrite, was nearly completely reduced while reduction of synthetic crystalline Fe(III) oxide such as goethite or hematite were only partly reduced (Zachara et al., 2002). However, laboratory studies have also shown that in many cases, natural crystalline Fe(III) oxide is more likely to be reduced than synthetic crystalline Fe(III) oxide (Roden and Urrutia, 2002). Thus, reduction of crystalline Fe(III) oxide in the environment is more important than indicated by many laboratory experiments.

7.5.1.3 Pyrite distribution

The *Eh*–pH stability diagram suggests that groundwater redox conditions are not ideal for pyrite formation (Figure 7–12). However, pyrite is evident throughout the study area with visual pyrite in the channel sand regolith unit being up to 1% and up to 3% in the flood plain and WBR regolith units. The rock chips (between 0 and 10 m depth) at the time of drilling were tested according to the field peroxide test (Section 4.3.2) which indicates the possible presence of sulfide (Hey et al., 2000). For numerous bores, within the first 10 m most of the pH_{FOX} were between 4 and 5.5 indicating potential acid soils (Figure 5–5).

Rock chip samples from depths greater than 10 m were tested in bores MU12A, MU42D and MU46D, yielding pH_{FOX} values indicative of the presence of pyrite throughout the sediments (Figure 5–5 and Figure 7–14). The poorly-sorted quartz dominated channel sand regolith unit yielded pH_{FOX} values of between 1.4 to 3.2, while the flood plain unit gave pH_{FOX} of between 1.3 and 1.6 (Figure 7–14). The weathered basement pH_{FOX} ranged from 1.7 to 6.7. The pH_F values shown in Figure 7–14 were measured on rock chip samples drilled two years previously, whereas in MU12A the pH_F was measured at the time of drilling (Figure 5–5). The low pH_F values from rock chips from bores MU42D and MU46D suggest that oxidation of the sulfides started after extraction of the rock chips.

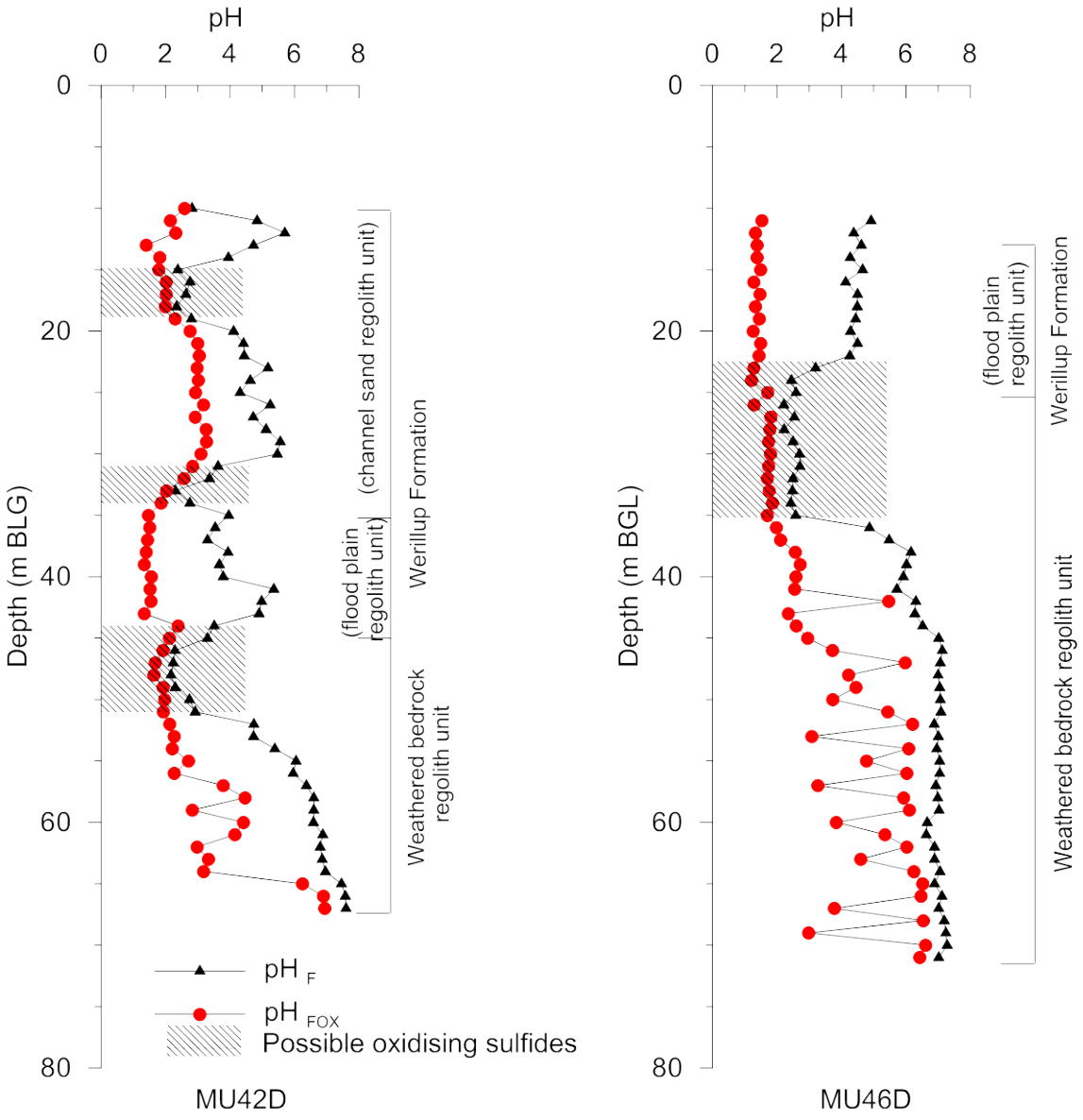

Figure 7–14 Comparison of pH_F and pH_{FOX} measured in bores MU42D and MU46D. The low pH_F values (stippled areas) suggest that sulfides had started to oxidise. The consistently low pH_{FOX} suggests that the sediments contain sulfide minerals. Rock chips were two years old at time of testing.

7.5.1.4 Oxidation of pyrite and Fe(II)

Oxidation of pyrite and Fe(II) is interpreted to be the major acid-generating process in the study area. Groundwaters with pH < 5 are present in all 3 aquifers and at various depths below surface (Table 7-1) and extensive iron staining is seen at many of the groundwater seeps, edges of swamps and lakes and in saline scolds in the study area (Figure 7–15). Detailed geochemical work would be required to determined the relative importance of pyrite and Fe(II) oxidation compared to Fe(II) oxidation only and this likely to change from site to site. The field peroxide test on regolith samples within the top 10 m mostly have $pH_{Fox} > 4$.

Table 7-1 Bores with groundwater pH < 5, trace metals and Net Acidity.

Bore no.	*Aquifer*	*Base of screen (m BGL)*	*pH (ground water)*	*Al (mg/L)*	*Fe (mg/L)*	*Mn (mg/L)*	*Net acidity (mg/L $CaCO_3$)*
MU07S	Sedimentary	21	4.18	4.25	28.2	0.3	78
MU13	Surficial	12	4.42	1.23	8.82	0.72	25
MU15S	Sedimentary	15	3.95	5.45	70.3	0.46	163
MU16S	Sedimentary	9	4.09	4.5	50.4	0.36	120
MU22D	WBR, sedimentary	14	4.49	0.79	15.9	0.49	32
MU22S	Surficial	7.5	4.83	0.2	15.6	1.94	19
MU23S	Sedimentary	15	4.52	0.3	9.34	0.33	13
MU25	Surficial	13	4.59		0.03	0.37	–40
MU37I	Sedimentary	34	4.94	0.09	40.7	0.32	57
MU39	WBR	19	4.2	1	24.8	0.07	53
MU56S	Sedimentary	8	3.45				
MU62I	Sedimentary	33	4.96	0.01	11.5	0.41	35
MU63S	Sedimentary	6	4.46	10.1	1.5	0.22	61
MU64S	Sedimentary	4	3.15	14.2	7.34	0.39	143
PM10	Sedimentary	37	4.9	0.12	19.1	0.43	9
PM12	Sedimentary	24	3.77	15.1	51.6	0.42	186

No pyrite was identified from samples at depths less than 10 m near the watertable (Table 4-3). Pyrite has been identified at depths > 10 m, thus potential oxidation of pyrite is more likely below 10 m depth (Figure 7–14).

Figure 7–15 Extensive Fe staining in the saline scald upslope of Yarnup Swamp.

7.5.1.5 Ferric hydrosulfate minerals

Ferric hydrosulfate minerals most commonly associated with groundwater acidification are alunite and jarosite. Alunite has not been identified in the study area, whereas jarosite and/or natrojarosite has been identified by SEM – EDAX. Alunite is known to occur in sedimentary low temperature environments and it has been reported in weathered profiles, intertidal marine environments, lacustrine environments and caves (Stoffregen et al., 2000).

Jarosite is commonly associated with natural and anthropogenicaly degraded acid soils. Highly acidic conditions exist at the loci of jarosite precipitation (Stoffregen et

al., 2000). In soil with no buffering capacity, drainage of these soils will enable oxidation of pyrite and the development of low pH values along with jarosite precipitation. Oxidation of sulfide minerals in anthropogenicaly degraded acid soils and mining spoils produce ideal conditions for jarosite formation. Jarosite commonly is found in clays as micro-concretions, seams and aggregates.

Brown (1971) investigated the stability fields for jarosite and goethite at 25 °C, 1 atm. In defining the stability field of jarosite, 5 variables were considered: *Eh*, pH, activity of total sulfur species, activity of dissolved iron and the activity of potassium. Four main conclusions were drawn. Jarosite is stable at low pH and moderately oxidizing *Eh* values. As the activity of dissolved iron or potassium increases the stability field of jarosite moves to increasingly lower *Eh* values i.e. jarosite may form if the activity of ferrous iron is greater than the activity of ferric iron. The jarosite field completely eliminates the Fe^{3+} stability field for high activities of Fe^{3+} and SO_4^{2-} and finally, the activities of H^+ and SO_4^{2-} are critical to jarosite precipitation or dissolution.

McArthur et al. (1989) noted stoichiometric K and sulfate depletion in groundwater from the Yilgarn Craton, which they suggested was due to alunite and jarosite precipitation. Alunite formation from kaolinite would be according to:

$$3Al_2Si_2O_5(OH)_4 + 4SO_4^{2-} + 6H^+ + 2K^+ \rightarrow 2KAl_3(SO_4)_2(OH)_6 + 6SiO_2 + 3H_2O \quad (7.8)$$

For every mole of K^+ used in the formation of alunite, two moles of SO_4^{2-} would be utilised. The K^+ deficit is calculated according to:

$$K^+_{(expected)} = \frac{Cl^-_{(actual)} \times K^+_{(seawater)}}{Cl^-_{(seawater)}} \quad (7.9)$$

$$K^+_{(deficit)} = K^+_{(expected)} - K^+_{(actual)} \quad (7.10)$$

where $K^+_{(expected)}$ is the concentration designated by the seawater potassium to chloride ratio. If the $K^+_{(actual)}$ is less than $K^+_{(expected)}$ depletion of the ion has occurred. Assuming that the $K^+_{(deficit)}$ was utilised in the formation of alunite the required SO_4^{2-} can be

calculated. The required SO_4^{2-} to form alunite was added to the actual groundwater SO_4^{2-}. From Figure 7–16 it can be seen that the initial groundwater samples would be enriched with sulfate and not represent the original marine aerosol signature. This suggests that not all the $K^+_{(deficit)}$ was utilised in the formation of alunite or jarosite.

The SI suggests that most of the groundwater is oversaturated with respect to alunite (Figure 7–6) but undersaturated with respect to jarosite (Figure 7–6). The formation of jarosite is restricted to very specific conditions occurring locally within the study area. Jarosite has been identified from a groundwater seep on the beach of Tordit-Gurrup Lagoon near the rock exposure (Figure 4–1). Down slope of the groundwater seep the beach is covered by a thin iron crust. The crust has a pH of 2.5 (1:5 paste). This is consistent with jarosite being stable at low pH and moderately oxidizing *Eh* values (Brown, 1971).

Formation of jarosite and alunite may account for some sulfate depletion in the groundwater of the study area. Potassium may be removed from groundwater by other processes, and the K to SO_4 ratio will be determined by other chemical processes, such as pyrite formation and dissolution.

7.5.1.6 Other oxidants

One aspect not addressed in this study is the influence of landuse on the groundwater acidity. Extensive areas east of Unicup Lake have been cleared of native vegetation for agricultural purposes. Fertilisers containing nitrogen will have been added as part of the farming practices. Nitrate levels are not available for the groundwater, but regional groundwater mapping shows the NO_3^- levels generally less than 1 mg/L (De Silva, 2004). Any addition of nitrogen via fertiliser may contribute to biotic Fe(II) oxidation with NO_3^- acting as the oxidant at near neutral pH (Kappler and Straub, 2005). This process would need further investigation.

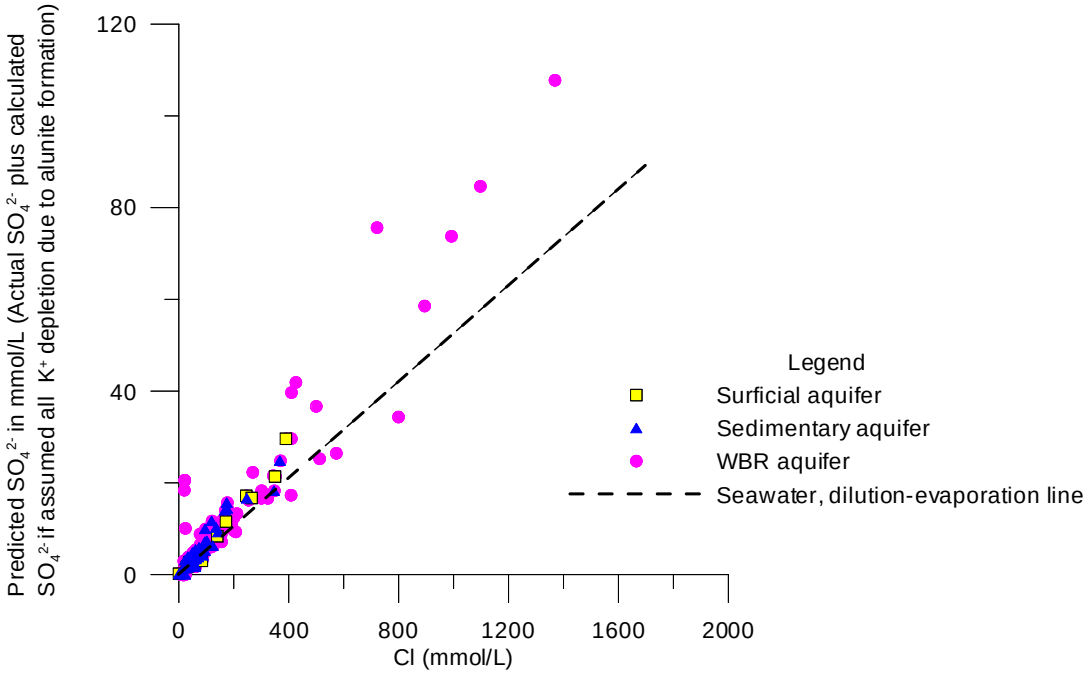

Figure 7–16 The predicted groundwater sulfate concentration if all K^+ depletion was due to formation of alunite or jarosite. The predicted sulfate concentration was obtained by adding the actual groundwater sulfate concentration to the calculated sulfate concentration required if all the K^+ depletion was due to formation of alunite or jarosite. By comparing the predicted sulfate concentration to the seawater dilution-evaporation line (dashed line) it can be seen that the groundwater samples would be enriched with sulfate as thus the initial groundwater would not represent the marine aerosol signature.

7.6 Ca–Na–Cl type water

The greatest enrichment of dissolved Ca^{2+} (Ca–Na–Cl type water) is seen in the WBR aquifer in the south of the study area associated with bores MU46A, MU46D and MU61D (Figure 4–1). Carbonate minerals huntite and siderite showing Mg substitution have been identified by XRD in regolith sample MU46-45.5. Huntite is typically a weathering product of dolomite- or magnesite-bearing rocks and is also sound in faults (Deer et al., 1992). Huntite is often associated with additional carbonate minerals, but besides siderite other carbonate minerals were not identified (Table 7-2). Huntite was identified in only one rock sample and is thus thought to be relatively rare in the study area.

Total calcium and exchangeable calcium have been extracted from the regolith sample MU46-45.5 using a total acid digestion and 1M ammonium acetate extraction at pH 5, respectively. Total calcium was just over 7000 mg/kg (MU46-45.5) of

which 2753 mg/kg was considered exchangeable. Total magnesium was about 1500 mg/kg, with 674 mg/kg being exchangeable. The quantity of total and extractible magnesium was low considering the stoichiometric formula for huntite is $Ca_3Mg_4CO_3$ and that the siderite had Mg substitution. If the increased concentration of Ca^{2+} was from the dissolution of huntite it would be expected for greater concentration of Mg^{2+} than is evident (Figure 7–3(d)). Quantative results of the XRD analysis for this sample are listed below Table 7-2. The analysis did not detect other carbonate minerals or Ca minerals such as gypsum.

Cation exchange cannot be discounted with 2753 mg/kg of the total calcium being exchangeable. While XRD analysis did not detect other Ca minerals work by BHP Minerals Pty. Ltd (2000) indicates a change in basement lithology that could explain the change in water type.

Table 7-2 XRD analysis of weathered basement regolith sample MU46–45.5.

Mineral phase	Weight (%)
Kaolin, BISH885	48.4
Quartz	38.6
Siderite (hex)	5.9
Huntite	5.0
Biotite, 1M	1.3
Sodium Chloride	0.4

To the west of the study area calcium values ranging from 2500 to 47 800 mg/kg from basement rock interpreted to be paragneiss have been documented (BHP Minerals Pty. Ltd, 2000). No groundwater chemistry is available for this area. The Ca–Na–Cl type water in the WBR aquifer was not found in the overlying sedimentary aquifer suggesting that dissolution of a carbonate mineral in the WBR aquifer contributed to this type of water. Additional work is needed to understand this groundwater type.

7.7 NA–MG–SO_4 TYPE WATER

Groundwater beneath Forty Acre Swamp is enriched in sulfate and is a Na–Mg–SO_4 type water. The swamp is located within a mining lease for peat. Although peat has not been mined at Forty Acre Swamp, the swamp lies within the area of changed hydrology resulting from peat mining at Cowerup Swamp (Figure 7–17). Historically, Forty Acre Swamp is thought to have had a water level of about 1 m above surface in winter, falling in summer to just above the peat surface: thus the peat was submerged throughout the year.

Currently the top 0.3 m of the 1 m thick peat is dry over summer with the lower section being moist. By the end of winter the full thickness of peat is wet. There is no well defined natural drainage entering or leaving the swamp. However, to enable mining of Cowerup Swamp, both Forty Acre Swamp and Cowerup Swamp were drained by an open channel cut between the two swamps and a second channel which extended from Cowerup Swamp to Lake Muir.

Peat deposits form where the oxidation of the organic matter is slower than the rate of accumulation. Organic material for peat formation is derived from a variety of plants ranging from sphagnum and grasses to debris of large forests on low-lying wet ground. Under aerobic conditions fungi degrade this organic matter to form cellulose, hemi cellulose and lignin. Once O_2 becomes depleted, anaerobic conditions prevail and the oxidants become NO_3^-, Fe(III), Mn(IV), SO_4^{2-} (Figure 2–5). Degradation of the organic material ceases when there is an accumulation of inhibitory waste products, lack of moisture or an insufficient quantity of oxidant (Ehrlich, 2002). During the formation of peat the deposits become enriched in lignin, ulmins and humic acid. On draining Forty Acre Swamp, the watertable was lowered to below the peat layer, but as noted the lower 0.7 m of peat is moist all year.

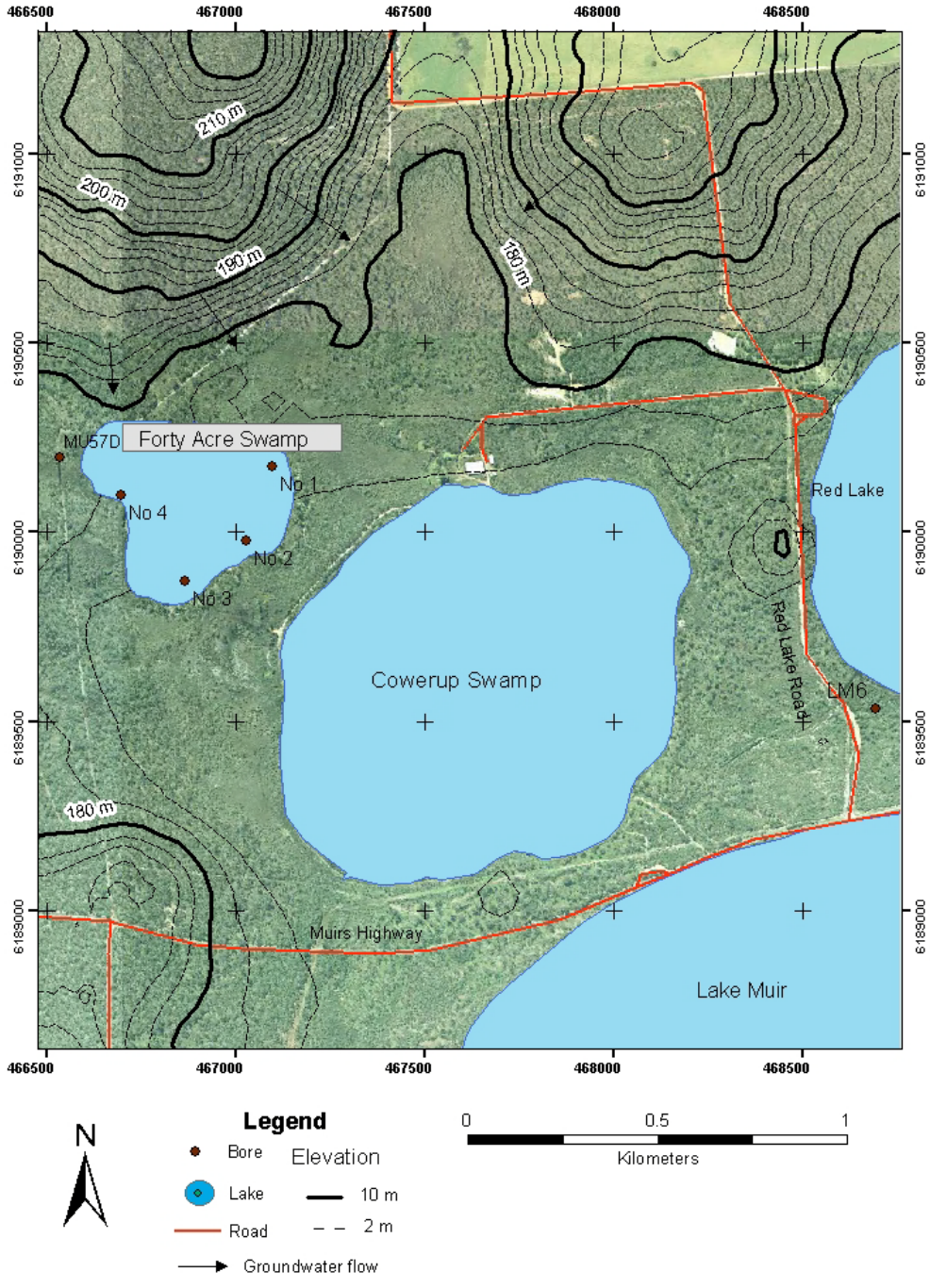

Figure 7–17 Forty Acre Swamp showing bore locations and groundwater flows into the swamp.

The surficial aquifer and the weathered basement aquifer are present in the vicinity of the swamp. The weathered basement aquifer is only 2 m thick in bore MU57D (Figure 7–17). Groundwater flow in these two aquifers is mainly characterised by local flow systems reflecting the local topographic slopes (Figure 7–17). Recharge to the surficial aquifer is from direct infiltration of rainfall. Discharge is via evapotranspiration from the shallow watertable, especially where the groundwater converges between the two hills as seen on Figure 7–17.

Table 7-3 Major ion concentrations showing the groundwater chemical variation in groundwater between the weathered basement aquifer to the west of the swamp and the groundwater under the swamp.

	Bore ID	*Cl (mg/L)*	*SO4 (mg/L)*	*HCO_3 (mg/L)*	*Na (mg/L)*	*Ca (mg/L)*	*Mg (mg/L)*	*K (mg/L)*
Bores located in Forty Acre Swamp	Forty Acre 1	880	2100	41	700	220	330	20
	Forty Acre 2	510	260	380	390	160	80	12
	Forty Acre 3	830	1800	373	730	470	220	28
	Forty Acre 4	910	1400	312	680	270	280	11
Bores west of Forty Acre Swamp	MU57S	2800	120	197	1600	88	220	23
	MU57D	4300	340	264	2300	160	340	31

The water under the peat swamp is sulfate dominated in contrast to the chloride dominated groundwater immediately west of the swamp in bores MU57S and MU57D (Table 7-3). The chloride levels in bores Forty Acre 1 to 4 are between 510 and 910 mg/L compared to 2800 and 4300 mg/L in bores MU57S and MU57D, suggesting a major fresh water component from direct infiltration of rainfall through the swamp. The marine sulfate/chloride weight ratio is 0.14 (Hem, 1970). The sulfate rich waters (bores Forty Acre 1, Forty Acre 3, Forty Acre 4) have ratios greater than 1.5 with bore Forty Acre 2 having a ratio of about 0.5. The local groundwater is depleted with a ratio of less than 0.04. Relative to the surrounding regional groundwater the HCO_3^- values are also elevated except for bore Forty Acre 1 (Table 7-3). Sodium is the major cation, but the proportions of Ca^{2+} and

Mg^{2+} have increased and the groundwater is enriched in both Ca^{2+} and Mg^{2+} relative to the seawater evaporation dilution line (Figure 7–3).

The groundwater has low levels of Al and Mn with values being below 1 mg/L. Iron in solution is between 1.86 and 17 mg/L. The groundwater has a Total Alkalinity > 450 mg/L CaCO3 in 3 of the 4 bores (Table 7-4). A low Total Acidity and elevated Total Alkalinity suggest that alkalinity-generating processes dominate in this swamp. In contrast, acidity-generating processes dominate at the mined peat swamp of Cowerup where the weekly recorded lake water pH ranges between 3.18 and 4.40 except for two values of > 4.4 in 2008.

Table 7-4 Total Alkalinity and Total Acidity for groundwater under Forty Acre Swamp

Bore ID	*pH*	*Al*	*Fe*	*Mn*	*Total acidity*	*Total alkalinity*	*Net Acidity*
		mg/L	*mg/L*	*mg/L*		*mg/L CaCO3*	
Forty Acre 1	5.95	0.46	7.4	0.5	17	61	–44
Forty Acre 2	6.74	0.12	10.3	0.86	21	560	–539
Forty Acre 3	6.72		1.86	0.45	4	550	–546
Forty Acre 4	6.56	0.02	17	0.33	31	460	–429

The groundwater SI with respect to calcite ranges from –1.88 to 0.08 with the groundwater being in equilibrium at bores Forty Acre 2 and Forty Acre 3. The SI with respect to gypsum suggests that only one of the four groundwater samples is in equilibrium with gypsum (bore Forty Acre 3). Since the groundwater is undersaturated with respect to gypsum and the TDS < 3100 mg/L the formation and dissolution of gypsum is unlikely to be a major source SO_4^{2-} or Ca^{2+} in the groundwater under Forty Acre Swamp as at Lake Muir.

Sulfate in the groundwater may result from oxidation of pyrite, and/or aerobic mineralization of organic matter. Pyrite is associated with many peat swamps (Howarth and Teal, 1979; Lopez-Buendia et al., 2007; Mandernack et al., 2000) and it is likely that pyrite is present in the peat at Fort Acre Swamp. Organic S has not been determined in the peats. However, elsewhere such peat is likely to have about 90% of the total S as organic S (McGill and Cole, 1981; Wieder and Lang, 1988).

The lowering of the watertable through drainage will have changed the environment of the peat from reducing to oxidising in the top 0.3 m in summer. Oxidation will proceed according to reaction (2.48) with O_2 being the major oxidant. Beneath Forty Acre Swamp the groundwater pH values are currently between 5.95 and 6.74. At this pH and under oxidising condition any aqueous Fe^{2+} released by pyrite oxidation will oxidise to aqueous Fe^{3+} (reaction (2.49)). The free ferric ion is unstable at these pH values and is precipitate as ferric oxyhydroxides (reaction (2.50)).

The SO_4^{2-} excess is calculated according to

$$SO_{4\,(excess)}^{2-} = SO_{4\ (actual)}^{2-} - \frac{Cl^-_{(actual)} \times SO_{4\ (seawater)}^{2-}}{Cl^-_{(seawater)}} \qquad (7.11)$$

To produce the excess aqueous sulfate concentrations in the groundwater between 1 and 9.85 mmol of pyrite would need to be oxidised (Table 7-5). This would result in pH values less than 2.35 assuming no buffering capacity.

Table 7-5 Pyrite required to oxidise to produce the excess sulfate (equation (7.11)) and expected pH assuming no buffering.

Bore Id	Excess SO_4 (mg/L)	SO_4 (mmol/L)	FeS_2 (mmol)	H^+ (mmol/L)	pH
1	1895	19.7	9.85	39.4	1.41
2	202	2.1	1	4.4	2.35
3	1715	17.8	8.9	35.6	1.45
4	822	8.5	4.25	17	1.77

The oxidation of organic matter (aerobic respiration) may be summarised as (Drever, 1997; Stumm and Morgan, 1996):

$$(C) + 2H_2O \rightarrow CO_{2(g)} + 4H^+ + 4e^- \qquad (7.12)$$

If S is present in the organic matter then SO_4^{2-} is an end product of the aerobic respiration (Ehrlich, 2002). One mole of organic matter will produce 4 moles of H^+, similar to the oxidation of pyrite by oxygen (reactions (2.48) to (2.50) and (7.12)).

Both these processes are acid-generating, but the water chemistry indicates that an alkalinity-generating process dominates the groundwater. The Net Acidity is between –429 and –546 mg/L $CaCO_3$ in three of the bores and –44 mg/L in bore Forty Acre 1 (Table 7-4). It is proposed that pyrite oxidation is occurring in the dry layer of peat and that the SO_4^{2-} and H^+ ions are being flushed through the moist peat in winter where alkalinity-generating processes are dominant. The acidity is buffered and the remaining SO_4^{2-} rich water infiltrates to the groundwater to produce the SO_4^{2-} rich groundwater. Additional work is required at Forty Acre Swamp to confirm this process.

8 Discussion and recommendations

8.1 DISCUSSION

Changes in hydrology are threatening lake habitat and vegetation in the Lake Muir–Unicup Natural Diversity Recovery Catchment. Recommendations made in the Catchment Management Plan (Department of Environment and Conservation, *in prep*) reflected the Department of Environment and Conservation's focus upon hydrological changes affecting individual lakes, in favour of a broader understanding of how the regional hydrogeology impacts upon the lakes. It quickly became apparent that a viable management plan could not be formulated until the hydrogeology and geochemistry were better known. In 2003, DEC initiated a groundwater exploration program. The geological information generated from this exploration program, and the groundwater and rock chemical data collected as part of this study have been combined with the reinterpreted geophysical survey data, to enabled this research project to establish the foundations for future detailed studies of wetland hydrology.

Specific outcomes of the present study that have implications for future lake hydrology research within the catchment include the identification of regolith units, assessment of the vertical and lateral extents of the aquifers especially the predominant sedimentary aquifer, directions of groundwater flow, and the distinct hydrochemical facies found within the catchment.

Five regolith units have been identified within the Lake Muir–Unicup Natural Diversity Recovery Catchment and form the bases of the 3 aquifers. Geological interpretation has increased our understanding of the lateral and vertical extent of the Eocene sedimentary rocks. The importance of this to the next stage of wetland research is that lakes, such as Kulunilup Lake, are a consequence of regional groundwater convergence within the sedimentary aquifer (Figure 6–4) and thus have a very different hydrology to that of Fort Acre Swamp located over the WBR aquifer with only local groundwater flows (Figure 7–17).

The present study has shown, for the first time, that the Lake Muir–Unicup Natural Diversity Recovery Catchment is a closed groundwater basin with groundwater

salinity being up to 3 times seawater in the south of the catchment. This has implications for the wetlands east of Lake Muir, as these important wetlands contain brackish lake water but are located over the extremely saline groundwater.

Three distinct hydrochemical facies have been identified with two groundwater types previously unidentified in the Lake Muir–Unicup Catchment. A Ca–Na–Cl type water probably reflects the mineralogy of the weathered basement rock in the south of the catchment, though cation exchange needs to be considered. An anthropogenic Na–Mg–SO_4 type water is caused by changing the hydrology of a Forty Acre Swamp (a peat wetland), illustrating the need to understand how human intervention in wetlands may impact on the local environment including groundwater. This wetland gives an indication of what can be expected if the drying climate continues and more peat wetlands dry through the summer month.

8.1.1 Landscape evolution

Rifting between Australia and Antarctica is the main tectonic event that has controlled the landscape evolution in southern Western Australia. Ultimately, it has determined the nature of the aquifers and the groundwater geochemistry in the region, including that of the Lake Muir–Unicup Natural Diversity Recovery Catchment. The separation of these two land masses resulted in the formation and preservation of five regolith units that provide three aquifers with distinct water chemistry in the catchment.

Cratonic uplift in the Early Cretaceous to middle Eocene resulted in south to southeast flowing rivers that eroded valleys to depths of at least 14 m below the pre-existing valley floor in the north of the catchment. The late Eocene topography has been interpreted from known depths to basement rock (model 1) and depth to magnetic basement (model 2). The resulting topographic surface predicted from these two independent data sets have been compared. Reasonable confidence can be placed on the position of a major river channel in the north of the catchment, but different topographic surfaces are predicted by the two models in the south of the catchment.

Existence of southeast trending segments, beneath Unicup Lake, and the southern segment south of Unicup Lake, predicted by both models, is supported by the

lithology. However, the southern trending segments (1B, 1C) north of Unicup Lake predicted by the depth to magnetic basement (model 2) is less certain.

In the vicinity of Lake Muir in the south of the catchment the Eocene topographic surface predicted from depth to magnetic basement (model 2) infers a palaeovalley system not predicted by the known depth to basement rock (model 1). Neither model at present can be discarded based on the known geology. Part of the reason for the low confidence in the predicted topographic surface under and to the east of Lake Muir is the lack of preserved sediment of the Werillup and Pallinup Formations. The thin sediments of the Werillup Formation are consistent with either a southern extension of the palaeovalley to the east of Byenup Lagoon (model 1) or an eastern extension of the palaeovalley beneath Byenup and Tordit-Gurrup Lagoons (model 2). An 11 m thickness of unconsolidated sands encountered in boreholes drilled around the Tordit-Gurrup and Byenup Lagoons exceeds that normally associated with sand dunes in the catchment. The sediments are thus more likely to be fluvial origin. The presence of fluvial deposits would lend support to the existence of the eastern extension of the palaeovalley predicted by the model 2.

The topographic surface present in the late Eocene was dominated by exposures of granitic gneiss with major albite, quartz and muscovite. The carbonate minerals huntite and siderite have been identified in the south of the catchment associated with a fault zone. Mineral exploration has identified a paragneiss (BHP Minerals Pty. Ltd, 2000) west of the Lake Muir–Unicup Catchment, although this rock type has not been identified in the catchment. Whether these carbonate minerals are related to a paragneiss or alteration of other rock types along the fault zone has not been determined in this study and warrants additional investigation in light of the increased abundance of dissolved Ca^{2+} occurring in the groundwater from this area. Crystalline basement exposed in the late Eocene forms the current weathered and/or fractured basement rock aquifer. This aquifer is laterally the most extensive within the study area. It is either exposed on the elevated ridges and hills or is overlain by the sedimentary and surficial aquifers within the broad valleys.

Differential land subsidence rates changed the erosional river system to one of deposition. The valleys present in the Eocene infilled with fluvial and marine sediment. These deposits form the sedimentary aquifer present today and can be subdivided into three regolith units: the channel sand regolith unit and the flood plain

regolith unit of the Werillup Formation and the marine regolith unit of the Pallinup Formation. Both the quartz dominated sands of the channel sand unit and the carbonaceous clays and silts of the flood plain unit are present throughout the study area, but the marine unit appears to be restricted to the northern part of the catchment. In the north, the sedimentary aquifer can be up to 70 m thick, but in the south it is much thinner where present.

The reduced thickness of the Werillup Formation and absence of the Pallinup Formation in the south of the catchment indicates that erosion has taken place. The timing of the erosion is poorly constrained but possibly post-dates the development of the ferricrete crust that is preserved on the Pallinup Formation and on elevated weathered bedrock rises and hillocks. In Western Australia, extensive ferricrete formed in the Oligocene and Miocene (Anand and Paine, 2002; Quilty, 1994) and one can therefore expect the erosion to have taken place since the Miocene. Assuming that a more or less uniform thickness of the marine Pallinup Formation was originally deposited over the Lake Muir–Unicup Catchment, at least 12 to 14 m of sediment has been eroded from the southern part.

Subsequent change of the erosional environment to one of deposition most probably reflects uplift of the plateau in the south combined with a drier climate. The climate of Australia is known to have changed with desiccation of inland Australia during the late Miocene (Norvick and Smith, 2001). The distinct difference in bedrock elevations between the Frankland River (~140 m AHD) and the crystalline basement beneath the broad valley east of Lake Muir (117 m AHD) suggests that the southern plateau has risen. Up to 11 m of recent sediments have been deposited on weathered bedrock and 7 m of recent sediments on the Werillup Formation. These young sediments form the surficial aquifer, with this aquifer being thicker in the south than the north.

8.1.2 Groundwater recharge and flow

The exposed aquifers in the study area are recharged by infiltration of rainfall. Leakage between the semi-confined aquifers is evident from the hydraulic head data.

The southern plateau prevents groundwater discharging to the south resulting in a closed basin with respect to groundwater. The groundwater flows have hydraulic heads (adjusted for density) that decrease from about 230 m AHD in the north to

about 175 m AHD in the south. The northeast hills, westerly sloping ridges and plateau along the southern boundary influence the groundwater flows beneath the broad-valley floors in the north and south (Figure 3–1 and Figure 6–4). In the north, a chain of lakes and swamps has developed on the broad-valley floor where northwest and southwest directed groundwater flows converge in both the north and south of the catchment.

Groundwater exits the Lake Muir–Unicup Catchment into the Tone River through a narrow valley in the northwest. Groundwater discharge into the Frankland River has not been identified and the greatest loss of groundwater is by evaporation through Lake Muir although further work is needed to quantify this loss. A dramatic increase in TDS of groundwater (up to about 95 000 mg/L) in the south of the catchment is due to evapo-concentration, consistent with there being groundwater discharge from Lake Muir.

8.1.3 Groundwater evolution

Three groundwater types have been identified in the Lake Muir–Unicup Catchment, a Na–Cl type, a Ca–Na–Cl type, and a Na–Mg–SO_4 type water. The Na–Cl type water has been identified in all three aquifers, whereas the Ca–Na–Cl type has only been identified in the WBR aquifer in the south of the catchment. The anthropogenic ally generated Na–Mg–SO_4 type water is located under Forty Acre Swamp.

Even though the groundwater moves in a closed basin with the TDS values increasing from less than 10 000 mg/L in the north to about 95 000 mg/L in the south of the Lake Muir–Unicup catchment, the groundwater evolution does not fit easily into the brine evolution model (Figure 2–3 and Figure 2–4) which describes a lacustrine rather than a marine origin for the groundwater (Long et al., 1992a) and assumes that evaporative concentration is the only process occurring (Hardie and Eugster, 1970). The groundwater in the study area is concentrated through evaporation though it also interacts with the aquifer media and is modified by processes such as chemical weathering of rocks, cation exchange and redox reactions.

The Na–Cl type water reflects the initial marine chemical signature rather than a classic groundwater evolution where the major anions evolve from HCO_3^- to Cl^-. In

the south of the catchment the groundwater evolves from the Na–Cl type water into a Ca–Na–Cl type water as the groundwater interacts with the WBR aquifer media in which siderite and huntite have been identified. The groundwater in the overlying quartz dominated sedimentary aquifer remains a Na–Cl type water retaining the original marine chemical signature.

8.1.3.1 Surficial aquifer

Groundwater in the surficial aquifer is mostly of Na–Cl type water but is influenced at a local scale by groundwater–lake water interactions and anthropogenic process. Reactions between groundwater and lake water beneath Lake Muir have resulted in a Na–Cl type that is enriched in SO_4^{2-} and Ca^{2+} relative to seawater, whereas anthropogenic impact has created a Na–Mg–SO_4 type water at Forty Acre Swamp.

Beneath Lake Muir, the enrichment in dissolved Ca^{2+} and SO_4^{2-} is attributed to the annual formation and dissolution of gypsum crust. Dissolution of a gypsum crust formed on the desiccated lake floor enriches infiltrating water with Ca^{2+} and SO_4^{2-}. The saturation index for calcite at the watertable directly under the lake, indicates that the water is oversaturated with respect of Ca. The groundwater under the lake has become enriched in sulfate relative to seawater.

The draining of Forty Acre Swamp to enable mining of peat at nearby Cowerup Swamp has produced a Na–Mg–SO_4 type water. The low TDS of the groundwater appears to preclude the formation and subsequent dissolution of gypsum to enrich the water with SO_4^{2-} as is the case at Lake Muir. The source of sulfate is likely to be the oxidation of pyrite in the peat. However, this process should produce groundwater acidification as seen in Cowerup Swamp, but in 3 of the 4 bores the Net Acidity is < -429 mg/L. This suggests that as pyrite oxidised the acid produced was buffered.

8.1.3.2 Sedimentary aquifer

The sedimentary aquifer contains a Na–Cl type water with TDS up to 10 000 mg/L in the north, and in excess of 30 000 mg/L in the south of the catchment. Minor increases in dissolved Na^+ relative to the seawater evaporation-dilution line implies an input from rock weathering. Kaolinite has been identified in the aquifer and is the chemical weathering product of plagioclase feldspar more so than orthoclase or

K-feldspar and other silicate minerals. However, it is very difficult to quantify the contribution from weathering as kaolinite will have been deposited as part of the fluvial sediments; and the chemical signature of the groundwater is overprinted by cation exchange.

Enrichment of groundwater in dissolved Ca^{2+} and Mg^{2+} along with Na^{+} depletion suggests that cation exchange is occurring within the aquifer. Organic clays normally have significantly greater cation exchange capacity than kaolinite clays, thus cation exchange is likely to have been more influential in the flood plain regolith unit than the other regolith units. This is supported by the results of selective chemical extraction analysis in which greater concentrations of readily exchangeable Ca and Mg were extracted from the carbonaceous clays and silts of the flood plain than the quartz dominated sands.

Pyrite has been identified in the quartz dominated sands and the carbonaceous clays within the sedimentary aquifer. Pyrite formation requires dissolved ferrous ion and sulfide. Analysis of groundwater from the aquifer has revealed dissolved $Fe_{(Total)}$ concentrations up to 142 mg/L. Sulfide has not been analysed for, but is indicated by comparing the values of total sulfur (recalculated as sulfate) to actual sulfate. Total sulfur (recalculated as sulfate) values are greater than the sulfate measured in some groundwaters and, together with a 'rotten egg' smell noted when purging bores, suggests the presence of hydrogen sulfide. The groundwater is depleted in SO_4^{2-} with respect to seawater Cl^{-} indicating that mineral formation is occurring. However, pyrite is not the only mineral that can cause sulfate depletion, and gypsum and alunite formation must be considered. For groundwaters with TDS less than 30 000 mg/L, gypsum will not form by chemical precipitation. Alunite formation is noted by other workers elsewhere on the Yilgarn Craton. They proposed that the deficit of K^{+} with respect of seawater Cl^{-} is the result of alunite formation. Although alunite has not been identified in the catchment, jarosite has. In the Lake Muir–Unicup catchment some sulfate is being removed by the formation of pyrite and jarosite.

8.1.3.3 WBR aquifer

Two groundwater types are found in the WBR aquifer. In the north of the catchment, the groundwater is a Na–Cl type water, whereas the closed groundwater basin the

south has a Ca–Na–Cl type water. Although huntite and siderite have been identified in the aquifer, dissolution of these minerals would normally produce a groundwater richer in aqueous Mg^{2+}. The Ca–Na–Cl type groundwater is found up hydraulic gradient from Lake Muir. Dissolution of gypsum is an unlikely source of Ca^{2+} east of Lake Muir as the groundwater is undersaturated with respect to gypsum. Additional work is needed to resolve the exact source of the aqueous Ca^{2+}.

8.1.4 Groundwater acidification risk

Groundwater with a positive Net Acidity is mostly found in the sedimentary aquifer, and to a lesser extent in the WBR aquifer. Groundwaters with pH < 5.5 tend to have a positive Net Acidity whereas, groundwaters with pH between 5.5 and 6.3 can have either a positive or negative Net Acidity. Groundwaters with a positive Net Acidity are potentially at risk of acidification should the prevailing conditions change.

The acidification process, both actual and potential, are related to oxidation of pyrite and, in the absence of pyrite, the oxidation of dissolved Fe^{2+}. While the oxidation of pyrite includes oxidation of Fe^{2+}, pyrite does not need to be present for Fe^{2+} oxidation. The pH_{FOX} suggests that pyrite is not generally present within 10 m of the surface unless associated with the peat swamps, but is common below 10 m in the sedimentary aquifer. The significant concentrations of dissolved $Fe_{(total)}$ in the groundwater and the presence of ferric oxyhydroxides on the ground surface indicate that oxidation of Fe^{2+} is occurring as groundwater is discharged. Oxidation of pyrite generally produces 4 moles of H^+, but can produce up to 16 moles of H^+ for every mole of pyrite oxidised (reaction (2.51)) (assuming Fe^{3+} is one of the oxidizing agents) whereas the oxidation of dissolved $Fe^{2+}$to ferric oxyhydroxides produces 2 protons in the form of H^+(reactions (2.49) and (2.50)). Thus these two processes consume differing amounts of alkalinity.

The groundwater potentially at greatest risk of acidification is the quartz dominated channel sand regolith unit of the sedimentary aquifer. This unit is particularly at risk where cropping out at the ground surface or exposed by engineering works such as road building and the cutting of drains. This regolith unit is extensive in the north of the Lake Muir–Unicup catchment, but is of uncertain extent in the south.

8.2 RECOMMENDATIONS

This study has increased understanding of the geology and groundwater evolution in the Lake Muir–Unicup Natural Diversity Recovery Catchment, while elucidating where additional work is required to address gaps in understanding. Recommended areas for further work have been noted in the individual chapters of the thesis, and are summarised below.

8.2.1 Geology

- Determine the nature and extent of the carbonate minerals
- Determine the presence or absence of the postulated 3rd palaeovalley system in the south of the catchment
- Map the sediments in greater detail and refine the extent and thickness of the sediments
- Establish the exit point of the Eocene palaeoriver

8.2.2 Hydrogeology

- Resolve the groundwater boundaries in the north east of the catchment near bore MU37D and in the west near bore MU49
- Determine hydraulic conductivity values for the aquifers
- Develop a robust water balance for the study area
- Refine the groundwater recharge rate in the north and south of the catchment
- Determine the evaporation rate and groundwater losses from Lake Muir

8.2.3 Hydrogeochemistry

- Investigated the increased dissolved Ca in the groundwater of the WBR aquifer in the south of the catchment
- Refine the models for groundwater evolution by establishing the roles of individual processes with greater confidence
- Ascertain the extent to which agricultural land use increases the risk of groundwater acidification

9 References

Ahern, C.R., Sullivan, L.A. and McElnea, A.E., 2003. Laboratory methods guidelines 2003 — Acid sulfate soils, Department of Natural Resources and Mines, Indooroopilly, Queensland, Australia.

Alkalali, A. and Rostron, B., 2003. Basin-scale analysis of variable-density groundwater flow: Nisku Aquifer, Western Canadian Sedimentary Basin. *Journal of Geochemical Exploration* Proceedings of Geofluids IV, 78–79: 313–316.

Allison, G.B. and Barnes, C.J., 1985. Estimation of evaporation from the normally "dry" Lake Frome in South Australia. *Journal of Hydrology*, 78(3–4): 229–242.

Alpers, C.N., Rye, R.O., Nordstrom, D.K., White, L.D. and King, B.-S., 1992. Chemical, crystallographic and stable isotopic properties of alunite and jarosite from acid — Hypersaline Australian lakes. *Chemical Geology*, 96(1–2): 203–226.

American Public Health Association, 1999. Standard methods for the examination of water and wastewater. American Public Health Association, the American Water Works Association and the Water Pollution.

Anand, R.R. and Paine, M., 2002. Regolith geology of the Yilgarn Craton, Western Australia: implications for exploration. *Australian Journal of Earth Sciences*, 49: 3–162.

Anand, R.R., Smith, R.E., Innes, J., Churchwood, H.M., Perdrix, J.L. and Grunsky, E.C., 1989. Laterite types and associated ferruginous materials, Yilgarn Block WA: terminology classification and atlas. 60R, Commonwealth Science Industry Research Organisation Australia Division of Exploration Geoscience Report.

Andreae, M.O. and Merlet, P., 2001. Emission of trace gases and aerosols from biomass burning. Global Biogeochemical Cycles, 15: 955–966.

Appelo, C.A.J. and Postma, D., 2005. Geochemistry, groundwater and pollution. A.A. Balkema Publishers Leiden/London/New York/Philadelphia/Singapore, 649p.

Australian Water Resources Council, 1988. Guidelines for the preparation of Australian hydrogeological maps. no. 13, Department of Primary Industries and Energy, Australian Water Resources Council.

Banks, D. and Frengstad, B., 2006. Evolution of groundwater chemical composition by plagioclase hydrolysis in Norwegian anorthosites. *Geochimica et Cosmochimica Acta*, 70: 1337–1355.

Bazuhair, A.S. and Wood, W.W., 1996. Chloride mass-balance method for estimating ground water recharge in arid areas: examples from western Saudi Arabia. *Journal of Hydrology*, 186(1–4): 153–159.

Beard, J.S., 1981. Vegetation survey of Western Australia, Swan 1:1 000 000 Vegetation Series, Explanatory notes to Sheet 7, The vegetation of the Swan Area. University of Western Australia Press.

Beard, J.S., 1999. Evolution of the river systems of the south-west drainage division, Western Australia. *Journal of the Royal Society of Western Australia*, 82: 147–164.

Berry, J.S., 1987. The history, landscape and heritage of the Warren District, on behalf of the National Trust of Australia (Western Australia) for the Shire of Manjimup, 83p.

BHP Minerals Pty. Ltd, 2000. Exploration Licences E70/2009, 2010, 2014, 2090, 2111, 2120, 2121 and 2205 Manjimup Project — Albany Fraser Orogen. Geological Survey of Western Australia, CR9807.

Bradshaw, B.E., 2006. The Bremer Sub-basin — a new deepwater petroleum opportunity. Issue 81, Geoscience Australia.

Bradshaw, B.E., Rollet, N., Totterdell, J.M. and Borissova, I., 2003. A revised structural framework for frontier basins on the southern and southwestern Australian continental margin. Geoscience Australia Record 2003/03.

Brown, J.B., 1971. Jarosite-goethite stabilities at 25 °C, 1 ATM. *Mineralium Deposita*, 6(3): 245–252.

Brown, T.L. and LeMay, H.E., 1977. Chemistry: The central science. Prentice Hall International Inc., Englewood Cliffs, New Jersey, 893p.

Butler, I.B., Böttcher, M.E., Rickard, D. and Oldroyd, A., 2004. Sulfur isotope partitioning during experimental formation of pyrite via the polysulfide and hydrogen sulfide pathways: implications for the interpretation of sedimentary and hydrothermal pyrite isotope records. *Earth and Planetary Science Letters*, 228(3-4): 495–509.

Canfield, D.E., Thamdrup, B. and Fleischer, S., 1998. Isotope fractionation and sulfur metabolism by pure and enrichment cultures of elemental sulfur-disproportionating bacteria. *Limnology and Oceanography*, 43(2): 253–264.

Chakravartula, P.N. and Street, G., 2000. Hydrogeological interpretation of airborne geophysical data Lake Muir–Unicup catchment, Western Australia, Agraria Limited, Western Australia (unpublished).

Chebotarev, I.I., 1955. Metamorphism of natural waters in the crust of weathering. *Geochimica et Cosmochimica Acta*, 8: 22–48, 137–170, 198–212.

Christensen, T.H., Bjerg, P.L., Banwart, S.A., Jakobsen, R., Heron, G. and Albrechtsen, H.-J., 2000. Characterization of redox conditions in groundwater contaminant plumes. *Journal of Contaminant Hydrology*, 45: 165–241.

Chu, C., Lin, C., Wu, Y., Lu, W. and Long, J., 2006. Organic matter increases jarosite dissolution in acid sulfate soils under inundation conditions. *Australian Journal of Soil Research*, 44: 11–16.

Clarke, C.J., George, R.J., Bennett, D.L. and Bell, R.W., 2000. Geologically relate variations in saturated hydraulic conductivity in the regolith of the western wheatbelt of Western Australia and its implications for the development of dryland salinity. *Australian Journal of Soil Research*, 38: 555–568.

Clarke, J.D.A., 1993. Stratigraphy of the Lefroy and Cowan palaeodrainages, Western Australia. *Journal of the Royal Society of Western Australia*, 76: 12–23.

Clarke, J.D.A., 1994. Evolution of the Lefroy and Cowan palaeodrainage channels, Western Australia. *Journal of Earth Sciences*, 41: 55–68.

Clarke, J.D.A., Bone, Y. and James, N.P., 1996. Cool-water carbonates in an Eocene palaeoestuary, Norseman Formation, Western Australia. *Sedimentary Geology*, 101(3–4): 213–226.

Clarke, J.D.A., Gammon, P.R., Hou, B. and Gallagher, S.J., 2003. Middle to upper Eocene stratigraphic nomenclature and deposition in the Eucla Basin. *Australian Journal of Earth Sciences*, 50(2): 231–248.

Climate Note 6/05, 15 August 2005. How extreme south-west rainfalls have changed. *In:* John Ruprecht, Yun Li, Eddy Campbell and Pandora Hope (Editors). Indian Ocean Climate Initiative, 2p.

Cockbain, A.E., 1968. The stratigraphy of the Plantagenet Group, Western Australia, Geological Survey of Western Australia.

Commander, D.P., Kern, A.M. and Smith, R.A., 1992. Hydrogeology of the Tertiary palaeochannels in the Kalgoorlie region. Record 1991/10, Geological Survey of Western Australia.

Cope, R.N., 1975. Tertiary epeirogeny in the southern part of Western Australia. 1974, Western Australia Geological Survey.

Commonwealth Science Industry Research Organisation Australia and Australian Bureau of Meteorology, 2007. Climate change in Australia, Commonwealth Science Industry Research Organisation Australia.

Dampier Mining Company Limited, 1981. Coal exploration in Lake Muir area. Geological Survey of Western Australia Microfiche Record C 68/2236.

Davies, P.B., 1987. Modeling areal, variable density, groundwater flow using equivalent freshwater head–analysis of potentially significant errors. , Proceedings of the NWWA/IGWMC Conference — Solving Groundwater Problems with Models. 10-12. National Water Well Association, Denver, Colorado, p. 888–903.

Davis, S.N., Whittemore, D.O. and Fabryka-Martin, J., 1998. Uses of chloride/bromide ratios in studies of potable water. *Ground Water*, 36(2): 338–350.

de Broekert, P. and Sandiford, M., 2005. Buried inset-valleys in the Eastern Yilgarn Craton, Western Australia: Geomorphology, Age, and Allogenic Control. *Journal of Geology*, 113(4): 471–493.

De Silva, J., 2000. Pemberton — Irwin Inlet 1:250 000 sheet, Western Australia. Sheet SI 50-10 and part of SI 50-14, Western Australia Water and Rivers Commission.

De Silva, J., 2004. Hydrogeology of the Pemberton — Irwin Inlet 1:250 000 sheet, Western Australia. Sheet SI 50–10 and part of SI 50–14. Report HM 8, Western Australia Department of Environment.

Deer, W.A., Howie, R.A. and Zussman, J., 1966. An introduction to the rock forming minerals. Longman, Harlow, Essex, England.

Deer, W.A., Howie, R.A. and Zussman, J., 1992. An introduction to the rock forming minerals. (2nd edition) Longman, Harlow, Essex, England.

Department of Environment and Conservation, in prep. The Lake Muir–Unicup Natural Diversity Recovery Catchment — Management Plan, Western Australia Department of Environment and Conservation.

Dolla, A., Fournier, M. and Dermoun, Z., 2006. Oxygen defense in sulfate-reducing bacteria. *Journal of Biotechnology*, 126(1): 87–100.

Drever, J.I., 1997. The Geochemistry of Natural Waters. Prentice Hall, Upper Saddle River, New Jersey, 436p.

Edwards, K.B. and Turney, D.C., 1997. The principal origin of lake acidity: Underground mines, minespoil, or buried gob? *International Journal of Mining, Reclamation and Environment*, 11: 139–144.

Eggleton, R.A. (Editor), 2001. The Regolith Glossary — Surficial geology, soils and landscapes. Cooperative Research Centre for Landscape Evolution & Mineral Exploration, Canberra, 144p.

Ehrlich, H.L., 2002. Geomicrobiology. Marcel Dekker, Inc., New York, 768 pp.

Eugster, H.P. and Hardie, L.A., 1978. Saline lakes. *In:* A. Lerman (Editor), Lakes — Chemistry, geology, physics. Springer-Verlag, New York, p. 237–292.

Eugster, H.P. and Jones, B.F., 1979. Behavior of major solutes during closed-basin brine evolution. *American Journal of Science*, 279: 609–631.

Exon, N.F., Hill, P.J., Mitchell, C. and Post, A., 2005. Nature and origin of the submarine Albany canyons off southwest Australia. *Australian Journal of Earth Sciences*, 52: 101–115.

Faure, G., 1998. Principles and applications of geochemistry. Prentice Hall, Upper Saddle River, New Jersey.

Ferdowsian, R., McCarron, C. and Majidi, R., 2001. HARTT manual — Hydrograph analysis: rainfall and time trends. Agriculture Western Australia (unpublished).

Field Geologists' Manual, 1989. Field geologists' manual. Monograph Series No. 9. The Australasian Institute of Mining and Metallurgy, Parkville, 382p.

Fitzpatrick, R.W., Merry, R.H., Cox, J.W., Rengasamy, P. and Davies, P.J., 2003. Assessment of physico-chemical changes in dryland saline soils when drained or disturbed for developing management options, Commonwealth Science Industry Research Organisation Australia Land and Water.

Fitzpatrick, R. and Shand, P.,(eds), 2008. Inland Acid Sulfate Soil Systems Across Australia. CRC LEME Open File Report No. 249. CRC LEME, Perth.

Fossing, H. and Jorgensen, B.B., 1990. Oxidation and reduction of radiolabeled inorganic sulfur compounds in an estuarine sediment, Kysing Fjord, Denmark. *Geochimica et Cosmochimica Acta*, 54: 2731–2742.

Freeze, R.A. and Cherry, J.A., 1979. Groundwater. Prentice Hall, Englewood Cliffs, New Jersey, 604p.

Gammon, P.R. and James, N.P., 2001. Palaeogeographical influence on late Eocene biosiliceous sponge-rich sedimentation, southern Western Australia. *Sedimentology*, 48(3): 559–584.

Gammon, P.R., James, N.P., Clarke, J.D.A. and Bone, Y., 2000a. Sedimentology and lithostratigraphy of the upper Eocene sponge-rich sediments, southern Western Australia. *Australian Journal of Earth Sciences*, 47: 1087–1103.

Gammon, P.R., James, N.P. and Pisera, A., 2000b. Eocene spiculites and spongolites in southwestern Australia: Not deep, not polar, but shallow and warm. *Geology*, 28: 855–858.

Garnett, S.T. and Crowley, G.M., 2000. The Action Plan for Australian Birds 2000, Natural Heritage Trust, Environment Australia, Birds Australia.

Garrels, R.M. and Mackenzie, F.T., 1967. Origin of the chemical composition of some springs and lakes, *In* Equilibrium Concepts in Natural Water Systems. American Chemistry Society Advances in Chemistry, pp. 222–242.

Geological Survey of Western Australia (Editor), 1990. Geology and mineral resources of Western Australia. Memoir 3. Western Australia Geological Survey, 827p.

George, R.J., 1992. Hydraulic properties of groundwater systems in the saprolite and sediments of the wheatbelt, Western Australia. *Journal of Hydrology*, 130(1-4): 251–278.

Gibson, N. and Keighery, G.J., 1999. Assessment of the nature conservation values of the Byenup-Muir wetland system, Report for Environment Australia prepared by Western Australia Department of Conservation and Land Management (unpublished).

Government of Western Australia, 1996a. Salinity: a situation statement for Western Australia, prepared by Agriculture Western Australia, Department of Conservation and Land Management, Department of Environmental Protection, Western Australia Water and Rivers Commission.

Government of Western Australia, 1996b. Western Australia: salinity action plan, prepared by Agriculture Western Australia, Department of Conservation and Land Management, Department of Environmental Protection, Western Australia Water and Rivers Commission.

Government of Western Australia, 2000. Salinity: a guide for land managers, prepared by Western Australia State Salinity Council.

Gradstein, F.M., Ogg, J.G. and Smith, A.G., 2004. A geologic time scale 2004. Cambridge University Press, 589p.

Gray, D.J., 1999. Selective and partial extraction analyses of transported overburden for gold exploration in the Yilgarn Craton, Western Australia. *Journal of Geochemical Exploration*, 67: 51–66.

Gray, D.J., 2001. Hydrogeochemistry in the Yilgarn Craton. *Geochemistry: Exploration, Environment, Analysis*, 1: 253–264.

Hardie, L.A. and Eugster, H.P., 1970. The evolution of closed-basin brines. *Mineral Society American Special Paper*, 3: 273–290.

Hedin, R.S., 2006. The use of measured and calculated acidity values to improve the quality of mine drainage datasets. *Mine Water and the Environment*, 25: 146–152.

Hedin, R.S., Nairn, R.W. and Kleinmann, L.P., 1994. Passive treatment of coal mine drainage. IC 9389, United States Department of the Interior.

Hem, J.D., 1970. Study and interpretation of the chemical characteristics of natural water. Water–supply paper 1473, Geological Survey.

Hengl, T., 2006. Finding the right pixel size. *Computers & Geosciences*, 32: 1283–1298.

Hey, K.M., Ahern, C.R. and Watling, K.M., 2000. Using chemical field tests to identify acid sulfate soils likelihood, Department of Natural Resources, Indooroopilly, Queensland.

Hingston, F.J. and Gailitis, V., 1976. The geographic variation of salt precipitated over Western Australia. *Australian Journal of Soil Research*, 14: 319–335.

Hjulstrom, F., 1939. Transportation of detritus by moving water. *In:* P.D. Trask (Editor), Recent Marine Sediments, A Symposium, Society of Economic Paleontologists and Mineralogists, Special Publication 4, p. 5–31.

Hocking, R.M., 1990. Bremer Basin. *In*: Geological Survey of Western Australia (Editor), Geology and Mineral Resources of Western Australia. Geological Survey of Western Australia, Memoir 3, Perth, p. 561–563.

Holdgate, G.R. and Clarke, J.D.A., 2000. A review of Tertiary brown coal deposits in Australia — Their depositional factors and eustatic correlations. *America Association of Petroleum and Geology Bulletin*, 84(8): 1129–1151.

Howarth, R.W. and Teal, J.M., 1979. Sulfate reduction in a New England salt Marsh. *Limnology and Oceanography*, 24: 999–1013.

Jarvis, I. and Jarvis, K.E., 1992. Plasma spectrometry in the earth sciences: techniques, applications and future trends. *Chemical Geology*, 95(1-2): 1–33.

Jarvis, K.E., Gray, A.L. and Houk, R.S., 1992. Handbook of inductively coupled plasma mass spectrometry. Blackie Academic & Professional, London, 380p.

Johnson, S.L., Commander, D.P. and O'Boy, C.A., 1999. Groundwater resources of the northern goldfields, Western Australia. Report HG 2, Western Australia Water and Rivers Commission.

Johnston, C.D., 1987. Distribution of environmental chloride in relation to subsurface hydrology. *Journal of Hydrology*, 94(1–2): 67–88.

Johnston, C.D., Williamson, D.R. and Trotter, C.L., 1982. Ionic composition and electrical conductivity relationships in soil water extracts from South-Western Australia. Commonwealth Science Industry Research Organisation Australia Land Resources Management Technical Paper, 12: 1–10.

Jorgensen, B.B., 1990a. A thiosulfate shunt in the sulfur cycle of marine sediments. *Science*, 249: 152–154.

Jorgensen, B.B., 1990b. The sulfur cycle of freshwater sediments: Role of thiosulfate. *Limnology and Oceanography*, 35(6): 1329–1342.

Jorgensen, B.B. and Bak, F., 1991. Pathways and Microbiology of Thiosulfate Transformations and Sulfate Reduction in a Marine Sediment (Kattegat, Denmark). *Applied and Environmental Microbiology*, 57(3): 847–855.

Kappler, A. and Straub, K.L., 2005. Geomicrobiological cycling of iron. *Reviews in Mineralogy & Geochemistry*, 59: 85–108.

Kennedy, V.C., Zellweger, G.W. and Jones, B.F., 1974. Filter pore-size effects on the analysis of Al, Fe, Mn, and Ti in water. *Water Resources Research*, 10(4): 785–790.

Kirby, C.S. and Cravotta III, C.A., 2005a. Net alkalinity and net acidity 1: Theoretical considerations. *Applied Geochemistry*, 20: 1920–1940.

Kirby, C.S. and Cravotta III, C.A., 2005b. Net alkalinity and net acidity 2: Practical considerations. *Applied Geochemistry*, 20: 1941–1964.

Kjeldsen, K.U., Joulian, C. and Ingvorsen, K., 2005. Effects of oxygen on respiratory activities of *Desulfovibrio desulfuricans* strain DvO1 isolated from activated sludge. FEMS Microbiology Ecology 53: 275–284.

Kohn, B.P., Gleadow, A.J.W., Brown, R.W., Gallagher, K., O'Sullivan, P.B. and Foster, D.A., 2002. Shaping the Australian crust over the last 300 million years: insights from fission track thermotectonic imaging and denudation studies of key terranes. *Australian Journal of Earth Sciences*, 49: 697–717.

Koryak, M., Stafford, L.J. and Reilly, R.J., 2004. Declining intensity of acid mine drainage in the Northern Appalachian bituminous coal fields: major allegheny river tributaries. *Journal of the American Water Resources Association*, 40: 677–689.

Langmuir, D., 1997. Aqueous environmental geochemistry. Prentice Hall, Upper Saddle River New Jersey, 600p.

Ledin, M. and Pedersen, K., 1996. The environmental impact of mine wastes — Roles of microorganisms and their significance in treatment of mine wastes. *Earth-Science Reviews*, 41(1–2): 67–108.

Li, Q., James, N.P. and McGowran, B., 2003. Middle and late Eocene Great Australian Bight lithobiostratigraphy and stepwise evolution of the southern Australian continental margin. *Australian Journal of Earth Sciences*, 50(1): 113–128.

Lindberg, R.D. and Runnells, D.D., 1984. Ground water redox reactions: An analysis of equilibrium state applied to *Eh* measurements and geochemical modeling. *Science*, 225: 925–927.

Liu, J.-y., Xiu, X.-x. and Cai, P., 2009. Study of formation of jarosite mediated by *Thiobacillus ferrooxidans* in 9K medium. *Procedia Earth and Planetary Science*, 1(1): 706–712.

Long, D.T., Fegan, N.E., Lyons, W.B., Hines, M.E., Macumber, P.G. and Giblin, A.M., 1992. Geochemistry of acid brines: Lake Tyrrell, Victoria, Australia. *Chemical Geology*, 96(1–2): 33–52.

Lopez-Buendia, A.M., Whateley, M.K.G., Bastida, J. and Urquiola, M.M., 2007. Origins of mineral matter in peat marsh and peat bog deposits, Spain. *International Journal of Coal Geology*, 71(2–3): 246–262.

Lusczynski, N.J., 1961. Head and flow of ground water of variable density. *Journal of Geophysical Research*, 66(12): 4247–4256.

Macphail, M.K., 1996. Palynostratigraphy of the Murray Basin, inland southeastern Australia. Australian Geological Survey Organisation Record 1996/57, Australian Geological Survey Organisation.

Macumber, P.G., 1992. Hydrological processes in the Tyrrell Basin, southeastern Australia. *Chemical Geology*, 96(1–2): 1–18.

Mandernack, K.W., Lynch, L., Krouse, H.R. and Morgan, M.D., 2000. Sulfur cycling in wetland peat of the New Jersey Pinelands and its effect on stream water chemistry. *Geochimica et Cosmochimica Acta*, 64(23): 3949–3964.

Mann, A.W., 1983. Hydrogeochemistry and weathering on the Yilgarn Block, Western Australia: ferrolysis and heavy metals in continental brines. *Geochimica et Cosmochimica Acta*, 47: 181–190.

Mano, S. and Andreae, O., 1994. Emission of methyl bromide from biomass burning. Science, 263: 1255–1257.

McArthur, J.M., Turner, J.V., Lyons, W.B., Osborn, A.O. and Thirlwall, M.F., 1991. Hydrochemistry on the Yilgarn Block, Western Australia: ferrolysis and mineralisation in acidic brines. *Geochimica et Cosmochimica Acta*, 55: 1273–1288.

McArthur, J.M., Turner, J.V., Lyons, W.B. and Thirlwall, M.F., 1989. Salt sources and water-rock interactions on the Yilgarn Block, Australia: isotopic and major element tracers. *Applied Geochemistry*, 4: 79–92.

McCutcheon, S.C., Martin, J.L. and Barnwell, T.O.J., 1992. Water Quality. *In*: D.R. Maidment (Editor), Handbook of Hydrology. McGraw-Hill, New York, p. 11.11–11.73.

McGill, W.B. and Cole, C.V., 1981. Comparative aspects of cycling of organic C, N, S and P through soil organic matter. *Geoderma*, 26(4): 267–286.

Merry, R.H., Spouncer, L.R., Fitzpatrick, R.W., Davies, P.J. and Bruce, D.A., 2002. Regional prediction of soil profile acidity and alkalinity. *In*: T.R. McVicar, Li Rui, J. Walker, R.W. Fitzpatrick and L. Changming (Editors), Regional water and soil assessment for managing sustainable agriculture in China and Australia, Australian Centre for International Agricultural Research Monograph No. 84, p. 155–164.

Milne, L.A., 2003. Palynological analysis of three samples from borehole 14. ME/BP 61, Report for the Western Australia Water and Rivers Commission (unpublished).

Morel, F.M. and Hering, J.G., 1993. Principles and application of aquatic chemistry. John Wiley & Son, Inc., New York.

Muller, R.D., Giana, C. and Clark, S., 2000. Seafloor spreading around Australia. *In*: J.J. Veevers (Editor), Billion-year earth history of Australia and neighbours in Gondwanaland. Gemoc Press, North Ryde, N.S.W.

Munsell Color, 2000. Munsell soil color charts. GretagMacbeth.

Myers, J.S., 1990. Albany–Fraser Orogen. *In:* Geological Survey of Western Australia (Editor), Geology and Mineral Resources of Western Australia. Geological Survey of Western Australia, Memoir 3, Perth, p. 255–264.

Myers, J.S., Shaw, R.D. and Tyler, I.M., 1996. Tectonic evolution of Proterozoic Australia. *Tectonics*, 15: 1431–1446.

Nahon, D. and Tardy, Y., 1992. The ferruginous laterites. *In:* C.R.M. Butt and H. Zeegers (Editors), Regolith exploration geochemistry in the tropical and subtropical terrains. Handbook of Exploration Geochemistry. Elsevier, Amsterdam, p. 41–55.

Neuendorf, K.K.E., Mehl, J.P.J. and Jackson, J.A., 2005. Glossary of geology. American Geological Institute, Alexandria, Virginia, 779p.

New, C., Hearn, R.W. and Smith, M.G., in prep. The Lake Muir–Unicup Natural Diversity Catchment — Bore completion report, Western Australia Department of Environment and Conservation.

Nicholls, N., Chambers, L., Haylock, M., Frederiksen, C., Jones, D. and Drosdowsky, W., no date. Climate variability and predictability for south west Western Australia. Bureau of Meteorology Research Centre.

Norvick, M.S. and Smith, M.A., 2001. Mapping the plate tectonic reconstruction of southern and southeastern Australia and implications for petroleum systems. *APPEA Journal*, 16: 15–34.

Nulsen, R.A., 1981. Critical depth to saline groundwater in non-irrigated situations. *Australian Journal of Soil Research*, 19: 83–86.

Oberlander, P.L., 1989. Fluid Density and Gravitational Variations in Deep Boreholes and Their Effect on Fluid Potential. *Ground Water*, 27(3): 341–350.

Panasiewicz, R., De Silva, J. and McGann, M.P., 1997. Pemberton and Blackwood Drilling Programs — Completion Report. HR86, Western Australia Water and Rivers Commission, Perth (unpublished).

Parkhurst, D.L. and Appelo, C.A.J., 1999. User's guide to PHREEQC (version 2) — a computer program for speciation, batch-reaction, one-dimensional transport, and inverse geochemical calculations. Water-Resources Investigations Report 99–4259, U.S Department of the Interior, U.S. Geological Survey.

Peck, A.J. and Williamson, D.R., 1987. Effects of forest clearing on groundwater. *Journal of Hydrology*, 94(1–2): 47–65.

Quilty, P.G., 1994. The background: 144 million years of Australian palaeoclimate and palaeogeography. *In*: R.S. Hill (Editor), History of the Australian vegetation: Cretaceous to Recent. Cambridge University Press, Cambridge, p. 14–43.

Reid, A.B., Allsop, J.M., Granser, H., Millett, A.J. and Somerton, I.W., 1990. Magnetic interpretation in three dimensions using Euler deconvolution. *Geophysics*, 55: 80–91.

Reineck, H.-E. and Singh, I.B., 1980. Depositional sedimentary environments. Springer-Verlag, Berlin, 551p.

Reynolds, D.A. and Marimuthu, S., 2007. Deuterium composition and flow path analysis as additional calibration targets to calibrate groundwater flow simulation in a coastal wetlands system. *Hydrogeology Journal*, 15: 515–535.

Rickard, D., 1995. Kinetics of FeS precipitation: Part 1. Competing reaction mechanisms. *Geochimica et Cosmochimica Acta*, 59(21): 4367–4379.

Rickard, D., 1997. Kinetics of pyrite formation by the H2S oxidation of iron (II) monosulfide in aqueous solutions between 25 and 125 ºC: The rate equation. *Geochimica et Cosmochimica Acta*, 61(1): 115–134.

Rickard, D. and Morse, J., 2005. Acid volatile sulfide: Authors' closing comments. *Marine Chemistry*, 97(3–4): 213–215.

Ritter, D.F., Kochel, R.C. and Miller, J.R., 1995. Process geomorphology. Mc Graw Hill, Boston, 546p.

Roden, E.E. and Urrutia, M.M., 2002. Influence of biogenic Fe(II) on bacterial crystalline Fe(III) oxide reduction. *Geomicrobiology Journal*, 19(2): 209–251.

Rosicky, M.A., Sullivan, L.A. and Slavich, P.G., 2002. Acid sulfate soil scalds: How they occur and best management practices for their revegetation, NSW Agriculture and Acid Sulfate Soil Management Advisory Committee.

Scheffer, F. and Schachtschabel, P., 2002. Lehrbuch der Bodenkunde. Elsevier, Amsterdam, 607p.

Schumm, S.A., 1977. The fluvial system. John Wiley & Son, New York, 338p.

Shand, P. and Degens, B., 2008. Avon Catchment acidic groundwater — geochemical risk assessment. CRC LEME open file report 191, Cooperative Research Centre for Landscape Environments and Mineral Exploration.

Shand, P., Degens, B. and Rogers, S., 2008. The geochemistry of acid-saline waters and drainage sediments in the Avon Catchment, Western Australian Wheatbelt Explore, 140: 1–11.

Smith, M.G., Dixon, R.N.M., Boniecka, L.H., Berti, L.H., Sparks, T., Bari, M.A. and Platt, J., 2005. Salinity situation statement: Warren River. WRT 32, Western Australia Department of Environment.

Smith, M.G., Hearn, R.W. and Wheeler, I.B., 2004. Groundwater acidification in the Lake Muir–Unicup Recovery Catchment. *In*: A. Waterhouse (Editor), 1st National Salinity Engineering Conference, Perth Western Australia.

Smith, R.A., 1997. Hydrogeology of the Mount Barker–Albany 1:250 000 sheet, Western Australia. Sheet SI 50-11 and SI 50-14. Report HM 1, Western Australia Water and Rivers Commission.

Smith, R.A., 2003. Hydrogeology of the Muir–Unicup catchments. Report No. SLUI 22, Western Australia Water and Rivers Commission.

Spencer, R.J., 2000. Sulfate minerals in evaporite deposits. *In:* C.N. Alpers, J.L. Jambor and D.K. Nordstrom (Editors), Sulfate Minerals: Crystallography, Geochemistry, and Environmental Significance. Mineralogical Society of America, Washington, DC, p. 173–192.

Stoffregen, R.E., Alpers, C.N. and Jambor, J.L., 2000. Alunite-jarosite crystallography, thermodynamics, and geochronology. *In*: C.N. Alpers, J.L. Jambor and D.K. Nordstrom (Editors), Sulfate minerals: crystallography, geochemistry and environmental significance. Reviews in Mineralogy and

Geochemistry. Mineralogical Society of America, Washington DC, p. 453–479.

Storey, A.W., 1998. Assessment of the nature conservation values of the Byenup–Muir peat swamp system, southwestern Australia: physico-chemistry, aquatic macroinvertebrates and fishes. Report for Western Australia Conservation and Land Management by UWA Wetland Research and Management Group (unpublished).

Stover, L.E. and Partridge, A.D., 1982. Eocene spore-pollen from the Werillup Formation, Western Australia. *Palynology*, 6: 69–96.

Stuart-Street, A. and Scholz, G., in prep. Tonebridge — Frankland land resource survey, Western Australia Department of Agriculture and Food.

Stumm, W. and Morgan, J.J., 1996. Aquatic chemistry: Chemical equilibria and rates in natural waters. John Wiley & Sons, Inc., New York, 1022p.

Syvitski, J.P.M., Kettner, A.J., Correggiari, A. and Nelson, B.W., 2005. Distributary channels and their impact on sediment dispersal. *Marine Geology*, 222–223: 75–94.

Tapley, I., Pirlo, M.C. and Gray, D.J., 2004. Spectral mineralogy, soil and water chemistry associated with the Narembeen drain network and Seagroatt Nature Reserve. 1235R, Report for Western Australia Department of Conservation and Land Management by Commonwealth Science Industry Research Organisation Australia Exploration and Mining.

Taylor, G. and Shirtliff, G., 2003. Weathering: cyclical or continuous? An Australian perspective*, Australian Journal of Earth Sciences. pp. 9-17.

Thompson, D.T., 1982. EULDPH: A new technique for making computer-assisted depth estimates from magnetic data. *Geophysics*, 47: 31–37.

Tucket, M., 1982. The field description of sedimentary rocks. Geological Society of London Handbook. Open University Press and Halsted Press, 112p.

Tyler, S.W., Kranz, S., Parlange, M.B., Albertson, J., Katul, G.G., Cochran, G.F., Lyles, B.A. and Holder, G., 1997. Estimation of groundwater evaporation and salt flux from Owens Lake, California, USA. *Journal of Hydrology*, 200(1–4): 110–135.

van Gool, D., Tille, P. and Moore, G., 2005. Land evaluation standards for land resource mapping. Resource Management Technical Report 298, 3th edition, Agriculture Western Australia.

Veevers, J.J., 2000. Change of tectono-stratigraphic regime in the Australian plate during the 99 Ma (mid-Cretaceous) and 43 Ma (mid-Eocene) swerves of the Pacific. *Geology*, 28: 47–50.

Welch, S.A., Christy, A.G., Kirste, D., Beavis, S.G. and Beavis, F., 2007. Jarosite dissolution I — Trace cation flux in acid sulfate soils. *Chemical Geology*, 245(3-4): 183–197.

Welch, S.A., Kirste, D., Christy, A.G., Beavis, F.R. and Beavis, S.G., 2008. Jarosite dissolution II--Reaction kinetics, stoichiometry and acid flux. *Chemical Geology*, 254(1-2): 73–86.

Wieder, R.K. and Lang, G.E., 1988. Cycling of inorganic and organic sulfur in peat from Big Run Bog, West Virginia. *Biogeochemistry*, 5(2): 221–242.

Wilde, S.A. and Walker, I.W., 1984. Pemberton – Irwin Inlet Western Australia, 1:250 000 Geological Series — Explanatory notes, Geological Survey of Western Australia.

Wood, W.W. and Sanford, W.E., 1995. Chemical and isotopic method for quantifying ground-water recharge in a regional, semiarid environment. *Ground Water*, 33: 458–486.

Zaccone, C., Cocozza, C., Shotyk, W. and Miano, T.M., 2008. Humic acids role in Br accumulation along two ombrotrophic peat bog profiles. *Geoderma*, 146: 26–31.

Zachara, J.M., Kukkadapu, R.K., Fredrickson, J.K., Gorby, Y.A. and Smith, S.C., 2002. Biomineralization of poorly crystalline Fe(III) oxides by dissimilatory metal reducing bacteria (DMRB). *Geomicrobiology Journal*, 19(2): 179–207.

10 Appendix

APPENDIX 1 ACRONYMS AND NOTATION

Chapter 1

BOM	Bureau of Meteorology
DEC	Department of Environment and Conservation

Chapter 2

β_I	activity of each exchangeable ion
ε_i	number of equivalents/mole of the i^{th} species
a	activity
C	moles/L of acid
C_B	moles/L of strong base
CEC	cation exchange capacity
EJH model	brine evolution model
f	reference condition
IAP	ion activity product
K	mass action constant
K_H	Henry's constant for liquid–gas equilibrium
m	molar concentrations
P	pressure
P_{CO2}	partial pressure CO_2
T	temperature (°C)
TIC	total inorganic carbon
X	soil exchanger

Chapter 3

AHD	Australian height datum
AMRR	accumulation monthly residual rainfall
CSIRO	Commonwealth Science Investigation and Research Organisation
Hwy.	Highway
i	month
j^{th}	month of year
M	rainfall
t	number of months since records started

Chapter 4

$\bar{x}$	mean
σ	standard deviation
A	bore suffix (drilled in 2006)
AAS	Atomic Absorption Spectrometry
ASS	acid sulfate soils
CI	confidence interval
D	bore suffix ie MU63D (bore drilled to basement)
EMU	bore prefix (Department of Conservation and Environment)

I	bore suffix (intermediate bore)
I	ionic strength
ICP–AES	Inductively Coupled Plasma--Atomic Emission Spectrometry
ICP–MS	Inductively Coupled Plasma--Mass Spectrometry
M	ion
MU	bore prefix (Department of Conservation and Environment)
n	number of samples
pH_F	field pH
pH_{FOX}	oxidised field pH
PM	bore prefix (Department of Water)
RSD	relative standard deviation
S	bore suffix (shallow bore)
SEM – EDAX	Scanning Electron Microscopy–energy dispersive x-ray microanalysis
t	dependent on degrees of freedom and degree of confidence
x	value of sample measurement
XRD	X-Ray Diffraction

Chapter 5

A	area in m^2
B	background level of the observed field
M	observed field at location (x, y, z)
N	degree of homogeneity or the interpreted structural index
N	number of sample points
p	grid resolution in m

Chapter 6

β_I	activity of exchangeable ion
ρ_o	density of pure water (kg/m^3) as a function of temperature
ρ	fluid density (kg/m^3)
ρ_a	average density
ρ_f	reference density which in this study is the fresh-water density
ρ_g	density of groundwater (kg/m^3)
ρ_p	density of the water at the screens
μ	fluid viscosity
a	cross-sectional area
A	coefficient (in this study 1)
a_i	empirical coefficients
b_i	empirical coefficients
BGL	below ground level
CEC	cation exchange capacities
Cl_{gw}	chloride concentration in the groundwater
Cl_{wap}	weight-average chloride concentration in precipitation
d_{10}	grain-size diameter
DFR	driving force ratio
E	elevation of the base of the aquifer
g	acceleration of gravity (m/s^2)
h	hydraulic head (m)
h_e	environmental pressure head

h_{eD}	deep bore environmental pressure head
h_{eS}	shallow bore environmental pressure head
h_f	fresh-water pressure head
h_p	pressure head (m)
i	hydraulic gradient
K	Hydraulic conductivity
k	intrinsic permeability
K	solubility product, mass action constant
P	average annual precipitation
p	fluid pressure (N/m^2)
q	recharge flux
Q	flow rate
R_T	ratio of electrical conductivity to the conductivity of seawater at 35 g/kg (~50 mS/cm)
S	salinity (g/kg)
SI	saturation index, log(*IAP/K*)
T	temperature (°C)
TDS	total dissolved solids (mg/L)
WBR aquifer	fractured and-or weathered basement rock aquifer
z	elevation above a reference datum (m)
Z_i	depth to the screen interval (m AHD)
Z_r	depth datum (m AHD) such as ground level

APPENDIX 2 BACKGROUND TO BASIN AND STRATIGRAPHIC NOMENCLATURE

Numerous workers (Clarke, 1993; Clarke, 1994; Cockbain, 1968; Commander et al., 1992; Gammon and James, 2001; Gammon et al., 2000a; Gammon et al., 2000b; Johnson et al., 1999) have investigated the Palaeogene sediments of the south-west of Australia. As a consequence, sediments of similar age and depositional history have been allotted different names, and sediments of different age given similar names. In a review of the nomenclature, Clarke et al. (2003) suggested that the basin names be redefined and the Eocene stratigraphy be rationalised. The proposed changes relevant to the study area are summarised below.

The onshore Eocene sedimentary sequence of the Bremer Basin is inseparable from the Eocene succession of the Eucla Basin (Clarke et al., 2003). Therefore, it is proposed that the term Bremer Basin be abandoned and that the rocks previously assigned to the basin be considered part of the Eucla Basin (Clarke et al., 2003). The term Bremer Sub-basin has been retained for the offshore Mesozoic sediments (Bradshaw et al., 2003; Clarke et al., 2003).

The Werillup Formation was original defined by Cockbain (1968). Clarke (1993) divided the formation into the upper Werillup Formation (containing an Upper *Nothofagidites asperus* palynoflora) and the lower Werillup Formation (containing a Lower *N. asperus* palynoflora) separated by the Norseman Formation (formerly referred to as the Norseman Limestone (Cockbain, 1968). Clarke et al. (2003) proposed that the upper and lower Werillup Formation be redefined and the term Werillup Formation be restricted to Eocene clastic sediments and lignites with the Upper *N. asperus* palynoflora and the older sediments containing the Lower *N. asperus* palynoflora be called the North Royal Formation.

The Pallinup Siltstone of Cockbain (1968) was redefined as the Pallinup Formation (Gammon et al., 2000a). Clarke et al. (2003) has extended the Pallinup Formation to include all spicular marine sediments along the margin of the Eucla Basin

APPENDIX 3 BORE LOCATIONS

Bore ID	*Date*	*Easting (m MGA)*	*Northing (m MGA)*	*RL (m AHD)*	*Drilling method*	*Depth (m BGL)*	*Screen top (m BGL)*	*Bottom (m BGL)*	*Length (m)*	*Aquifer code*
EMU01	21/02/2000	487576	6195760	232.44	?RAB	26.6	14.6	26.6	12	Not known
EMU02	21/02/2000	486844	6195501	246.17	?RAB	30	27.8	29.8	2	Not known
EMU03	22/02/2000	486895	6195327	245.50	?RAB	11.7	9.7	11.7	2	Not known
EMU04	21/02/2000	486916	6195133	255.88	?RAB	18.0	15.9	17.9	2	Not known
EMU05	22/02/2000	487058	6195735	243.49	?RAB	14.0	12.0	14.0	2	Not known
EMU06	22/02/2000	487106	6195464	239.64	?RAB	34	28.0	34.0	6	Not known
EMU07	23/02/2000	487480	6196791	228.78	?RAB	40.0	11.5	29.5	18	Not known
EMU08	23/02/2000	488071	6196538	240.26	?RAB	16.7	12.6	16.6	4	Not known
EMU09	30/02/2001	484740	6195985	258.10	?RAB	24.4	22.4	24.4	2	Not known
EMU10	30/02/2001	484815	6196126	261.19	?RAB	11.1	9.1	11.1	2	Not known
EMU11	30/02/2001	484837	6196177	265.53	?RAB	7.9	5.9	7.9	2	Not known
EMU12	30/02/2001	484886	6195941	260.60	?RAB	25.5	23.5	25.5	2	Not known
EMU13	30/02/2001	484953	6195934	261.93	?RAB	24	22.0	24.0	2	Not known
EMU14	30/02/2001	485026	6195895	264.07	?RAB	27.1	25.0	27.0	2	Not known
EMU15	31/03/2001	483772	6192056	243.68	?RAB	25.3	23.3	25.3	2	Not known
EMU16	01/04/2001	483788	6191920	238.99	?RAB	22.4	20.4	22.4	2	Not known
EMU17	01/04/2001	483796	6191794	242.04	?RAB	49.7	47.7	49.7	2	Not known
EMU18	31/03/2001	484299	6191794	245.79	?RAB	40.5	38.5	40.5	2	Not known

Bore ID	*Date*	*Easting (m MGA)*	*Northing (m MGA)*	*RL (m AHD)*	*Drilling method*	*Depth (m BGL)*	*Screen top (m BGL)*	*Bottom (m BGL)*	*Length (m)*	*Aquifer code*
EMU19	31/03/2001	484715	6191933	262.82	?RAB	5	3.0	5.0	2	Not known
EMU20	01/04/2001	468882	6191261	182.21	?RAB	16.5	14.5	16.5	2	Surficial and WBR
EMU21	01/04/2001	469020	6191273	179.22	?RAB	17.5	15.3	17.3	2	Surficial and WBR
EMU22D	02/04/2001	469166	6191287	176.27	?RAB	45	39.6	41.6		WBR
EMU22S	03/04/2001	469166	6191287	176.27	?RAB	12	8	11		Sedimentary
EMU23	02/04/2001	469341	6191303	175.68	?RAB	7	4.6	6.6	2	Surficial and sedimentary
EMU24D	22/05/2000	476410	6182420	175.51	?RAB	11	9.0	11.0	2	Sedimentary
EMU24S	22/05/2000	476410	6182420	175.51	?RAB	4	2.0	4.0	2	Surficial
EMU25D	23/05/2000	476396	6185009	175.92	?RAB	11	9.0	11.0	2	Sedimentary
EMU25S	23/05/2000	476396	6185009	175.92	?RAB	4	2.0	4.0	2	Surficial
EMU26	23/05/2000	476750	6184010	175.60	?RAB	11.8	9.8	11.8	2	Sedimentary
EMU27D	24/05/2000	474773	6182425	176.10	?RAB	20	17.8	19.8	2	WBR
EMU27S	24/05/2000	474773	6182425	176.10	?RAB	2	1.0	2.0	1	Surficial
EMU28	24/05/2000	474769	6184658	176.54	?RAB	20.6	18.6	20.6	2	WBR
EMU29D	25/05/2000	474556	6183813	177.94	?RAB	26			0	WBR
EMU29S	25/05/2000	474556	6183813	177.94	?RAB	5	3.0	5.0	2	Surficial
EMU30	25/05/2000	474341	6183820	187.58	?RAB	26			0	WBR
Forty-acre1	?2006	467098	6190176	173.71	Air core	6.1				Surficial
Forty-acre2	?2006	467027	6189979	173.86	Air core	6.1				Surficial
Forty-acre3	?2006	466865	6189873	173.83	Air core	5.3				Surficial
Forty-acre4	?2006	466696	6190099	173.76	Air core	4.8				Surficial
MU01	19/05/2003	485296	6206168	286.08	Air core	22.0	19.0	22.0	3	WBR

Bore ID	*Date*	*Easting (m MGA)*	*Northing (m MGA)*	*RL (m AHD)*	*Drilling method*	*Depth (m BGL)*	*Screen top (m BGL)*	*Bottom (m BGL)*	*Length (m)*	*Aquifer code*
MU02	15/05/2003	482704	6204593	231.72	Air core	21.0	18.0	21.0	3	WBR
MU03	24/01/2003	472201	6200726	202.16	Air core	56.0	48.0	54.0	6	
MU03D	24/01/2003	472201	6200726	202.16	Air core	56.0	48.0	54.0	6	WBR and sedimentary
MU03S	5/05/2005	472201	6200726	202.16	Air core	6.0	4.0	6.0	2	Surficial and sedimentary
MU04	28/01/2003	472323	6203573	211.66	Air core	57.0	54.0	57.0	3	WBR
MU05D	20/01/2003	474498	6203340	203.41	Air core	36.0	17.3	23.3	6	Sedimentary
MU05S	20/01/2003	474498	6203340	203.41	Air core	12.0	3.0	12.0	9	Sedimentary
MU06	1/05/2003	476894	6203029	211.23	Air core	21.0	15.0	21.0	6	WBR
MU07D	12/05/2003	479658	6202003	211.57	Air core	40.5	37.5	40.5	3	WBR
MU07S	12/05/2003	479658	6202003	211.57	Air core	21.0	15.0	21.0	6	Sedimentary
MU08	9/05/2003	485964	6201546	223.58	Air core	13.0	7.0	13.0	6	WBR and sedimentary
MU09D	19/04/2004	487166	6202751	237.57	Air core	27.0	24.0	27.0	3	WBR
MU09S	19/04/2004	487165	6202749	237.52	Air core	18.0	11.0	17.0	6	Sedimentary
MU10D	21/01/2003	474260	6200065	203.00	Air core	73.0	30.0	36.0	6	WBR and sedimentary
MU10I	25/04/2006	474264	6200065	203.07	Wireline core	15.0	11.0	14.0	3	Sedimentary
MU10S	5/04/2004	474260	6200065	203.00	Air core	6.0	3.0	6.0	3	Surficial and sedimentary
MU11D	7/05/2003	483875	6200240	217.83	Air core	66.0	63.0	66.0	3	WBR
MU11I	7/05/2003	483875	6200240	217.83	Air core	43.0	37.0	43.0	6	Sedimentary
MU12A	26/04/2006	487236	6200173	222.44	Wireline core	48.3	30.0	36.0	6	Sedimentary
MU12D	6/05/2003	487236	6200178	222.50	Air core	49.0	40.0	49.0	9	WBR and sedimentary

Bore ID	*Date*	*Easting (m MGA)*	*Northing (m MGA)*	*RL (m AHD)*	*Drilling method*	*Depth (m BGL)*	*Screen top (m BGL)*	*Bottom (m BGL)*	*Length (m)*	*Aquifer code*
MU12S	6/05/2003	487236	6200178	222.50	Air core	14.0	11.0	14.0	3	Sedimentary
MU13	30/04/2003	472220	6198263	200.21	Air core	39.0	9.0	12.0	3	Surficial
MU14D	3/02/2003	479189	6198621	210.72	Air core	42.0	33.0	39.0	6	WBR
MU14S	3/02/2003	479189	6198621	210.72	Air core	22.5	16.5	22.5	6	Sedimentary
MU15A	25/04/2006	480493	6199187	212.25	Wireline core	5.0	1.0	4.0	3	Surficial
MU15D	30/01/2003	480493	6199187	212.25	Air core	31.0	25.5	28.5	3	WBR
MU15S	30/01/2003	480493	6199187	212.25	Air core	15.0	12.0	15.0	3	Sedimentary
MU16D	19/05/2003	485454	6199388	220.48	Air core	55.5	52.5	55.5	3	WBR
MU16S	19/05/2003	485454	6199388	220.48	Air core	9.0	6.0	9.0	3	Sedimentary
MU17	29/01/2003	472539	6197330	205.41	Air core	24.0	18.0	24.0	6	WBR
MU18D	28/04/2003	474370	6196483	201.02	Air core	54.0	51.0	54.0	3	WBR
MU18S	28/04/2003	474370	6196483	201.02	Air core	18.0	12.0	18.0	6	Sedimentary
MU19D	29/01/2003	476914	6197514	209.36	Air core	44.0	14.5	17.5	3	Sedimentary
MU19S	5/05/2005	476914	6197514	209.36	Air core	4.0	2.0	4.0	2	Surficial and sedimentary
MU20	1/05/2003	487910	6195438	251.90	Air core	22.0	19.0	22.0	3	WBR
MU21	2/05/2003	488685	6196232	226.69	Air core	25.0	22.0	25.0	3	WBR
MU22D	19/02/2003	480694	6193836	221.35	Air core	50.0	8.0	14.0	6	WBR and sedimentary
MU22S	30/04/2006	480705	6193805	221.48	Wireline core	8.5	4.5	7.5	3	Surficial
MU23D	10/02/2003	479962	6192950	220.56	Air core	53.5	47.5	53.5	6	WBR
MU23S	10/02/2003	479962	6192950	220.56	Air core	15.0	9.0	15.0	6	Sedimentary

Bore ID	*Date*	*Easting (m MGA)*	*Northing (m MGA)*	*RL (m AHD)*	*Drilling method*	*Depth (m BGL)*	*Screen top (m BGL)*	*Bottom (m BGL)*	*Length (m)*	*Aquifer code*
MU24	14/04/2003	474343	6191083	193.06	Air core	34.5	31.5	34.5	3	Surficial and WBR
MU25	20/02/2003	479338	6189385	222.55	Air core	13.0	7.0	13.0	6	Surficial
MU26	8/04/2003	485128	6188045	205.88	Air core	19.5	11.5	17.5	6	Surficial and WBR
MU27D	24/02/2003	483930	6187201	196.83	Air core	37.0	34.0	37.0	3	WBR
MU27S	24/02/2003	483930	6187201	196.83	Air core	7.5	4.5	7.5	3	Surficial
MU28D	20/02/2003	485136	6187029	199.96	Air core	35.0	32.0	35.0	3	WBR
MU28S	20/02/2003	485136	6187029	199.96	Air core	15.0	12.0	15.0	3	Surficial and WBR
MU29D	9/04/2003	478616	6180945	178.56	Air core	25.0	22.0	25.0	3	WBR
MU29S	9/04/2003	478616	6180945	178.56	Air core	10.5	7.5	10.5	3	Sedimentary
MU30D	8/04/2003	477620	6180603	178.98	Air core	33.0	30.0	33.0	3	WBR
MU30S	8/04/2003	477620	6180603	178.98	Air core	7.5	4.5	7.5	3	Surficial and sedimentary
MU31D	10/04/2003	480088	6181283	177.56	Air core	32.0	29.0	32.0	3	WBR
MU31S	10/04/2003	480088	6181283	177.56	Air core	16.5	10.5	16.5	6	Surficial and sedimentary
MU32	14/04/2003	479117	6184163	179.21	Air core	18.5	6.5	12.5	6	WBR and sedimentary
MU33D	16/04/2003	468142	6197058	186.91	Air core	51.0	48.0	51.0	3	WBR
MU33S	16/04/2003	468142	6197058	186.91	Air core	13.0	10.0	13.0	3	Surficial and sedimentary
MU34	15/05/2003	473090	6205073	200.65	Air core	19.5	16.5	19.5	3	Surficial and WBR
MU35	29/04/2003	472194	6197480	213.93	Air core	25.0	22.0	25.0	3	WBR
MU36D	15/04/2003	469593	6191813	177.16	Air core	43.0	30.0	36.0	6	Sedimentary
MU36S	15/04/2003	469593	6191813	177.16	Air core	27.0	21.0	27.0	6	Sedimentary

Bore ID	*Date*	*Easting (m MGA)*	*Northing (m MGA)*	*RL (m AHD)*	*Drilling method*	*Depth (m BGL)*	*Screen top (m BGL)*	*Bottom (m BGL)*	*Length (m)*	*Aquifer code*
MU37D	5/05/2003	487555	6199636	223.30	Air core	48.0	45.0	48.0	3	WBR
MU37I	5/05/2003	487555	6199636	223.30	Air core	34.0	28.0	34.0	6	Sedimentary
MU37S	5/05/2003	487555	6199636	223.30	Air core	12.0	9.0	12.0	3	Sedimentary
MU38D	8/04/2004	471418	6203540	205.40	Air core	39.0	17.0	20.0	3	Surficial and WBR
MU38S	8/04/2004	471419	6203538	205.36	Air core	7.5	3.0	6.0	3	Surficial
MU39	31/03/2004	472322	6202375	218.20	Air core	19.0	16.0	19.0	3	WBR
MU40D	7/04/2004	468234	6199579	188.58	Air core	29.5	26.5	29.5	3	WBR
MU40S	7/04/2004	468236	6199579	188.66	Air core	15.0	9.0	15.0	6	Surficial
MU41D	14/04/2004	470343	6196390	186.47	Air core	50.0	16.0	19.0	3	Sedimentary
MU41S	15/04/2004	470342	6196391	186.50	Air core	16.5	10.5	16.5	6	Sedimentary
MU42A	19/04/2006	474241	6193285	192.51	Wireline core	67.0	59.0	65.0	6	WBR
MU42D	19/04/2004	474242	6193281	192.72	Air core	69.0	40.5	43.5	3	Sedimentary
MU42I	19/04/2004	474244	6193281	192.76	Air core	36.0	29.0	35.0	6	Sedimentary
MU42S	19/04/2004	474246	6193281	192.84	Air core	12.0	5.0	11.0	6	Sedimentary
MU43D	19/04/2004	475021	6189254	178.31	Air core	30.0	12.0	15.0	3	Sedimentary
MU43S	21/04/2004	475019	6189254	178.33	Air core	9.0	6.0	9.0	3	Sedimentary
MU44	29/03/2004	467064	6181284	174.73	Air core	19.5	10.5	16.5	6	Surficial and WBR
MU45D	25/03/2004	472088	6179777	174.99	Air core	33.0	24.0	30.0	6	WBR
MU45S	25/03/2004	472088	6179775	175.03	Air core	9.0	6.0	9.0	3	Surficial
MU46A	2/04/2006	476491	6195485	178.17	Wireline core	80.0	41.0	47.0	6	WBR
MU46D	22/03/2004	476501	6177084	177.29	Air core	72.0	65.0	71.0	6	WBR

Bore ID	*Date*	*Easting (m MGA)*	*Northing (m MGA)*	*RL (m AHD)*	*Drilling method*	*Depth (m BGL)*	*Screen top (m BGL)*	*Bottom (m BGL)*	*Length (m)*	*Aquifer code*
MU46S	22/03/2004	476500	6177082	177.32	Air core	27.0	20.0	26.0	6	WBR and sedimentary
MU47	18/03/2000	479823	6178486	192.87	Air core	30.0	23.5	26.5	3	WBR
MU48	18/03/2004	481524	6181847	176.49	Air core	19.5	8.0	11.0	3	WBR and sedimentary
MU49	13/04/2004	467350	6194594	177.75	Air core	42.0	35.0	41.0	6	WBR
MU50	25/03/2004	479123	6177193	188.36	Air core	6.0			0	
MU51	29/03/2004	477584	6178735	181.40	Air core	20.0	14.0	20.0	6	WBR
MU52A	1/05/2006	475961	6176929	176.58	Wireline core	5.5	2.0	5.0	3	Surficial
MU52D	30/03/2004	475956	6176928	176.71	Air core	28.5	20.5	26.5	6	WBR
MU52S	30/03/2004	475957	6176928	176.69	Air core	12.0	5.0	11.0	6	Surficial and sedimentary
MU53	8/04/2004	467233	6199580	192.35	Air core	27.0	23.5	26.5	3	WBR
MU54D	22/04/2004	468633	6196056	182.82	Air core	30.5	10.0	13.0	3	Surficial and WBR
MU54S		468619	6196055	182.83	Air core		6.0	8.0	2	Surficial
MU55D		469473	6194747	180.73	Air core	51.5	48.0	50.0	2	Sedimentary
MU55S		469473	6194747	180.73	Air core		9.0	11.0	2	Sedimentary
MU56D	4/05/2005	468369	6194950	179.37	Air core	29.0	21.0	23.0	2	Sedimentary
MU56S		468369	6194950	179.37	Air core		6.0	8.0	2	Sedimentary
MU57D	19/04/2005	466535	6190199	175.27	Air core	16.0	14.0	16.0	2	Surficial and WBR
MU57S	20/04/2005	466535	6190198	175.20	Air core	7.3	5.3	7.3	2	Surficial
MU58D	19/04/2005	474567	6188153	175.66	Air core	14.0	12.0	14.0	2	WBR
MU58S	19/04/2005	474567	6188154	175.64	Air core	3.0	1.0	3.0	2	Surficial
MU59D	16/02/2006	473849	6187091	175.11	Air core	58.0	39.0	42.0	3	WBR and sedimentary

Bore ID	*Date*	*Easting (m MGA)*	*Northing (m MGA)*	*RL (m AHD)*	*Drilling method*	*Depth (m BGL)*	*Screen top (m BGL)*	*Bottom (m BGL)*	*Length (m)*	*Aquifer code*
MU59I	16/02/2006	473849	6187092	175.11	Air core	22.5	19.5	22.5	3	Sedimentary
MU59S	16/02/2006	473850	6187093	175.14	Air core	7.2	4.2	7.2	3	Surficial and sedimentary
MU60D	15/02/2006	473704	6186443	174.85	Air core	16.0	13.0	16.0	3	WBR
MU60S	15/02/2006	473706	6186443	174.85	Air core	6.0	3.0	6.0	3	Surficial
MU61D	22/02/2006	476364	6186329	175.31	Air core	54.0	47.8	53.8	6	WBR and sedimentary
MU61I	22/02/2006	476366	6186330	175.35	Air core	33.0	26.0	32.0	6	Sedimentary
MU61S	22/02/2006	476366	6186330	175.30	Air core	12.0	9.0	12.0	3	Surficial and sedimentary
MU62D	20/04/2005	476911	6199146	203.75	Air core	66.0	43.0	45.0	2	Sedimentary
MU62I	22/04/2005	476911	6199147	203.74	Air core	33.0	31.0	33.0	2	Sedimentary
MU62S	22/04/2005	476912	6199148	203.76	Air core	6.0	4.0	6.0	2	Sedimentary
MU63D	3/05/2005	474580	6197241	201.12	Air core	68.5	52.0	54.0	2	Sedimentary
MU63S	3/05/2005	474579	6197242	201.12	Air core	6.0	4.0	6.0	2	Sedimentary
MU64D	26/04/2005	475218	6197024	204.83	Air core	69.0	46.5	48.5	2	Sedimentary
MU64I	28/04/2005	475217	6197024	204.81	Air core	42.0	31.0	33.0	2	Sedimentary
MU64S	28/04/2005	475216	6197025	204.87	Air core	4.0	2.0	4.0	2	Sedimentary
MU65D	4/05/2005	476735	6189155	184.59	Air core	39.0	37.0	39.0	2	WBR
MU65S	5/05/2005	476735	6189155	184.57	Air core	6.0	4.0	6.0	2	Surficial
MU66D	7/03/2006	473834	6206759	203.47	Air core	60.0	53.0	59.0	6	WBR
MU66S	7/03/2006	473835	6206759	203.48	Air core	15.0	7.5	13.5	6	Sedimentary
MU67D	23/02/2006	482389	6186599	187.74	Air core	54.0	48.0	54.0	6	WBR
MU67I	23/02/2006	482386	6186600	187.73	Air core	33.0	27.0	33.0	6	WBR

Bore ID	*Date*	*Easting (m MGA)*	*Northing (m MGA)*	*RL (m AHD)*	*Drilling method*	*Depth (m BGL)*	*Screen top (m BGL)*	*Bottom (m BGL)*	*Length (m)*	*Aquifer code*
MU67S	23/02/2006	482385	6186600	187.72	Air core	18.0	15.0	18.0	3	Sedimentary
MU68D	2/03/2006	481515	6184586	181.86	Air core	43.0	35.5	41.5	6	WBR and sedimentary
MU68S	2/03/2006	481513	6184586	181.87	Air core	18.0	13.0	18.0	5	Sedimentary
MU69	2/03/2006	481721	6182936	183.53	Air core	28.0	21.0	27.0	6	Surficial and WBR
MU70	3/03/2006	473933	6176283	186.18	Air core	20.5	14.5	20.5	6	WBR
MU71	8/03/2006	474775	6182625	176.00	Air core	14.0	10.5	13.5	3	WBR
MU72	30/04/2006	487072	6195485	239.51	Wireline core	8.0	4.0	7.0	3	Surficial
Muir1	18/01/2007	468537	6186002	Lake floor	Hand dug	1.0		1.0	0	Surficial
Muir2	18/01/2007	471896	6183461	Lake floor	Hand dug	1.0		1.0	0	Surficial
Muir3	18/01/2007	471707	6183451	Lake floor	Hand dug	1.0		1.0	0	Surficial
Muir4	18/01/2007	470659	6179136	Lake floor	Hand dug	1.0		1.0	0	Surficial
PM01	3/05/1997	472084	6188975	174.93	Air core	43.0	13.6	19.6	6	Sedimentary
PM02	5/05/1997	468023	6200722	194.17	Air core	18.0	12.0	18.0	6	WBR
PM03	5/05/1997	473415	6195295	194.15	Air core	51.0	16.0	40.0	24	Sedimentary
PM04	7/05/1997	476914	6200044	205.74	Air core	42.0	34.5	40.5	6	Sedimentary
PM05	8/05/1997	483037	6202696	220.05	Air core	39.0	6.0	39.0	33	
PM10	16/05/1997	479128	6193960	218.28	Air core	54.0	31.0	37.0	6	Sedimentary
PM12	19/05/1997	481571	6201141	211.90	Air core	39.0	18.0	24.0	6	Sedimentary

APPENDIX 4 RESULTS

Table 6 Results for XRD. Results in weight %.

	MU09–27	MU10–5.1	MU12–5.4	MU12–49	MU32-18	MU42-23.5	MU42–29	MU42–31	MU46–21.45	MU46–45.5
Albite	48.7			46.9	32.2			0.7	0.3	
Biotite					1.3					1.3
Calcite					1.5					
Chlorite	8			4.4						
Gibbsite	0.1	1.3	0.5					2.6	5.5	
Huntite										5
Kaolin		35.5	16.9	2.2	2.3	0.8	0.2	82.3	6.9	48.6
Magnetite						0.1		1.1		
Microcline			10.6		31.3	0.1	0.1	0.2		
Muscovite	11.3									
Quartz	29.5	62	72	43.2	31.4	99	99.7	13.1	87.3	38.8
Rutile	2.4	1.2		trace						
Siderite										5.9
Sodium Chloride										0.4

Table 7 Results for total acid extraction

			Al (%)	*Ca (%)*	*K (%)*	*Mg (%)*	*Na (%)*	*P (%)*	*S (%)*	*Fe (ppm)*	*Mn (ppm)*
MU10-4.75	Werillup Formation	Clay	11.875	0.0418	0.3561	0.0879	0.0593	0.019	0.1755	10642	264.99
MU10-5.1	Werillup Formation	Sandy clay	8.8989	0.0365	0.1902	0.0645	0.0526	0.0155	0.1094	8973.6	311.52
MU12-10	Pallinup Formation	Fine-grained quartz sand	3.2161	0.015	1.5383	0.0248	0.0807	<0.01	0.0413	3637.1	41.367
MU12-5.4	Pallinup Formation	Fine-grained quartz sand	5.4619	0.0168	1.4463	0.0377	0.1062	<0.01	0.01	2900.1	10.282
MU42-29	Werillup Formation	Coarse-grained quartz sand	0.2233	0.0242	0.0327	<0.01	0.0284	<0.01	0.0079	1777.4	19.697
MU42-31.4	Werillup Formation	Carbonaceous clay	13.856	0.1633	0.1598	0.1828	0.3444	0.0247	1.2028	6323.6	48.313
MU46-21.45	Werillup Formation	Carbonaceous sandy silt	3.5831	0.2335	0.1354	0.0802	0.086	0.0144	0.6233	6100.7	181.59
MU46-45.5	Weathered basement rock		10.075	0.7075	0.6659	0.1459	0.1583	0.0581	1.5866	57166	2593.7
MU52-2.35	Recent sediment	Silty clay	2.5656	0.0264	0.0502	0.0412	0.0586	<0.01	0.0279	29245	14.109
YARNUP CREEK	Recent sediment	Sandy silt	6.8151	0.0372	0.1168	0.1429	0.2519	0.01	0.0562	19798	54.554

Table 8 Results for exchangeable element extraction

			Al (mg/kg)	*Ca* (mg/kg)	*Fe* (mg/kg)	*K* (mg/kg)	*Mg* (mg/kg)	*Mn* (mg/kg)	*Na* (mg/kg)	*S* (mg/kg)	*P* (mg/kg)
MU10-4.75	Werillup Formation	Clay	439.45	340.68	12.90	144.28	456.91	0.58	321.36	15.28	<0.01
MU10-5.1	Werillup Formation	Sandy clay	424.42	285.23	232.14	132.44	326.39	2.76	280.91	9.87	<0.01
MU12-10	Pallinup Formation	Fine-grained quartz sand	189.57	43.07	230.15	193.73	41.22	2.14	93.85	10.77	<0.01
MU12-5.4	Pallinup Formation	Fine-grained quartz sand	181.79	61.23	31.61	113.32	123.07	0.25	349.68	37.74	<0.01
MU42-29	Werillup Formation	Coarse-grained quartz sand	11.30	114.99	35.91	12.39		3.37	135.65	9.55	0.39
MU42-31.4	Werillup Formation	Carbonaceous clay	51.56	702.96	2.00	83.43	763.65	2.41	1687.95	93.63	2.03
MU46-21.45	Werillup Formation	Carbonaceous sandy silt	26.57	1096.71	134.03	16.17	275.52	6.11	376.61	20.32	<0.01
MU46-45.5	Weathered basement rock		326.83	2753.85	995.11	176.88	673.93	66.17	1304.41	124.96	0.54
MU52-2.35	Recent sediment	Silty clay	173.46	157.62	47.58	46.11	205.88	0.85	345.27	126.87	<0.01
YARNUP CREEK	Recent sediment	Sandy silt	673.27	223.48	120.87	179.53	937.31	3.05	2133.19	279.85	<0.01

Table 9 Field measurements at time of chemical sample collection

Bore ID	*Date*	*EC* (mS/cm)*	*T (°C)*	*pH*	*EC** (mS/cm)*	*TDS (mg/L)*	*SWL (m BGL)*	*Eh (V)*	*DO (mg/L)*
Forty-acre 1	20/03/07	5.04	20.6	5.95	5.52	3050	2.05	0.29	1
Forty-acre 2	20/03/07	2.82	19.4	6.74	3.17	1665	2.13	0.17	5.98
Forty-acre 3	20/03/07	5.09	21.8	6.72	5.44	2998	2.34	0.15	1.67
Forty-acre 4	20/03/07	4.4	21.1	6.56	4.77	2607	2.65	0.17	0.68
MU01	22/05/07	14	20.9	5.61	15.25	8776	5.87	0.40	7.56
MU02	22/05/07	14.52	17.5	5.99	17.02	9823	1.54	0.38	0.23
MU03D	27/03/07	25	18.6	6.08	28.63	18886	3.3	0.17	1.12
MU03S	14/03/07	1.396	20.5	5.73	1.53	788	2.83	0.13	0.55
MU04	29/03/07	5.65	24.2	5.94	5.74	3178	7.94	0.18	0.56
MU05D	3/03/05	3.5	18.4	5.99	3.97	2133	2.27		0.1
MU05S	3/03/05	0.5	18.0	6.45	0.62	325	2.28		0.1
MU06	13/03/07	26.8	20.8	5.81	29.25	19373	1.13	0.37	0.23
MU07D	10/03/05	17.7	21.1		19.17	11493	1.92		1.7
MU07S	8/03/05	17.7	20.5	4.18	19.39	11661	2.93		18.7
MU08	14/03/07	18.86	20.5	6.11	20.71	12700	0	0.10	0.16
MU09D	9/03/05	19.5	19.5	6.22	21.87	13601	-0.31		0.4
MU09S	10/03/05	14	19.1	6.18	15.87	9141	0.01		3
MU10D	3/03/05	2.3	18.8	6.37	2.58	1317	3.48		0.1
MU10I	1/12/06	3.07	22.3	6.42	3.24	1707	3.03	-0.07	0.04
MU10S	3/03/05	1	17.8	8.10	1.17	605	3.48		1.2
MU11D	16/03/05	7.3	20.1	7.33	8.04	4533	3.5	0.10	2.5
MU11I	16/03/05	6.7	18.0	6.39	7.76	4367	3.67	0.20	1.2
MU12A	28/03/07	9.97	17.6	6.06	11.66	6667	4.67	0.05	0.15
MU12D	16/03/05	15.5	18.3	6.86	17.86	10471	4.65	0.13	0.3
MU12S	16/03/05	2.9	19.5	6.02	3.21	1688	2.09	0.16	0.5
MU13	10/05/07		16.8	4.42			-0.15	0.07	0.08
MU14D	14/03/05	8	17.4	5.77	9.38	5319	3.1		15.5
MU14S	14/03/05	5	17.2	5.40	5.91	3279	2.91		9.4
MU15A	13/03/07	24	20.2	6.22	26.53	17246	3.81		
MU15D	15/03/05	8.4	20.0	6.00	9.34	5295	3.44	0.16	0.3
MU15S	15/03/05	13.1	17.9	3.95	15.22	8759	3.87	0.25	0.4
MU16D	15/03/05	3.6	19.1	7.48	4.02	2165	2.17		0.2
MU16S	15/03/05	11.8	17.8	4.09	13.69	7859	4.38	0.17	2.2
MU17	10/05/07	17.35	18.5	5.05	19.91	12070	-0.73	0.43	0.029
MU18D	15/03/05	7.3	21.6	6.24	7.82	4402	8.94	0.07	2
MU18S	15/03/05	2.5	18.0	5.23	2.87	1484	9.22	0.39	5.1
MU19D	7/12/06	9.4	16.2	5.55	11.33	6468	3.74	0.17	
MU22D	22/03/07	8.84	19.4	4.49	9.95	5654	1.45	0.09	0.23
MU22S	26/03/07	15.61	17.0	4.83	18.50	10967	1.8	0.31	1.14

Bore ID	*Date*	*EC* (mS/cm)*	*T (°C)*	*pH*	*EC** (mS/cm)*	*TDS (mg/L)*	*SWL (m BGL)*	*Eh (V)*	*DO (mg/L)*
MU23D	17/03/05	13.7	20.6	6.59	14.97	8614	0.67	0.02	0.3
MU23S	17/03/05	6.3	20.4	4.52	6.93	3881	1.02	0.15	0.5
MU24	21/05/07	12.41	15.9	5.99	15.05	8659	1.28	0.25	0.13
MU25	15/05/07	4.07	15.3	4.59	5.00	2739	5.88	0.22	
MU26	15/05/07	3.9	16.6	5.66	4.66	2542	3.38	0.28	0.3
MU27D	17/03/05	4	24.3	6.36	4.03	2168	3.05	0.18	0.6
MU27S	17/03/05	3.8	18.4	5.64	4.34	2350	3.67	0.41	2.9
MU28D	17/03/05	1.5	20.4	6.73	1.63	838	5.81		0.2
MU28S	17/03/05	0.9	19.4	6.16	1.06	548	6.16	0.13	0.3
MU29D	9/03/05	23.4	19.2	6.53	26.44	17179	3.38		0.4
MU29S	9/03/05	22.1	20.1	6.47	24.48	15644	3.37		3.6
MU30D	9/03/05	29.5	23.7	5.96	30.27	20170	3.26		6.1
MU30S	9/03/05	2.6	21.9	6.42	2.81	1454	3.1		7
MU31D	10/03/05	29.1	18.2	6.16	33.61	22785	1.51	0.17	3.8
MU31S	10/03/05	9.9	17.6	5.77	11.57	6612	1.57	0.39	4.4
MU32	27/02/07	8.05	17.5	5.96	9.44	5356	2.65	0.16	0.11
MU33D	2/03/05	11.7	23.6	6.38	11.98	6850	3.02		0.8
MU33S	1/03/05	5.8	20.0	5.76	6.39	3562	3.85	0.25	0.1
MU34	14/03/07	5.48	17.9	6.42	6.37	3549	3.01	0.17	1.02
MU35	17/05/07	16.33	17.3	5.32	19.23	11538	0.81	0.24	0.23
MU36D	18/03/05	4.8	17.6	5.99	5.56	3070	2.75	0.11	0.5
MU36S	18/03/05	3	17.6	6.00	3.45	1830	2.8	0.03	2.3
MU37D	16/03/05	9.3	22.7	6.90	9.73	5525	5.92	0.13	0.4
MU37I	16/03/05	5.4	18.3	4.94	6.26	3482	5.77	0.26	0.3
MU37S	16/03/05	6.1	23.5	5.18	6.29	3503	5.95	0.04	4.7
MU38D	3/03/05	0.9	17.4	6.02	1.09	562	1.32	0.07	0.3
MU38S	3/03/05	0.4	21.9	5.79	0.45	240	3.42	0.23	0.7
MU39	14/03/07	15.42	20.4	4.20	16.97	9792	7.98		
MU40D	2/03/05	20.1	23.5	6.05	20.70	12691	-0.18		1.2
MU40S	2/03/05	19.7	19.5	5.78	22.11	13794	-0.02		0.1
MU41D	1/03/05	6.3	18.2	5.64	7.30	4096	1.28		0.1
MU41S	1/03/05	3.3	18.2	5.87	3.81	2042	1.7	0.07	0.1
MU42A	28/03/07	9.05	18.0	6.37	10.50	5980	2.25	0.12	0.72
MU42D	24/02/05	6.7	22.3	6.00	7.07	3959	2.1	0.33	0.5
MU42I	24/02/05	11.2	19.3	5.45	12.64	7241	2.31		2.5
MU42S	24/02/05	3.5	21.1	5.76	3.74	2000	2.17		0.7
MU43D	24/02/05	6.8	17.4	5.61	8.03	4523	0.36	0.05	0.6
MU43S	24/02/05	5.9	17.6	5.56	6.90	3862	-0.05		1.2
MU44	28/11/06	40.9	16.9	6.20	48.57	34482	2.36	0.26	

Bore ID	*Date*	*EC* (mS/cm)*	*T (°C)*	*pH*	*EC** (mS/cm)*	*TDS (mg/L)*	*SWL (m BGL)*	*Eh (V)*	*DO (mg/L)*
MU45D	22/02/05	102.8	18.7	6.54	117.45	88346	3.43		0.1
MU45S	22/02/05	6.1	17.3	6.73	7.19	4034	2.46		0
MU46A	28/11/06	43.5	22.3	6.06	45.95	32435	3.1	0.19	
MU46D	23/02/05	66.8	20.9	6.30	72.75	53388	3.97		0.4
MU46S	23/02/05	19.4	16.6	5.80	23.22	14658	2.87		0.1
MU47	29/11/06	15.13	21.9	6.22	16.12	9293	13.39	0.26	1.31
MU48	29/11/06	35.2	18.2	5.48	40.66	28294	1.59	0.16	0.07
MU49	22/05/07	4.46	17.7	6.09	5.21	2864	1.6	0.18	0.09
MU51	29/11/06	16.69	16.1	5.79	20.15	12261	3.74	0.29	0.11
MU52A	27/11/06	8.36	21.9	5.29	8.91	5044	1.43		
MU52D	22/02/05	18.1	17.7	6.14	21.17	13054	2.03	0.36	0.1
MU52S	22/02/05	8.3	16.2	5.21	9.99	5680	1.93		0.5
MU53	20/03/07	12.89	20.1	5.72	14.28	8206	0.72		
MU54D	15/03/07	2.24	19.3	6.30	2.53	1291	2.3	0.14	0.14
MU54S	15/03/07	5.18	24.3	6.68	5.25	2890	2.32	0.12	3.22
MU55D	15/03/07	6.05	16.5	5.92	7.24	4064	3.54	0.09	0.15
MU55S	27/03/07	4.18	17.6	5.61	4.89	2677	3.4	0.05	0.89
MU56D	27/03/07	1.25	20.2	5.79	1.38	711	2.51	0.05	0.18
MU57D	15/03/07	11.52	16.8	6.56	13.71	7870	4.09	0.20	0.89
MU57S	1/03/07	7.88	15.8	6.15	9.57	5435	3.9	0.18	0.7
MU58D	30/11/06	33.6	19.9	6.26	37.38	25732	1.83	0.13	0.86
MU58S	30/11/06	33.4	22.3	6.27	35.28	24091	1.43		
MU59D	30/11/06	78.3	17.4	5.66	92.00	68447	1.32	0.23	0.08
MU59I	30/11/06	36.6	18.0	5.79	42.46	29702	0.7	0.14	0.23
MU59S	30/11/06	14.44	15.8	6.06	17.54	10221	0.8	0.15	0.37
MU60D	5/12/06	39.2	22.3	6.31	41.41	28883	0.85	0.18	0.81
MU60S	5/12/06	35.7	22.3	6.05	37.71	25991	0.82	0.27	0.62
MU61D	6/12/06	51.2	20.3	6.17	56.47	40664	0.35	0.19	3.02
MU61I	6/12/06	12.93	22.3	6.09	13.66	7841	-0.41	0.16	0.08
MU61S	6/12/06	10.24	22.3	6.02	10.82	6167	0.15	0.18	0.1
MU62D	22/03/07	9.9	18.7	6.00	11.31	6458	3.63	0.14	0.14
MU62I	28/02/07	5.79	15.8	4.96	7.03	3940	3.27	0.30	0.5
MU62S	28/02/07	3.87	20.7	5.54	4.23	2290	3.01		
MU63D	7/12/06	8.8	17.7	5.70	10.27	5848	3.95		
MU63S	6/12/06	3.78	16.1	4.46	4.56	2485	3.15	0.54	2.02
MU64D	22/03/07	8.3	19.5	5.65	9.32	5284	5.03	0.16	0.18
MU64I	27/02/07	6.52	18.8	5.67	7.43	4174	4.93	0.20	0.16
MU64S	27/02/07	3.11	21.1	3.15	3.37	1783	2.35	0.23	2.26
MU65D	13/03/07	4.72	19.2	5.86	5.33	2938	2.51	0.17	0.15

Bore ID	*Date*	*EC* (mS/cm)*	*T (°C)*	*pH*	*EC** (mS/cm)*	*TDS (mg/L)*	*SWL (m BGL)*	*Eh (V)*	*DO (mg/L)*
MU65S	12/03/07	3.21	19.1	5.50	3.64	1938	2.83	0.05	0.6
MU66D	29/03/07	5.59	19.8	6.21	6.23	3468	2.6	0.15	0.2
MU66S	29/03/07	6.76	19.3	5.97	7.62	4286	2.63	0.08	0.43
MU67D	21/03/07	7.16	26.7	10.32	6.92	3870	2.27	0.12	0.57
MU67I	1/03/07	6.96	18.4	5.82	8.00	4511	2.22	0.19	0.15
MU67S	28/02/07	4.87	16.7	5.76	5.81	3217	2.13	0.11	0.35
MU68D	21/03/07	6.66	25.3	5.50	6.62	3696	3.66	0.19	0.16
MU68S	21/03/07	2.76	19.2	5.58	3.12	1634	3.6	0.10	0.21
MU69	21/03/07	34.1	17.8	6.03	39.73	27567	6.53	0.20	2.2
MU70	16/05/07	11.62	16.8	5.82	13.83	7941	6.01	0.24	0.39
MU71	17/05/07	3.22	18.0	6.50	3.74	1997	3.47	0.21	0.53
MU72	15/05/07	13.65	17.9	5.65	15.87	9142	0.06	0.17	1.02
Muir1	16/01/07	66.2	23.5	6.69	68.19	49823	1		
Muir2	18/01/07	87.2	20.2	7.54	96.39	71874	1		
Muir3	18/01/07	93.9	20.1	7.45	104.01	77837	1		
Muir4	18/01/07	43.2	19.9	7.01	48.06	34084	1		
PM01	23/05/07	31.7	17.6	5.13	37.09	25505	0.99	0.23	0.11
PM02	24/05/07	11.79	20.2	5.73	13.03	7472	3.16	0.31	0.23
PM03	24/05/07	4.9	17.7	5.75	5.72	3166	3.14	0.07	0.08
PM04	24/05/07	5.04	18.0	5.44	5.85	3240	5.49	0.10	0.07
PM10	23/05/07	7.95	17.7	4.90	9.28	5263	0.88	0.13	0.5
PM12	23/05/07	17.25	18.0	3.77	20.01	12149	0.99	0.13	0.23

- EC uncompensated, ** EC Compensated

Table 10 Results of major ion chemical analyses for groundwater. na not determined

Bore ID	*Electron balance*	*F (mg/L)*	*Cl (mg/L)*	*Br (mg/L)*	*SO4 (mg/L)*	*HCO3 (mg/L)*	*CO3 (mg/L)*	*Ca (mg/L)*	*K (mg/L)*	*Mg (mg/L)*	*Mn (mg/L)*	*Na (mg/L)*	*Alkalinity (mg CaCO3/L)*
Forty-acre 1	1.16	0.23	811.0	1.0	2010.8	69		247	22.8	314	0.5	670	57
Forty-acre 2	-1.97	0.49	687.3	1.5	300.3	656		204	16.4	73	0.86	430	538
Forty-acre 3	1.74	0.54	762.0	1.3	1823.5	378		468	26	194	0.45	656	310
Forty-acre 4	2.23	0.74	898.2	1.5	950.0	438		220	13.8	186	0.33	650	359
MU01	7.15	0.19	5099.7	14.9	495.3	126		80.1	9.5	407	0.224	3270	103
MU02	3.92	0.28	5495.8	18.2	315.4	272		338	2.4	969	1.17	1900	223
MU03D	1.84	0.33	9623.2	14.9	1757.0	171		236	114	698	0.36	5800	140
MU03S	0.61	0.07	462.8	0.9	9.2	86		16.8	4.9	31.6	0.004	261	70
MU04	3.19	0.27	1759.5	4.5	158.4	145		41.3	16.2	166	2.2	990	119
MU05D	3.56	0.16	1324.3	4.1	117.1	115		47.8	3.7	146	0.14	695	94
MU05S	0.86	0.00	141.6	0.7	0.0	110		9	1.4	14.2	0.01	98	90
MU06	2.66	0.36	10755.0	25.9	742.3	236		376	8.5	1440	2.12	4650	193
MU07D	15.92	0.25	4634.9	12.9	350.7	na		970	86.5	0.4	-0.02	2730	-999
MU07S	3.13	0.00	6273.6	17.9	1034.6			266	29	597	0.3	3410	0
MU08	2.61	0.75	6886.1	19.4	553.2	319		121	32	638	0.69	3750	262
MU09D	2.85	0.87	7553.3	21.6	617.6	346		305	16.5	1080	3.96	3230	284
MU09S	2.73	0.58	5176.7	14.7	444.3	281		190	12.5	647	1.52	2430	230
MU10D	3.90	0.15	686.4	1.0	0.0	229		26.1	15.8	46.9	0.07	454	188
MU10I	-0.94	0.11	897.1	1.1	3.4	240		34.5	17.5	58.5	0.11	509	197
MU10S	1.76	0.32	236.2	0.0	0.0	143		26.8	9.2	12.2	-0.01	160	122
MU11D	3.45	0.23	2348.6	6.5	383.1	290		212	17.9	231	0.22	1260	238
MU11I	3.08	0.00	2234.6	6.3	403.9	220		125	19.5	183	0.37	1340	180

Bore ID	*Electron balance*	*F (mg/L)*	*Cl (mg/L)*	*Br (mg/L)*	*SO4 (mg/L)*	*HCO3 (mg/L)*	*CO3 (mg/L)*	*Ca (mg/L)*	*K (mg/L)*	*Mg (mg/L)*	*Mn (mg/L)*	*Na (mg/L)*	*Alkalinity (mg CaCO3/L)*
MU12A	3.95	0.27	3681.2	10.2	402.7	154		143	20.3	361	1.38	2000	126
MU12D	2.17	0.53	5758.0	17.2	719.7	351		297	27	568	0.18	2970	288
MU12S	4.12	0.17	856.3	2.6	111.1	198		14.3	10.4	55.5	0.02	618	162
MU13	4.79	0.72	2253.7	6.4	139.8	1		45.5	9.1	209	0.728	1230	1
MU14D	1.30	0.56	2823.5	7.9	484.6	115		143	25.7	228	1	1560	94
MU14S	1.49	0.21	2705.8	6.8	397.9	88		72.5	18.9	232	0.19	1510	72
MU15A	2.26	0.48	9481.7	22.2	703.3	189		124	6	802	1.12	5180	155
MU15D	0.98	0.26	2844.4	7.9	412.7	151		122	22.7	203	0.31	1610	124
MU15S	2.04	0.30	4909.7	13.0	629.6			107	25.5	416	0.46	2710	0
MU16D	4.20	0.29	1047.2	2.9	127.8	348		74.9	11.7	86.2	0.06	696	286
MU16S	12.79	0.26	3452.6	9.4	471.3			90.5	24.5	351	0.36	2410	0
MU17	3.79	0.28	6223.0	13.2	561.3	39		132	22.5	626	0.93	3310	32
MU18D	2.14	0.21	2479.4	7.0	175.0	171		259	17.9	233	3.61	1090	140
MU18S	4.17	0.00	842.0	2.2	78.4	24		16.1	3.7	72.8	0.19	486	20
MU19D	-0.86	0.32	3509.0	9.0	352.2	66		73.5	15.5	267	0.32	1830	54
MU22D	4.66	0.39	3256.8	11.0	264.4	3		48.8	13.7	283	0.49	1860	3
MU22S	3.22	0.18	6168.2	9.3	535.1	17		68.2	6	393	1.94	3710	14
MU23D	2.63	0.60	4785.6	10.9	568.5	251		303	23.5	396	0.64	2550	206
MU23S	2.11	0.00	2204.2	5.1	208.6	10		39.8	10.4	232	0.33	1110	8
MU24	4.59	0.09	4333.7	13.7	591.1	179		110	39.7	332	0.978	2700	147
MU25	3.81	0.02	1201.2	4.4	82.6	53		21.4	5.3	105	0.372	679	43
MU26	3.71	0.19	1255.6	3.2	89.4	81		45.9	8.7	150	0.534	617	66
MU27D	2.78	0.58	1095.8	1.9	179.4	171		30	13.5	91.4	0.72	700	140

Bore ID	*Electron balance*	*F (mg/L)*	*Cl (mg/L)*	*Br (mg/L)*	*SO4 (mg/L)*	*HCO3 (mg/L)*	*CO3 (mg/L)*	*Ca (mg/L)*	*K (mg/L)*	*Mg (mg/L)*	*Mn (mg/L)*	*Na (mg/L)*	*Alkalinity (mg CaCO3/L)*
MU27S	-1.52	0.00	1414.1	2.8	135.9	37		16.5	4	90	0.04	774	30
MU28D	6.21	1.19	377.2	1.0	0.0	202		14.7	6.1	24.4	0.63	299	166
MU28S	3.97	0.33	269.9	0.0	0.0	119		7.62	4.5	17.2	0.14	196	98
MU29D	87.54	0.49	0.0	27.4	800.8	188		762	27	951	1.58	4150	154
MU29S	0.65	0.84	8858.7	27.5	800.0	232		421	15	844	0.6	4200	190
MU30D	1.24	0.00	11544.6	29.7	700.2	117		1010	48	1340	4.74	4350	96
MU30S	4.52	0.16	797.4	2.2	96.8	44		20	2.3	86.8	0.27	446	36
MU31D	90.42	0.81	0.0	32.7	799.5	161		2400	51.5	1010	4	4130	132
MU31S	-0.62	0.18	3799.6	9.6	318.9	78		293	17	349	0.92	1610	64
MU32	5.23	0.21	3891.3	9.9	405.2	134		151	18.8	360	0.342	2210	110
MU33D	0.32	0.46	3861.0	7.7	429.6	166		193	17	413	1.46	1780	136
MU33S	2.79	0.12	1990.9	4.7	146.0	122		46	5	180	0.17	1090	100
MU34	3.37	0.21	1918.2	4.5	149.4	137		109	11	139	0.396	1070	112
MU35	8.15	0.11	5930.0	17.0	608.8	76		92	25.5	494	0.4	3850	62
MU36D	2.93	0.07	1693.7	3.1	116.0	90		80.5	8.3	152	0.25	876	74
MU36S	4.46	0.00	1002.3	2.1	65.3	102		34.2	4.5	84.2	0.1	586	84
MU37D	2.47	0.23	2801.0	7.0	684.0	232		235	22.1	258	0.33	1580	190
MU37I	1.05	0.06	1840.9	4.7	368.5	22		66.7	17.5	157	0.32	1030	18
MU37S	-0.91	0.00	1887.7	5.1	222.3	34		29.9	24.6	106	0.06	1080	28
MU38D	2.26	0.00	288.8	0.0	0.0	90		8.15	6	13.9	0.03	195	74
MU38S	0.75	0.00	108.5	0.0	0.0	41		4.42	1.2	13.9	-0.01	55.5	34
MU39	2.95	0.18	5532.6	12.9	322.5			33.6	5.5	417	0.07	3130	0
MU40D	1.64	0.72	7178.0	13.5	655.7	134		394	34	804	2.08	3200	110

Bore ID	*Electron balance*	*F (mg/L)*	*Cl (mg/L)*	*Br (mg/L)*	*SO4 (mg/L)*	*HCO3 (mg/L)*	*CO3 (mg/L)*	*Ca (mg/L)*	*K (mg/L)*	*Mg (mg/L)*	*Mn (mg/L)*	*Na (mg/L)*	*Alkalinity (mg CaCO3/L)*
MU40S	-5.28	0.39	8786.0	16.6	908.2	107		271	24.5	627	0.62	4040	88
MU41D	5.73	0.27	2217.5	4.0	63.1	59		111	18	174	0.73	1210	48
MU41S	4.28	0.00	1130.8	3.0	90.5	78		37.7	6.7	116	0.23	613	64
MU42A	3.66	0.20	3302.1	7.2	295.0	56		314	17.7	403	4.21	1350	46
MU42D	3.74	0.26	2184.2	5.3	143.6	134		83.4	39.1	145	0.53	1280	110
MU42I	1.26	0.20	3706.0	8.4	537.8	29		115	39.5	264	0.38	2100	24
MU42S	4.18	0.00	793.6	1.9	85.3	68		17.1	5.1	63	0.09	491	56
MU43D	3.02	0.00	2586.6	6.6	159.3	95		94.1	9.4	279	0.39	1260	78
MU43S	1.73	0.22	2258.0	5.7	134.9	71		65.6	5.8	217	1.05	1120	58
MU44	3.44	0.00	17812.1	24.3	2376.1	279		433	123	1410	0.46	10500	229
MU45D	1.53	1.35	48593.9	77.9	7621.8	393		688	418	3970	0.65	28000	322
MU45S	2.98	0.95	2074.9	4.2	134.1	224		56.3	20.6	109	0.09	1310	184
MU46A	2.42	0.00	18222.3	27.7	913.0	76		4950	57	1520	12.5	4310	62
MU46D	5.44	0.90	28407.8	40.4	966.3	88		8980	94	2520	7.7	5980	72
MU46S	6.23	0.60	7426.7	13.0	333.2	na		1560	34	851	2	1800	-999
MU47	1.61	0.75	4816.8	12.0	308.3	345		84.5	15	346	0.86	2750	283
MU48	-2.02	0.36	14594.9	25.3	1530.3	26		1230	24	1330	0.86	5850	22
MU49	4.31	0.27	1447.2	2.3	88.2	90		64.9	7.7	136	2.09	771	74
MU51	0.23	0.54	5581.4	13.5	274.4	84		209	27.5	576	3.81	2460	69
MU52A	-1.09	0.30	2852.3	5.9	89.4			129	9	253	2.1	1220	0
MU52D	0.85	0.48	7166.2	12.7	362.1	251		1720	29	653	2.2	1780	206
MU52S	0.91	0.21	3179.2	7.3	162.1	51		183	14.5	313	1.66	1390	42
MU53	3.38	0.14	4922.0	16.6	412.7	109		98.7	18	389	0.9	2810	89

Bore ID	*Electron balance*	*F (mg/L)*	*Cl (mg/L)*	*Br (mg/L)*	*SO4 (mg/L)*	*HCO3 (mg/L)*	*CO3 (mg/L)*	*Ca (mg/L)*	*K (mg/L)*	*Mg (mg/L)*	*Mn (mg/L)*	*Na (mg/L)*	*Alkalinity (mg CaCO3/L)*
MU54D	2.30	0.57	684.1	1.6	48.2	207		69.3	8.3	41.3	0.15	411	170
MU54S	2.32	0.25	2011.7	3.5	122.8	200		37.3	2.7	185	0.08	1110	164
MU55D	4.00	0.36	2258.5	4.8	219.4	75		107	8.5	245	0.404	1140	61
MU55S	3.46	0.17	1529.5	2.9	93.5	59		34.1	9.7	110	0.002	884	49
MU56D	2.87	0.06	380.3	0.8	22.4	38		11.5	2.1	29.4	0.012	218	31
MU57D	6.44	0.17	4608.8	12.5	380.9	392		160	37.2	381	1.79	2860	321
MU57S	5.84	0.00	3062.9	8.1	120.6	305		104	26.5	238	0.346	1850	250
MU58D	3.92	1.12	12242.6	20.9	937.4	37		695	14	1240	1.81	5920	31
MU58S	4.66	0.00	12497.9	21.4	852.4	38		771	5.5	1290	2.97	6010	31
MU59D	4.55	1.26	31798.5	53.9	3232.0	86		1740	150	2670	3.05	17200	70
MU59I	4.49	0.00	13125.6	22.6	1449.8	95		973	72.5	1140	1.39	6810	78
MU59S	3.12	0.60	4319.2	6.0	809.9	251		293	22.5	470	0.18	2260	206
MU60D	0.17	0.00	14583.4	23.0	2678.2	246		867	61	1530	0.78	6950	202
MU60S	4.26	1.98	13900.9	24.7	1650.0	160		1350	35	1770	0.74	5820	131
MU61D	3.12	0.00	20397.8	37.6	728.6	90		4930	39.5	1770	4.31	5450	74
MU61I	-0.30	0.60	4467.5	10.3	220.8	117		425	11	361	0.43	1850	96
MU61S	1.60	0.56	3449.4	8.7	198.5	106		129	7	314	0.21	1700	87
MU62D	3.76	0.00	3476.8	11.8	739.7	116		275	25.1	294	0.848	1980	95
MU62I	3.13	0.10	2121.2	5.4	363.1			117	17	180	0.412	1170	0
MU62S	2.16	0.07	1229.4	2.7	61.8	25		42.7	5.7	114	0.042	606	20
MU63D	-4.04	0.35	3132.4	7.6	727.8	67		183	28	207	0.56	1610	55
MU63S	0.51	0.81	1262.0	3.1	283.2			47.5	6.5	98.5	0.22	720	0
MU64D	2.69	0.10	3045.2	10.2	238.8	47		214	14.6	244	1.24	1510	38

Bore ID	*Electron balance*	*F (mg/L)*	*Cl (mg/L)*	*Br (mg/L)*	*SO4 (mg/L)*	*HCO3 (mg/L)*	*CO3 (mg/L)*	*Ca (mg/L)*	*K (mg/L)*	*Mg (mg/L)*	*Mn (mg/L)*	*Na (mg/L)*	*Alkalinity (mg CaCO3/L)*
MU64I	3.96	0.15	2304.3	5.6	174.6	70		51.1	11	197	0.394	1300	58
MU64S	2.89	0.14	882.6	1.4	233.8			45.2	3.7	77.2	0.258	525	0
MU65D	1.63	0.28	1645.1	4.0	111.1	115		70.9	13.2	198	1.39	743	94
MU65S	2.47	0.13	1122.2	2.8	72.4	41		38.5	3.9	131	0.454	523	34
MU66D	2.28	0.14	1915.0	4.2	183.3	96		75.8	5.9	163	0.394	1030	79
MU66S	4.15	0.11	2407.3	5.2	198.0	107		76.6	6	206	0.112	1360	88
MU67D	-0.62	0.16	2234.7	5.8	90.1	263		507	14.1	33.6	-0.002	922	215
MU67I	3.40	0.30	2444.8	6.1	206.8	67		136	11.6	285	1.21	1130	55
MU67S	2.71	0.40	1718.8	4.3	101.9	89		75.3	6.8	213	0.682	771	73
MU68D	3.47	0.18	2070.5	5.2	207.9	56		78.5	9.9	255	1.19	992	46
MU68S	1.91	0.09	954.1	2.4	72.2	46		32.1	4.1	101	0.41	467	38
MU69	0.32	0.75	14569.8	26.8	603.9	306		171	76	919	1.58	7950	251
MU70	3.84	0.24	4252.0	13.5	284.0	123		209	24.8	511	2.75	1960	101
MU71	4.54	2.48	914.0	1.6	69.4	310		8.3	16.1	21.6	0.01	760	254
MU72	4.88	0.29	5053.1	17.4	346.5	126		135	7.7	583	2	2580	103
Muir1	0.42	0.00	25619.9	26.1	6071.2	301		1520	270	2220	1.1	13800	247
Muir2	4.83	1.70	35228.4	34.5	5386.1	506	1.0	1540	360	3100	1.1	20500	416
Muir3	-2.24	0.00	38959.5	36.3	6260.9	433	1.0	1510	400	3260	1.1	19200	356
Muir4	0.41	0.00	15158.2	14.6	3296.3	649		1060	155	1300	0.6	8040	533
PM01	1.92	0.44	12356.0	21.2	868.0	33		740	66.5	870	1.03	6250	27
PM02	4.26	0.30	4439.1	14.6	267.9	127		124	10.9	537	1.25	2160	104
PM03	4.45	0.16	1529.3	3.8	163.5	87		44.5	9.4	132	0.184	901	72
PM04	1.77	0.23	1687.6	6.0	232.1	43		65.5	10.4	131	0.216	939	35

Bore ID	*Electron balance*	*F (mg/L)*	*Cl (mg/L)*	*Br (mg/L)*	*SO4 (mg/L)*	*HCO3 (mg/L)*	*CO3 (mg/L)*	*Ca (mg/L)*	*K (mg/L)*	*Mg (mg/L)*	*Mn (mg/L)*	*Na (mg/L)*	*Alkalinity (mg CaCO3/L)*
PM10	5.55	0.17	2623.8	6.3	329.5	32		47.4	24.6	164	0.428	1720	27
PM12	1.01	0.30	6313.9	23.1	847.2			203	17	553	0.42	3300	0

Table 11 Results of trace metals in groundwater. Negative values represent the detection limits with -0.0001 representing a detection limit of 0.0001 of designated unit

Bore ID	*Au (mg/L)*	*Pt (mg/L)*	*Pd (mg/L)*	*Ag (mg/L)*	*Al (mg/L)*	*As (mg/L)*	*B (mg/L)*	*Ba (mg/L)*	*Be (mg/L)*	*Bi (mg/L)*	*Cd (mg/L)*	*Ce (mg/L)*	*Co (mg/L)*	*Cr (mg/L)*
Forty-acre 1	-0.00005	-0.0001	-0.0005	-0.001	0.46	-0.01	0.12	0.15	-0.001	-0.001	-0.002	0.073	0.046	-0.01
Forty-acre 2	-0.00005	-0.0001	-0.0005	-0.001	0.12	-0.01	0.16	0.42	-0.001	-0.001	-0.002	0.002	0.008	-0.01
Forty-acre 3	-0.00005	-0.0001	-0.0005	-0.001	-0.02	-0.01	0.14	0.09	-0.001	-0.001	-0.002	-0.001	0.008	-0.01
Forty-acre 4	-0.00005	-0.0001	-0.0005	-0.001	0.02	-0.01	0.08	0.2	-0.001	-0.001	-0.002	-0.001	0.006	-0.01
MU01	-0.00005	-0.0001	-0.0005	-0.001	-0.01	-0.01	0.15	0.04	-0.001	-0.001	-0.002	-0.001	0.035	-0.005
MU02	-0.00005	-0.0001	0.001	-0.001	-0.01	-0.01	0.1	0.16	-0.001	-0.001	-0.002	-0.001	0.03	-0.005
MU03D	-0.00005	-0.0001	0.0015	-0.001	-0.05	0.01	1.3	0.02	-0.001	-0.001	-0.002	0.001	-0.02	0.01
MU03S	-0.00005	-0.0001	-0.0005	-0.001	2.02	-0.01	0.07	0.02	-0.001	-0.001	-0.002	0.003	-0.005	0.005
MU04	-0.00005	-0.0001	-0.0005	-0.001	-0.01	-0.01	0.09	0.12	-0.001	-0.001	-0.002	-0.001	0.03	-0.005
MU05D	-0.00001	-0.00005	-0.0005	-0.001	-0.01	0.01	0.07	0.05	-0.001	-0.001	-0.01	-0.001	0.01	0.01
MU05S	-0.00001	-0.00005	-0.0005	-0.001	0.04	-0.01	0.08	0.03	-0.001	-0.001	-0.01	0.001	-0.01	-0.01
MU06	-0.00005	-0.0001	0.002	-0.001	0.05	0.01	0.15	0.06	-0.001	-0.001	-0.002	-0.001	0.06	0.01
MU07D	-0.00001	-0.00005	-0.0005	-0.001	0.35	-0.01	-0.05	0.41	-0.001	-0.001	-0.01	-0.001	0.02	0.15
MU07S	-0.00001	-0.00005	-0.0005	-0.001	4.25	0.01	0.45	0.03	-0.001	-0.001	-0.01	0.035	0.02	0.1
MU08	-0.00005	-0.0001	-0.0005	-0.001	0.1	-0.01	0.45	0.11	-0.001	-0.001	-0.002	-0.001	-0.02	0.04
MU09D	-0.00001	-0.00005	-0.0005	-0.001	-0.05	0.01	0.2	0.05	-0.001	-0.001	-0.01	-0.001	0.02	0.15
MU09S	-0.00001	-0.00005	-0.0005	-0.001	0.25	0.01	0.1	0.04	-0.001	-0.001	-0.01	-0.001	0.04	0.05
MU10D	-0.00001	-0.00005	-0.0005	-0.001	0.01	-0.01	0.25	0.14	-0.001	-0.001	-0.01	-0.001	-0.01	0.02
MU10I	-0.00005	-0.0001	-0.0005	-0.001	0.2	-0.01	0.3	0.14	-0.001	-0.001	0.004	-0.001	0.02	0.02
MU10S	-0.00001	-0.00005	-0.0005	-0.001	0.31	-0.01	0.07	-0.01	-0.001	-0.001	-0.01	-0.001	0.01	-0.01
MU11D	-0.00001	-0.00005	-0.0005	-0.001	-0.01	-0.01	0.15	0.05	-0.001	-0.001	-0.01	-0.001	-0.01	0.02

Bore ID	*Au (mg/L)*	*Pt (mg/L)*	*Pd (mg/L)*	*Ag (mg/L)*	*Al (mg/L)*	*As (mg/L)*	*B (mg/L)*	*Ba (mg/L)*	*Be (mg/L)*	*Bi (mg/L)*	*Cd (mg/L)*	*Ce (mg/L)*	*Co (mg/L)*	*Cr (mg/L)*
MU11I	-0.00001	-0.00005	-0.0005	-0.001	0.03	-0.01	0.28	0.04	-0.001	-0.001	-0.01	-0.001	0.01	0.03
MU12A	-0.00005	-0.0001	-0.0005	-0.001	-0.01	-0.01	0.24	0.09	-0.001	-0.001	-0.002	-0.001	-0.005	-0.005
MU12D	-0.00001	-0.00005	-0.0005	-0.001	0.2	-0.01	0.3	0.04	-0.001	-0.001	-0.01	-0.001	-0.02	0.1
MU12S	-0.00001	-0.00005	-0.0005	-0.001	0.01	0.15	0.16	0.04	-0.001	-0.001	-0.01	0.002	0.01	0.02
MU13	-0.00005	-0.0001	-0.0005	-0.001	1.23	-0.01	0.11	0.14	-0.001	-0.001	-0.002	0.008	0.015	-0.005
MU14D	-0.00001	-0.00005	-0.0005	-0.001	0.05	-0.01	0.23	0.03	-0.001	-0.001	-0.01	-0.001	-0.01	0.01
MU14S	-0.00001	-0.00005	-0.0005	-0.001	0.06	-0.01	0.29	0.05	-0.001	-0.001	-0.01	0.002	0.02	0.01
MU15A	-0.00005	-0.0001	0.0015	-0.001	-0.05	0.01	1.55	0.17	-0.001	-0.001	-0.002	-0.001	-0.02	0.01
MU15D	-0.00001	-0.00005	-0.0005	-0.001	0.02	-0.01	0.21	0.03	-0.001	-0.001	-0.01	-0.001	0.02	-0.01
MU15S	-0.00001	-0.00005	-0.0005	-0.001	5.45	0.01	0.25	0.04	-0.001	-0.001	-0.01	0.046	0.02	0.1
MU16D	-0.00001	-0.00005	-0.0005	-0.001	0.02	-0.01	0.17	0.05	-0.001	-0.001	-0.01	-0.001	-0.01	0.02
MU16S	-0.00001	-0.00005	-0.0005	-0.001	4.5	0.01	0.3	0.04	-0.001	-0.001	-0.01	0.055	-0.02	0.1
MU17	-0.00005	-0.0001	-0.0005	-0.001	0.05	-0.01	0.05	0.04	-0.001	-0.001	-0.002	-0.001	0.06	0.03
MU18D	-0.00001	-0.00005	-0.0005	-0.001	-0.01	-0.01	0.07	0.17	-0.001	-0.001	-0.01	-0.001	0.01	0.02
MU18S	-0.00001	-0.00005	-0.0005	-0.001	0.01	-0.01	0.04	0.04	-0.001	-0.001	-0.01	-0.001	0.01	0.01
MU19D	-0.00005	-0.0001	-0.0005	-0.001	-0.1	-0.01	0.25	0.06	-0.001	-0.001	-0.002	-0.001	-0.02	-0.02
MU22D	-0.00005	-0.0001	-0.0005	-0.001	0.79	-0.01	0.15	0.05	-0.001	-0.001	-0.002	0.006	-0.005	-0.005
MU22S	-0.00005	-0.0001	-0.0005	-0.001	0.2	-0.01	0.1	0.06	-0.001	-0.001	-0.002	0.037	0.02	0.08
MU23D	-0.00001	-0.00005	-0.0005	-0.001	0.2	-0.01	0.1	0.04	-0.001	-0.001	-0.01	-0.001	0.02	0.1
MU23S	-0.00001	-0.00005	-0.0005	-0.001	0.3	-0.01	0.07	0.21	-0.001	-0.001	-0.01	0.005	-0.01	0.01
MU24	-0.00005	-0.0001	-0.0005	-0.001	-0.01	-0.01	0.07	0.05	-0.001	-0.001	-0.002	-0.001	0.01	-0.005
MU25	-0.00005	-0.0001	-0.0005	-0.001	-0.01	-0.01	0.04	0.32	-0.001	-0.001	-0.002	-0.001	0.02	-0.005
MU26	-0.00005	-0.0001	-0.0005	-0.001	-0.01	-0.01	0.04	0.1	-0.001	-0.001	-0.002	0.004	0.015	-0.005

Bore ID	*Au (mg/L)*	*Pt (mg/L)*	*Pd (mg/L)*	*Ag (mg/L)*	*Al (mg/L)*	*As (mg/L)*	*B (mg/L)*	*Ba (mg/L)*	*Be (mg/L)*	*Bi (mg/L)*	*Cd (mg/L)*	*Ce (mg/L)*	*Co (mg/L)*	*Cr (mg/L)*
MU27D	-0.00001	-0.00005	-0.0005	-0.001	-0.01	-0.01	0.11	0.07	-0.001	-0.001	-0.01	-0.001	-0.01	0.01
MU27S	-0.00001	-0.00005	-0.0005	-0.001	0.25	-0.01	0.15	0.04	-0.001	-0.001	-0.01	-0.001	0.02	0.05
MU28D	-0.00001	-0.00005	-0.0005	-0.001	0.02	-0.01	0.15	0.04	-0.001	-0.001	-0.01	-0.001	-0.01	0.02
MU28S	-0.00001	-0.00005	-0.0005	-0.001	0.2	-0.01	0.13	0.01	-0.001	-0.001	-0.01	0.001	0.01	-0.01
MU29D	-0.00001	-0.00005	-0.0005	-0.001	-0.05	0.01	0.25	0.06	-0.001	-0.001	-0.01	-0.001	0.04	0.1
MU29S	-0.00001	-0.00005	-0.0005	-0.001	0.1	0.01	0.25	0.07	-0.001	-0.001	-0.01	-0.001	0.04	0.1
MU30D	-0.00001	-0.00005	-0.0005	-0.001	0.1	-0.01	0.2	0.25	-0.001	-0.001	-0.01	-0.001	0.06	0.2
MU30S	-0.00001	-0.00005	-0.0005	-0.001	-0.01	-0.01	0.09	0.05	-0.001	-0.001	-0.01	-0.001	-0.01	0.01
MU31D	-0.00001	-0.00005	-0.0005	-0.001	0.15	0.02	0.1	0.1	-0.001	-0.001	-0.01	0.006	-0.02	0.1
MU31S	-0.00001	-0.00005	-0.0005	-0.001	0.35	-0.01	0.05	0.06	-0.001	-0.001	-0.01	0.002	0.02	-0.05
MU32	-0.00005	-0.0001	0.0005	-0.001	-0.01	-0.01	0.13	0.05	-0.001	-0.001	-0.002	-0.001	-0.005	-0.005
MU33D	-0.00001	-0.00005	-0.0005	-0.001	0.15	-0.01	0.15	0.07	-0.001	-0.001	-0.01	-0.001	-0.02	-0.05
MU33S	-0.00001	-0.00005	-0.0005	-0.001	0.14	-0.01	0.09	0.08	-0.001	-0.001	-0.01	0.016	0.01	0.02
MU34	-0.00005	-0.0001	-0.0005	-0.001	-0.01	-0.01	0.11	0.05	-0.001	-0.001	0.002	-0.001	-0.005	-0.005
MU35	-0.00005	-0.0001	-0.0005	-0.001	-0.01	-0.01	0.04	0.03	-0.001	-0.001	-0.002	-0.001	0.015	-0.005
MU36D	-0.00001	-0.00005	-0.0005	-0.001	-0.01	-0.01	0.05	0.05	-0.001	-0.001	-0.01	0.002	-0.01	0.01
MU36S	-0.00001	-0.00005	-0.0005	-0.001	0.03	-0.01	0.05	0.02	-0.001	-0.001	-0.01	0.003	-0.01	0.01
MU37D	-0.00001	-0.00005	0.0005	-0.001	-0.01	-0.01	0.32	0.05	-0.001	-0.001	-0.01	-0.001	0.01	0.02
MU37I	-0.00001	-0.00005	-0.0005	-0.001	0.09	-0.01	0.28	0.06	-0.001	-0.001	-0.01	0.003	-0.01	0.01
MU37S	-0.00001	-0.00005	-0.0005	-0.001	-0.01	0.05	0.14	0.13	-0.001	-0.001	-0.01	0.006	0.01	0.01
MU38D	-0.00001	-0.00005	-0.0005	-0.001	1.88	-0.01	0.04	0.01	-0.001	-0.001	-0.01	0.005	0.01	0.02
MU38S	-0.00001	-0.00005	-0.0005	-0.001	0.05	-0.01	0.08	-0.01	-0.001	-0.001	-0.01	0.008	0.01	0.01
MU39	-0.00005	-0.0001	-0.0005	-0.001	1	-0.01	0.05	0.05	-0.001	-0.001	-0.002	0.029	0.02	0.07

Bore ID	*Au (mg/L)*	*Pt (mg/L)*	*Pd (mg/L)*	*Ag (mg/L)*	*Al (mg/L)*	*As (mg/L)*	*B (mg/L)*	*Ba (mg/L)*	*Be (mg/L)*	*Bi (mg/L)*	*Cd (mg/L)*	*Ce (mg/L)*	*Co (mg/L)*	*Cr (mg/L)*
MU40D	-0.00001	-0.00005	-0.0005	-0.001	0.15	-0.01	0.15	0.04	-0.001	-0.001	-0.01	-0.001	0.06	0.1
MU40S	-0.00001	-0.00005	-0.0005	-0.001	0.05	-0.01	0.15	0.04	-0.001	-0.001	-0.01	0.002	-0.02	0.15
MU41D	-0.00001	-0.00005	-0.0005	-0.001	0.05	-0.01	0.11	0.04	-0.001	-0.001	-0.01	-0.001	-0.01	0.02
MU41S	-0.00001	-0.00005	-0.0005	-0.001	0.04	-0.01	0.11	0.06	-0.001	-0.001	-0.01	0.001	0.01	0.01
MU42A	-0.00005	-0.0001	0.0005	-0.001	-0.01	-0.01	0.05	0.28	-0.001	-0.001	-0.002	-0.001	0.015	0.01
MU42D	-0.00001	-0.00005	-0.0005	-0.001	0.02	-0.01	0.05	0.08	-0.001	-0.001	-0.01	-0.001	-0.01	-0.01
MU42I	-0.00001	-0.00005	-0.0005	-0.001	0.25	0.02	0.15	0.1	-0.001	-0.001	-0.01	0.006	0.02	0.1
MU42S	-0.00001	-0.00005	-0.0005	-0.001	-0.01	0.01	0.09	0.07	-0.001	-0.001	-0.01	-0.001	0.01	0.01
MU43D	-0.00001	-0.00005	-0.0005	-0.001	0.04	-0.01	0.08	0.22	-0.001	-0.001	-0.01	-0.001	-0.01	0.01
MU43S	-0.00001	-0.00005	-0.0005	-0.001	-0.01	-0.01	0.07	0.1	-0.001	-0.001	-0.01	-0.001	0.02	0.01
MU44	-0.00005	-0.0001	-0.0005	-0.001	0.1	0.01	0.8	0.04	-0.001	-0.001	-0.002	-0.001	-0.02	-0.02
MU45D	-0.00001	-0.00005	-0.0005	-0.001	0.4	0.04	1.6	0.04	-0.001	-0.001	-0.01	-0.001	-0.1	0.2
MU45S	-0.00001	-0.00005	-0.0005	-0.001	-0.01	-0.01	0.07	0.06	-0.001	-0.001	-0.01	-0.001	0.01	0.02
MU46A	-0.00005	-0.0001	-0.0005	-0.001	0.1	0.02	0.05	0.72	-0.001	-0.001	-0.002	-0.001	0.06	0.02
MU46D	-0.00001	-0.00005	-0.0005	-0.001	-0.2	0.02	-0.2	0.14	-0.001	-0.001	-0.01	-0.001	-0.1	0.2
MU46S	-0.00001	-0.00005	-0.0005	-0.001	0.25	-0.01	0.1	0.22	-0.001	-0.001	-0.01	-0.001	0.06	0.15
MU47	-0.00005	-0.0001	-0.0005	-0.001	0.1	-0.01	0.5	0.07	-0.001	-0.001	-0.002	-0.001	0.04	-0.02
MU48	-0.00005	-0.0001	-0.0005	-0.001	0.2	0.01	0.2	0.06	-0.001	-0.001	-0.002	0.016	-0.02	-0.02
MU49	-0.00005	-0.0001	-0.0005	-0.001	-0.01	-0.01	0.07	0.06	-0.001	-0.001	0.008	-0.001	0.02	-0.005
MU51	-0.00005	-0.0001	-0.0005	-0.001	0.1	-0.01	0.15	0.05	-0.001	-0.001	-0.002	-0.001	0.06	-0.02
MU52A	-0.00005	-0.0001	-0.0005	-0.001	0.1	-0.01	0.1	0.18	-0.001	-0.001	0.002	0.002	-0.02	-0.02
MU52D	-0.00001	-0.00005	-0.0005	-0.001	0.2	-0.01	0.15	0.1	-0.001	-0.001	-0.01	-0.001	0.06	0.2
MU52S	-0.00001	-0.00005	0.0005	0.002	0.1	-0.01	0.08	0.15	-0.001	-0.001	-0.01	0.001	0.01	-0.01

Bore ID	*Au (mg/L)*	*Pt (mg/L)*	*Pd (mg/L)*	*Ag (mg/L)*	*Al (mg/L)*	*As (mg/L)*	*B (mg/L)*	*Ba (mg/L)*	*Be (mg/L)*	*Bi (mg/L)*	*Cd (mg/L)*	*Ce (mg/L)*	*Co (mg/L)*	*Cr (mg/L)*
MU53	-0.00005	-0.0001	-0.0005	-0.001	-0.01	-0.01	0.04	0.04	-0.001	-0.001	-0.002	-0.001	0.02	-0.005
MU54D	-0.00001	-0.00005	-0.0005	-0.001	0.12	-0.01	0.05	0.07	-0.001	-0.001	-0.01	-0.001	-0.01	0.01
MU54S	-0.00001	-0.00005	-0.0005	-0.001	-0.01	-0.01	0.05	0.03	-0.001	-0.001	-0.01	0.005	-0.01	0.02
MU55D	-0.00005	-0.0001	-0.0005	-0.001	-0.01	-0.01	0.08	0.06	-0.001	-0.001	-0.002	-0.001	-0.005	-0.005
MU55S	-0.00005	-0.0001	-0.0005	-0.001	0.47	-0.01	0.08	0.03	-0.001	-0.001	-0.002	0.001	-0.005	-0.005
MU56D	-0.00005	-0.0001	-0.0005	-0.001	0.02	-0.01	0.04	0.01	-0.001	-0.001	-0.002	0.001	-0.005	-0.005
MU57D	-0.00005	-0.0001	0.001	-0.001	-0.01	-0.01	0.33	0.19	-0.001	-0.001	-0.002	-0.001	0.015	0.005
MU57S	-0.00005	-0.0001	-0.0005	-0.001	0.01	-0.01	0.2	0.12	-0.001	-0.001	-0.002	0.019	-0.005	0.005
MU58D	-0.00005	-0.0001	-0.0005	-0.001	-0.1	0.01	0.25	0.07	-0.001	-0.001	0.004	-0.001	0.06	-0.02
MU58S	-0.00005	-0.0001	-0.0005	-0.001	0.1	0.01	0.15	0.11	-0.001	-0.001	-0.002	-0.001	-0.02	-0.02
MU59D	-0.00005	-0.0001	-0.0005	-0.001	-0.1	0.02	0.15	0.05	-0.001	-0.001	-0.002	-0.001	-0.02	-0.02
MU59I	-0.00005	-0.0001	-0.0005	-0.001	0.1	0.01	0.25	0.03	-0.001	-0.001	-0.002	-0.001	0.02	0.02
MU59S	-0.00005	-0.0001	-0.0005	-0.001	-0.1	-0.01	0.35	0.2	-0.001	-0.001	-0.002	0.007	0.04	0.02
MU60D	-0.00005	-0.0001	-0.0005	-0.001	0.1	0.01	0.45	0.04	-0.001	-0.001	0.002	-0.001	-0.02	-0.02
MU60S	-0.00005	-0.0001	-0.0005	-0.001	0.1	0.01	0.2	0.06	-0.001	-0.001	-0.002	0.002	-0.02	-0.02
MU61D	-0.00005	-0.0001	-0.0005	-0.001	0.2	0.02	0.1	0.15	-0.001	-0.001	-0.002	-0.001	-0.02	-0.02
MU61I	-0.00005	-0.0001	-0.0005	-0.001	0.1	-0.01	0.2	0.08	-0.001	-0.001	-0.002	-0.001	0.02	-0.02
MU61S	-0.00005	-0.0001	-0.0005	-0.001	0.2	-0.01	0.2	0.11	-0.001	-0.001	0.002	-0.001	-0.02	-0.02
MU62D	-0.00005	-0.0001	0.0005	-0.001	-0.01	-0.01	0.3	0.02	-0.001	-0.001	-0.002	-0.001	-0.005	-0.005
MU62I	-0.00005	-0.0001	-0.0005	-0.001	0.1	0.1	0.19	0.05	-0.001	-0.001	-0.002	0.004	0.11	-0.005
MU62S	-0.00005	-0.0001	-0.0005	-0.001	0.12	-0.01	0.18	0.04	-0.001	-0.001	-0.002	0.001	-0.005	-0.005
MU63D	-0.00005	-0.0001	-0.0005	-0.001	-0.1	-0.01	0.35	0.04	-0.001	-0.001	0.004	0.002	0.04	-0.02
MU63S	-0.00005	-0.0001	-0.0005	-0.001	10.1	-0.01	0.1	0.05	-0.001	-0.001	0.002	0.009	0.04	0.02

Bore ID	*Au (mg/L)*	*Pt (mg/L)*	*Pd (mg/L)*	*Ag (mg/L)*	*Al (mg/L)*	*As (mg/L)*	*B (mg/L)*	*Ba (mg/L)*	*Be (mg/L)*	*Bi (mg/L)*	*Cd (mg/L)*	*Ce (mg/L)*	*Co (mg/L)*	*Cr (mg/L)*
MU64D	-0.00005	-0.0001	-0.0005	-0.001	-0.01	0.02	0.12	0.07	-0.001	-0.001	-0.002	0.002	0.005	0.005
MU64I	-0.00005	-0.0001	-0.0005	-0.001	-0.01	0.01	0.15	0.08	-0.001	-0.001	-0.002	-0.001	0.01	-0.005
MU64S	-0.00005	-0.0001	-0.0005	-0.001	14.2	-0.01	0.02	0.05	-0.001	-0.001	0.002	0.024	0.065	0.01
MU65D	-0.00005	-0.0001	-0.0005	-0.001	-0.01	-0.01	0.05	0.1	-0.001	-0.001	-0.002	-0.001	0.04	-0.005
MU65S	-0.00005	-0.0001	-0.0005	-0.001	0.03	-0.01	0.05	0.12	-0.001	-0.001	-0.002	0.003	-0.005	-0.005
MU66D	-0.00005	-0.0001	-0.0005	-0.001	-0.01	-0.01	0.08	0.05	-0.001	-0.001	-0.002	-0.001	0.005	-0.005
MU66S	-0.00005	-0.0001	-0.0005	-0.001	-0.01	-0.01	0.07	0.04	-0.001	-0.001	-0.002	0.001	-0.005	-0.005
MU67D	-0.00005	-0.0001	0.0015	-0.001	-0.01	-0.01	0.01	0.09	-0.001	-0.001	-0.002	-0.001	-0.005	-0.005
MU67I	-0.00005	-0.0001	-0.0005	-0.001	-0.01	0.03	0.06	0.15	-0.001	-0.001	-0.002	-0.001	0.48	-0.005
MU67S	-0.00005	-0.0001	-0.0005	-0.001	0.01	-0.01	0.05	0.07	-0.001	-0.001	-0.002	-0.001	-0.005	-0.005
MU68D	-0.00005	-0.0001	-0.0005	-0.001	-0.01	0.24	0.08	0.14	-0.001	-0.001	-0.002	-0.001	0.615	-0.005
MU68S	-0.00005	-0.0001	-0.0005	-0.001	-0.01	-0.01	0.05	0.05	-0.001	-0.001	-0.002	0.002	-0.005	-0.005
MU69	-0.00005	-0.0001	0.002	-0.001	-0.05	0.01	0.3	0.11	-0.001	-0.001	-0.002	-0.001	0.02	0.01
MU70	-0.00005	-0.0001	0.0005	-0.001	-0.01	-0.01	0.04	0.06	-0.001	-0.001	-0.002	-0.001	0.03	-0.005
MU71	-0.00005	-0.0001	-0.0005	-0.001	0.03	-0.01	0.56	0.05	-0.001	-0.001	-0.002	-0.001	-0.005	-0.005
MU72	-0.00005	-0.0001	0.0005	-0.001	-0.01	-0.01	0.06	0.12	-0.001	-0.001	-0.002	0.001	0.035	-0.005
Muir1	-0.00005	-0.0001	0.0015	-0.001	-0.5	0.02	2.4	0.14	-0.001	-0.001	-0.002	-0.001	-0.005	-0.1
Muir2	-0.00005	-0.0001	0.001	-0.001	-0.5	0.03	1.2	0.22	-0.001	-0.001	-0.002	-0.001	0.005	-0.1
Muir3	-0.00005	-0.0001	0.001	-0.001	-0.5	0.03	1.2	0.17	-0.001	-0.001	-0.002	0.001	0.005	-0.1
Muir4	-0.00005	-0.0001	-0.0005	-0.001	-0.5	0.01	1	0.15	-0.001	-0.001	-0.002	-0.001	-0.005	-0.1
PM01	-0.00005	-0.0001	0.0045	-0.001	0.1	0.01	0.1	0.14	-0.001	-0.001	-0.002	0.015	-0.02	0.01
PM02	-0.00005	-0.0001	-0.0005	-0.001	-0.01	-0.01	0.14	0.06	-0.001	-0.001	-0.002	-0.001	0.02	-0.005
PM03	-0.00005	-0.0001	-0.0005	-0.001	-0.01	-0.01	0.12	0.06	-0.001	-0.001	-0.002	0.002	-0.005	-0.005

Bore ID	*Au (mg/L)*	*Pt (mg/L)*	*Pd (mg/L)*	*Ag (mg/L)*	*Al (mg/L)*	*As (mg/L)*	*B (mg/L)*	*Ba (mg/L)*	*Be (mg/L)*	*Bi (mg/L)*	*Cd (mg/L)*	*Ce (mg/L)*	*Co (mg/L)*	*Cr (mg/L)*
PM04	-0.00005	-0.0001	-0.0005	-0.001	0.02	-0.01	0.14	0.06	-0.001	-0.001	-0.002	0.002	-0.005	-0.005
PM10	-0.00005	-0.0001	-0.0005	-0.001	0.12	-0.01	0.14	0.03	-0.001	-0.001	-0.002	-0.001	-0.005	-0.005
PM12	-0.00005	-0.0001	0.001	-0.001	15.1	0.01	0.4	0.03	0.001	-0.001	-0.002	0.091	-0.02	0.02

Table 12 Results of trace metals in groundwater continued. Negative values represent the detection limits with -0.0001 representing a detection limit of 0.0001 of designated unit.

Bore ID	*Cs (mg/L)*	*Cu (mg/L)*	*Dy (mg/L)*	*Er (mg/L)*	*Eu (mg/L)*	*Fe (mg/L)*	*Ga (mg/L)*	*Gd (mg/L)*	*Ge (mg/L)*	*Hf (mg/L)*	*Hg (mg/L)*	*Ho (mg/L)*	*In (mg/L)*	*La (mg/L)*	*Li (mg/L)*
Forty-acre 1	-0.001	-0.01	0.003	0.001	-0.001	7.4	-0.001	0.004	-0.002		-0.0005	-0.001	-0.001	0.031	0.02
Forty-acre 2	-0.001	-0.01	-0.001	-0.001	-0.001	10.3	-0.001	-0.001	-0.002		-0.0005	-0.001	-0.001	0.001	-0.01
Forty-acre 3	-0.001	-0.01	-0.001	-0.001	-0.001	1.86	-0.001	-0.001	-0.002		-0.0005	-0.001	-0.001	-0.001	-0.01
Forty-acre 4	-0.001	-0.01	-0.001	-0.001	-0.001	17	-0.001	-0.001	-0.002		-0.0005	-0.001	-0.001	-0.001	-0.01
MU01	-0.001	0.002	-0.001	-0.001	-0.001	0.03	-0.001	-0.001	-0.002		0.0005	-0.001	-0.001	-0.001	0.01
MU02	-0.001	0.002	-0.001	-0.001	-0.001	0.02	-0.001	-0.001	-0.002		-0.0005	-0.001	-0.001	-0.001	0.02
MU03D	-0.001	-0.01	-0.001	-0.001	-0.001	13.3	-0.001	-0.001	-0.002		-0.0005	-0.001	-0.001	-0.001	0.02
MU03S	-0.001	0.004	-0.001	-0.001	-0.001	17.5	-0.001	-0.001	-0.002		-0.0005	-0.001	-0.001	0.001	-0.01
MU04	-0.001	0.002	-0.001	-0.001	-0.001	9.19	-0.001	-0.001	-0.002		-0.0005	-0.001	-0.001	-0.001	0.03
MU05D	-0.001	-0.01	-0.001	-0.001	-0.001	4.5	-0.005	-0.005	-0.1	-0.01	-0.001	-0.001	-0.001	-0.001	-0.01
MU05S	-0.001	-0.01	-0.001	-0.001	-0.001	0.96	-0.005	-0.005	-0.1	-0.01	-0.001	-0.001	-0.001	-0.001	-0.01
MU06	-0.001	0.01	-0.001	-0.001	-0.001	0.1	-0.001	-0.001	-0.002		-0.0005	-0.001	-0.001	-0.001	0.03
MU07D	0.013	-0.02	-0.001	-0.001	-0.001	0.25	-0.005	-0.005	-0.1	-0.01	-0.001	-0.001	-0.001	-0.001	0.31
MU07S	-0.001	-0.02	-0.001	-0.001	-0.001	28.2	-0.005	-0.005	-0.1	-0.01	-0.001	-0.001	-0.001	0.018	0.1
MU08	-0.001	-0.01	-0.001	-0.001	-0.001	8.44	-0.001	-0.001	-0.002		-0.0005	-0.001	-0.001	-0.001	0.11
MU09D	-0.001	0.02	-0.001	-0.001	-0.001	0.5	-0.005	-0.005	-0.1	-0.01	-0.001	-0.001	-0.001	-0.001	0.07
MU09S	-0.001	0.06	-0.001	-0.001	-0.001	0.2	-0.005	-0.005	-0.1	-0.01	-0.001	-0.001	-0.001	-0.001	0.03
MU10D	-0.001	-0.01	-0.001	-0.001	-0.001	0.78	-0.005	-0.005	-0.1	-0.01	-0.001	-0.001	-0.001	-0.001	-0.01
MU10I	-0.001	0.02	-0.001	-0.001	-0.001	2.25	-0.001	-0.001	-0.002		-0.0005	-0.001	-0.001	-0.001	-0.01
MU10S	-0.001	-0.01	-0.001	-0.001	-0.001	0.14	-0.005	-0.005	-0.1	-0.01	-0.001	-0.001	-0.001	-0.001	-0.01
MU11D	-0.001	-0.01	-0.001	-0.001	-0.001	3.21	-0.005	-0.005	-0.1	-0.01	-0.001	-0.001	-0.001	-0.001	-0.01

Bore ID	*Cs (mg/L)*	*Cu (mg/L)*	*Dy (mg/L)*	*Er (mg/L)*	*Eu (mg/L)*	*Fe (mg/L)*	*Ga (mg/L)*	*Gd (mg/L)*	*Ge (mg/L)*	*Hf (mg/L)*	*Hg (mg/L)*	*Ho (mg/L)*	*In (mg/L)*	*La (mg/L)*	*Li (mg/L)*
MU11I	-0.001	-0.01	-0.001	-0.001	-0.001	20.2	-0.005	-0.005	-0.1	-0.01	-0.001	-0.001	-0.001	-0.001	0.04
MU12A	-0.001	0.004	-0.001	-0.001	-0.001	85.3	-0.001	-0.001	-0.002		-0.0005	-0.001	-0.001	-0.001	0.15
MU12D	-0.001	-0.02	-0.001	-0.001	-0.001	5.7	-0.005	-0.005	-0.1	-0.01	-0.001	-0.001	-0.001	-0.001	0.16
MU12S	-0.001	-0.01	-0.001	-0.001	-0.001	11.4	-0.005	-0.005	-0.1	-0.01	-0.001	-0.001	-0.001	-0.001	-0.01
MU13	-0.001	0.002	-0.001	-0.001	-0.001	8.82	-0.001	-0.001	-0.002		-0.0005	-0.001	-0.001	0.003	0.03
MU14D	-0.001	-0.01	-0.001	-0.001	-0.001	65.5	-0.005	-0.005	-0.1	-0.01	-0.001	-0.001	-0.001	-0.001	0.04
MU14S	-0.001	-0.01	-0.001	-0.001	-0.001	24.8	-0.005	-0.005	-0.1	-0.01	-0.001	-0.001	-0.001	-0.001	0.02
MU15A	-0.001	0.01	-0.001	-0.001	-0.001	0.16	-0.001	-0.001	-0.002		-0.0005	-0.001	-0.001	-0.001	-0.01
MU15D	-0.001	-0.01	-0.001	-0.001	-0.001	63.5	-0.005	-0.005	-0.1	-0.01	-0.001	-0.001	-0.001	-0.001	0.02
MU15S	-0.001	-0.02	0.001	-0.001	-0.001	70.3	-0.005	-0.005	-0.1	-0.01	-0.001	-0.001	-0.001	0.02	0.08
MU16D	-0.001	-0.01	-0.001	-0.001	-0.001	0.16	-0.005	-0.005	-0.1	-0.01	-0.001	-0.001	-0.001	-0.001	0.02
MU16S	-0.001	-0.02	0.001	-0.001	-0.001	50.4	-0.005	-0.005	-0.1	-0.01	-0.001	-0.001	-0.001	0.023	0.07
MU17	-0.001	0.01	-0.001	-0.001	-0.001	0.2	-0.001	-0.001	-0.002		-0.0005	-0.001	-0.001	-0.001	0.02
MU18D	-0.001	-0.01	-0.001	-0.001	-0.001	31.3	-0.005	-0.005	-0.1	-0.01	-0.001	-0.001	-0.001	-0.001	0.03
MU18S	-0.001	-0.01	-0.001	-0.001	-0.001	2.21	-0.005	-0.005	-0.1	-0.01	-0.001	-0.001	-0.001	-0.001	-0.01
MU19D	-0.001	0.02	0.001	-0.001	-0.001	31.5	-0.001	-0.001	-0.002		-0.0005	-0.001	-0.001	-0.001	0.03
MU22D	-0.001	0.002	-0.001	-0.001	-0.001	15.9	-0.001	-0.001	-0.002		-0.0005	-0.001	-0.001	0.002	0.05
MU22S	-0.001	0.01	0.001	-0.001	-0.001	15.6	-0.001	0.002	-0.002		-0.0005	-0.001	-0.001	0.022	0.03
MU23D	-0.001	-0.02	-0.001	-0.001	-0.001	9.1	-0.005	-0.005	-0.1	-0.01	-0.001	-0.001	-0.001	-0.001	-0.01
MU23S	-0.001	-0.01	-0.001	-0.001	-0.001	9.34	-0.005	-0.005	-0.1	-0.01	-0.001	-0.001	-0.001	0.002	0.02
MU24	-0.001	0.012	-0.001	-0.001	-0.001	41	-0.001	-0.001	-0.002		-0.0005	-0.001	-0.001	-0.001	0.03
MU25	-0.001	0.012	-0.001	-0.001	-0.001	0.03	-0.001	-0.001	-0.002		-0.0005	-0.001	-0.001	-0.001	0.01
MU26	-0.001	0.032	-0.001	-0.001	-0.001	5.91	-0.001	-0.001	-0.002		-0.0005	-0.001	-0.001	-0.001	-0.01

Bore ID	*Cs (mg/L)*	*Cu (mg/L)*	*Dy (mg/L)*	*Er (mg/L)*	*Eu (mg/L)*	*Fe (mg/L)*	*Ga (mg/L)*	*Gd (mg/L)*	*Ge (mg/L)*	*Hf (mg/L)*	*Hg (mg/L)*	*Ho (mg/L)*	*In (mg/L)*	*La (mg/L)*	*Li (mg/L)*
MU27D	-0.001	-0.01	-0.001	-0.001	-0.001	12.7	-0.005	-0.005	-0.1	-0.01	-0.001	-0.001	-0.001	-0.001	0.04
MU27S	-0.001	-0.02	-0.001	-0.001	-0.001	0.4	-0.005	-0.005	-0.1	-0.01	-0.001	-0.001	-0.001	-0.001	-0.01
MU28D	-0.001	-0.01	-0.001	-0.001	-0.001	6.43	-0.005	-0.005	-0.1	-0.01	-0.001	-0.001	-0.001	-0.001	-0.01
MU28S	-0.001	-0.01	-0.001	-0.001	-0.001	3.2	-0.005	-0.005	-0.1	-0.01	-0.001	-0.001	-0.001	-0.001	-0.01
MU29D	-0.001	0.02	-0.001	-0.001	-0.001	55.5	-0.005	-0.005	-0.1	-0.01	-0.001	-0.001	-0.001	-0.001	0.1
MU29S	-0.001	-0.02	-0.001	-0.001	-0.001	10.3	-0.005	-0.005	-0.1	-0.01	-0.001	-0.001	-0.001	-0.001	0.07
MU30D	-0.001	0.04	-0.001	-0.001	-0.001	15.9	-0.005	-0.005	-0.1	-0.01	-0.001	-0.001	-0.001	-0.001	0.12
MU30S	-0.001	-0.01	-0.001	-0.001	-0.001	0.03	-0.005	-0.005	-0.1	-0.01	-0.001	-0.001	-0.001	-0.001	-0.01
MU31D	-0.001	-0.02	-0.001	-0.001	-0.001	67.3	-0.005	-0.005	-0.1	-0.01	-0.001	-0.001	-0.001	0.003	0.13
MU31S	-0.001	-0.02	-0.001	-0.001	-0.001	17	-0.005	-0.005	-0.1	-0.01	-0.001	-0.001	-0.001	0.001	0.04
MU32	-0.001	-0.002	-0.001	-0.001	-0.001	7.43	-0.001	-0.001	-0.002		-0.0005	-0.001	-0.001	-0.001	0.01
MU33D	-0.001	-0.02	-0.001	-0.001	-0.001	25	-0.005	-0.005	-0.1	-0.01	-0.001	-0.001	-0.001	-0.001	0.04
MU33S	-0.001	-0.01	-0.001	-0.001	-0.001	6.47	-0.005	-0.005	-0.1	-0.01	-0.001	-0.001	-0.001	0.007	-0.01
MU34	-0.001	0.002	-0.001	-0.001	-0.001	21.5	-0.001	-0.001	-0.002		-0.0005	-0.001	-0.001	-0.001	-0.01
MU35	-0.001	0.002	-0.001	-0.001	-0.001	0.18	-0.001	-0.001	-0.002		-0.0005	-0.001	-0.001	-0.001	0.01
MU36D	-0.001	-0.01	-0.001	-0.001	-0.001	5.43	-0.005	-0.005	-0.1	-0.01	-0.001	-0.001	-0.001	-0.001	-0.01
MU36S	-0.001	-0.01	-0.001	-0.001	-0.001	0.5	-0.005	-0.005	-0.1	-0.01	-0.001	-0.001	-0.001	0.001	-0.01
MU37D	-0.001	-0.01	-0.001	-0.001	-0.001	7	-0.005	-0.005	-0.1	-0.01	-0.001	-0.001	-0.001	-0.001	0.08
MU37I	-0.001	-0.01	-0.001	-0.001	-0.001	40.7	-0.005	-0.005	-0.1	-0.01	-0.001	-0.001	-0.001	-0.001	0.08
MU37S	0.001	-0.01	-0.001	-0.001	-0.001	142	-0.005	-0.005	-0.1	-0.01	-0.001	-0.001	-0.001	0.002	0.02
MU38D	-0.001	-0.01	-0.001	-0.001	-0.001	1.58	-0.005	-0.005	-0.1	-0.01	-0.001	-0.001	-0.001	0.002	-0.01
MU38S	-0.001	-0.01	-0.001	-0.001	-0.001	0.77	-0.005	-0.005	-0.1	-0.01	-0.001	-0.001	-0.001	0.005	-0.01
MU39	-0.001	0.08	0.001	-0.001	-0.001	24.8	-0.001	0.002	-0.002		-0.0005	-0.001	-0.001	0.009	0.02

Bore ID	*Cs (mg/L)*	*Cu (mg/L)*	*Dy (mg/L)*	*Er (mg/L)*	*Eu (mg/L)*	*Fe (mg/L)*	*Ga (mg/L)*	*Gd (mg/L)*	*Ge (mg/L)*	*Hf (mg/L)*	*Hg (mg/L)*	*Ho (mg/L)*	*In (mg/L)*	*La (mg/L)*	*Li (mg/L)*
MU40D	-0.001	0.02	-0.001	-0.001	-0.001	109	-0.005	-0.005	-0.1	-0.01	-0.001	-0.001	-0.001	-0.001	0.02
MU40S	-0.001	-0.02	-0.001	-0.001	-0.001	10.9	-0.005	-0.005	-0.1	-0.01	-0.001	-0.001	-0.001	-0.001	0.02
MU41D	-0.001	-0.01	-0.001	-0.001	-0.001	44.7	-0.005	-0.005	-0.1	-0.01	-0.001	-0.001	-0.001	-0.001	0.03
MU41S	-0.001	-0.01	-0.001	-0.001	-0.001	7.67	-0.005	-0.005	-0.1	-0.01	-0.001	-0.001	-0.001	-0.001	-0.01
MU42A	-0.001	0.002	-0.001	-0.001	-0.001	23.5	-0.001	-0.001	-0.002		-0.0005	-0.001	-0.001	-0.001	0.01
MU42D	0.001	-0.01	-0.001	-0.001	-0.001	1.99	-0.005	-0.005	-0.1	-0.01	-0.001	-0.001	-0.001	-0.001	0.02
MU42I	-0.001	0.82	-0.001	-0.001	-0.001	0.35	-0.005	-0.005	-0.1	-0.01	-0.001	-0.001	-0.001	0.003	0.01
MU42S	-0.001	-0.01	-0.001	-0.001	-0.001	5.89	-0.005	-0.005	-0.1	-0.01	-0.001	-0.001	-0.001	-0.001	-0.01
MU43D	-0.001	-0.01	-0.001	-0.001	-0.001	2.23	-0.005	-0.005	-0.1	-0.01	-0.001	-0.001	-0.001	-0.001	-0.01
MU43S	-0.001	-0.01	-0.001	-0.001	-0.001	2.49	-0.005	-0.005	-0.1	-0.01	-0.001	-0.001	-0.001	-0.001	-0.01
MU44	-0.001	0.04	-0.001	-0.001	-0.001	24.3	-0.001	-0.001	-0.002		-0.0005	-0.001	-0.001	-0.001	0.09
MU45D	-0.001	-0.05	-0.001	-0.001	-0.001	13.2	-0.005	-0.005	-0.1	-0.01	-0.001	-0.001	-0.001	-0.001	0.15
MU45S	-0.001	-0.01	-0.001	-0.001	-0.001	31.1	-0.005	-0.005	-0.1	-0.01	-0.001	-0.001	-0.001	-0.001	-0.01
MU46A	-0.001	0.02	-0.001	-0.001	-0.001	35.7	-0.001	-0.001	-0.002		-0.0005	-0.001	-0.001	-0.001	0.03
MU46D	0.002	-0.05	-0.001	-0.001	-0.001	99.8	-0.005	-0.005	-0.1	-0.01	-0.001	-0.001	-0.001	-0.001	0.01
MU46S	0.002	-0.02	-0.001	-0.001	-0.001	56.2	-0.005	-0.005	-0.1	-0.01	-0.001	-0.001	-0.001	-0.001	0.04
MU47	-0.001	0.02	-0.001	-0.001	-0.001	2.45	-0.001	-0.001	-0.002		-0.0005	-0.001	-0.001	-0.001	0.06
MU48	-0.001	0.02	-0.001	-0.001	-0.001	16.7	-0.001	-0.001	-0.002		-0.0005	-0.001	-0.001	0.006	0.03
MU49	0.001	0.004	-0.001	-0.001	-0.001	24.2	-0.001	-0.001	-0.002		-0.0005	-0.001	-0.001	-0.001	0.02
MU51	-0.001	0.02	-0.001	-0.001	-0.001	4.7	-0.001	-0.001	-0.002		-0.0005	-0.001	-0.001	-0.001	0.17
MU52A	-0.001	0.04	-0.001	-0.001	-0.001	19.6	-0.001	-0.001	-0.002		-0.0005	-0.001	-0.001	-0.001	-0.01
MU52D	-0.001	-0.02	-0.001	-0.001	-0.001	68.2	-0.005	-0.005	-0.1	-0.01	-0.001	-0.001	-0.001	-0.001	0.11
MU52S	-0.001	-0.01	-0.001	-0.001	-0.001	38.5	-0.005	-0.005	-0.1	-0.01	-0.001	-0.001	-0.001	-0.001	-0.01

Bore ID	*Cs (mg/L)*	*Cu (mg/L)*	*Dy (mg/L)*	*Er (mg/L)*	*Eu (mg/L)*	*Fe (mg/L)*	*Ga (mg/L)*	*Gd (mg/L)*	*Ge (mg/L)*	*Hf (mg/L)*	*Hg (mg/L)*	*Ho (mg/L)*	*In (mg/L)*	*La (mg/L)*	*Li (mg/L)*
MU53	-0.001	-0.002	-0.001	-0.001	-0.001	0.37	-0.001	-0.001	-0.002		0.0005	-0.001	-0.001	-0.001	0.02
MU54D	-0.001	-0.01	-0.001	-0.001	-0.001	5.25	-0.005	-0.005	-0.1	-0.01	-0.001	-0.001	-0.001	-0.001	-0.01
MU54S	-0.001	-0.01	-0.001	-0.001	-0.001	2.36	-0.005	-0.005	-0.1	-0.01	-0.001	-0.001	-0.001	0.003	-0.01
MU55D	-0.001	0.002	-0.001	-0.001	-0.001	14.5	-0.001	-0.001	-0.002		-0.0005	-0.001	-0.001	-0.001	0.01
MU55S	-0.001	0.002	-0.001	-0.001	-0.001	0.98	-0.001	-0.001	-0.002		-0.0005	-0.001	-0.001	-0.001	-0.01
MU56D	-0.001	0.008	-0.001	-0.001	-0.001	0.16	-0.001	-0.001	-0.002		-0.0005	-0.001	-0.001	-0.001	-0.01
MU57D	-0.001	0.002	-0.001	-0.001	-0.001	5.86	-0.001	-0.001	-0.002		-0.0005	-0.001	-0.001	-0.001	0.02
MU57S	-0.001	0.002	-0.001	-0.001	-0.001	3.48	-0.001	0.001	-0.002		-0.0005	-0.001	-0.001	0.008	-0.01
MU58D	-0.001	-0.02	-0.001	-0.001	-0.001	42.6	-0.001	-0.001	-0.002		-0.0005	-0.001	-0.001	-0.001	0.03
MU58S	-0.001	-0.02	-0.001	-0.001	-0.001	24.2	-0.001	-0.001	-0.002		-0.0005	-0.001	-0.001	-0.001	0.01
MU59D	0.003	0.04	-0.001	-0.001	-0.001	59	-0.001	-0.001	-0.002		-0.0005	-0.001	-0.001	-0.001	0.06
MU59I	0.001	0.02	-0.001	-0.001	-0.001	34.9	-0.001	-0.001	-0.002		-0.0005	-0.001	-0.001	-0.001	0.05
MU59S	-0.001	-0.02	-0.001	-0.001	-0.001	59.8	-0.001	-0.001	-0.002		-0.0005	-0.001	-0.001	0.002	0.03
MU60D	0.001	0.06	-0.001	-0.001	-0.001	25.3	-0.001	-0.001	-0.002		-0.0005	-0.001	-0.001	-0.001	0.05
MU60S	-0.001	0.08	-0.001	-0.001	-0.001	15.5	-0.001	-0.001	-0.002		-0.0005	-0.001	-0.001	-0.001	0.02
MU61D	-0.001	0.02	-0.001	-0.001	-0.001	50.2	-0.001	-0.001	-0.002		-0.0005	-0.001	-0.001	-0.001	0.07
MU61I	-0.001	-0.02	-0.001	-0.001	-0.001	11.5	-0.001	-0.001	-0.002		-0.0005	-0.001	-0.001	-0.001	0.01
MU61S	-0.001	0.02	-0.001	-0.001	-0.001	3.9	-0.001	-0.001	-0.002		-0.0005	-0.001	-0.001	-0.001	-0.01
MU62D	-0.001	0.002	-0.001	-0.001	-0.001	30.9	-0.001	-0.001	-0.002		-0.0005	-0.001	-0.001	-0.001	0.04
MU62I	-0.001	0.026	-0.001	-0.001	-0.001	18.7	-0.001	-0.001	-0.002		-0.0005	-0.001	-0.001	0.002	0.01
MU62S	-0.001	0.026	-0.001	-0.001	-0.001	2.28	-0.001	-0.001	-0.002		-0.0005	-0.001	-0.001	-0.001	-0.01
MU63D	-0.001	0.04	-0.001	-0.001	-0.001	39.5	-0.001	-0.001	-0.002		-0.0005	-0.001	-0.001	-0.001	0.02
MU63S	-0.001	0.04	-0.001	-0.001	-0.001	1.5	-0.001	-0.001	-0.002		-0.0005	-0.001	-0.001	0.004	-0.01

Bore ID	*Cs (mg/L)*	*Cu (mg/L)*	*Dy (mg/L)*	*Er (mg/L)*	*Eu (mg/L)*	*Fe (mg/L)*	*Ga (mg/L)*	*Gd (mg/L)*	*Ge (mg/L)*	*Hf (mg/L)*	*Hg (mg/L)*	*Ho (mg/L)*	*In (mg/L)*	*La (mg/L)*	*Li (mg/L)*
MU64D	-0.001	0.002	-0.001	0.001	-0.001	30.7	0.001	0.001	-0.002		-0.0005	0.001	-0.001	0.002	0.01
MU64I	-0.001	0.002	-0.001	-0.001	-0.001	7.34	-0.001	-0.001	-0.002		-0.0005	-0.001	-0.001	-0.001	-0.01
MU64S	-0.001	0.068	0.002	0.001	-0.001	15.8	0.002	0.002	-0.002		-0.0005	-0.001	-0.001	0.012	0.01
MU65D	0.002	0.002	-0.001	-0.001	-0.001	33.6	-0.001	-0.001	-0.002		-0.0005	-0.001	-0.001	-0.001	0.03
MU65S	-0.001	0.002	-0.001	-0.001	-0.001	4.36	-0.001	-0.001	-0.002		-0.0005	-0.001	-0.001	0.002	-0.01
MU66D	-0.001	0.004	-0.001	-0.001	-0.001	57.1	-0.001	-0.001	-0.002		-0.0005	-0.001	-0.001	-0.001	0.01
MU66S	-0.001	-0.002	-0.001	-0.001	-0.001	7.75	-0.001	-0.001	-0.002		-0.0005	-0.001	-0.001	-0.001	-0.01
MU67D	-0.001	0.004	-0.001	-0.001	-0.001	-0.01	-0.001	-0.001	-0.002		-0.0005	-0.001	-0.001	-0.001	0.02
MU67I	-0.001	-0.002	-0.001	-0.001	-0.001	17.2	-0.001	-0.001	-0.002		-0.0005	-0.001	-0.001	-0.001	0.02
MU67S	-0.001	0.002	-0.001	-0.001	-0.001	8.42	-0.001	-0.001	-0.002		-0.0005	-0.001	-0.001	-0.001	0.02
MU68D	-0.001	0.002	-0.001	-0.001	-0.001	22.1	-0.001	-0.001	-0.002		-0.0005	-0.001	-0.001	-0.001	0.01
MU68S	-0.001	0.002	-0.001	-0.001	-0.001	4.06	-0.001	-0.001	-0.002		-0.0005	-0.001	-0.001	-0.001	-0.01
MU69	-0.001	0.01	-0.001	-0.001	-0.001	35.1	-0.001	-0.001	-0.002		-0.0005	-0.001	-0.001	-0.001	0.06
MU70	-0.001	0.006	-0.001	-0.001	-0.001	51.3	-0.001	-0.001	-0.002		-0.0005	-0.001	-0.001	-0.001	0.09
MU71	-0.001	0.002	-0.001	-0.001	-0.001	0.17	-0.001	-0.001	-0.002		-0.0005	-0.001	-0.001	-0.001	-0.01
MU72	-0.001	0.002	-0.001	-0.001	-0.001	0.72	-0.001	-0.001	-0.002		-0.0005	-0.001	-0.001	-0.001	0.08
Muir 1	-0.001	-0.1	-0.001	-0.001	-0.001	0.7	-0.001	-0.001	-0.002		-0.0005	-0.001	-0.001	-0.001	0.13
Muir 2	-0.001	-0.1	-0.001	-0.001	-0.001	0.1	-0.001	-0.001	-0.002		-0.0005	-0.001	-0.001	-0.001	0.09
Muir 3	-0.001	-0.1	-0.001	-0.001	-0.001	0.1	-0.001	-0.001	-0.002		-0.0005	-0.001	-0.001	-0.001	0.12
Muir 4	-0.001	-0.1	-0.001	-0.001	-0.001	-0.1	-0.001	-0.001	-0.002		-0.0005	-0.001	-0.001	-0.001	0.06
PM01	-0.001	-0.01	-0.001	-0.001	-0.001	36.8	-0.001	-0.001	-0.002		-0.0005	-0.001	-0.001	0.011	0.02
PM02	-0.001	0.026	-0.001	-0.001	-0.001	5.54	-0.001	-0.001	-0.002		-0.0005	-0.001	-0.001	-0.001	0.02
PM03	-0.001	0.002	-0.001	-0.001	-0.001	18.4	-0.001	-0.001	-0.002		-0.0005	-0.001	-0.001	-0.001	-0.01

Bore ID	*Cs (mg/L)*	*Cu (mg/L)*	*Dy (mg/L)*	*Er (mg/L)*	*Eu (mg/L)*	*Fe (mg/L)*	*Ga (mg/L)*	*Gd (mg/L)*	*Ge (mg/L)*	*Hf (mg/L)*	*Hg (mg/L)*	*Ho (mg/L)*	*In (mg/L)*	*La (mg/L)*	*Li (mg/L)*
PM04	-0.001	0.004	-0.001	-0.001	-0.001	14.6	-0.001	-0.001	-0.002		-0.0005	-0.001	-0.001	-0.001	-0.01
PM10	-0.001	0.002	-0.001	-0.001	-0.001	19.1	-0.001	-0.001	-0.002		-0.0005	-0.001	-0.001	-0.001	0.05
PM12	0.001	0.01	0.003	0.001	-0.001	51.6	-0.001	0.004	-0.002		-0.0005	-0.001	-0.001	0.038	0.12

Table 13 Results of trace metals in groundwater continued. Negative values represent the detection limits with -0.0001 representing a detection limit of 0.0001 of designated unit.

Bore ID	*Lu (mg/L)*	*Mo (mg/L)*	*Nb (mg/L)*	*Nd (mg/L)*	*Ni (mg/L)*	*P (mg/L)*	*Pb (mg/L)*	*Pr (mg/L)*	*Rb 9mg/L)*	*Re (mg/L)*	*S (mg/L)*	*Sb (mg/L)*	*Sc (mg/L)*	*Se (mg/L)*	*Si (mg/L)*	*Sm (mg/L)*
Forty-acre 1	-0.001	0.004	-0.001	0.027	0.05	-0.1	-0.01	0.007	0.02	-0.001	697	-0.002	-0.01	-0.01	9.3	0.005
Forty-acre 2	-0.001	-0.002	-0.001	-0.001	0.02	-0.1	-0.01	-0.001	-0.01	-0.001	90.6	-0.002	-0.01	-0.01	15.1	-0.001
Forty-acre 3	-0.001	0.004	-0.001	-0.001	0.01	-0.1	-0.01	-0.001	0.01	-0.001	646	-0.002	-0.01	-0.01	15.9	-0.001
Forty-acre 4	-0.001	-0.002	-0.001	-0.001	0.02	-0.1	-0.01	-0.001	-0.01	-0.001	339	-0.002	-0.01	-0.01	9.7	-0.001
MU01	-0.001	-0.002		-0.001	0.02	-0.1	-0.01	-0.001	-0.01		172	-0.002	-0.001		25.7	-0.001
MU02	-0.001	-0.002		-0.001	0.02	-0.1	-0.01	-0.001	-0.01		110	-0.002	-0.001		26.8	-0.001
MU03D	-0.001	0.012		-0.001	0.02	-0.2	-0.01	-0.001	0.04		623	-0.002	-0.01		4.2	-0.001
MU03S	-0.001	-0.002		0.001	-0.01	-0.1	-0.01	-0.001	-0.01		3.2	-0.002	0.002		5.8	-0.001
MU04	-0.001	0.002		-0.001	0.04	-0.1	-0.01	-0.001	-0.01		56.9	-0.002	0.001		29.6	-0.001
MU05D	-0.001	-0.01	-0.01	-0.001	0.02	0.1	-0.05	-0.001	0.004	-0.005	42.1	-0.005	-0.01	-0.1	7.5	-0.001
MU05S	-0.001	-0.01	-0.01	-0.001	0.01	0.25	-0.05	-0.001	0.002	-0.005	6.4	-0.005	-0.01	-0.1	5.8	-0.001
MU06	-0.001	-0.002		-0.001	0.04	0.2	-0.01	-0.001	-0.01		271	-0.002	-0.01		26.6	-0.001
MU07D	-0.001	0.01	-0.01	-0.001	0.1	0.5	-0.05	-0.001	0.236	-0.005	123	-0.005	-0.01	-0.1	1	-0.001
MU07S	-0.001	-0.01	-0.01	0.009	0.1	1	-0.05	0.003	0.034	-0.005	388	-0.005	-0.01	-0.1	16	0.001
MU08	-0.001	-0.002		-0.001	0.02	-0.2	-0.01	-0.001	0.02		211	-0.002	-0.01		24.6	-0.001
MU09D	-0.001	-0.01	-0.01	-0.001	0.1	0.5	-0.05	-0.001	0.007	-0.005	227	-0.005	-0.01	-0.1	13.5	-0.001
MU09S	-0.001	-0.01	-0.01	-0.001	-0.05	-0.5	-0.05	-0.001	0.007	-0.005	160	-0.005	-0.01	-0.1	17.5	-0.001
MU10D	-0.001	-0.01	-0.01	-0.001	0.02	0.05	0.05	-0.001	0.013	-0.005	1.35	-0.005	-0.01	-0.1	14.2	-0.001
MU10I	-0.001	-0.002		-0.001	0.05	-0.5	-0.01	-0.001	0.02		2	-0.002	-0.01		21	-0.001
MU10S	-0.001	-0.01	-0.01	-0.001	0.02	-0.05	-0.05	-0.001	0.011	-0.005	10	-0.005	-0.01	-0.1	6.3	-0.001
MU11D	-0.001	-0.01	-0.01	-0.001	-0.01	0.1	-0.05	-0.001	0.033	-0.005	140	-0.005	-0.01	-0.1	11.8	-0.001

Bore ID	*Lu (mg/L)*	*Mo (mg/L)*	*Nb (mg/L)*	*Nd (mg/L)*	*Ni (mg/L)*	*P (mg/L)*	*Pb (mg/L)*	*Pr (mg/L)*	*Rb 9mg/L)*	*Re (mg/L)*	*S (mg/L)*	*Sb (mg/L)*	*Sc (mg/L)*	*Se (mg/L)*	*Si (mg/L)*	*Sm (mg/L)*
MU11I	-0.001	-0.01	-0.01	-0.001	-0.01	0.15	-0.05	-0.001	0.04	-0.005	149	-0.005	-0.01	-0.1	8.2	-0.001
MU12A	-0.001	-0.002		-0.001	-0.01	0.4	-0.01	-0.001	0.05		150	-0.002	0.001		11.2	-0.001
MU12D	-0.001	-0.01	-0.01	-0.001	0.05	-0.5	-0.05	-0.001	0.059	-0.005	262	-0.005	-0.01	-0.1	29	-0.001
MU12S	-0.001	-0.01	-0.01	-0.001	0.01	0.05	-0.05	-0.001	0.016	-0.005	40.2	-0.005	-0.01	-0.1	28.2	-0.001
MU13	-0.001	-0.002		0.002	0.01	-0.1	-0.01	-0.001	-0.01		51.3	-0.002	0.003		3	-0.001
MU14D	-0.001	-0.01	-0.01	-0.001	0.02	0.1	-0.05	-0.001	0.036	-0.005	173	-0.005	-0.01	-0.1	4.1	-0.001
MU14S	-0.001	-0.01	-0.01	-0.001	0.01	0.2	-0.05	-0.001	0.02	-0.005	146	-0.005	-0.01	-0.1	18.1	-0.001
MU15A	-0.001	-0.002		-0.001	0.04	0.2	-0.01	-0.001	-0.01		258	-0.002	-0.01		15.4	-0.001
MU15D	-0.001	-0.01	-0.01	-0.001	-0.01	0.1	-0.05	-0.001	0.032	-0.005	148	-0.005	-0.01	-0.1	7	-0.001
MU15S	-0.001	-0.01	-0.01	0.012	-0.05	-0.5	-0.05	0.004	0.043	-0.005	230	-0.005	-0.01	-0.1	32	0.002
MU16D	-0.001	-0.01	-0.01	-0.001	-0.01	0.2	-0.05	-0.001	0.022	-0.005	46.7	-0.005	-0.01	-0.1	17.9	-0.001
MU16S	-0.001	-0.01	-0.01	0.013	-0.05	-0.5	-0.05	0.004	0.04	-0.005	214	-0.005	-0.01	-0.1	31	0.002
MU17	-0.001	-0.002		-0.001	0.06	0.2	-0.01	-0.001	-0.01		202	-0.002	-0.01		26.8	-0.001
MU18D	-0.001	-0.01	-0.01	-0.001	0.01	0.1	-0.05	-0.001	0.019	-0.005	60.4	-0.005	-0.01	-0.1	28.4	-0.001
MU18S	-0.001	-0.01	-0.01	-0.001	0.02	0.15	-0.05	-0.001	0.003	-0.005	25.3	-0.005	-0.01	-0.1	4.5	-0.001
MU19D	-0.001	-0.002		-0.001	-0.05	-0.5	-0.01	-0.001	0.02		140	-0.002	-0.01		20	-0.001
MU22D	-0.001	-0.002		0.002	-0.01	-0.1	-0.01	-0.001	0.01		93.7	-0.002	-0.001		6.6	-0.001
MU22S	-0.001	-0.002		0.014	0.14	-0.2	-0.01	0.004	0.01		200	-0.002	-0.01		31.2	0.002
MU23D	-0.001	-0.01	-0.01	-0.001	-0.05	-0.5	-0.05	-0.001	0.042	-0.005	212	-0.005	-0.01	-0.1	19.5	-0.001
MU23S	-0.001	-0.01	-0.01	0.001	-0.01	0.05	-0.05	-0.001	0.013	-0.005	75.3	-0.005	-0.01	-0.1	9.5	-0.001
MU24	-0.001	-0.002		-0.001	0.01	0.1	-0.01	-0.001	0.03		207	-0.002	0.002		28.6	-0.001
MU25	-0.001	-0.002		-0.001	0.02	-0.1	-0.01	-0.001	-0.01		29.7	-0.002	-0.001		21.3	-0.001
MU26	-0.001	-0.002		-0.001	0.01	-0.1	-0.01	-0.001	-0.01		33.3	-0.002	-0.001		11.5	-0.001

Bore ID	*Lu (mg/L)*	*Mo (mg/L)*	*Nb (mg/L)*	*Nd (mg/L)*	*Ni (mg/L)*	*P (mg/L)*	*Pb (mg/L)*	*Pr (mg/L)*	*Rb 9mg/L)*	*Re (mg/L)*	*S (mg/L)*	*Sb (mg/L)*	*Sc (mg/L)*	*Se (mg/L)*	*Si (mg/L)*	*Sm (mg/L)*
MU27D	-0.001	-0.01	-0.01	-0.001	0.02	0.2	-0.05	-0.001	0.052	-0.005	66.8	-0.005	-0.01	-0.1	30.8	-0.001
MU27S	-0.001	-0.01	-0.01	-0.001	0.1	-0.5	-0.05	-0.001	0.007	-0.005	44	-0.005	-0.01	-0.1	6.5	-0.001
MU28D	-0.001	-0.01	-0.01	-0.001	0.01	0.7	-0.05	-0.001	0.012	-0.005	15.5	-0.005	-0.01	-0.1	17.7	-0.001
MU28S	-0.001	-0.01	-0.01	-0.001	0.01	0.15	-0.05	-0.001	0.005	-0.005	9.25	-0.005	-0.01	-0.1	5.1	-0.001
MU29D	-0.001	-0.01	-0.01	-0.001	0.05	-0.5	-0.05	-0.001	0.078	-0.005	254	-0.005	-0.01	-0.1	28.5	-0.001
MU29S	-0.001	-0.01	-0.01	-0.001	-0.05	0.5	-0.05	-0.001	0.04	-0.005	251	-0.005	-0.01	-0.1	20.5	-0.001
MU30D	-0.001	-0.01	-0.01	-0.001	0.05	0.5	-0.05	-0.001	0.054	-0.005	221	-0.005	-0.01	-0.1	27	-0.001
MU30S	-0.001	0.03	-0.01	-0.001	0.01	0.1	-0.05	-0.001	0.002	-0.005	35.3	-0.005	-0.01	-0.1	10.9	-0.001
MU31D	-0.001	-0.01	-0.01	0.001	0.1	0.5	-0.05	-0.001	0.124	-0.005	247	-0.005	-0.01	-0.1	25	-0.001
MU31S	-0.001	-0.01	-0.01	-0.001	0.05	-0.5	-0.05	-0.001	0.051	-0.005	116	-0.005	-0.01	-0.1	14	-0.001
MU32	-0.001	-0.002		-0.001	-0.01	-0.1	-0.01	-0.001	0.02		144	-0.002	0.001		7.3	-0.001
MU33D	-0.001	-0.01	-0.01	-0.001	-0.05	-0.5	-0.05	-0.001	0.036	-0.005	161	-0.005	0.01	-0.1	23.5	-0.001
MU33S	-0.001	-0.01	-0.01	0.007	0.01	0.15	-0.05	0.002	0.006	-0.005	52.4	-0.005	-0.01	-0.1	5.3	0.001
MU34	-0.001	-0.002		-0.001	-0.01	-0.1	-0.01	-0.001	0.03		55.6	-0.002	-0.001		25.1	-0.001
MU35	-0.001	-0.002		-0.001	0.02	0.1	-0.01	-0.001	-0.01		212	-0.002	-0.001		25.2	-0.001
MU36D	-0.001	-0.01	-0.01	0.001	0.02	0.05	-0.05	-0.001	0.013	-0.005	42.1	-0.005	-0.01	-0.1	4.8	-0.001
MU36S	-0.001	-0.01	-0.01	0.002	0.01	0.1	-0.05	-0.001	0.006	-0.005	20.4	-0.005	-0.01	-0.1	5	-0.001
MU37D	-0.001	-0.01	-0.01	-0.001	0.01	0.15	-0.05	-0.001	0.048	-0.005	249	-0.005	-0.01	-0.1	10.7	-0.001
MU37I	-0.001	-0.01	-0.01	0.001	0.02	0.1	-0.05	-0.001	0.035	-0.005	133	-0.005	-0.01	-0.1	7.4	-0.001
MU37S	-0.001	-0.01	-0.01	0.002	0.09	0.05	-0.05	-0.001	0.062	-0.005	81.2	-0.005	-0.01	-0.1	46.8	-0.001
MU38D	-0.001	-0.01	-0.01	0.002	0.04	0.1	-0.05	-0.001	0.011	-0.005	2.55	-0.005	-0.01	-0.1	5.4	-0.001
MU38S	-0.001	-0.01	-0.01	0.004	-0.01	0.05	-0.05	0.001	0.001	-0.005	5.45	-0.005	-0.01	-0.1	3.6	-0.001
MU39	-0.001	-0.002		0.01	0.06	0.2	-0.01	0.002	-0.01		121	-0.002	-0.01		25.6	0.002

Bore ID	*Lu (mg/L)*	*Mo (mg/L)*	*Nb (mg/L)*	*Nd (mg/L)*	*Ni (mg/L)*	*P (mg/L)*	*Pb (mg/L)*	*Pr (mg/L)*	*Rb 9mg/L)*	*Re (mg/L)*	*S (mg/L)*	*Sb (mg/L)*	*Sc (mg/L)*	*Se (mg/L)*	*Si (mg/L)*	*Sm (mg/L)*
MU40D	-0.001	-0.01	-0.01	-0.001	0.05	0.5	-0.05	-0.001	0.069	-0.005	242	-0.005	-0.01	-0.1	19.5	-0.001
MU40S	-0.001	0.01	-0.01	-0.001	0.15	1	-0.05	-0.001	0.017	-0.005	287	-0.005	-0.01	-0.1	5.5	-0.001
MU41D	-0.001	-0.01	-0.01	-0.001	-0.01	0.1	-0.05	-0.001	0.021	-0.005	97.7	-0.005	-0.01	-0.1	5.2	-0.001
MU41S	-0.001	-0.01	-0.01	-0.001	-0.01	0.1	-0.05	-0.001	0.008	-0.005	32.5	-0.005	-0.01	-0.1	6.7	-0.001
MU42A	-0.001	-0.002		-0.001	0.03	1.4	-0.01	-0.001	0.06		112	-0.002	-0.001		24	-0.001
MU42D	-0.001	0.01	-0.01	-0.001	0.01	0.05	-0.05	-0.001	0.084	-0.005	49.4	-0.005	-0.01	-0.1	12.6	-0.001
MU42I	-0.001	0.01	-0.01	0.001	-0.05	-0.5	-0.05	-0.001	0.023	-0.005	198	-0.005	-0.01	-0.1	6	-0.001
MU42S	-0.001	0.01	-0.01	-0.001	0.01	0.05	-0.05	-0.001	0.004	-0.005	30	-0.005	-0.01	-0.1	7.5	-0.001
MU43D	-0.001	-0.01	-0.01	-0.001	-0.01	0.15	-0.05	-0.001	0.011	-0.005	55.2	-0.005	-0.01	-0.1	6.7	-0.001
MU43S	-0.001	-0.01	-0.01	-0.001	0.01	0.1	-0.05	-0.001	0.005	-0.005	47.9	-0.005	-0.01	-0.1	15.8	-0.001
MU44	-0.001	-0.002		-0.001	0.1	-0.5	-0.01	-0.001	0.05		831	-0.002	-0.01		15.5	-0.001
MU45D	-0.001	0.01	-0.01	-0.001	0.2	-1	-0.05	-0.001	0.092	-0.005	2530	-0.005	-0.05	0.1	7	-0.001
MU45S	-0.001	-0.01	-0.01	-0.001	0.01	0.1	-0.05	-0.001	0.012	-0.005	46.9	-0.005	-0.01	-0.1	3.7	-0.001
MU46A	-0.001	0.004		-0.001	0.1	1	-0.01	-0.001	0.16		335	-0.002	-0.01		17.5	-0.001
MU46D	-0.001	-0.01	-0.01	-0.001	-0.2	1	-0.05	-0.001	0.311	-0.005	412	-0.005	-0.05	-0.1	15	-0.001
MU46S	-0.001	-0.01	-0.01	-0.001	-0.05	-0.5	-0.05	-0.001	0.098	-0.005	119	-0.005	-0.01	-0.1	6	-0.001
MU47	-0.001	0.006		-0.001	0.05	-0.5	-0.01	-0.001	-0.01		133	-0.002	-0.01		20.5	-0.001
MU48	-0.001	-0.002		0.004	-0.05	-0.5	-0.01	0.001	0.04		491	-0.002	-0.01		5	-0.001
MU49	-0.001	-0.002		-0.001	0.01	0.4	-0.01	-0.001	0.02		32.8	-0.002	-0.001		4.6	-0.001
MU51	-0.001	-0.002		-0.001	0.1	-0.5	-0.01	-0.001	-0.01		119	-0.002	-0.01		33	-0.001
MU52A	-0.001	-0.002		-0.001	0.1	-0.5	-0.01	-0.001	0.01		42	-0.002	-0.01		5.5	-0.001
MU52D	-0.001	-0.01	-0.01	-0.001	0.15	0.5	-0.05	-0.001	0.089	-0.005	129	-0.005	-0.01	-0.1	26	-0.001
MU52S	-0.001	-0.01	-0.01	-0.001	0.01	-0.05	0.05	-0.001	0.023	-0.005	54.2	-0.005	-0.01	-0.1	4.6	-0.001

Bore ID	*Lu (mg/L)*	*Mo (mg/L)*	*Nb (mg/L)*	*Nd (mg/L)*	*Ni (mg/L)*	*P (mg/L)*	*Pb (mg/L)*	*Pr (mg/L)*	*Rb 9mg/L)*	*Re (mg/L)*	*S (mg/L)*	*Sb (mg/L)*	*Sc (mg/L)*	*Se (mg/L)*	*Si (mg/L)*	*Sm (mg/L)*
MU53	-0.001	-0.002		-0.001	0.03	0.2	-0.01	-0.001	-0.01		134	-0.002	-0.001		28.5	-0.001
MU54D	-0.001	-0.01	-0.01	-0.001	-0.01	0.1	-0.05	-0.001	0.017	-0.005	14.2	-0.005	-0.01	-0.1	4	-0.001
MU54S	-0.001	0.01	-0.01	0.002	0.01	0.05	-0.05	-0.001	0.003	-0.005	44	-0.005	-0.01	-0.1	3.6	-0.001
MU55D	-0.001	-0.002		-0.001	-0.01	-0.1	-0.01	-0.001	0.01		79.8	-0.002	0.001		7.3	-0.001
MU55S	-0.001	-0.002		-0.001	-0.01	-0.1	-0.01	-0.001	-0.01		34.6	-0.002	-0.001		3.4	-0.001
MU56D	-0.001	-0.002		-0.001	-0.01	-0.1	-0.01	-0.001	-0.01		8.2	-0.002	-0.001		4	-0.001
MU57D	-0.001	0.002		-0.001	0.01	-0.1	-0.01	-0.001	0.02		136	-0.002	-0.001		10.7	-0.001
MU57S	-0.001	-0.002		0.009	-0.01	-0.1	-0.01	0.002	0.02		46.6	-0.002	0.003		21.1	0.002
MU58D	-0.001	-0.002		-0.001	-0.05	-0.5	-0.01	-0.001	0.03		348	-0.002	-0.01		12	-0.001
MU58S	-0.001	-0.002		-0.001	0.05	-0.5	-0.01	-0.001	-0.01		377	-0.002	-0.01		3	-0.001
MU59D	-0.001	-0.002		-0.001	-0.05	-0.5	-0.01	-0.001	0.22		1120	-0.002	-0.01		4.5	-0.001
MU59I	-0.001	-0.002		-0.001	-0.05	-0.5	-0.01	-0.001	0.08		530	-0.002	-0.01		5.5	-0.001
MU59S	-0.001	-0.002		-0.001	-0.05	-0.5	-0.01	-0.001	0.03		316	-0.002	-0.01		12.5	-0.001
MU60D	-0.001	-0.002		-0.001	0.1	-0.5	-0.01	-0.001	0.06		942	-0.002	-0.01		8	-0.001
MU60S	-0.001	-0.002		-0.001	0.1	-0.5	-0.01	-0.001	0.04		645	-0.002	-0.01		4	-0.001
MU61D	-0.001	-0.002		-0.001	0.05	-0.5	-0.01	-0.001	0.13		284	-0.002	-0.01		14.5	-0.001
MU61I	-0.001	-0.002		-0.001	0.05	-0.5	-0.01	-0.001	0.04		94	-0.002	-0.01		5.5	-0.001
MU61S	-0.001	-0.002		-0.001	0.05	-0.5	-0.01	-0.001	0.02		88	-0.002	-0.01		5	-0.001
MU62D	-0.001	-0.002		-0.001	-0.01	-0.1	-0.01	-0.001	0.05		249	-0.002	-0.001		5.1	-0.001
MU62I	-0.001	-0.002		0.001	0.09	-0.1	-0.01	-0.001	0.03		129	-0.002	0.002		4.4	-0.001
MU62S	-0.001	-0.002		-0.001	0.01	-0.1	-0.01	-0.001	-0.01		21.3	-0.002	-0.001		6.8	-0.001
MU63D	-0.001	-0.002		-0.001	0.1	-0.5	-0.01	-0.001	0.03		231	-0.002	-0.01		5	-0.001
MU63S	-0.001	-0.002		0.003	0.1	-0.5	-0.01	-0.001	-0.01		107	-0.002	-0.01		8.5	-0.001

Bore ID	*Lu (mg/L)*	*Mo (mg/L)*	*Nb (mg/L)*	*Nd (mg/L)*	*Ni (mg/L)*	*P (mg/L)*	*Pb (mg/L)*	*Pr (mg/L)*	*Rb 9mg/L)*	*Re (mg/L)*	*S (mg/L)*	*Sb (mg/L)*	*Sc (mg/L)*	*Se (mg/L)*	*Si (mg/L)*	*Sm (mg/L)*
MU64D	-0.001	0.002		0.001	-0.01	-0.1	-0.01	0.001	0.03		85.6	-0.002	0.002		5.9	0.001
MU64I	-0.001	-0.002		-0.001	-0.01	-0.1	-0.01	-0.001	0.01		63.9	-0.002	0.001		10.3	-0.001
MU64S	-0.001	-0.002		0.007	0.04	-0.1	0.03	0.002	-0.01		90.9	-0.002	0.003		11	0.001
MU65D	-0.001	-0.002		-0.001	0.03	0.1	-0.01	-0.001	0.04		39.9	-0.002	-0.001		29.6	-0.001
MU65S	-0.001	-0.002		0.001	-0.01	-0.1	-0.01	-0.001	-0.01		25.5	-0.002	-0.001		12.2	-0.001
MU66D	-0.001	-0.002		-0.001	0.02	0.1	-0.01	-0.001	0.01		66.7	-0.002	-0.001		7	-0.001
MU66S	-0.001	-0.002		-0.001	-0.01	-0.1	-0.01	-0.001	-0.01		72.1	-0.002	-0.001		4.1	-0.001
MU67D	-0.001	0.002		-0.001	0.01	-0.1	-0.01	-0.001	0.04		32.4	-0.002	-0.001		1.6	-0.001
MU67I	-0.001	-0.002		-0.001	0.21	-0.1	-0.01	-0.001	0.02		77.4	-0.002	-0.001		6.9	-0.001
MU67S	-0.001	-0.002		-0.001	-0.01	-0.1	-0.01	-0.001	-0.01		36.2	-0.002	-0.001		5	-0.001
MU68D	-0.001	0.018		-0.001	0.86	-0.1	-0.01	-0.001	0.02		75.8	-0.002	-0.001		5.8	-0.001
MU68S	-0.001	-0.002		-0.001	-0.01	-0.1	-0.01	-0.001	-0.01		25.9	-0.002	0.002		4.5	-0.001
MU69	-0.001	-0.002		-0.001	0.04	-0.2	-0.01	-0.001	0.04		224	-0.002	-0.01		17.6	-0.001
MU70	-0.001	-0.002		-0.001	0.02	0.1	-0.01	-0.001	0.06		101	-0.002	-0.001		20	-0.001
MU71	-0.001	-0.002		-0.001	-0.01	0.1	-0.01	-0.001	-0.01		25.4	-0.002	-0.001		23	-0.001
MU72	-0.001	-0.002		-0.001	0.04	-0.1	-0.01	-0.001	-0.01		121	-0.002	-0.001		26.6	-0.001
Muir1	-0.001	0.002	-0.001	-0.001	-0.1	-2	-0.01	-0.001	0.11	-0.001	1930	-0.002	-0.05	0.05	8	-0.001
Muir2	-0.001	0.004	-0.001	-0.001	-0.1	-2	-0.01	-0.001	0.13	-0.001	1960	-0.002	-0.05	0.08	8	-0.001
Muir3	-0.001	0.018	-0.001	-0.001	-0.1	-2	-0.01	-0.001	0.16	-0.001	2180	-0.002	-0.05	0.08	6	-0.001
Muir4	-0.001	-0.002	-0.001	-0.001	-0.1	-2	-0.01	-0.001	0.06	-0.001	1170	-0.002	-0.05	0.03	16	-0.001
PM01	-0.001	-0.002		0.003	0.02	-0.2	-0.01	-0.001	0.09		308	-0.002	-0.01		4.4	-0.001
PM02	-0.001	-0.002		-0.001	-0.01	0.1	-0.01	-0.001	-0.01		95.8	-0.002	0.001		23.3	-0.001
PM03	-0.001	-0.002		-0.001	-0.01	-0.1	-0.01	-0.001	0.01		60	-0.002	-0.001		6	-0.001

Bore ID	*Lu (mg/L)*	*Mo (mg/L)*	*Nb (mg/L)*	*Nd (mg/L)*	*Ni (mg/L)*	*P (mg/L)*	*Pb (mg/L)*	*Pr (mg/L)*	*Rb 9mg/L)*	*Re (mg/L)*	*S (mg/L)*	*Sb (mg/L)*	*Sc (mg/L)*	*Se (mg/L)*	*Si (mg/L)*	*Sm (mg/L)*
PM04	-0.001	-0.002		-0.001	-0.01	-0.1	-0.01	-0.001	0.01		81.1	-0.002	-0.001		6.2	-0.001
PM10	-0.001	-0.002		-0.001	-0.01	-0.1	-0.01	-0.001	0.03		122	-0.002	-0.001		4.3	-0.001
PM12	-0.001	-0.002		0.025	0.02	-0.2	-0.01	0.007	0.03		306	-0.002	-0.01		21.6	0.004

Table 14 Results of trace metals in groundwater continued. Negative values represent the detection limits with -0.0001 representing a detection limit of 0.0001 of designated unit.

Bore ID	*Sn (mg/L)*	*Sr (mg/L)*	*Ta (mg/L)*	*Tb (mg/L)*	*Te (mg/L)*	*Th (mg/L)*	*Ti (mg/L)*	*Tl (mg/L)*	*Tm (mg/L)*	*U (mg/L)*	*V (mg/L)*	*Y (mg/L)*	*W (mg/L)*	*Yb (mg/L)*	*Zn (mg/L)*	*Zr (mg/L)*
Forty-acre 1	-1	2.46	-0.001	-0.001	-1	0.001	-0.01	-0.001	-0.001	0.006	0.02	0.017	-0.001	0.001	0.34	
Forty-acre 2	-1	1.26	-0.001	-0.001	-1	-0.001	-0.01	-0.001	-0.001	-0.002	-0.02	-0.001	-0.001	-0.001	-0.01	
Forty-acre 3	-1	2.58	-0.001	-0.001	-1	-0.001	-0.01	-0.001	-0.001	-0.002	-0.02	-0.001	-0.001	-0.001	0.01	
Forty-acre 4	-1	1.7	-0.001	-0.001	-1	-0.001	-0.01	-0.001	-0.001	0.016	-0.02	-0.001	-0.001	-0.001	0.22	
MU01		1.06		-0.001	-1	-0.001	-0.005	-0.001	-0.001	-0.002	-0.005	0.001	-0.001	-0.001	0.015	
MU02		2.42		-0.001	-1	-0.001	-0.005	-0.001	-0.001	0.006	-0.005	-0.001	-0.001	-0.001	-0.005	
MU03D		3.76		-0.001	-1	-0.001	-0.02	-0.001	-0.001	-0.002	-0.02	-0.001	-0.001	-0.001	-0.02	
MU03S		0.16		-0.001	-1	0.001	0.015	-0.001	-0.001	-0.002	0.02	-0.001	-0.001	-0.001	0.015	
MU04		0.28		-0.001	-1	-0.001	-0.005	-0.001	-0.001	-0.002	-0.005	-0.001	-0.001	-0.001	0.035	
MU05D	-0.02	0.415	-0.001	-0.001	-0.01	-0.001	-0.01	-0.005	-0.001	-0.001	-0.02	-0.005	-0.01	-0.001	-0.01	-0.01
MU05S	-0.02	0.055	-0.001	-0.001	-0.01	-0.001	-0.01	-0.005	-0.001	-0.001	-0.02	-0.005	-0.01	-0.001	-0.01	-0.01
MU06		4.38		-0.001	-1	-0.001	-0.02	-0.001	-0.001	-0.002	-0.02	-0.001	-0.001	-0.001	0.02	
MU07D	-0.02	10.2	-0.001	-0.001	-0.01	-0.001	-0.05	-0.005	-0.001	-0.001	-0.05	-0.005	-0.01	-0.001	0.08	-0.01
MU07S	-0.02	2.97	-0.001	-0.001	-0.01	-0.001	0.05	-0.005	-0.001	-0.001	-0.05	0.005	-0.01	-0.001	0.02	-0.01
MU08		1		-0.001	-1	-0.001	-0.02	-0.001	-0.001	-0.002	-0.02	-0.001	-0.001	-0.001	-0.02	
MU09D	-0.02	1.8	-0.001	-0.001	-0.01	-0.001	-0.05	-0.005	-0.001	0.03	0.05	-0.005	-0.01	-0.001	0.08	-0.01
MU09S	-0.02	1.32	-0.001	-0.001	-0.01	-0.001	-0.05	-0.005	-0.001	0.009	-0.05	-0.005	-0.01	-0.001	0.04	-0.01
MU10D	-0.02	0.26	-0.001	-0.001	-0.01	-0.001	-0.01	-0.005	-0.001	-0.001	-0.02	-0.005	-0.01	-0.001	-0.01	-0.01
MU10I		0.42		-0.001	-1	-0.001	-0.02	-0.001	-0.001	-0.002	-0.05	-0.001	-0.001	-0.001	0.04	
MU10S	-0.02	0.195	-0.001	-0.001	-0.01	-0.001	-0.01	-0.005	-0.001	0.003	-0.02	-0.005	-0.01	-0.001	0.02	-0.01
MU11D	-0.02	1.56	-0.001	-0.001	-0.01	-0.001	-0.01	-0.005	-0.001	-0.001	-0.02	-0.005	-0.01	-0.001	-0.01	-0.01

Bore ID	*Sn (mg/L)*	*Sr (mg/L)*	*Ta (mg/L)*	*Tb (mg/L)*	*Te (mg/L)*	*Th (mg/L)*	*Ti (mg/L)*	*Tl (mg/L)*	*Tm (mg/L)*	*U (mg/L)*	*V (mg/L)*	*Y (mg/L)*	*W (mg/L)*	*Yb (mg/L)*	*Zn (mg/L)*	*Zr (mg/L)*
MU11I	-0.02	1.06	-0.001	-0.001	-0.01	-0.001	-0.01	-0.005	-0.001	-0.001	-0.02	-0.005	-0.01	-0.001	-0.01	-0.01
MU12A		1.22		-0.001	-1	-0.001	-0.005	-0.001	-0.001	-0.002	0.01	-0.001	-0.001	-0.001	0.01	
MU12D	-0.02	2.39	-0.001	-0.001	-0.01	-0.001	-0.05	-0.005	-0.001	-0.001	-0.05	-0.005	-0.01	-0.001	0.02	-0.01
MU12S	-0.02	0.275	-0.001	-0.001	-0.01	-0.001	-0.01	-0.005	-0.001	-0.001	-0.02	-0.005	-0.01	-0.001	0.01	-0.01
MU13		0.44		-0.001	-1	-0.001	0.005	-0.001	-0.001	-0.002	0.005	0.002	-0.001	-0.001	0.03	
MU14D	-0.02	1.01	-0.001	-0.001	-0.01	-0.001	-0.01	-0.005	-0.001	-0.001	-0.02	-0.005	-0.01	-0.001	0.03	-0.01
MU14S	-0.02	1.13	-0.001	-0.001	-0.01	-0.001	-0.01	-0.005	-0.001	0.001	-0.02	-0.005	-0.01	-0.001	-0.01	-0.01
MU15A		3.28		-0.001	-1	-0.001	-0.02	-0.001	-0.001	-0.002	-0.02	-0.001	-0.001	-0.001	0.04	
MU15D	-0.02	0.78	-0.001	-0.001	-0.01	-0.001	-0.01	-0.005	-0.001	-0.001	-0.02	-0.005	-0.01	-0.001	0.02	-0.01
MU15S	-0.02	2.34	-0.001	-0.001	-0.01	-0.001	-0.05	-0.005	-0.001	-0.001	-0.05	0.01	-0.01	-0.001	0.04	-0.01
MU16D	-0.02	0.42	-0.001	-0.001	-0.01	-0.001	-0.01	-0.005	-0.001	-0.001	-0.02	-0.005	-0.01	-0.001	-0.01	-0.01
MU16S	-0.02	2.15	-0.001	-0.001	-0.01	-0.001	-0.05	-0.005	-0.001	-0.001	-0.05	0.01	-0.01	-0.001	0.08	-0.01
MU17		1.1		-0.001	-1	-0.001	-0.02	-0.001	-0.001	-0.002	-0.02	0.001	-0.001	-0.001	0.04	
MU18D	-0.02	1.53	-0.001	-0.001	-0.01	-0.001	-0.01	-0.005	-0.001	-0.001	-0.02	-0.005	-0.01	-0.001	0.02	-0.01
MU18S	-0.02	0.17	-0.001	-0.001	-0.01	-0.001	-0.01	-0.005	-0.001	-0.001	-0.02	-0.005	-0.01	-0.001	0.03	-0.01
MU19D		1.48		-0.001	-1	-0.001	-0.02	-0.001	-0.001	-0.002	-0.05	-0.001	-0.001	-0.001	0.04	
MU22D		0.34		-0.001	-1	-0.001	-0.005	-0.001	-0.001	-0.002	0.005	0.002	-0.001	-0.001	0.01	
MU22S		1.02		-0.001	-1	-0.001	-0.02	-0.001	-0.001	-0.002	-0.02	0.01	-0.001	-0.001	0.04	
MU23D	-0.02	2.28	-0.001	-0.001	-0.01	-0.001	-0.05	-0.005	-0.001	-0.001	-0.05	-0.005	-0.01	-0.001	-0.02	-0.01
MU23S	-0.02	0.5	-0.001	-0.001	-0.01	-0.001	-0.01	-0.005	-0.001	-0.001	-0.02	-0.005	-0.01	-0.001	-0.01	-0.01
MU24		0.94		-0.001	-1	-0.001	-0.005	-0.001	-0.001	-0.002	0.005	-0.001	-0.001	-0.001	0.02	
MU25		0.18		-0.001	-1	-0.001	-0.005	-0.001	-0.001	-0.002	-0.005	-0.001	-0.001	-0.001	0.035	
MU26		0.4		-0.001	-1	-0.001	-0.005	-0.001	-0.001	-0.002	-0.005	0.002	-0.001	-0.001	0.015	

Bore ID	*Sn (mg/L)*	*Sr (mg/L)*	*Ta (mg/L)*	*Tb (mg/L)*	*Te (mg/L)*	*Th (mg/L)*	*Ti (mg/L)*	*Tl (mg/L)*	*Tm (mg/L)*	*U (mg/L)*	*V (mg/L)*	*Y (mg/L)*	*W (mg/L)*	*Yb (mg/L)*	*Zn (mg/L)*	*Zr (mg/L)*
MU27D	-0.02	0.32	-0.001	-0.001	-0.01	-0.001	-0.01	-0.005	-0.001	-0.001	-0.02	-0.005	-0.01	-0.001	0.02	-0.01
MU27S	-0.02	0.31	-0.001	-0.001	-0.01	-0.001	-0.05	-0.005	-0.001	0.001	-0.05	-0.005	-0.01	-0.001	0.04	-0.01
MU28D	-0.02	0.05	-0.001	-0.001	-0.01	-0.001	-0.01	-0.005	-0.001	-0.001	-0.02	-0.005	-0.01	-0.001	-0.01	-0.01
MU28S	-0.02	0.05	-0.001	-0.001	-0.01	-0.001	-0.01	-0.005	-0.001	0.001	-0.02	-0.005	-0.01	-0.001	0.04	-0.01
MU29D	-0.02	8.8	-0.001	-0.001	-0.01	-0.001	-0.05	-0.005	-0.001	-0.001	-0.05	-0.005	-0.01	-0.001	0.04	-0.01
MU29S	-0.02	5.53	-0.001	-0.001	-0.01	-0.001	0.1	-0.005	-0.001	0.003	-0.05	-0.005	-0.01	-0.001	-0.02	-0.01
MU30D	-0.02	8.08	-0.001	-0.001	-0.01	-0.001	0.1	-0.005	-0.001	-0.001	-0.05	-0.005	-0.01	-0.001	0.14	-0.01
MU30S	-0.02	0.275	-0.001	-0.001	-0.01	-0.001	-0.01	-0.005	-0.001	-0.001	-0.02	-0.005	-0.01	-0.001	0.09	-0.01
MU31D	-0.02	18.1	-0.001	-0.001	-0.01	-0.001	0.05	-0.005	-0.001	-0.001	-0.05	-0.005	-0.01	-0.001	0.08	-0.01
MU31S	-0.02	2.57	-0.001	-0.001	-0.01	-0.001	-0.05	-0.005	-0.001	-0.001	-0.05	-0.005	-0.01	-0.001	0.02	-0.01
MU32		1.74		-0.001	-1	-0.001	-0.005	-0.001	-0.001	-0.002	0.005	-0.001	-0.001	-0.001	0.02	
MU33D	-0.02	2.15	-0.001	-0.001	-0.01	-0.001	-0.05	-0.005	-0.001	-0.001	-0.05	-0.005	-0.01	-0.001	0.2	-0.01
MU33S	-0.02	0.65	-0.001	-0.001	-0.01	-0.001	-0.01	-0.005	-0.001	-0.001	-0.02	-0.005	-0.01	-0.001	-0.01	0.01
MU34		0.76		-0.001	-1	-0.001	-0.005	-0.001	-0.001	-0.002	-0.005	-0.001	-0.001	-0.001	0.015	
MU35		0.86		-0.001	-1	-0.001	-0.005	-0.001	-0.001	-0.002	-0.005	0.004	-0.001	-0.001	0.055	
MU36D	-0.02	0.79	-0.001	-0.001	-0.01	-0.001	-0.01	-0.005	-0.001	-0.001	-0.02	-0.005	-0.01	-0.001	0.01	-0.01
MU36S	-0.02	0.32	-0.001	-0.001	-0.01	-0.001	-0.01	-0.005	-0.001	-0.001	-0.02	-0.005	-0.01	-0.001	-0.01	-0.01
MU37D	-0.02	1.88	-0.001	-0.001	-0.01	-0.001	-0.01	-0.005	-0.001	-0.001	-0.02	-0.005	-0.01	-0.001	0.02	-0.01
MU37I	-0.02	0.775	-0.001	-0.001	-0.01	-0.001	-0.01	-0.005	-0.001	-0.001	-0.02	-0.005	-0.01	-0.001	-0.01	-0.01
MU37S	-0.02	1.33	-0.001	-0.001	-0.01	-0.001	-0.01	-0.005	-0.001	-0.001	-0.02	-0.005	-0.01	-0.001	0.44	-0.01
MU38D	-0.02	0.145	-0.001	-0.001	-0.01	-0.001	0.2	-0.005	-0.001	0.001	0.12	-0.005	-0.01	-0.001	0.03	0.03
MU38S	-0.02	0.065	-0.001	-0.001	-0.01	-0.001	-0.01	-0.005	-0.001	-0.001	-0.02	-0.005	-0.01	-0.001	-0.01	-0.01
MU39		0.38		-0.001	-1	-0.001	0.06	-0.001	-0.001	-0.002	0.08	0.011	-0.001	-0.001	0.16	

Bore ID	*Sn (mg/L)*	*Sr (mg/L)*	*Ta (mg/L)*	*Tb (mg/L)*	*Te (mg/L)*	*Th (mg/L)*	*Ti (mg/L)*	*Tl (mg/L)*	*Tm (mg/L)*	*U (mg/L)*	*V (mg/L)*	*Y (mg/L)*	*W (mg/L)*	*Yb (mg/L)*	*Zn (mg/L)*	*Zr (mg/L)*
MU40D	-0.02	3.34	-0.001	-0.001	-0.01	-0.001	0.05	-0.005	-0.001	-0.001	-0.05	-0.005	-0.01	-0.001	0.2	-0.01
MU40S	-0.02	2.96	-0.001	-0.001	-0.01	-0.001	-0.05	-0.005	-0.001	-0.001	-0.05	-0.005	-0.01	-0.001	0.02	-0.01
MU41D	-0.02	0.87	-0.001	-0.001	-0.01	-0.001	-0.01	-0.005	-0.001	-0.001	-0.02	-0.005	-0.01	-0.001	-0.01	-0.01
MU41S	-0.02	0.445	-0.001	-0.001	-0.01	-0.001	-0.01	-0.005	-0.001	-0.001	-0.02	-0.005	-0.01	-0.001	-0.01	-0.01
MU42A		1.7		-0.001	-1	-0.001	-0.005	-0.001	-0.001	-0.002	0.01	-0.001	0.002	-0.001	0.015	
MU42D	-0.02	0.78	-0.001	-0.001	-0.01	-0.001	-0.01	-0.005	-0.001	-0.001	-0.02	-0.005	-0.01	-0.001	-0.01	-0.01
MU42I	-0.02	1.21	-0.001	-0.001	-0.01	-0.001	-0.05	-0.005	-0.001	-0.001	-0.05	-0.005	-0.01	-0.001	0.1	-0.01
MU42S	-0.02	0.235	-0.001	-0.001	-0.01	-0.001	-0.01	-0.005	-0.001	-0.001	-0.02	-0.005	-0.01	-0.001	0.03	-0.01
MU43D	-0.02	0.97	-0.001	-0.001	-0.01	-0.001	-0.01	-0.005	-0.001	-0.001	-0.02	-0.005	-0.01	-0.001	-0.01	-0.01
MU43S	-0.02	0.695	-0.001	-0.001	-0.01	-0.001	-0.01	-0.005	-0.001	-0.001	-0.02	-0.005	-0.01	-0.001	0.7	-0.01
MU44		8.08		-0.001	-1	-0.001	-0.02	-0.001	-0.001	-0.002	-0.05	-0.001	-0.001	-0.001	0.04	
MU45D	-0.02	15.7	-0.001	-0.001	-0.01	-0.001	-0.2	-0.005	-0.001	0.001	-0.2	-0.005	-0.01	-0.001	0.1	-0.01
MU45S	-0.02	0.745	-0.001	-0.001	-0.01	-0.001	-0.01	-0.005	-0.001	-0.001	-0.02	-0.005	-0.01	-0.001	0.04	-0.01
MU46A		39.5		-0.001	-1	-0.001	0.02	-0.001	-0.001	0.002	-0.05	-0.001	-0.001	-0.001	0.06	
MU46D	-0.02	71.4	-0.001	-0.001	-0.01	-0.001	-0.2	-0.005	-0.001	-0.001	-0.2	-0.005	-0.01	-0.001	0.2	-0.01
MU46S	-0.02	11.1	-0.001	-0.001	-0.01	-0.001	0.05	-0.005	-0.001	-0.001	-0.05	-0.005	-0.01	-0.001	0.2	-0.01
MU47		1.62		-0.001	-1	-0.001	-0.02	-0.001	-0.001	-0.002	-0.05	-0.001	-0.001	-0.001	0.04	
MU48		20		-0.001	-1	-0.001	-0.02	-0.001	-0.001	-0.002	-0.05	0.004	-0.001	-0.001	0.04	
MU49		0.44		-0.001	-1	-0.001	-0.005	-0.001	-0.001	-0.002	0.005	-0.001	-0.001	-0.001	0.01	
MU51		2.5		-0.001	-1	-0.001	-0.02	-0.001	-0.001	-0.002	-0.05	-0.001	-0.001	-0.001	0.02	
MU52A		1.22		-0.001	-1	-0.001	-0.02	-0.001	-0.001	-0.002	-0.05	-0.001	-0.001	-0.001	0.16	
MU52D	-0.02	10.5	-0.001	-0.001	-0.01	-0.001	0.05	-0.005	-0.001	-0.001	-0.05	-0.005	-0.01	-0.001	0.08	-0.01
MU52S	-0.02	1.59	-0.001	-0.001	-0.01	-0.001	-0.01	-0.005	-0.001	-0.001	-0.02	-0.005	-0.01	-0.001	0.05	-0.01

Bore ID	*Sn (mg/L)*	*Sr (mg/L)*	*Ta (mg/L)*	*Tb (mg/L)*	*Te (mg/L)*	*Th (mg/L)*	*Ti (mg/L)*	*Tl (mg/L)*	*Tm (mg/L)*	*U (mg/L)*	*V (mg/L)*	*Y (mg/L)*	*W (mg/L)*	*Yb (mg/L)*	*Zn (mg/L)*	*Zr (mg/L)*
MU53		0.94		-0.001	-1	-0.001	-0.005	-0.001	-0.001	-0.002	-0.005	-0.001	-0.001	-0.001	0.045	
MU54D	-0.02	0.64	-0.001	-0.001	-0.01	-0.001	-0.01	-0.005	-0.001	-0.001	-0.02	-0.005	-0.01	-0.001	-0.01	-0.01
MU54S	-0.02	0.245	-0.001	-0.001	-0.01	-0.001	-0.01	-0.005	-0.001	-0.001	-0.02	-0.005	-0.01	-0.001	0.01	-0.01
MU55D		0.9		-0.001	-1	-0.001	-0.005	-0.001	-0.001	-0.002	0.005	-0.001	-0.001	-0.001	0.005	
MU55S		0.36		-0.001	-1	-0.001	-0.005	-0.001	-0.001	-0.002	0.005	-0.001	-0.001	-0.001	0.01	
MU56D		0.1		-0.001	-1	-0.001	-0.005	-0.001	-0.001	-0.002	-0.005	-0.001	-0.001	-0.001	0.09	
MU57D		2.12		-0.001	-1	-0.001	-0.005	-0.001	-0.001	-0.002	-0.005	-0.001	-0.001	-0.001	0.025	
MU57S		1.32		-0.001	-1	-0.001	-0.005	-0.001	-0.001	-0.002	0.02	0.005	-0.001	-0.001	0.015	
MU58D		6.9		-0.001	-1	-0.001	-0.02	-0.001	-0.001	-0.002	-0.05	-0.001	-0.001	-0.001	0.04	
MU58S		7.16		-0.001	-1	-0.001	-0.02	-0.001	-0.001	-0.002	-0.05	-0.001	-0.001	-0.001	0.06	
MU59D		29.6		-0.001	-1	-0.001	0.02	-0.001	-0.001	-0.002	-0.05	-0.001	-0.001	-0.001	0.02	
MU59I		13.1		-0.001	-1	-0.001	-0.02	-0.001	-0.001	-0.002	-0.05	-0.001	-0.001	-0.001	0.02	
MU59S		4.22		-0.001	-1	-0.001	-0.02	-0.001	-0.001	-0.002	-0.05	0.003	-0.001	-0.001	-0.02	
MU60D		12.6		-0.001	-1	-0.001	-0.02	-0.001	-0.001	-0.002	-0.05	-0.001	-0.001	-0.001	0.04	
MU60S		18.5		-0.001	-1	-0.001	0.04	-0.001	-0.001	-0.002	-0.05	-0.001	-0.001	-0.001	0.38	
MU61D		67.2		-0.001	-1	-0.001	0.02	-0.001	-0.001	-0.002	-0.05	-0.001	-0.001	-0.001	0.06	
MU61I		5.62		-0.001	-1	-0.001	0.02	-0.001	-0.001	-0.002	-0.05	-0.001	-0.001	-0.001	-0.02	
MU61S		1.96		-0.001	-1	-0.001	0.02	-0.001	-0.001	-0.002	-0.05	-0.001	-0.001	-0.001	0.02	
MU62D		2.04		-0.001	-1	-0.001	-0.005	-0.001	-0.001	-0.002	-0.005	-0.001	-0.001	-0.001	0.015	
MU62I		0.94		-0.001	-1	-0.001	-0.005	-0.001	-0.001	-0.002	-0.005	-0.001	-0.001	-0.001	0.18	
MU62S		0.3		-0.001	-1	-0.001	-0.005	-0.001	-0.001	-0.002	0.01	-0.001	-0.001	-0.001	0.225	
MU63D		1.8		-0.001	-1	-0.001	-0.02	-0.001	-0.001	-0.002	-0.05	-0.001	-0.001	-0.001	0.06	
MU63S		0.4		-0.001	-1	-0.001	-0.02	-0.001	-0.001	-0.002	-0.05	0.003	-0.001	-0.001	0.16	

Bore ID	*Sn (mg/L)*	*Sr (mg/L)*	*Ta (mg/L)*	*Tb (mg/L)*	*Te (mg/L)*	*Th (mg/L)*	*Ti (mg/L)*	*Tl (mg/L)*	*Tm (mg/L)*	*U (mg/L)*	*V (mg/L)*	*Y (mg/L)*	*W (mg/L)*	*Yb (mg/L)*	*Zn (mg/L)*	*Zr (mg/L)*
MU64D		1.6		0.001	-1	-0.001	-0.005	-0.001	-0.001	-0.002	0.01	0.001	-0.001	-0.001	0.025	
MU64I		0.6		-0.001	-1	-0.001	-0.005	-0.001	-0.001	-0.002	-0.005	-0.001	-0.001	-0.001	0.07	
MU64S		0.4		-0.001	-1	0.001	0.24	-0.001	-0.001	-0.002	0.02	0.01	-0.001	-0.001	0.18	
MU65D		0.56		-0.001	-1	-0.001	-0.005	-0.001	-0.001	-0.002	0.005	-0.001	-0.001	-0.001	0.03	
MU65S		0.46		-0.001	-1	-0.001	-0.005	-0.001	-0.001	-0.002	0.005	0.001	-0.001	-0.001	0.02	
MU66D		0.48		-0.001	-1	-0.001	-0.005	-0.001	-0.001	-0.002	0.01	-0.001	-0.001	-0.001	0.015	
MU66S		0.62		-0.001	-1	-0.001	-0.005	-0.001	-0.001	-0.002	0.005	-0.001	-0.001	-0.001	0.005	
MU67D		2.96		-0.001	-1	-0.001	-0.005	-0.001	-0.001	-0.002	-0.005	-0.001	-0.001	-0.001	0.005	
MU67I		0.86		-0.001	-1	-0.001	-0.005	-0.001	-0.001	-0.002	-0.005	-0.001	-0.001	-0.001	0.035	
MU67S		0.44		-0.001	-1	-0.001	-0.005	-0.001	-0.001	-0.002	0.005	-0.001	-0.001	-0.001	0.03	
MU68D		0.62		-0.001	-1	-0.001	-0.005	-0.001	-0.001	-0.002	-0.005	-0.001	-0.001	-0.001	0.075	
MU68S		0.26		-0.001	-1	-0.001	-0.005	-0.001	-0.001	-0.002	0.01	-0.001	-0.001	-0.001	0.02	
MU69		4.32		-0.001	-1	-0.001	-0.02	-0.001	-0.001	-0.002	-0.02	-0.001	-0.001	-0.001	0.04	
MU70		1.36		-0.001	-1	-0.001	-0.005	-0.001	-0.001	-0.002	-0.005	-0.001	-0.001	-0.001	0.055	
MU71		0.12		-0.001	-1	-0.001	-0.005	-0.001	-0.001	-0.002	0.005	-0.001	-0.001	-0.001	-0.005	
MU72		1.4		-0.001	-1	-0.001	0.005	-0.001	-0.001	-0.002	-0.005	-0.001	-0.001	-0.001	0.02	
Muir1	-1	36.8	-0.001	-0.001	-1	-0.001	-0.1	-0.001	-0.001	0.004	-0.2	-0.001	-0.001	-0.001	-0.1	
Muir2	-1	33.2	-0.001	-0.001	-1	-0.001	-0.1	-0.001	-0.001	0.004	-0.2	-0.001	-0.001	-0.001	-0.1	
Muir3	-1	39.6	-0.001	-0.001	-1	-0.001	-0.1	-0.001	-0.001	0.008	-0.2	0.003	-0.001	-0.001	-0.1	
Muir4	-1	15.8	-0.001	-0.001	-1	-0.001	-0.1	-0.001	-0.001	-0.002	-0.2	-0.001	-0.001	-0.001	-0.1	
PM01		10.3		-0.001	-1	-0.001	-0.02	-0.001	-0.001	-0.002	-0.02	0.002	-0.001	-0.001	0.32	
PM02		0.94		-0.001	-1	-0.001	-0.005	-0.001	-0.001	-0.002	-0.005	-0.001	-0.001	-0.001	0.175	
PM03		0.54		-0.001	-1	-0.001	-0.005	-0.001	-0.001	-0.002	0.005	-0.001	-0.001	-0.001	0.015	

Bore ID	*Sn (mg/L)*	*Sr (mg/L)*	*Ta (mg/L)*	*Tb (mg/L)*	*Te (mg/L)*	*Th (mg/L)*	*Ti (mg/L)*	*Tl (mg/L)*	*Tm (mg/L)*	*U (mg/L)*	*V (mg/L)*	*Y (mg/L)*	*W (mg/L)*	*Yb (mg/L)*	*Zn (mg/L)*	*Zr (mg/L)*
PM04		0.56		-0.001	-1	-0.001	-0.005	-0.001	-0.001	-0.002	0.005	-0.001	-0.001	-0.001	0.02	
PM10		0.4		-0.001	-1	-0.001	-0.005	-0.001	-0.001	-0.002	0.01	-0.001	-0.001	-0.001	0.015	
PM12		2.46		-0.001	-1	-0.001	-0.02	-0.001	-0.001	-0.002	0.02	0.019	-0.001	0.001	0.06	